Bulletin 36
Part 5
(of 7 Parts)

THE
SHOCK AND VIBRATION
BULLETIN

JANUARY 1967

A Publication of
**THE SHOCK AND VIBRATION
INFORMATION CENTER**
Naval Research Laboratory, Washington, D.C.
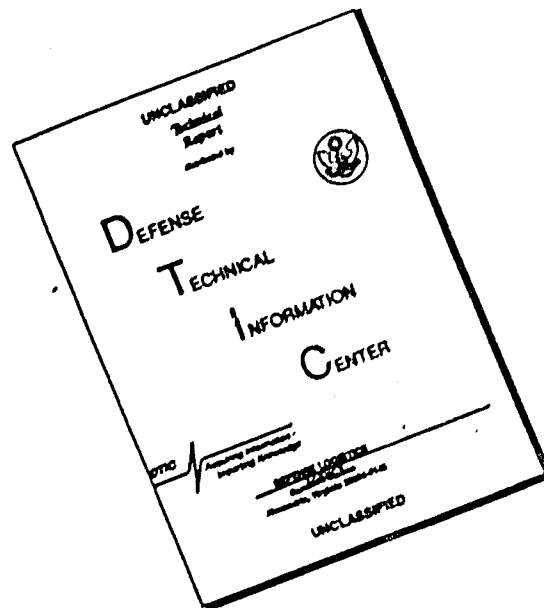
Office of
The Director of Defense
Research and Engineering

DISCLAIMER NOTICE

THIS DOCUMENT IS BEST
QUALITY AVAILABLE. THE COPY
FURNISHED TO DTIC CONTAINED
A SIGNIFICANT NUMBER OF
PAGES WHICH DO NOT
REPRODUCE LEGIBLY.

THE
SHOCK AND VIBRATION
BULLETIN

JANUARY 1967

A Publication of
THE SHOCK AND VIBRATION
INFORMATION CENTER
Naval Research Laboratory, Washington, D.C.

Office of
The Director of Defense
Research and Engineering

SYMPOSIUM MANAGEMENT

The Shock and Vibration Information Center

William W. Mutch, Director

Henry C. Pusey, Coordinator

Rudolph H. Volin, Coordinator

Jean B. Goldbecker, Editor

Katherine G. Jahnel, Administrative Secretary

36th Program Committee

William R. Forlifer, NASA Goddard Space Flight Center

Edward H. Schell, Air Force Flight Dynamics Laboratory

George Stathopoulos, Naval Ordnance Laboratory

James M. Taylor, U.S. Army Missile Command

Air Force Liaison

Los Angeles Scientific and Technical Liaison Office, Research and Technology
Division, Air Force Systems Command

Lt. Col. Kenneth W. Cook

Arthur E. Kimberly

Bulletin Production

Graphic Arts Branch, Technical Information Division,
Naval Research Laboratory

CONTENTS

PART 5

Analysis and Prediction

PAPERS APPEARING IN PART 1
Part 1 - Confidential
(Titles Unclassified)

EFFECT OF AIR DAMPING ON STRUCTURAL FATIGUE FAILURE
    John R. Fagan, Radio Corporation of America, Princeton, New Jersey

DEVELOPMENT OF DAMPED MACHINERY FOUNDATIONS
    W. Blasingame and E. V. Thomas, Navy Marine Engineering Laboratory,
    Annapolis, Maryland, and R. A. DiTaranto, Pennsylvania Military Colleges,
    Chester, Pennsylvania

DYNAMIC MECHANICAL STUDIES OF A COMPOSITE MATERIAL
    M. G. Sharma, M. Critchfield, and W. F. St. Lawrence, The Pennsylvania
    State University, University Park, Pennsylvania

PAPERS APPEARING IN PART 6

Data Analysis and Instrumentation

ANALYSIS AND PREDICTION

METHOD FOR IMPROVING A DYNAMIC MODEL USING EXPERIMENTAL TRANSIENT RESPONSE DATA

Ching-u Ip, Eli P. Howard and Richard J. Sylvester
Aerospace Corporation
San Bernardino, California

A rational method is developed for improving the mathematical dynamic model of a linear system by utilizing experimental results. The data required as input to the method consist of measurements of the applied load and some limited response information. Two examples demonstrate the improvement in the mathematical model of a six-degree-of-freedom system when the loading and limited response information is known without experimental error. Future efforts are outlined to study effects of error in experimental input data and feasibility of application to systems of many degrees of freedom.

E. P. Howard

INTRODUCTION

The dynamic analyses performed to determine the responses of a structure subjected to dynamic loads involve the formulation of a mathematical model that represents the physical structure. When the structure and loading are particularly complex, confirmatory experiments are devised to gain confidence in the results of the mathematical model or to demonstrate structural integrity, or both.

A certain degree of confidence in the mathematical analysis can be achieved by a ground vibration test in which the entire structure is vibrated at a low level and the resonant frequencies are identified. However, limitations in this experimental technique usually preclude obtaining the mode shapes of the structure with

the same accuracy as the resonant frequencies. In addition to a ground vibration survey, dynamic load tests are often conducted that subject full-scale reentry vehicles to a blast wave in a large shock tube. A facility currently being utilized for this purpose is the Sandia Corporation "Thunderpipe" facility at Albuquerque, New Mexico.

It is the purpose of this paper to present a method or technique for utilizing experimental results from such facilities as the "Thunderpipe" to improve the mathematical model representing the structure that was tested. The improvement is achieved by revising the theoretically computed mode shapes to be in better agreement with experimental results.

LIST OF SYMBOLS

$[c]$	Square matrix, damping matrix
$\{F(t)\}$	Column matrix giving forces acting on various stations (nodes) of system
i	Subscript
$[I]$	Identity matrix
j	Subscript

1

$[k]$ Square matrix, stiffness matrix

$[m]$ Square matrix, mass matrix

n Number of modes

$\{q(t)\}$ Column matrix of generalized displacements

s Laplace transform variable

$[T]$ Transformation matrix relating strains to displacements

T Superscript, transpose of a matrix

$\{x\}, \{\dot{x}\}, \{\ddot{x}\}$ Column matrices representing displacements and their time derivative

a Scale factor

$\beta(t)$ Parameter associated with input forces and defined as quantity inside large parentheses of Eq. (11)

γ_{xy} Shear strain

$\{\gamma(t)\}$ Parameter associated with input forces and defined by Eq. (15)

$\{\epsilon\}$ Column matrix of strains

ζ $\mu_i / 2\omega_i$

μ Diagonal matrix of generalized modal damping

$[\phi]$ Modal matrix normalized so that $[\phi]^T [m] [\phi] = [I]$

ψ_i Function to be minimized and defined by Eq. (2)

$[\omega^2]$ Diagonal matrix of squares of circular frequencies

DESCRIPTION OF METHOD

Thunderpipe Tests

The "Thunderpipe" test series subjects a full-size reentry vehicle structure to blasts of conventional explosive, confined in a closed-end tube. One objective of the tests is to compare the measured dynamic response with the theoretical predictions to verify the analytical approach. Specifically, the pressure-time histories at various stations on the reentry vehicle are measured and are used as the forcing

functions in the analytical model. Measurements by strain gages and accelerometers at selected locations on the vehicle constitute the measured responses. These are used to compare with the calculated response of the preselected mathematical model of the dynamic system subjected to the measured forcing function.

Comparison of Experiment and Theory

An exact duplication of measured and computed response never occurs in practice. Hence a quantitative assessment of the degree of correlation is desired to assess the validity of the mathematical model used in the dynamic analysis. This study was conducted to determine the feasibility of improving the dynamic model using measured data from "Thunderpipe" experiments. This study assumes that the instrumentation and experimental technique are adequate, and that discrepancies are due to errors in formulating the mathematical model or establishing values of parameters for use in the model.

This feasibility study is idealized by considering linear mass-spring-dashpot mechanical systems subjected to transient response experiments in general, rather than the specific problem of the response of a reentry vehicle in a shock tube.

Summary of Method

In analyzing the continuous structure to which the shock is applied, the structure is approximated by a system of finite elements consisting of masses, springs, and dashpots. Since the structure is assumed to experience small vibrations due to the shock loading, the finite elements are considered to behave linearly. Hence, the linear response of the structure at the mass locations can be determined by the solution of the equations of motion of the system of finite elements if the system indeed represents the structure correctly. The problem is formulated utilizing matrix notation to facilitate the treatment since the mathematical aspects of the problem usually involve solving a large number of differential equations simultaneously. The large number results from the large number of finite elements used to represent the continuous system. The finite element are represented by $(n \times n)$ square matrices with n being the number of degrees of freedom. The shock or external disturbance is represented by a column matrix of forces, with each force

element being a function of time acting on a finite element or mass.

In the discussion that follows, a formal solution of the equations of motion is derived in matrix form. The responses of the system, calculated and measured, should agree with one another. If these do not agree, one has to adjust the values of the $3n^2$ elements in the mass, spring, and dashpot matrices until agreement between calculated and measured response is reached. Since the system is assumed to be linear, the response can be assumed to be a linear superposition of its normal modes. Hence, by filtering the measured response by adjusting the filter to the measured resonant frequencies (obtained from a vibration survey), its modal components can be obtained. This can be compared with the normal mode solution obtained analytically and has the advantage that one has to adjust the values of only n elements at one time. This was done in this report with the aid of a method developed and computerized at Aerospace Corporation. In this method, the difference between the calculated and measured values of the response in a particular mode, i, constitutes an error. The ψ function derived in the body of this report represents the sum of the squares of all the errors in the ith mode. This function is to be minimized so that the experimental data and the calculated results agree as closely as possible. By adjusting the values of the n modal elements in the neighborhood of the calculated values in a random manner and choosing the better set after each adjustment, one can find the values of the modal elements for closest agreement. The method described in this report accomplishes this result in a systematic way.

Derivation of Method for a Mass-
Spring-Dashpot System

The equations of motion of a linear system with viscous damping can be written concisely in the form of a matrix equation:

$$[m]\{\ddot{x}\} + [c]\{\dot{x}\} + [k]\{x\} = \{F(t)\}, \qquad (1)$$

where

$[m]$ = square matrix called the mass matrix,

$[c]$ = square matrix called the damping coefficient matrix,

$[k]$ = square matrix called the stiffness matrix,

$\{x\}, \{\dot{x}\}, \{\ddot{x}\}$ = column matrices representing displacements and their time derivatives, and

$\{F(t)\}$ = column matrix giving the forces acting on various stations (called nodes) of the system.

The solution to this equation will be derived in terms of the normal modes of the system. Not only $\{x(t)\}$, the displacement, but $\{\dot{x}(t)\}$, the velocity, and $\{\ddot{x}(t)\}$, the acceleration, were derived in terms of the normal modes and are given, respectively, in Eqs. (11), (12), and (13) which appear later.

It is convenient to treat the transient responses of the dynamic system as the summation of the responses of its normal modes. For a linear dynamic system with damping, the existence of normal modes is given by a theorem of Caughey [1] which can be stated as follows: "A necessary and sufficient condition that a linear damped dynamical system possess classical normal modes is that the damping matrix be diagonalized by the same transformation which uncouples the undamped system." However, if the transformation matrix $[\phi]$, which diagonalizes the $[m]$ and $[k]$ matrices of the undamped system, is found, it will not necessarily diagonalize the $[c]$ matrix of the damped system; but, for a realistic vibrating system, the off-diagonal terms of the transformed $[c]$ matrix will be small compared with the diagonal terms. Hence, the calculated responses by considering the system possesses classical normal modes would not differ much from the actual responses, and the generally accepted procedure is to ignore the off-diagonal terms of the modal damping matrix.

Consider the modal transformation as defined by

$$\{x(t)\} = [\phi]\{q(t)\}, \qquad (2)$$

where $[\phi]$ is the modal matrix, normalized such that $[\phi]^T[m][\phi] = \lceil I \rfloor$, and $\{q(t)\}$ is a column matrix representing the generalized displacements.

Substituting Eq. (2) into Eq. (1) and premultiplying by $[\phi]^T$ results in

$$\{\ddot{q}\} + \lceil \mu \rfloor \{\dot{q}\} + \lceil \omega^2 \rfloor \{q\} = [\phi]^T\{F(t)\}, \qquad (3)$$

where $\lceil \mu \rfloor$ and $\lceil \omega^2 \rfloor$ are diagonal matrices representing the generalized modal damping

3

and the normalized stiffness (or the square of circular frequency), respectively. $[\phi]^T$ is the transpose of the $[\phi]$ matrix. Thus, we obtain

$$[\phi]^T [m] [\phi] = \lceil I \rfloor .$$

$$[\phi]^T [k] [\phi] = \lceil \omega^2 \rfloor . \qquad (4)$$

and

$$[\phi]^T [c] [\phi] = \lceil \mu \rfloor .$$

where $\lceil I \rfloor$ is the identity matrix.

Taking the Laplace transformation of Eq. (3), we obtain the transformed equation, after using the following notations:

$$\{\bar{q}(s)\} = \int_0^\infty \{q(t)\} e^{-st} dt .$$

$$\{\bar{F}(s)\} = \int_0^\infty \{F(t)\} e^{-st} dt .$$

$$(5)$$

$$\{\bar{x}(s)\} = [\phi] \{\bar{q}(s)\} .$$

and

$$\left(s^2 \lceil I \rfloor + s \lceil \mu \rfloor + \lceil \omega^2 \rfloor \right) \{\bar{q}(s)\} = [\phi]^T \{\bar{F}(s)\}$$
$$+ \left(s \lceil I \rfloor + \lceil \mu \rfloor \{q(0)\} \right) + \{\dot{q}(0)\} .$$

Premultiplying Eq. (2) by $[\phi]^T [m]$ and using the normalization property given in Eq. (4), we obtain the following equation:

$$\{q(t)\} = [\phi]^T [m] \{x(t)\} , \qquad (6)$$

where the initial conditions are given by

$$\{q(0)\} = [\phi]^T [m] \{x(0)\}$$
and $\qquad (7)$
$$\{\dot{q}(0)\} = [\phi]^T [m] \{\dot{x}(0)\} .$$

From Eq. (5) we obtain

$$\{\bar{x}(s)\} = [\phi] \{\bar{q}(s)\}$$

$$= [\phi] \left[\frac{1}{s^2 + s\mu_i + \omega_i^2} \right] [\phi]^T \{\bar{F}(s)\}$$

$$+ [\phi] \left[\frac{s + \mu_i}{s^2 + s\mu_i + \omega_i^2} \right] [\phi]^T [m] \{x(0)\}$$

$$+ [\phi] \left[\frac{1}{s^2 + s\mu_i + \omega_i^2} \right] [\phi]^T [m] \{\dot{x}(0)\} .$$

$$(8)$$

where i is the index for the ith row of the diagonal matrix. Now we observe that

$$[\phi] \left[\frac{1}{s^2 + s\mu_i + \omega_i^2} \right] [\phi]^T = \sum_i \frac{1}{s^2 + s\mu_i + \omega_i^2} \{\phi\}_i \{\phi\}_i^T .$$

$$(9)$$

where $\{\phi\}_i$ is a column matrix formed from the ith column of the $[\phi]$ matrix or the ith mode of the dynamic system. Hence, Eq. (8) becomes

$$\{\bar{x}(s)\} = \sum_i \{\phi\}_i \{\phi\}_i^T \left(\frac{1}{s^2 + s\mu_i + \omega_i^2} \{\bar{F}(s)\} \right.$$

$$+ \frac{s + \mu_i}{s^2 + s\mu_i + \omega_i^2} [m] \{x(0)\}$$

$$+ \left. \frac{1}{s^2 + s\mu_i + \omega_i^2} [m] \{\dot{x}(0)\} \right) . \qquad (10)$$

Taking the inverse Laplace transform of Eq. (10) and differentiating the resulting function, we obtain the displacement, velocity, and acceleration matrices of the linear dynamic system as follows:

$$\{x(t)\} = \sum_i \{\phi\}_i \{\phi\}_i^T \left\{ \int_0^t \frac{e^{-\zeta_i \omega_i (t-\tau)}}{\omega_i \sqrt{1 - \zeta_i^2}} \right.$$

$$\times \sin \left(\omega_i (t - \tau) \sqrt{1 - \zeta_i^2} \right) \{F(\tau)\} d\tau$$

$$+ [m] \{x(0)\} e^{-\zeta_i \omega_i t} \left[\cos \left(\omega_i t \sqrt{1 - \zeta_i^2} \right) \right.$$

$$+ \left. \frac{\zeta_i}{\sqrt{1 - \zeta_i^2}} \sin \left(\omega_i t \sqrt{1 - \zeta_i^2} \right) \right]$$

$$+ \left. [m] \{\dot{x}(0)\} \frac{e^{-\zeta_i \omega_i t}}{\omega_i \sqrt{1 - \zeta_i^2}} \sin \omega_i t \sqrt{1 - \zeta_i^2} \right\} ,$$

$$(11)$$

$$\{\dot{x}(t)\} = \sum_i \{\phi\}_i \{\phi\}_i^T \left[\int_0^t e^{-\zeta_i \omega_i (t-\tau)} \right.$$

$$\times \{F(\tau)\} \left(\cos \sqrt{1 - \zeta_i^2} \omega_i (t - \tau) \right.$$

$$- \left. \left. \frac{\zeta_i}{\sqrt{1 - \zeta_i^2}} \sin \sqrt{1 - \zeta_i^2} \omega_i (t - \tau) \right) \right] d\tau$$

$$(12)$$
(Cont.)

4

$$-[m]\{x(0)\} \frac{\omega_i e^{-\zeta_i \omega_i t}}{\sqrt{1-\zeta_i^2}} \sin\left(\omega_i t \sqrt{1-\zeta_i^2}\right)$$

$$+[m]\{\dot{x}(0)\} e^{-\zeta_i \omega_i t} \left[\cos\left(\omega_i t \sqrt{1-\zeta_i^2}\right)\right.$$

$$\left. - \frac{\zeta_i \omega_i}{\sqrt{1-\zeta_i^2}} \sin\left(\omega_i t \sqrt{1-\zeta_i^2}\right)\right] . \qquad (12)$$

and

$$\{\ddot{x}(t)\} = \sum_i \{\phi\}_i \{\phi\}_i^T \left\{ \{F(t)\} - \int_0^t e^{-\zeta_i \omega_i (t-\tau)} \right.$$

$$\times \{F(\tau)\}\left[\frac{\omega_i(1-2\zeta_i^2)}{\sqrt{1-\zeta_i^2}} \sin\left(\omega_i(t-\tau)\sqrt{1-\zeta_i^2}\right)\right.$$

$$\left. + 2\omega_i \zeta_i \cos\left(\omega_i(t-\tau)\sqrt{1-\zeta_i^2}\right)\right] d\tau$$

$$- [m]\{x(0)\} e^{-\zeta_i \omega_i t} \left[\omega_i^2 \cos\left(\omega_i t \sqrt{1-\zeta_i^2}\right)\right.$$

$$\left. - \frac{\zeta_i \omega_i}{\sqrt{1-\zeta_i^2}} \sin\left(\omega_i t \sqrt{1-\zeta_i^2}\right)\right] + [m]\{\dot{x}(0)\}$$

$$\times e^{-\zeta_i \omega_i t} \left[\frac{\omega_i(2\zeta_i^2-1)}{\sqrt{1-\zeta_i^2}} \sin\left(\omega_i t\sqrt{1-\zeta_i^2}\right)\right.$$

$$\left.\left. - 2\zeta_i \omega_i \cos\left(\omega_i t \sqrt{1-\zeta_i^2}\right)\right]\right\} . \qquad (13)$$

where $\zeta_i = \mu_i / 2\omega_i$.

Equations (11), (12), and (13) represent the displacement, velocity, and acceleration responses of the total system of finite elements in terms of its normal modes. Considering, for example, Eq. (13), one may interpret that the elements in $\{\ddot{x}(t)\}$ are obtainable from accelerometer readings, those in $\{F(\tau)\}$ are obtainable from pressure measurements, the values of ω_i are obtainable from a vibration survey, and $\{\phi\}_i$ are the unknown quantities needed to satisfy the equation.

Also, it may be observed from Eq. (13) that the acceleration signals consist only of components of the damped frequencies $\omega_i \sqrt{1-\zeta_i^2}$. It

is then feasible that a narrow-band filter (whether it is an electronic circuit or a digital computer filter) may be used to separate the components. The filtered acceleration components are derived below and given in Eq. (19).

Filtered Signal - Consider the acceleration column matrix, Eq. (13), which can be written as

$$\{\ddot{x}(t)\} = \sum_i \{\phi\}_i \{\phi\}_i^T \{\gamma(t)\}_i . \qquad (14)$$

where $\{\gamma(t)\}_i$ is the column matrix representing the quantity inside the braces in Eq. (13). For an undamped system where $\zeta_i = 0$,

$$\{\gamma(t)\}_i = \{F(t)\} - \int_0^t \{F(\tau)\} \omega_i \sin \omega_i(t-\tau)d\tau$$

$$- [m]\{x(0)\} \omega_i^2 \cos \omega_i t$$

$$- [m]\{\dot{x}(0)\} \omega_i \sin \omega_i t . \qquad (15)$$

Let the acceleration column matrix be decomposed into its modal components,

$$\{\ddot{x}(t)\} = \sum_i \{\ddot{x}(t)\}_i . \qquad (16)$$

which gives, from Eq. (14),

$$\{\ddot{x}(t)\}_i = \{\phi\}_i \{\phi\}_i^T \{\gamma(t)\}_i . \qquad (17)$$

Writing Eq. (17) in detail gives

$$\begin{Bmatrix} \ddot{x}_{1i} \\ \ddot{x}_{2i} \\ \cdot \\ \cdot \\ \cdot \\ \ddot{x}_{ji} \\ \cdot \\ \cdot \\ \ddot{x}_{ni} \end{Bmatrix} = \begin{Bmatrix} \phi_{1i} \\ \phi_{2i} \\ \cdot \\ \cdot \\ \cdot \\ \phi_{ji} \\ \cdot \\ \cdot \\ \phi_{ni} \end{Bmatrix} [\phi_{1i}\phi_{2i}\cdots\phi_{ji}\cdots\phi_{ni}] \begin{Bmatrix} \gamma_{1i} \\ \gamma_{2i} \\ \cdot \\ \cdot \\ \cdot \\ \gamma_{ji} \\ \cdot \\ \cdot \\ \gamma_{ni} \end{Bmatrix}$$

$$(18)$$

where

n is the number of degrees of freedom,
j denotes the jth mass, and
i denotes the ith mode.

From Eq. (18),

$$\ddot{x}_{ji}(t) = \phi_{ji} \sum_{k=1}^{n} \phi_{ki} \gamma_{ki}(t) . \qquad (19)$$

5

which is the filtered acceleration response at station j (filter set at the ith frequency).

Prior to the transient response experiment, a vibration survey (frequency response experiment) is made to determine accurately the natural frequencies (actually the damped frequencies) of the system. The applied forces $\{F(t)\}$ are measured during the transient response experiment. (It is assumed that the applied forces at each mass point representing the external structure are measured or can be extrapolated.) Then the quantities $\gamma_{ki}(t)$ can be determined from $\{F(t)\}$ and the initial conditions of the system. Hence, on examining Eqs. (15) and (19), it would appear that a set of $\{\phi\}_i$ could be determined if the values of $\ddot{x}_{ji}(t)$ and $\gamma_{ki}(t)$ are computed for a sufficient number of instants of observation.

In general, however, Eq. (19) will not be satisfied exactly for all instants of observation, due to inaccuracies in the formulation of the mathematical dynamic model. Consequently, a least squares criterion was generated for the determination of the best $\{\phi\}_i$ that would satisfy Eq. (19).

For the ith mode, this least squares criterion may be written

$$\psi_i(\phi_{1i}, \phi_{2i}, \ldots \phi_{ni})$$

$$= \sum_{t=1}^{p} \left[\sum_{j=1}^{m} \left(\ddot{x}_{ji} - \phi_{ji} \sum_{k=1}^{n} \gamma_{ki} \gamma_{ki} \right)^2 \right]_t$$

$$= \text{minimum} \tag{20}$$

or

$$-\psi = \text{maximum},$$

where

k = 1, 2, ..., n;
j = 1, 2, ..., m, number of responses measured; and
t = 1, 2, ..., p, number of instants of observation.

It should be pointed out that the number of responses measured, m, can be less than n, the number of degrees of freedom.

Recapitulating, we have shown that, on the basis of a dynamic analysis, an estimate of the natural mode shapes $\{\phi\}$ could be made. Together with this information and the natural frequencies ω_i obtained from a ground vibration survey of the structure and the measured

response at various locations on the structure, we are able to construct ψ_i. This function expresses in a general way the difference between the computed and measured responses. Hence, minimizing this function will result in a set of mode shapes that will fit the experimental data.

The minimization of Eq. (20) was accomplished by means of a method developed by Brooks [2]. This method is described in the following paragraphs.

Brooks' Monte Carlo Method for Finding a Maximum - A customary method for determining maxima is the gradient method, which requires determining the direction of maximum change of the function by evaluating its partial derivatives with respect to its independent variables. One then proceeds along the direction of the gradient until a local maximum is determined. At this point, another gradient direction is established.

Because of the amount of computation in derivative determination, a more efficient method is to maximize along a line in a random direction. One can show that the expectation of the change is in the gradient direction, yet the partial derivatives associated with the gradient need not be determined.

To simplify the discussion of the method, we consider ψ_i to be a function of a two-dimensional space (ϕ_{1i}, ϕ_{2i}) (Fig. 1). Starting with an initial guess of ϕ_{1i}, ϕ_{2i}, which corresponds to the point 0 in the space, one evaluates $-\psi_i$. From 0, a random direction is chosen. A point 1 in the vicinity of 0 in the chosen direction is then selected and the corresponding value of $-\psi_i$ is evaluated. The second value of $-\psi_i$ is compared with the first. If the second value is higher, select point 2 in the direction of 0-1 at twice the step size. If point 2 is still higher, select point 3 at again twice the step size. If point 2 is still higher, select point 3 at again twice the second step size. If point 3 gives a
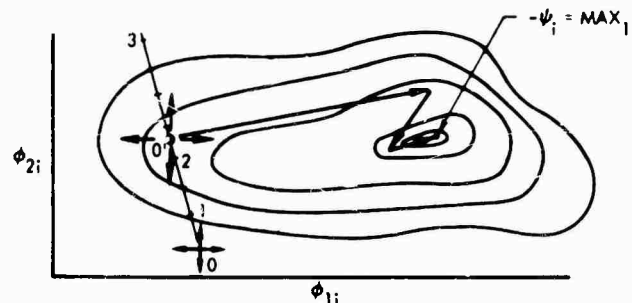
Fig. 1. Monte Carlo method

lower value of $-\psi_i$ than point 2, a parabolic curve is drawn through points 1, 2, and 3. Point 0' corresponds to the highest point on the parabolic curve, which should be close to the position of a local maximum in that one direction. From 0', another random direction is chosen and the process is repeated. The process terminates when an exhaustive search of a vicinity yields no better $-\psi_i$.

It may be seen that this method has some of the characteristics of the method of steepest descent, but seems to be more efficient in that the gradients in n-dimensional space need not be evaluated for each step.

EXAMPLE PROBLEMS AND DISCUSSION

Two problems were solved to illustrate the method of this report. Both of these problems considered a lumped parameter model having only six degrees of freedom, but it is felt that the essence of the method was demonstrated nevertheless. In the absence of test data, the mass and stiffness parameters in the problems were arbitrarily changed in an attempt to introduce errors due to shortcomings of the dynamic analyst who formulated the problems. The mode shapes computed from this erroneous formulation were obviously different from the true mode shapes one would obtain from an experimental modal survey if this could be accomplished accurately.

In the first problem, it was assumed that there was measured disturbance or response information at all points corresponding to the degrees of freedom of the mathematical model. In the second problem, this was not true. In fact, no information was available at two of the stations used in the mathematical formulation.

The convergence to the true mode shapes was excellent in the first example despite the fact that the analytically derived mode shapes differed considerably from the true ones. In the second example, improvement in the computed mode shapes was shown as a result of processing the "experimental data" according to the method of this report, although the improvement was not as dramatic as in the first example. These results seem to imply that one can anticipate considerable improvement in a poorly formulated mathematical dynamic model when a large amount of experimental data are available.

Example Problem Number 1

Statement of Problem - To illustrate the application of the previously derived results, an example was constructed that contains the main features of a typical problem. The problem might represent the case in which it is desired to determine the transient response of a reentry vehicle subjected to a blast loading. Based on the physical properties of the structure, a spring-mass analog was constructed, consisting of 6 masses and 5 springs (Fig. 2). The applied force is represented by a triangular pulse with a peak of 1000 lb and a duration of 0.001 sec that travels over the reentry vehicle at a speed of 12,000 ips.

Let the true (actual) masses and springs be of the following values:

$$w_1 = m_1 g = 28.309 \text{ lb}$$

$$w_2 = m_2 g = 19.709 \text{ lb}$$

$$w_3 = m_3 g = 16.110 \text{ lb}$$

$$w_4 = m_4 g = 14.919 \text{ lb}$$

$$w_5 = m_5 g = 19.319 \text{ lb}$$

$$w_6 = m_6 g = 19.427 \text{ lb}$$

$$k_1 = 1.251 \times 10^4 \text{ lb/in.}$$

$$k_2 = 1.528 \times 10^4 \text{ lb/in.}$$
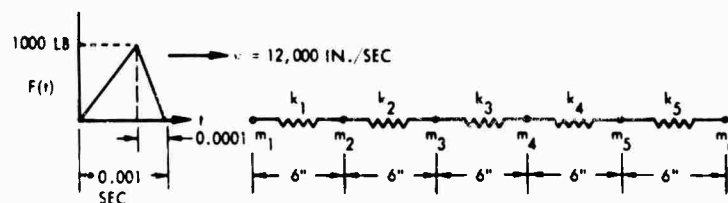
Fig. 2. Spring-mass system subjected to traveling pulse

7

$$k_3 = 1.063 \times 10^4 \text{ lb/in.}$$

$$k_4 = 1.144 \times 10^4 \text{ lb/in.}$$

$$k_5 = 1.012 \times 10^4 \text{ lb/in.}$$

Let the dynamicist who formulates the dynamic model calculate these values to be

$$w_1 = 25.000 \text{ lb}$$

$$w_2 = 19.709 \text{ lb}$$

$$w_3 = 16.110 \text{ lb}$$

$$w_4 = 17.000 \text{ lb}$$

$$w_5 = 19.319 \text{ lb}$$

$$w_6 = 19.427 \text{ lb}$$

$$k_1 = 1.25 \times 10^4 \text{ lb/in.}$$

$$k_2 = 1.300 \times 10^4 \text{ lb/in.}$$

$$k_3 = 0.900 \times 10^4 \text{ lb/in.}$$

$$k_4 = 1.144 \times 10^4 \text{ lb/in.}$$

$$k_5 = 1.012 \times 10^4 \text{ lb/in.}$$

which are different from the true values; i.e., some errors were made in formulating the values due to limitations of the theory employed.

An eigenvalue analysis would furnish the following frequencies and mode shapes.

a. True Frequencies and Mode Shapes - The true frequencies and mode shapes are based on actual masses and springs of the system.

$$\omega_1^2 = 0 \text{ (rigid body mode)} \qquad \{\phi\}_1 = \begin{Bmatrix} 1.0 \\ 1.0 \\ 1.0 \\ 1.0 \\ 1.0 \\ 1.0 \end{Bmatrix},$$

$$\omega_2^2 = 5.6617794 \times 10^4 \text{ (1st flexible mode)} \qquad \{\phi\}_2 = \begin{Bmatrix} 2.1832192 \\ 1.4587241 \\ 0.5896454 \\ -0.7540531 \\ -1.8584049 \\ -2.5865483 \end{Bmatrix},$$

$$\omega_3^2 = 2.5711003 \times 10^5 \qquad \{\phi\}_3 = \begin{Bmatrix} 1.7488900 \\ -0.8866337 \\ -2.2827900 \\ -2.6291799 \\ -0.6677005 \\ 2.3984586 \end{Bmatrix},$$

$$\omega_4^2 = 4.5687757 \times 10^5 \qquad \{\phi\}_4 = \begin{Bmatrix} 1.4134544 \\ -2.3715559 \\ -1.8505419 \\ 1.2303420 \\ 2.2175386 \\ -1.7438144 \end{Bmatrix},$$

$$\omega_5^2 = 7.5677902 \times 10^5 \qquad \{\phi\}_5 = \begin{Bmatrix} 0.5546950 \\ -1.9057222 \\ 0.8981284 \\ 3.0055750 \\ -2.7191541 \\ 0.9841980 \end{Bmatrix},$$

and

$$\omega_6^2 = 1.2522949 \times 10^6 \qquad \{\phi\}_6 = \begin{Bmatrix} 0.3159087 \\ -2.0028400 \\ 4.4781486 \\ -2.0715276 \\ 0.6050650 \\ -0.1157667 \end{Bmatrix}.$$

b. Calculated Frequencies and Mode Shapes - The calculated frequencies and mode shapes are based on masses and springs estimated by analysis.

$$\omega_1^2 = 0 \qquad \{\phi\}_1 = \begin{Bmatrix} 1.0 \\ 1.0 \\ 1.0 \\ 1.0 \\ 1.0 \\ 1.0 \end{Bmatrix},$$

$$\omega_2^2 = 5.3594196 \times 10^4 \qquad \{\phi\}_2 = \begin{Bmatrix} 2.2822298 \\ 1.6491218 \\ 0.6928123 \\ -0.8125969 \\ -1.8292985 \\ -2.4938566 \end{Bmatrix},$$

$$\omega_3^2 = 2.4823731 \times 10^5 \qquad \{\phi\}_3 = \begin{Bmatrix} 1.7012653 \\ -0.4846835 \\ -2.1157792 \\ -2.7167839 \\ -0.5938498 \\ 2.5348854 \end{Bmatrix},$$

$$\omega_4^2 = 4.4476042 \times 10^5 \qquad \{\phi\}_4 = \begin{Bmatrix} 1.8014632 \\ -2.3457125 \\ -2.2398130 \\ 1.2419185 \\ 1.8550571 \\ -1.5313187 \end{Bmatrix},$$

$$\omega_5^2 = 7.0651811 \times 10^5 \qquad \{\phi\}_5 = \begin{Bmatrix} 0.6474993 \\ -1.7204015 \\ 0.7739617 \\ 2.5497223 \\ -2.9868394 \\ 1.1885990 \end{Bmatrix},$$

and

$$\omega_6^2 = 1.0675415 \times 10^6 \qquad \{\phi\}_6 = \begin{Bmatrix} 0.4804274 \\ -2.1742601 \\ 4.3856738 \\ -1.7835363 \\ 0.6914416 \\ -0.1605030 \end{Bmatrix} .$$

It should be noted that the true and calculated values of the frequencies and mode shapes are different and that, after a hypothetical frequency survey has been performed, the set of true ω_i^2 in case a is found. The sets of $\{\phi\}_i$ in case a are not known, however, whereas those in case b have been calculated by the dynamicist. It is assumed that, during the frequency survey, either the mode shapes were not measured or they were not obtained with the same accuracy as the measured frequencies. A computer program has been written to compute the quantities $\ddot{x}_{ji}(t)$ and $\phi_{ji}(t)$ using Eqs. (14) and (15). The values of the quantities for 3 time instants and the 5 flexible modes are given in Table 1.

Example Problem Results - The numerical values from Table 1 were entered as inputs to the "Creeping Random Computer Program," previously discussed, which minimizes ψ_i in Eq. (20). This computer program requires as input an initial trial value for ϕ_{ji}. Instead of using the calculated values of ϕ_{ji} only (the results of the dynamic analysis), two cases of initial trial values of ϕ_{ji} were attempted: (a) the calculated values of ϕ_{ji} (from the dynamic analysis), and (b) all elements of ϕ_{ji} equal to 1.0.

a. Calculated ϕ_{ji} as Initial Values

$[\phi] = [\{\phi\}_2 \{\phi\}_3 \dots \{\phi\}_6]$

$$= \begin{bmatrix} 2.1832193 & 1.7489067 & 1.4134545 \\ 1.4587253 & -0.88650611 & -2.3715565 \\ 0.58964542 & -2.2828123 & -1.8505421 \\ -0.75405318 & -2.6292058 & 1.2903421 \\ -1.8584052 & -0.6677963 & 2.2175393 \\ -2.5865485 & 2.3984812 & -1.7438146 \end{bmatrix}$$

No. of Trials	(71,001)	(245,000)	(81,002)

$$\begin{bmatrix} 0.55469529 & 0.32092342 \\ -1.9057233 & -2.0454205 \\ 0.89812871 & 4.5181893 \\ 3.0055761 & -2.0922921 \\ -2.7191556 & 0.59756558 \\ 0.98419836 & -0.11567424 \end{bmatrix}$$

No. of Trials		(139,002)	(285,000 not yet converged)

b. All Elements of ϕ_{ji} Equal to 1.0 as Initial Values

$[\phi] = [\{\phi\}_2 \{\phi\}_3 \{\phi\}_4 \{\phi\}_5]$

$$= \begin{bmatrix} -2.1832198 & -1.7464479 & -1.4134545 \\ -1.4587201 & 0.90395607 & 2.3715562 \\ -0.58964556 & 2.2796787 & 1.8505420 \\ 0.75405333 & 2.6254416 & -1.2903421 \\ 1.8584022 & 0.65576761 & -2.2175390 \\ 2.5865490 & -2.3956199 & 1.7438145 \end{bmatrix}$$

No. of Trials	(108,002)	(186,002)	(152,001)

$$\begin{bmatrix} 0.55469514 \\ -1.9057231 \\ 0.89812867 \\ 3.0055761 \\ -2.7191556 \\ 0.98419835 \end{bmatrix}$$

No. of Trials	(177,002)

Discussion of Example Problem Number 1 Results - Comparing the results obtained with the true mode shapes, it may be observed that the computer results are accurate and repeatable as they converge to the values known to be correct a priori.

It is interesting to note that ϕ_{ji} converges to the same numerical value, but with a minus sign for $i = 2, 3,$ and 4 in the case of the initial values of 1.0. For $i = 5$, the obtained result is the same for cases a and b. For our physical problem, the mode shape $-\{\phi\}_i$ is the same as the mode shape $\{\phi\}_i$.

Not every set of ϕ_{ji} which minimizes Eq. (20) is necessarily a modal vector. If only a few response measurements are made and if there are many more unknowns than are represented in Eq. (20), more than one set of ϕ_{ji} will render ψ_i equal or close to zero. An additional mathematical constraint is required to produce an acceptable solution. This restraint is supplied by confining in some manner the mode shape $\{\phi\}_i$ to a neighborhood of the theoretically calculated mode shape.

If the $[m]$ matrix is chosen somewhat arbitrarily, as is often the case in the original model formulation, a test to evaluate whether the correct set of $\{\phi\}_i$ is obtained is that the vectors should be orthogonal with respect to the $[m]$ matrix. After the correct $[\phi]$ matrix, $[\phi] = [\{\phi\}_1 \{\phi\}_2 \dots \{\phi\}_6]$, is obtained from the Monte Carlo computation, the correct mass and stiffness matrices can then be evaluated from the following equations:

9

TABLE 1
Computed Values of Shear Strain and Acceleration

Flexible Mode		t₁ = 0.0028 Shear Strain		t₁ = 0.0028 Acceleration		t₂ = 0.0032 Shear Strain		t₂ = 0.0032 Acceleration		t₃ = 0.004 Shear Strain		t₃ = 0.004 Acceleration
1st (i = 2)	γ_{12}	-65.00842	$\ddot{x}_{12}$	-5731.2386	γ_{12}	-74.16420	$\ddot{x}_{12}$	-2298.7115	γ_{12}	-90.38496	$\ddot{x}_{12}$	-320.69656
	γ_{22}	-52.74640			γ_{22}	-62.62416			γ_{22}	-80.59479		
	γ_{32}	-39.73866	$\ddot{x}_{32}$	-1547.8970	γ_{32}	-50.19876	$\ddot{x}_{32}$	-620.83764	γ_{32}	-69.86516	$\ddot{x}_{32}$	-86.61396
	γ_{42}	-26.16911	$\ddot{x}_{42}$	1979.4890	γ_{42}	-37.06366	$\ddot{x}_{42}$	793.94253	γ_{42}	-57.75066	$\ddot{x}_{42}$	110.76407
	γ_{52}	211.8798			γ_{52}	-23.40456			γ_{52}	-45.01968		
	γ_{62}	776.6351	$\ddot{x}_{62}$	6790.0307	γ_{62}	325.3275	$\ddot{x}_{62}$	2723.3767	γ_{62}	-31.65222	$\ddot{x}_{62}$	379.94222
2nd (i = 3)	γ_{13}	-237.7336	$\ddot{x}_{13}$	3829.2716	γ_{13}	-249.6289	$\ddot{x}_{13}$	2496.3131	γ_{13}	-242.6493	$\ddot{x}_{13}$	1291.0348
	γ_{23}	-209.2545			γ_{23}	-233.2089			γ_{23}	-251.8453		
	γ_{33}	-167.3969	$\ddot{x}_{33}$	-4998.2691	γ_{33}	-201.8790	$\ddot{x}_{33}$	-3258.3860	γ_{33}	-244.9397	$\ddot{x}_{33}$	-1685.1611
	γ_{43}	-114.8369	$\ddot{x}_{43}$	-5756.7051	γ_{43}	-157.6421	$\ddot{x}_{43}$	-3752.8125	γ_{43}	-222.3742	$\ddot{x}_{43}$	-1940.8669
	γ_{53}	175.6890			γ_{53}	-103.3266			γ_{53}	-185.5915		
	γ_{63}	772.5922	$\ddot{x}_{63}$	5251.5306	γ_{63}	297.2178	$\ddot{x}_{63}$	3423.4879	γ_{63}	-136.9431	$\ddot{x}_{63}$	1770.5479
3rd (i = 4)	γ_{14}	-333.1573	$\ddot{x}_{14}$	-678.23450	γ_{14}	-314.4325	$\ddot{x}_{14}$	-383.7759	γ_{14}	-211.4668	$\ddot{x}_{14}$	419.99511
	γ_{24}	-322.5316			γ_{24}	-334.0710			γ_{24}	-285.2581		
	γ_{34}	-275.4158	$\ddot{x}_{34}$	887.96736	γ_{34}	-315.9140	$\ddot{x}_{34}$	502.45229	γ_{34}	-326.7763	$\ddot{x}_{34}$	-549.87169
	γ_{44}	-197.1405	$\ddot{x}_{44}$	-619.16003	γ_{44}	-262.0156	$\ddot{x}_{44}$	-350.34899	γ_{44}	-331.3242	$\ddot{x}_{44}$	383.41338
	γ_{54}	140.2857			γ_{54}	-178.4737			γ_{54}	-298.3873		
	γ_{64}	768.5691	$\ddot{x}_{64}$	836.75504	γ_{64}	269.5805	$\ddot{x}_{64}$	473.4740	γ_{64}	-231.6919	$\ddot{x}_{64}$	-518.15858
4th (i = 5)	γ_{15}	-364.5087	$\ddot{x}_{15}$	-99.045287	γ_{15}	-267.0165	$\ddot{x}_{15}$	9.1807959	γ_{15}	8.465248	$\ddot{x}_{15}$	-215.61766
	γ_{25}	-424.0461			γ_{25}	-382.4045			γ_{25}	-172.0933		
	γ_{35}	-404.6132	$\ddot{x}_{35}$	-160.36809	γ_{35}	-426.5772	$\ddot{x}_{35}$	14.864985	γ_{35}	-320.6029	$\ddot{x}_{35}$	-349.11497
	γ_{45}	-309.8289	$\ddot{x}_{45}$	-536.66976	γ_{45}	-391.3081	$\ddot{x}_{45}$	49.745482	γ_{45}	-409.4063	$\ddot{x}_{45}$	-1168.3088
	γ_{55}	88.39577			γ_{55}	-283.1654			γ_{55}	-121.9658		
	γ_{65}	762.5390	$\ddot{x}_{65}$	-175.73653	γ_{65}	228.7785	$\ddot{x}_{65}$	16.289530	γ_{65}	-355.9423	$\ddot{x}_{65}$	-382.57145
5th (i = 6)	γ_{16}	-219.5771	$\ddot{x}_{16}$	-223.53334	γ_{16}	16.55304	$\ddot{x}_{16}$	-240.31514	γ_{16}	433.1431	$\ddot{x}_{16}$	-65.692784
	γ_{26}	-449.1377			γ_{26}	-273.5458			γ_{26}	194.1195		
	γ_{36}	-541.7155	$\ddot{x}_{36}$	-3168.6856	γ_{36}	-480.2158	$\ddot{x}_{36}$	-3406.5751	γ_{36}	-104.1087	$\ddot{x}_{36}$	-931.22473
	γ_{46}	-469.0752	$\ddot{x}_{46}$	1465.7887	γ_{46}	-540.4245	$\ddot{x}_{46}$	1575.8330	γ_{46}	-370.5847	$\ddot{x}_{46}$	430.77126
	γ_{56}	5.834434			γ_{56}	-435.8088			γ_{56}	-524.0359		
	γ_{66}	752.6010	$\ddot{x}_{66}$	81.915198	γ_{66}	163.1514	$\ddot{x}_{66}$	88.064994	γ_{66}	-517.6611	$\ddot{x}_{66}$	24.073534

10

$$[m] = ([\phi]^T)^{-1} [\phi]^{-1}$$

and   (21)

$$[m] = ([\phi]^T)^{-1} \lceil \omega^2 \rfloor [\phi]^{-1} .$$

Example Problem Number 2

Statement of Problem - Referring to Example No. 1 and Eq. (20), we note that if neither a forcing function measurement nor a transient response measurement is made on any node in the dynamic model, then the modal value at that node does not appear in the equation. Hence, its value can then be arbitrary. In this example problem, we shall investigate methods for overcoming this deficiency.

When a dynamicist first formulates a mathematical model, the choice of nodes is perfectly arbitrary and is subject solely to his judgment. To a lesser degree, the assignment of the masses at the nodes is also arbitrary. For most dynamic analyses, knowing the correct frequencies and mode shapes should be sufficient to describe the system analytically. In this example we shall assume that the correct mass matrix is formulated; hence, the mass matrix is not going to be changed in the improvement of the model.

The same transient loading as that in the previous example is used except that the traveling pulse hits the first two particles only. The acceleration measurements are made on particles 1, 3, and 6. No experimental data are available for particles 4 and 5. This may correspond to the case in which there are internal components 3, 4, 5 and 6, and 1 and 2 represent the external structure of a vehicle subjected to a blast loading. Compared with the 6 force measurements and 4 acceleration measurements of example 1, this example presents a more restrictive requirement.

It is noted here that the orthogonality properties of the modal matrix normalized with respect to the mass matrix might be used as a supplemental restraint in addition to the comparison of analytical results with experimental data. The following equation is chosen for minimization in the Monte Carlo method:

$$\psi_2(\phi_{12}, \phi_{22}, \ldots, \phi_{n2})$$

$$= \sum_{t=1}^{p} \left[\sum_{j=1}^{m} \left(\ddot{x}_{j2} - \phi_{j2} \sum_{k=1}^{q} \phi_{k2} \gamma_{k2} \right)^2 \right]_t$$

$$+ c_1 \left[\sum_{\ell=1}^{n} w_{\ell\ell} \phi_{\ell 2}^2 - 386.08401 \right]^2 = minimum, \quad (22)$$

for $i \neq 2$, the first flexible mode,

$$\psi_i(\phi_{1i}, \ldots, \phi_{ni}) = \sum_{t=1}^{p} \left[\sum_{j=1}^{m} \left(\ddot{x}_{ji} - \phi_{ji} \sum_{k=1}^{q} \phi_{ki} \gamma_{ki} \right)^2 \right]_t$$

$$+ c_1 \left[\sum_{\ell=1}^{n} w_{\ell\ell} \phi_{\ell i}^2 - 386.08401 \right]^2$$

$$+ c_2 \left[\sum_{\ell=1}^{n} w_{\ell\ell} \phi_{\ell i} \phi_{\ell 2} \right]^2 = minimum, \quad (23)$$

where

    $k = 1, 2, \ldots q$, number of forces measured;

    $w_{\ell\ell}$ = diagonal element of weight matrix ("correct" set);

    $j = 1, 2, \ldots, m$, number of accelerations measured;

    c_1, c_2 = weighting constants; and

    $t = 1, 2, \ldots, p$, number of instants of observation.

Table 2 constitutes the input data to the "Creeping Random Computer Program" for the improvement of the first three flexible modes. For initial trial values of the ϕ's, the calculated values mentioned previously are used. Values of 1.0 are taken for the constants c_1 and c_2, giving equal weights to the experimental data and conditions of orthogonality.

Example Problem Results - Results from the computer program are given in Table 3. The true values of ϕ's are repeated for comparison in the same table.

Discussion of Example Problem No. 2 Results - The results show that improvement of the modal values, at nodes where there are no experimental data, can be obtained by the use of the orthogonality properties of modes.

The orthogonality property introduces one additional equation (in the case of $\{\phi\}_2$) to equations containing experimental data when there are n unknown ϕ's to be found. The value of n can be much larger than m. The question remains whether the orthogonality equation can improve all the ϕ's in a somewhat uniform manner.

To investigate this question, a value of 10^6 is taken for c_1 in Eq. (22), thus magnifying the

11

TABLE 2
Creeping Random Computer Program Input Data

Flexible Mode	t₁ = 0.0028		t₂ = 0.0032		t₃ = 0.004	
	Shear Strain	Acceleration	Shear Strain	Acceleration	Shear Strain	Acceleration
1st (i = 2)	γ_{12} -65.00842 γ_{22} -52.74640	$\ddot{x}_{12}$ -477.84119 $\ddot{x}_{32}$ -129.05569 $\ddot{x}_{62}$ 566.11783	γ_{12} -74.16420 γ_{22} -62.62416	$\ddot{x}_{12}$ -552.93978 $\ddot{x}_{32}$ -149.33837 $\ddot{x}_{62}$ 655.09017	γ_{12} -90.38496 γ_{22} -80.59479	$\ddot{x}_{12}$ -687.48634 $\ddot{x}_{32}$ -185.67680 $\ddot{x}_{62}$ 814.49294
2nd (i = 3)	γ_{13} -237.7336 γ_{23} -209.2545	$\ddot{x}_{13}$ -402.66076 $\ddot{x}_{33}$ 525.58478 $\ddot{x}_{63}$ -552.21607	γ_{13} -249.6289 γ_{23} -233.2089	$\ddot{x}_{13}$ -401.89947 $\ddot{x}_{33}$ 524.59108 $\ddot{x}_{63}$ -551.17202	γ_{13} -242 6493 γ_{23} -251.8453	$\ddot{x}_{13}$ -351.65368 $\ddot{x}_{33}$ 459.00629 $\ddot{x}_{63}$ -482.26407
3rd (i = 4)	γ_{14} -333.1573 γ_{24} -322.5316	$\ddot{x}_{14}$ 415.55418 $\ddot{x}_{34}$ -544.05747 $\ddot{x}_{64}$ -512.67969	γ_{14} -314.4325 γ_{24} -334.0710	$\ddot{x}_{14}$ 491.64481 $\ddot{x}_{34}$ -643.67788 $\ddot{x}_{64}$ -606.55462	γ_{14} -211.4668 γ_{24} -285.2581	$\ddot{x}_{14}$ 533.72985 $\ddot{x}_{34}$ -698.77702 $\ddot{x}_{64}$ -658.47600

TABLE 3
Comparison of Computed and True ϕ's for Example 2

ϕ_2 [a]		ϕ_3 [b]		ϕ_4 [c]	
Computed	True	Computed	True	Computed	True
2.1823435	2.1832192	1.7488908	1.7488900	1.4134613	1.4134544
1.4613510	1.4587241	-0.88663371	-0.88663372	-2.3715563	-2.3715559
0.58940554	0.58964540	-2.2827910	-2.2827900	-1.8505515	-1.8505419
-0.76825231	-0.75405312	-2.6339910	-2.6291799	1.3490425	1.2903420
-1.8548189	-1.8584049	-0.65287925	-0.66770054	2.1903482	2.2175386
-2.5855092	-2.5865483	2.3984598	2.3984586	-1.7438244	-1.7438144

[a] 294,002 trials.
[b] 170,002 trials.
[c] 106,001 trials.

effects of orthogonality in comparison to those of the experimental data.

Table 4 shows the results of computed $\{\phi\}_2$ compared with the starting values and the true values. A general improvement of $\{\phi\}_2$ is noted.

MIXED RESPONSE DATA FROM STRAIN GAGES AND ACCELEROMETERS—AN EXTENSION OF THE METHOD

In the preceding examples it was implied that only acceleration measurements were made. In practice, however, both acceleration

TABLE 4
Effects of Orthogonality Equation (C₁ = 10⁶)

Calculated $\{\phi\}_2$ [a]	Computed $\{\phi\}_2$ [b]	True $\{\phi\}_2$
2.2822298	2.1391473	2.1832192
1.6491218	1.5925472	1.4587241
0.69281230	0.57770646	0.58964540
-0.81259693	-0.81575419	-0.75405312
-1.8292985	-1.8758526	-1.8584049
-2.4938566	-2.5343082	-2.5865483

[a] Starting values.
[b] From random program.

and strain measurements are used. In formulating the dynamic model, we postulate that the dynamicist uses a finite element approach of some kind where masses are concentrated at a network of stations called nodes. The displacement and acceleration responses are also measured at the nodes. If the strains of the structure between the nodes are measured by strain gages, these measurements can be related to the relative displacements of the two nodes. The exact nature of this relationship would have been determined by the dynamicist in his original stress analysis.

Before proceeding with the development of the method for handling strain data, we will digress briefly to derive some strain-displacement relationships that will be needed in the subsequent derivation.

Let the transformation matrix $[T]$ relate the strains $\{\epsilon\}$ and the displacements $\{x\}$ of the system. The matrix $[T]$ is called the "strain transformation" matrix. This relationship may be expressed as follows:

$$\{\epsilon\} = [T]\{x\} . \qquad (24)$$

As an illustration of the form of $[T]$, two examples are shown. Example 1 is the case of an axially loaded bar of varying cross section (Fig. 3). For this case, Eq. (24) takes the form:

$$\left\{\begin{array}{c} \epsilon_a \\ \\ \epsilon_b \end{array}\right\} = \left[\begin{array}{c|c|c} 1/\ell_a & 1/\ell_a & 0 \\ \hline 0 & -1/\ell_b & 1/\ell_b \end{array}\right] \left\{\begin{array}{c} x_1 \\ x_2 \\ x_3 \end{array}\right\} . \qquad (25)$$
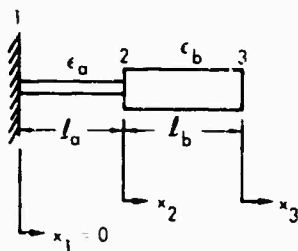
Fig. 3. Example 1, longitudinal bar of varying cross section

The second example (Fig. 4) is slightly more complex and considers the case of a triangular membrane element subjected to in-plane forces. The strain-displacement relationship is expressed by Eq. (26):

Fig. 4. Example 2, triangular membrane element
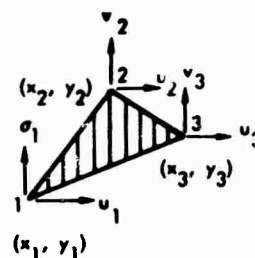
$$\left\{\begin{array}{c} \epsilon_x \\ \\ \epsilon_y \\ \\ \gamma_{xy} \end{array}\right\} = \frac{1}{2A} \left[\begin{array}{cccccc} y_{23} & 0 & y_{31} & 0 & y_{12} & 0 \\ 0 & x_{23} & 0 & x_{31} & 0 & x_{12} \\ x_{32} & y_{23} & x_{13} & y_{31} & x_{21} & y_{12} \end{array}\right] \left\{\begin{array}{c} u_1 \\ v_1 \\ u_2 \\ v_2 \\ u_3 \\ v_3 \end{array}\right\} , \qquad (26)$$

where

$\epsilon_x, \epsilon_y, \gamma_{xy}$ = strains in x- and y-directions and shear strain, respectively, considered to be uniform in small triangular element;

A = area of triangle;

$y_{23} = y_2 - y_3$, etc., where x and y are coordinates from reference point; and

u, v = displacements in the x- and y-directions, respectively.

Now, proceeding in a manner analogous to the treatment of acceleration data, we have from Eq. (11), the filtered signal for the displacement,

$$\{x(t)\}_i = \{\phi\}_i \{\phi\}_i^T \{\beta(t)\}_i , \qquad (27)$$

where $\{\beta(t)\}_i$ are the terms included in the braces in Eq. (11).

Substituting Eq. (24) into Eq. (27) gives

$$\{\epsilon\}_i = [T]\{\phi\}_i \{\phi\}_i^T \{\beta\}_i , \qquad (28)$$

which, when written out in expanded form, becomes

13

$$\begin{Bmatrix} \epsilon_{1i} \\ \epsilon_{2i} \\ \cdot \\ \cdot \\ \cdot \\ \epsilon_{\ell i} \\ \cdot \\ \cdot \\ \cdot \\ \epsilon_r \end{Bmatrix} = \begin{bmatrix} T_{11} & T_{12} & \cdots & T_{1n} \\ & & & \\ & & & \\ \cdots & \cdots & \cdots & \cdots \\ T_{\ell 1} & T_{\ell 2} & \cdots & T_{\ell n} \\ & & & \\ \cdots & \cdots & \cdots & \cdots \\ T_{r1} & T_{r2} & \cdots & T_{rn} \end{bmatrix}$$

$$\begin{Bmatrix} \phi_{1i} \\ \phi_{2i} \\ \cdot \\ \cdot \\ \cdot \\ \cdot \\ \cdot \\ \cdot \\ \phi_{ni} \end{Bmatrix} [\phi_{1i} \phi_{2i} \cdots \phi_{ni}] \begin{Bmatrix} \beta_{1i} \\ \beta_{2i} \\ \cdot \\ \cdot \\ \cdot \\ \cdot \\ \cdot \\ \cdot \\ \beta_{ni} \end{Bmatrix} . \tag{29}$$

where ϵ_{1i} is the strain measurement filtered to the ith mode between nodes ℓ and $\ell + 1$, and there are r strain measurements.

It follows that ϵ_ℓ is given by

$$\epsilon_{\ell i} = \left(\sum_{p=1}^{n} T_{\ell p} \, \phi_{pi} \right) \left(\sum_{k=1}^{n} \phi_{ki} \, \beta_{ki} \right) . \tag{30}$$

Hence, the ψ_i function to be minimized for mixed measurements of strain and acceleration responses will be given by

$$\psi_i(\phi_{1i}, \phi_{2i}, \ldots, \phi_{ni})$$

$$= \sum_t \left[\sum_{j=1}^{m} \left(\ddot{x}_{ji} - \phi_{ji} \sum_{k=1}^{n} \phi_{ji} \, \gamma_{ji} \right)^2 + \alpha \sum_{\ell=1}^{r} \right.$$

$$\left. \times \left\{ \epsilon_{\ell i} - \left(\sum_{p=1}^{n} T_{\ell p} \, \phi_{pi} \right) \left(\sum_{k=1}^{n} \phi_{ki} \, \beta_{ki} \right) \right\}^2 \right]_t . \tag{31}$$

where there are m acceleration and r strain measurements, $m + r \leq n$ and α = scale factor, which is introduced because the strains, numerically, are so much smaller than the accelerations.

Similarly, one can gather together the experimental data of more than one transient response experiment to form the ψ_i function to be minimized. The subsequent dynamic model obtained from a single computing operation will best fit all the experimental data so treated.

CONCLUSIONS

This report demonstrates that it is feasible to improve an analytically derived linear structural-dynamic model based on transient response experiments. Although the data used in this report were "manufactured" from analyses and were not actual measured data, the basic concept has been demonstrated.

In the examples presented, attempts were made to represent typical transient response experiments, albeit on a smaller scale; i.e., only a six-degree-of-freedom model was used although it is recognized that most practical problems in the aerospace industry require many more degrees of freedom for adequate simulation. In addition, the essence of the transient response experiments was maintained, especially in the second example, where the forcing function was assumed to be applied at only the first two particles and acceleration measurements were made on particles 1, 3, and 6. This example typifies the experiment in which the external structure, represented by particles 1 and 2, is subjected to a load, and response measurements are made on the external structure and on some, but not all, of the internal components. (No measurements were made on particles 4 and 5.)

The basic logic of the method has been established, even though feasibility was demonstrated only on a six-degree-of-freedom system with input data (loading and response) known exactly. A study of the effect of errors in data should form a next step in the evolution of the method.

FUTURE EFFORT

Although this report, in its present form, can be utilized for assessing the validity of a structural dynamic analysis based on experimental results, certain questions have arisen during the course of this study that require additional effort to find the answers. In an effort to demonstrate the principles of the method involved, relatively simple examples were chosen in the report. To obtain a better simulation of the physical system, more complex analytical dynamic models involving more than six degrees of freedom are often generated. It is planned to demonstrate that the methods of this report are feasible and economical (in terms of

14

computer time) in handling systems represented by many degrees of freedom.

In the simple examples given, it was assumed that four, and then three, accelerometer measurements were made during the tests. An investigation is planned in which it is hoped that general criteria for the number and location of transducers required for successful application of this method can be achieved. These criteria will then serve as a guide for future planning of experiments.

Measurement inaccuracies due to transducers and associated circuitry always arise due to factors such as manufacturing tolerances or noise in the system. It is planned to employ statistical concepts in the representation of the loading and response measurements obtained from experiments. This study should result in a "best fit" solution to the dynamic model based on test data. In addition, it is hoped to formulate a criterion for measurement accuracy to yield adequate results for revision of the analytical model.

REFERENCES

1. T. K. Caughey, "Classical Normal Modes in Damped Linear Systems," J. Appl. Mech., Vol. 27, Trans. ASME, pp. 269-271, '960

2. S. H. Brooks, "A Discussion of Random Methods for Seeking Maxima," Operations Res., Vol. 6, No. 2, March-April 1958

*   *   *

DIGITAL ANALYSIS OF FATIGUE DAMAGE TO A MULTI-MODAL SYSTEM SUBJECTED TO LOGARITHMICALLY SWEPT SINUSOIDAL VIBRATION SPECTRA

Seymour Fogelson
The Marquardt Corporation
Van Nuys, California

To qualify a component for use in missiles of space vehicles, it is normally required that its fatigue strength be demonstrated by test. Such a test generally requires that the component be subjected to a random vibration input for a specified time and to a sinusoidal vibration spectrum that is swept linearly or logarithmically at a given rate. One of the functions of the stress analyst is thus to verify that the component has a fatigue life sufficient to pass these tests without failure. The purpose of this paper is to present the analyst with a digital computer program that will predict the fatigue damage done to a structure with up to six degrees of freedom that is subject to logarithmically swept sinusoidal vibration spectra.

A method for calculating the fatigue damage of structures subjected to sinusoidal vibration spectra that are swept logarithmically at a given rate was developed and programmed for analysis by digital computer. It is assumed that the structure is a damped spring-mass system with each mass having three translational and three rotational degrees of freedom. Only lumped mass structures are considered. It is further assumed that the resonant amplification factors and the overall damping ratio of the structure are known.

Based on this analysis, the resulting digital computer program yields the damage accumulated in each mode of response for each axis of applied excitation, the total damage accruing for each input axis, and the total damage caused by sweeping the spectrum a given number of times.

J. Fogelson

INTRODUCTION

When a damped resonator is subjected to a sinusoidal excitation of a given amplitude and frequency, its response peak acceleration and frequency is constant with time. The stresses induced in the structure, which are functions of the response accelerations, and the number of times these stresses are repeated are therefore readily determined.

The "allowable" number of times this induced stress may be repeated is obtained from the S-N curve of the material and the resulting damage to the structure is directly obtained.

When a number of sinusoids differing in both amplitude and frequency are applied to the structure in sequence, the resulting damage is the sum of the damage caused by each resulting stress level, i.e.,

$$D = \sum_i \frac{n_i}{N_i} \qquad (1)$$

according to the Palmgren-Miner hypothesis of cumulative damage.

It is often required to determine the damage done to a structure when a frequency range is swept at a given rate. Within this range the magnitude of the applied excitation may remain constant for all frequencies or only over specified frequency ranges, as shown in Fig. 1. When this range of frequencies is swept, the response accelerations and, therefore, stresses are now time dependent and Eq. (1) is no longer applicable. In short-lived structures, such as missiles and space vehicles, the rate of sweep is adjusted to provide equal time increments for each frequency band [1, p. 24-22]. In this type of sweep the frequency varies logarithmically with time as shown in Fig. 2.
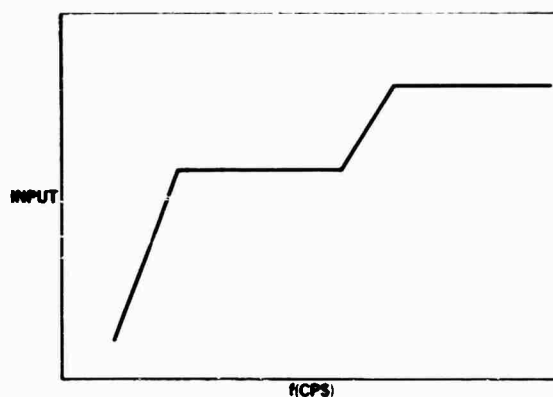
Fig. 1. Input spectrum

The response of a damped resonator subjected to a logarithmic swept sinusoidal spectrum was investigated by Grumman Aircraft Engineering Corp. [2]. This investigation resulted in an equation for predicting the number of times a specific amplification factor and, therefore, stress is exceeded when a spectrum

such as that shown in Fig. 1 is logarithmically swept at a given rate. This paper describes the utilization of that equation, and the resulting digital computer program, for predicting the fatigue damage in a lumped mass system having six degrees of freedom.

LIST OF SYMBOLS

b Slope of material S-N curve

D Damage

Δn Number of applied cycles occurring between two specified stress levels

f Frequency of applied acceleration (cps)

f_n Natural frequency, simple resonator (cps)

f_r Natural frequency in mode r, multimodal system (cps)

F.T Force, torque (lb, in.-lb)

γ Damping ratio

H Linear or generalized magnification factor

I Weight moment of inertia (psi)

K Percentage of maximum magnification factor

m Mass

M Generalized weight (lb)

$\ddot{u}$ Response acceleration (in./sec^2)

n Number of applied cycles
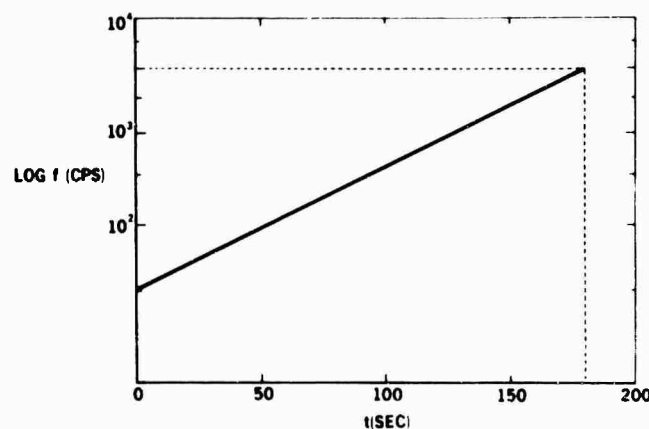
Fig. 2. Frequency-time relationship for logarithmic sweep

18

N   Number of allowable cycles from material S-N curve

Q   Generalized force (lb, in.-lb), "quality" factor = $1/2\gamma$, single-degree-of-freedom system

R   Applied load factor (g)

S   Stress (psi)

SR   Sweep rate (octaves/min)

T   Sweep period (sec/octave)

W   Weight (lb)

$\ddot{x}$ Applied acceleration (in./sec^2)

β Torsional mode magnification factor

Subscripts

i   General index, response coordinate

j   Input coordinate

k   General index

L   Subincremental index

r   Mode

Matrix Notation

$[A]^T$ Transpose of matrix A

$\lceil\ \rfloor$ Diagonal matrix

FAILURE CRITERIA

A typical material S-N curve is shown in Fig. 3. If a stress of intensity S_i is cyclically applied n_i times, the resulting damage is

$$D_i = \frac{n_i}{N_i} . \tag{2}$$

and the fatigue margin of safety may be expressed as

$$M.S. = \frac{1}{D} - 1 . \tag{3}$$

If the peak stress intensities vary during the life of the structure, the damage, according to the Miner hypothesis, is cumulative and is expressed as
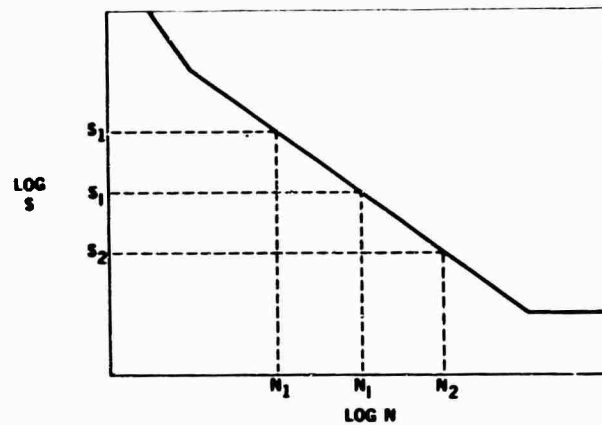
Fig. 3. Typical material S-N curve

$$D = \sum_{i=1}^{m} \frac{n_i}{N_i} . \tag{4}$$

where m is the total number of different stress intensities applied to the structure. In a piecewise fashion the S-N curve shown in Fig. 3 may be expressed as

$$N_i = N_1 (S_i/S_1)^{-b} . \tag{5}$$

where

$$-b = \frac{\log (N_2/N_1)}{\log (S_2/S_1)} . \tag{6}$$

By substituting Eq. (5) into Eq. (4), the damage is expressed as

$$D = \sum_{i=1}^{m} \frac{n_i}{N_1} \left(\frac{S_i}{S_1}\right)^b . \tag{7}$$

Equation (7) demonstrates that, for a given material, the damage depends on the magnitude of the applied stress S_i and the number of times n_i that it is applied. According to test data [1, p. 24-12], failure of a multiple-loaded material occurs when

$$D \geq 1/2 . \tag{8}$$
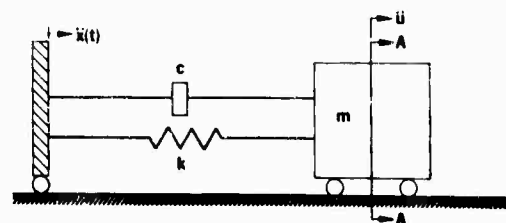
Fig. 4. Stress-time history

19

For clarity, the calculation processes for determining S_i and n_i will be illustrated for a single-degree-of-freedom system.

SINGLE-DEGREE-OF-FREEDOM SYSTEM

Determination of Stress

A resonator, such as shown in Fig. 4, responds to an excitation with the acceleration of

$$\ddot{u}_i = H_i \ddot{x} , \qquad (9)$$

where H, the magnification factor, is given by

$$H_i = \left\{ \left[1 - (f_i/f_n)^2 \right]^2 + 4\gamma^2 (f_i/f_n)^2 \right\}^{1/2} . \qquad (10)$$

$$\ddot{x}(t) = \ddot{x}_o \sin \omega t . \qquad (11)$$

and $\ddot{u}_i$ = response acceleration. When

$$f_i = f_n . \qquad (12)$$

Eq. (10) reduces to

$$H_i = \frac{1}{2\gamma} = Q .$$

When $f_i \neq f_n$, the magnification factor can be expressed as

$$H_i = K_i Q , \qquad (13)$$

where K_i is some fraction less than unity. The stress on section A-A (Fig. 4) of the mass is given by

$$S_i = \frac{m_{A-A} \ddot{u}_i}{A_{A-A}} . \qquad (14)$$

where

m_{A-A} is the mass to the right of section A-A, and

A_{A-A} is the cross-sectional area at A-A.

Substitution of Eqs. (9) and (13) into Eq. (14), setting $m_{A-A} = W_{A-A}/g$, yields

$$S_i = \frac{W_{A-A}}{A_{A-A}} K_i Q \frac{\ddot{x}}{g} \qquad (15)$$

or

$$S_i = S_s K_i QN , \qquad (16)$$

where S_s is the stress due to a 1-g loading and N is the applied load factor. If

$$S_{max} = S_s QN . \qquad (17)$$

the stress at any nonresonant condition can be expressed as

$$S_i = K_i S_{max} . \qquad (18)$$

Determination of Applied Cycles

The number of times the stress S_i (Eq. (18)) is equaled or exceeded was found by Grumman [1, p. 24-22] to be

$$n_i = 2.041 T f_n \sqrt{1 - \sqrt{(1 + \gamma^2) \left[1 - (1/K_i Q)^2 \right]}} . \qquad (19)$$

in which T is the sweep period in seconds per octave.

Since n_i counts all of the peak stresses greater than S_i, it also includes the number of times the stress S_k is exceeded (where $S_k > S_i$), as illustrated in Fig. 5.
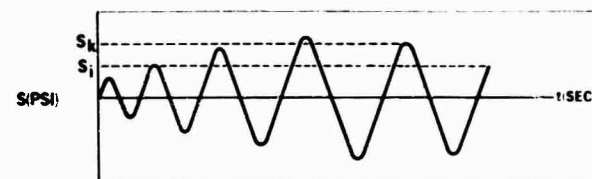
Fig. 5. Simple resonator

To preclude counting S_k and all higher values of S more than once, the increment between n_i and n_k is used and the number of times the peak stress level is between S_i and S_k is counted. Thus, the quantity

$$\Delta n_i = n_i - n_k \qquad (20)$$

is used in Eq. (7) in lieu of n_i. The stress magnitude now used in Eq. (7) is the average of S_i and S_k, i.e.,

$$\bar{S}_i = \frac{1}{2} (S_i + S_k) . \qquad (21)$$

If $K_k - K_i$ is small enough, the resulting error will also be small. Since the greatest damage is done at the higher stress levels, this difference should be initially small, e.g., 2.5 percent, increased to 10 percent for $K = 0.6$.
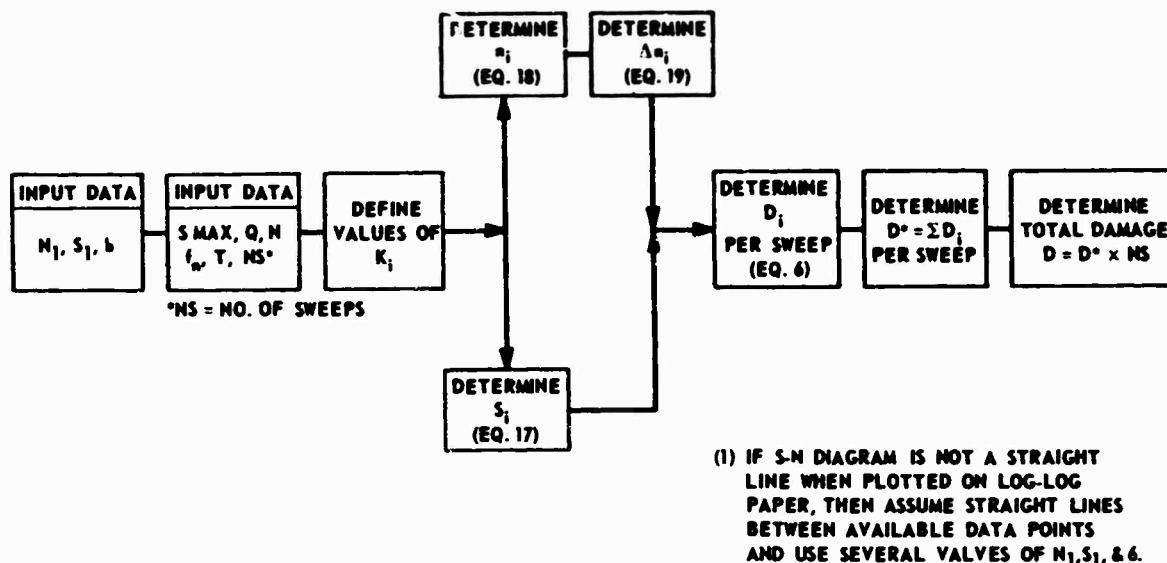
Fig. 6. Flow diagram for single-degree-of-freedom system

The procedure to be used to determine the damage factor D for a single-degree-of-freedom system is outlined in Fig. 6, and will now be adapted to a multi-modal system.

MULTI-MODAL SYSTEM

Discussion

This analysis is limited to a lumped mass system, supported on lightly damped springs, with each mass having three translational and three rotational modes of vibration. This system may be typified by equipment supported at various points on a space framework with structural damping. A sinusoidal excitation, such as shown in Fig. 1, is logarithmically swept and applied to the system along each of the three orthogonal system axes in succession. This input excites all six modal responses as the frequency range of the spectrum is swept, as shown in Fig. 7.

As in the simple resonator, the procedure to be followed is (a) determine the applied stress intensity; (b) determine the number of times each stress intensity is applied; (c) determine, from the S-N curve, the number of times each stress intensity may be applied; and (d) compute the damage.

In a weakly coupled system, the damage from each mode must be computed separately and then summed. Each of the procedures outlined above will now be discussed in detail.
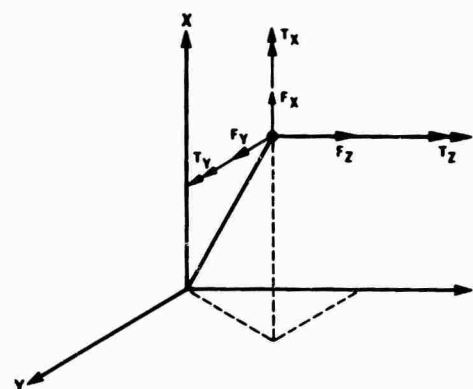
Fig. 7. Response inertia forces and moments

Determination of Stress Intensities

Each inertia load shown in Fig. 7 is derived from the mass properties at its centroid, the corresponding amplification factor, and the applied excitation. These loads are expressed as

$$
\left.
\begin{aligned}
F_{rij} &= W H_{rij} R_r \\
\\
\text{and} \qquad\qquad\qquad& \\
\\
T_{rij} &= I_i \theta_{rij} R_r
\end{aligned}
\right\} \qquad (22)
$$

Let each load be indexed as

21

$$\begin{Bmatrix} F_{rxj} \\ F_{ryj} \\ F_{rzj} \\ T_{rxj} \\ T_{ryj} \\ T_{rzj} \end{Bmatrix} = \begin{Bmatrix} Q_{r1j} \\ Q_{r2j} \\ Q_{r3j} \\ Q_{r4j} \\ Q_{r5j} \\ Q_{r6j} \end{Bmatrix} = Q_{rij}$$

where

    r is the mode,

    i is the response coordinate, and

    j is the input coordinate ($j = 1$ on x-axis, $j = 2$ on y-axis, and $j = 3$ on z-axis).

Similarly, let

$$\begin{bmatrix} W \\ & W \\ & & W \\ & & & I_X \\ & & & & I_Y \\ & & & & & I_Z \end{bmatrix} = \begin{bmatrix} M_1 \\ & M_2 \\ & & M_3 \\ & & & M_4 \\ & & & & M_5 \\ & & & & & M_6 \end{bmatrix} = \begin{bmatrix} M_i \end{bmatrix}$$

$$\begin{bmatrix} H_{1xj} & H_{1yj} & H_{1zj} & \theta_{1xj} & \theta_{1yj} & \theta_{1zj} \\ H_{2xj} & H_{2yj} & H_{2zj} & \theta_{2xj} & \theta_{2yj} & \theta_{2zj} \\ H_{3xj} & H_{3yj} & H_{3zj} & \theta_{3xj} & \theta_{3yj} & \theta_{3zj} \\ H_{4xj} & H_{4yj} & H_{4zj} & \theta_{4xj} & \theta_{4yj} & \theta_{4zj} \\ H_{5xj} & H_{5yj} & H_{5zj} & \theta_{5xj} & \theta_{5yj} & \theta_{5zj} \\ H_{6xj} & H_{6yj} & H_{6zj} & \theta_{6xj} & \theta_{6yj} & \theta_{6zj} \end{bmatrix}$$

$$\begin{bmatrix} H_{11j} & H_{12j} & \cdot & \cdot & \cdot & H_{16j} \\ H_{21j} & & \cdot & \cdot & \cdot & H_{26j} \\ \cdot & \cdot & \cdot & \cdot & \cdot & \cdot \\ \cdot & \cdot & \cdot & \cdot & \cdot & \cdot \\ \cdot & \cdot & \cdot & \cdot & \cdot & \cdot \\ H_{61j} & & \cdot & \cdot & \cdot & H_{66j} \end{bmatrix} = [H_{rij}]$$

and

$$\begin{bmatrix} R_1 \\ & R_2 \\ & & R_3 \\ & & & R_4 \\ & & & & R_5 \\ & & & & & R_6 \end{bmatrix} = [R_r]$$

Let the full force matrix be

$$\{Q_{rij}\} = \left[\{Q_{1ij}\} \{Q_{2ij}\} \ldots \{Q_{6ij}\} \right]^T$$

which, from Eq. (22) and the matrices defined above is

$$\begin{bmatrix} Q_{rij} \end{bmatrix} = \begin{bmatrix} R_r \end{bmatrix} \begin{bmatrix} H_{rij} \end{bmatrix} \begin{bmatrix} M_i \end{bmatrix} \quad (23)$$

At any point in the structure, the stress induced by one of the Q_{rij} forces is

$$S_{rij} = Q_{rij} A_i \quad (24)$$

where A_i is the coefficient relating S_{rij} to Q_{rij} as found by stress analysis. If Eq. (24) is written as a matrix, with the columns corresponding to the response axes and the rows corresponding to the modes,

$$\begin{bmatrix} S_{rij} \end{bmatrix}^T = \begin{bmatrix} Q_{rij} \end{bmatrix} \begin{bmatrix} A_i \end{bmatrix} \quad (25)$$

and using Eq. (23), these stresses may be expressed as

$$\begin{bmatrix} S_{rij} \end{bmatrix} = \begin{bmatrix} R_r \end{bmatrix} \begin{bmatrix} H_{rij} \end{bmatrix} \begin{bmatrix} M_i \end{bmatrix} \begin{bmatrix} A_i \end{bmatrix} \quad (26)$$

where

$$S_{rij} = \left[\{S_{1ij}\} \{S_{2ij}\} \ldots \{S_{6ij}\} \right]^T$$

and

$$\{S_{rij}\} = \begin{Bmatrix} S_{r1j} \\ S_{r2j} \\ \cdot \\ \cdot \\ \cdot \\ S_{r6j} \end{Bmatrix}$$

For the nonresonant frequencies, as in Eq. (18), Eq. (26) becomes

22

$$\left[S_{krij}\right] = K_k \left[R_r\right]\left[H_{rij}\right]\left[M_i\right]\left[A_i\right] . \quad (27)$$

Determination of Applied Cycles

It is shown by Eq. (19) that, for a simple resonator, the number of times a stress of intensity S_k is exceeded is a function of the corresponding magnification factor $K_k Q$. In a multi-degree-of-freedom system, however, the maximum magnification factor is H, which is different from $Q = 1/2\gamma$. Equation (19) is, therefore, expressed as

$$n_{krij} = \frac{122.46}{SR} f_r \sqrt{1 - \sqrt{\left[1 + \gamma^2\right]\left[1 - (1/K_k H_{rij})^2\right]}} , \quad (28)$$

where

f_r = rth modal frequency, and

SR = sweep rate (octaves/min) = $60/T$.

Equation (28) indicates that for a given mode and sweep rate, the stress components S_{krij} will each be exceeded a different number of times, depending on the magnitudes of the corresponding magnification factor $(K_k H_{rij})$.

Consider a two-degree-of-freedom system with response directions q_1 and q_2 and the corresponding resonant amplification factors in mode 1, H_{11} and H_{12}, for an input in direction 1, and assume that $H_{11} > H_{12}$. Equation (28) indicates that as $(K_k H_{ri})$ diminishes, the number of times the stress corresponding to $(K_k H_{ri})$ is exceeded increases. Thus

$$n_{k11} < n_{k12} .$$

The number of times the peak stresses fall in the intervals

$$S_{k11} < S_{11} < S_{(k+\Delta k)11}$$

and

$$S_{k12} < S_{12} < S_{(k+\Delta k)12}$$

is given by

$$\Delta n_{k11} = n_{k11} - n_{(k+\Delta k)11}$$

and

$$\Delta n_{k12} = n_{k12} - n_{(k+\Delta k)12} .$$

Since

$$n_{k11} < n_{k12}$$

and

$$n_{(k+\Delta k)11} < n_{(k+\Delta k)12} , \quad (29)$$

$$\Delta n_{k11} < \Delta n_k . .$$

Since Eq. (29) must hold for all values of k, it is inferred that, on a time basis, the stress S_{k12} is applied to the structure before the stress S_{k11}. This means that the stress S_{k12} is applied to the structure a number of times equal to

$$\Delta\Delta n_{k11} = \Delta n_{k12} - \Delta n_{k11} \quad (30)$$

more than S_{k11}. Also, since S_{k11} and S_{k12} are applied symmetrically about a central frequency, $\Delta n_{k12}/2$ and $\Delta n_{k11}/2$ must occur simultaneously. The total stress

$$S_k = S_{k11} + S_{k12} ,$$

is thus applied to the structure a number of times equal to

$$\Delta\Delta n_{k12} = \Delta n_{k11} . \quad (31)$$

This reasoning has been extended to cover the six-degree-of-freedom problem under consideration.

This concept is best illustrated in Fig. 8 where the Δn_i and S_i values are chosen arbitrarily. In this figure, $\Delta n_i/2$ is plotted against S_i to emphasize the temporal relationship between the various response directions.

It is seen from Fig. 8 that the initial stress intensity applied to the structure is $S_{(1)} = S_1 = 5$ ksi, which is applied $(2)(300 - 200)(10^3) = 200 \times 10^3$ times. Since the total stress applied to the structure is the sum of the component stresses, the stress $S_{(2)} = S_1 + S_4 = 5 + 10 = 15$ ksi is applied to the structure $(2)(200 - 150)(10^3) = 100 \times 10^3$ times before S_3 is applied. The summation of stress versus cycles continues until the maximum stress is reached. This method is illustrated in Table 1 which lists the total number of applied cycles for each $S_{(L)}$ value.

The stresses, $S_{(L)}$, as found in Table 1, are then used in Eq. (5) to determine the corresponding allowable number of cycles, N_i.

Allowable Cycles and Total Damage

In any interval of stress, where

$$S_k \leq S < S_{k+\Delta k} ,$$

it is assumed that S_k may be used as the reference stress to determine the allowable number

23
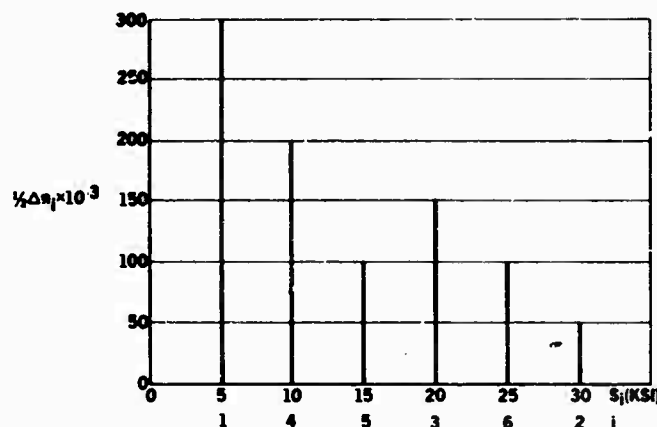
Fig. 8. Example relationship
between Δn_i and S_i

TABLE 1
Total Stress vs Number of Applied Cycles[a]

Increment, L	No. of Applied Cycles, $\Delta n_{(L)}$	Total Stress, $S_{(L)}$ (ksi)
1	$(2)(300-200)(10^3) = 200 \times 10^3$	5
2	$(2)(200-150)(10^3) = 100 \times 10^3$	$10+5 = 15$
3	$(2)(150-100)(10^3) = 100 \times 10^3$	$20+15 = 35$
4	$(2)(100-50)(10^3) = 100 \times 10^3$	$15+25+35 = 75$
5	$(2)(50)(10^3) = 100 \times 10^3$	$30+75 = 105$

[a]See Fig. 7.

of cycles, as given in Eq. (5). By using the subscripts k, r, and j as before, and introducing the subscript L to denote the subincrements as illustrated in Table 1, Eq. (5) is written as

$$\frac{1}{N_{krLj}} = \frac{1}{N_1}\left(\frac{S_{krLj}}{S_1}\right)^b . \tag{32}$$

The total damage per spectrum per sweep is then, from Eq. (7),

$$D = \sum_{j=1}^{3}\sum_{r=1}^{6}\sum_{k=1}^{m+1}\sum_{L=1}^{n}\frac{\Delta n_{krLj}}{N_1}\left(\frac{S_{krLj}}{S_1}\right)^b , \tag{33}$$

where

m is the number of nonresonant stress intensities,

n is the number of subincrements resulting when the component stresses are summed, and

b is the slope of S-N curve (see Eq. (6)).

PROGRAMMING

The calculations indicated in this analysis were programmed, in Fortran IV, for the IBM 7040 digital computer. A flow chart of the program is shown in Fig. 9. A listing of the main program, with the subroutines SORT and SUM, is given in Appendix A. A sample problem based on the LEM Propulsion System/Thrust Chamber Assembly (PS/TCA) analysis [3] is given in Appendix B.

24
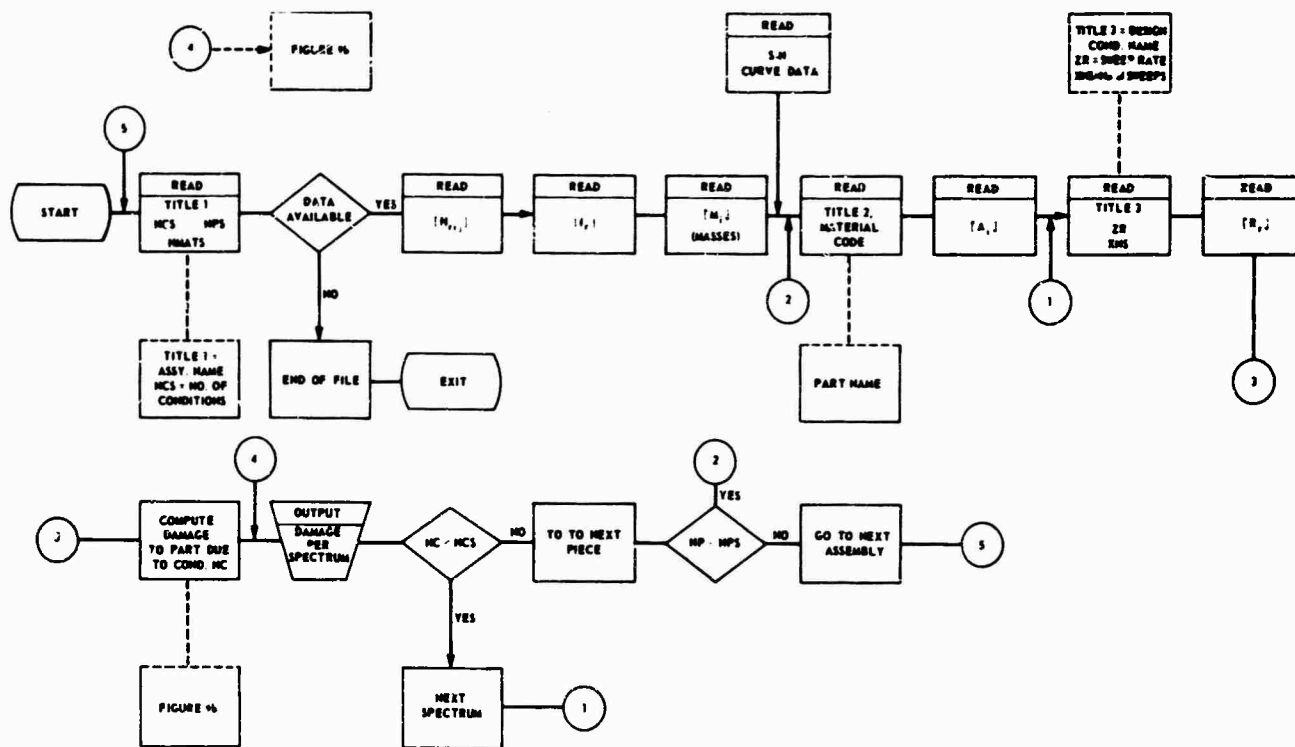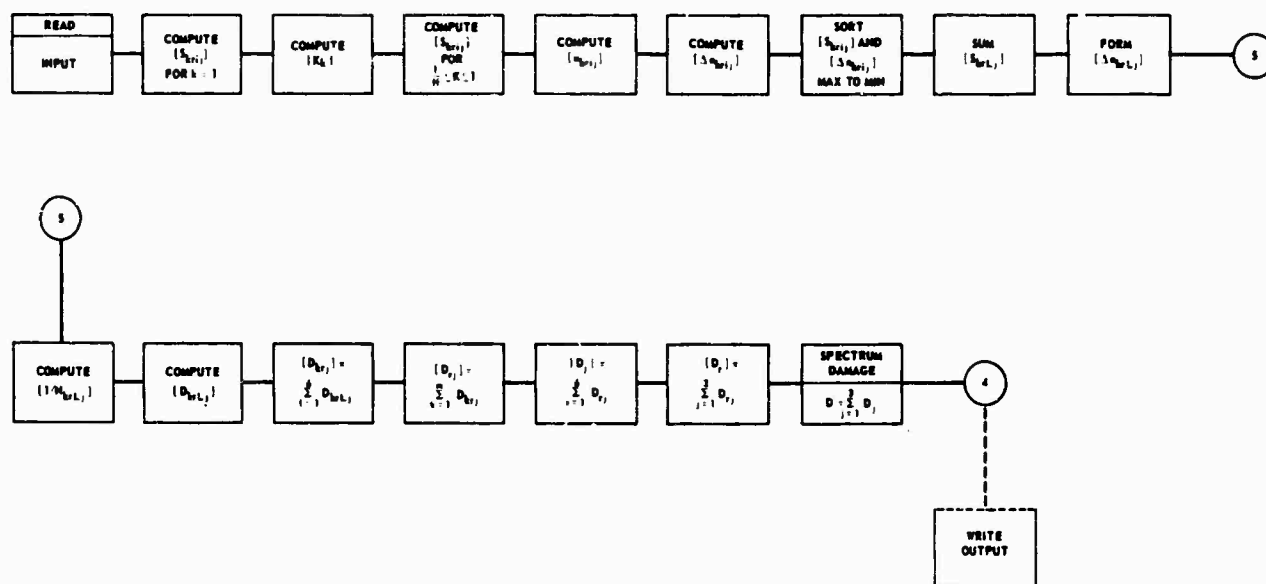
Fig. 9. (a) Fatigue program input-output flow chart, and (b) computation of damage

REFERENCES

1. Cyril M. Harris and C. E. Crede, Shock and Vibration Handbook, McGraw-Hill, New York, 1961

2. M. Pasyanos, Grumman Aircraft Engineering Corp., Unpublished Memo., Dec. 1964

3. S. Fogelson, "Stress Analysis of the LEM PS/TCA RCS Cluster Mount," Marquardt Corp. Rept. L-1034, 14 March 1966

Appendix A

PROGRAM LISTING

```
     0 $IBFTC 34C2
       L        PRCGRAM      -FATIGUE ANALYSIS,G.A.E.C. METHCD
       C        DATED 19 APRIL,1966
       C        ANALYSIS AND PKCGKAM BY S.FCGELSGN
       C
     1          DIMENSION SSI5,1D),VVA(5,1D),BBSN(5,10),NAME2(4,10),MAT(10),AB(6,
              210),NAME3(4,10),ZZR(10),XXNS(10),XXR(6,1D)
     2          DIMENSICN A)2),M)6,6,3),FN)6),TITLE1(4),TITLE2(4),TITLE3(4),
              2    XM)6),SOX(6,6),SOY)6,6),SDZ(6,6),AK)IT),SFDX(6,17,6),SIDY(6,17
              3,6),SFOZ(6,17,6),EAX)17,6,6),ENY(17,6,6),ENZ(17,6,6),DELENX)17,6,6
              4),DELENY)17,6,6),DELENZ(17,6,6),AA)6),B)6),C)6),SUMNX(6,17,6),FSDX
              5(17,6,6), SUPNY(6,17,6),SUMRZ(6,17,6),FSDY(17,6,6),FSUZ(17,6,6),
              6RDX(17,6,6),RDY(17,6,6),RDZ)17,6,6),DELDOX(17,6,),DELOOY(17,6),
              7DELODZ(17,6),SDMDX(6),SDMDY(6),SDMDZ(6),DDM)6),XXX)6),XM)6)
     3          DIMENSION S(5),VN(5),BSN(5)
     4          DIMENSIGN X)6),Y)6),Z)6)
     5          REAL NAPE2,NAME3
     6     50   READ(5,1DC)TITLE1,NPS,NCS,NPATS
    12     10C  FORMAT(4A6,2X,313)
       C
       C        TITLE1= ASSEMBLY NAME, NPS= NO. OF PARTS TC BE CHECKED, NCS=NO.
       C        OF LGAU CCNWITIONS, NPATS IS THE NUMBER OF DIFFERENT MATERIALS IN
       C        THE ASSEMBLY
       C
    13     11C  READ)5,12C)(((H(I,J,K),J=1,6),I=1,6),K=1,3)
    3D     12D  FORMAT(6F6.3)
       C
       C        H(I,J,K)=PAGNIFICATION FACTOR IN MCDE I,FOR A RESPONSE IN DIRECTI-
       C        ON J,TO AN INPUT LCAD FACTOR IN OIRECTION K
       C
    31          READ(5,13C))FN)I),I=1,6)
    36     130  FORMAT(6E12.6)
       C
       C        FN)I)=NATURAL FREGUENCY IN MCDE I
       C
    37          READ)5,)20))XM)J),J=1,6)
       C
       C        XM)J),J=1,3 = ASSEMBLY WEIGHT, XP)J),J=4,6 =II)X),I(Y),I(Z)
```

26

```
        C
   44         READ(5,135)((SS(N,P),N=1,5),P=1,NMATS)
   55         REAU(5,135)((VVN(N,P),N=1,5),P=1,NMATS)
   66         READ(5,135)((BBSN(N,M),N=1,5),M=1,NMATS)
   77     135 FORMAT(5E12.6)
        C
        C     SSN IS THE CRDINATE OF THE MATERIAL S-N CURVE
        C     VVN IS THE ABSCISSA OF THE MATERIAL S-N CUVE
        C     BBSN IS THE SLCPE CF THE MATERIAL S-N CURVE
        C
  1CO         READ(5,140)((NAME2(I,NP),I=1,4),MAT(NP),NP=1,NPS)
  111     140 FCRMAT(4A6,2X,I3)
        C
        C     NAME2 IS THE NAME OF THE PART BEING ANALIZED. MAT IS THE MATERIAL
        C     CODE NUMBER
        C
  112         READ(5,130)((AB(J,NP),J=1,6),NP=1,NPS)
        C     AB(J,NP) IS THE STRESS INFLUENCE COEFFICIENT FCR A RESPONSE IN
        C     DIRECTION J FOR PART NUMBER NP.
        C
  123         READ(5,150)((NAME3(I,NC),I=1,4),ZZR(NC),XXNS(NC),NC=1,NCS)
  134     150 FORMAT(4A6,2X,F6.3,2X,F6.3)
        C
        C     NAME3 IS THE NAME OF THE NC(TH) CONDITION BEING CHECKED.
        C
  135         READ(5,13C)((XXR(I,NC),I=1,6),NC=1,NCS)
        C
        C     XXR(I,NC) IS THE INPUT CF MCDE I DURING CONDITION NC.
        C
  146         DO 2000 NP=1,NPS
  147         M=MAT(NP)
  150         DO 155 I=1,4
  151     155 TITLE2(I)=NAME2(I,NP)
  153         DO 16C N=1,5
  154         S(N)=SS(N,M)
  155         VN(N)=VVN(N,P)
  156     16C BSN(N)=BBSN(N,M)
  16C         DO 165 J=1,6
```

```
  161     165 A(J)=AB(J,NP)
  163         DO 1000 NC=1,NCS
  164         DO 167 I=1,4
  165     167 TITLE3(I)=NAME3(I,NC)
  167         ZR=ZZR(NC)
  170         XNS=XXNS(NC)
  171         DO 170 I=1,6
  172     170 XR(I)=XXR(I,NC)
  174         DO 180 I=1,6
  175         DO 180 J=1,6
  176         SDX(I,J)=XR(I)*H(I,J,1)*A(J)*XM(J)
  177         SDY(I,J)=XR(I)*H(I,J,2)*A(J)*XM(J)
  200     180 SDZ(I,J)=XR(I)*H(I,J,3)*A(J)*XM(J)
        C
        C     SDX,SDY,SDZ ARE PART STRESSES FOR LOADING IN X,Y,Z AXES DIRECTIONS
        C
        C     AK=PERCENT CF MAXIMUM STRESS LEVEL
        C
  2C3         AK(1)=1.0
  2C4         DO 192 N=2,5
  2C5     192 AK(N)=AK(N-1)-0.025
  2C7         DO 194 N=6,13
  210     194 AK(N)=AK(N-1)-0.05C
  212         DO 196 N=14,17
  213     196 AK(N)=AK(N-1)-C.1C
  215         DO 200 J=1,6
  216         DO 200 I=1,6
  217         DO 2C0 N=1,17
        C
        C     SFOX,SFCY,ETC.,ARE MAX.STRESSES, FOR X,Y,AND Z LOADING,TIMES AK
        C
  22C         SFOX(I,N,J)=AK(N)*SDX(I,J)
  221         SFOY(I,N,J)=AK(N)*SDY(I,J)
  222     2C0 SFUZ(I,N,J)=AK(N)*SDZ(I,J)
        C
        C     ENX,ENY,ENZ ARE THE APPLIED CYCLES FOR X,Y,AND Z-AXES LOADING.SUB-
        C     SCRIPTS N=PERCENT LCADING I=MODE J=RESPONSE AXIS,I.E.,1=X-TRANSLA-
        C     TION 2=Y-TRANSLATICN 5=Y-AXIS ROTATION 6=Z-AXIS ROTATION
```

27

```
         C
226         OC 300 I=1,6
227         XXX(I)=122.4*FA(I)*XNS/ZR
230         DO 300 J=1,6
231         CO 300 N=1,17
232         FHX        =AK(N)*H(I,J,1)
233         FHY        =AK(N)*H(I,J,2)
234         FHZ        =AK(N)*H(I,J,3)
235         IF(ABS(FHY).LE.1.C)GO TC 225
240         ENY(N,I,J)=XXX(I)*SCRT(1.0-SCRT(1.00444*(1.0-1.0/(FHY**2))))
241         GC TC 230
242     225 ENY(N,I,J)=XXX(I)
243     23C IF(ABS(FHZ).LE.1.0)GO TC 250
246         ENZ(N,I,J)=XXX(I)*SQRT(1.0-SCRT(1.00444*(I.C-1.0/(FHZ**2))))
247         GC TC 260
250     25C ENZ(N,I,J)=XXX(I)
251     260 IF(ABS(FHX).LE.1.C)GU TC 270
254         ENX(N,I,J)=XXX(I)*SQRT(I.0-SCRT(I.00444*(I.0-1.0/(FHX**2))))
255         GC TO 300
256     27C ENX(N,I,J)=XXX(I)
257     3CO CCNTINUE
         C
         C     DELENX(N,I,J)=INCREMENT OF ENX BETWEEN N PERCENT AND (N-1) PERCENT
         C
263         DO 310 I=1,6
264         DO 310 J=1,6
265         DELEAX(1,I,J)=ENX(1,I,J)
266         DELEAY(1,I,J)=ENY(1,I,J)
267         DELEAZ(1,I,J)=ENZ(1,I,J)
270         DO 310 N=2,17
271         DELEAX(N,I,J)=ENX(N,I,J)-ENX(N-1,I,J)
272         DELENY(N,I,J)=ENY(N,I,J)-EAY(N-1,I,J)
273     310 DELEAZ(N,I,J)=ENZ(N,I,J)-ENZ(N-1,I,J)
         C
         C     SUMAX=TCTAL NC. CF TIMES A PARTICULAR STRESS LEVEL IS APPLIED DUE
         C     LOADING ON X-AXIS,AT K ( GF MAX.,IN MCDE I.
         C     FSCX=STRESS LEVEL APPLIEC SUMAX TIMES CUE TC X-LCADING
         C
```

```
277         DO 322 I=1,6
300         CO 322 N=1,6
301         DO 322 K=1,6
302         SUMAX(K,N,I)=0.0
303         SUMAY(K,N,I)=0.0
304         SUMAZ(K,N,I)=0.0
305         FSOX(N,K,I)=C.0
306         FSOY(N,K,I)=0.0
307         FSOZ(N,K,I)=0.0
310     322 CCNTINLE
314         OC 400 N=1,17
315         DC 400 I=1,5
316         DC 320 J=1,6
317         AA(J)=DELENX(N,I,J)
320     320 B(J)=SFOX(I,N,J)
322         CALL SCRT(AA,B,6)
323         CALL SUM(AA,B,C,6,JX,X,Y,Z)
324         OC 340 K=1,JX
325         SUMNX(K,N,I)=X(K)
326         FSOX(N,K,I)=Y(K)
327     34C CCNTINUE
331         CO 350 J=1,6
332         AA(J)=DELENY(N,I,J)
333     350 B(J)=SFOY(I,N,J)
335         CALL SCRT(AA,B,6)
336         CALL SUM(AA,B,C,6,JY,X,Y,Z)
337         DO 370 K=1,JY
340         SUMNY(K,N,I)=X(K)
341         FSOY(N,K,I)=Y(K)
342     37C CCNTINLE
344         DC 38C J=1,6
345         AA(J)=DELENZ(N,I,J)
346     380 B(J)=SFOZ(I,N,J)
350         CALL SCRT(AA,B,6)
351         CALL SUM(AA,B,C,6,JZ,X,Y,Z)
352         DC 395 K=1,JZ
353         SUMNZ(K,N,I)=X(K)
354         FSOZ(N,K,I)=Y(K)
```

```
  355   355 CONTINLE
  357   400 CCNTINUE
        C
        C      ROX(N,K,I)=RECIPRCCAL OF ALLCWABLE CYCLES WFEN X-AXIS IS LUAOED,AT
        C      N PERCENT LOADING CCRRESPCNUINU TO THE KITH) STRESS LEVEL,IN MOUE
        C      1.
        C
  362         DC 600 I=1,6
  363         OC 600 N=1,17
  364         JO 430 K=1,6
  365         IF(ABSIFSDX(N,K,I)).LT.S(1))GC TO 420
  370         ROX(N,K,I)=1.0/VN(1)
  371         GC TO 430
  372   420 IF(ABSIFSDX(N,K,I)).LT.S(3))GC TC 421
  375         ROX(N,K,I)=((FSDX(N,K,I)/S(2))**BSN(1))/VN(2)
  376         GC TC 430
  377   421 IF(ABSIFSDX(N,K,I)).LT.S(4))GC TC 422
  402         ROX(N,K,I)=((FSDX(N,K,I)/S(3))**BSN(3))/VN(3)
  4C3         GC TO 430
  404   422 IF(ABSIFSDX(N,K,I)).LT.S(5))GC TC 425
  407         ROX(N,K,I)=((FSDX(N,K,I)/S(4))**BSN(4))/VN(4)
  410         GO TC 430
  411   425 RDX(N,K,I)=0.0
  412   430 CCNTINUE
  414         DO 450 K=1,6
  415         IF(ABSIFSDY(N,K,I)).LT.S(1))GC TC 440
  420         ROY(N,K,I)=1.0/VN(1)
  421         GC TO 450
  422   440 IF(ABSIFSDY(N,K,I)).LT.S(3))GC TO 441
  425         RDY(N,K,I)=((FSDY(N,K,I)/S(2))**BSN(1))/VN(2)
  426         GO TC 450
  427   441 IF(ABSIFSDY(N,K,I)).LT.S(4))GC TC 442
  432         RDY(N,K,I)=((FSDY(N,K,I)/S(3))**BSN(3))/VN(3)
  433         GO TC 450
  434   442 IF(ABSIFSDY(N,K,I)).LT.S(5))GC TC 445
  437         ROY(N,K,I)=((FSDY(N,K,I)/S(4))**BSN(4))/VN(4)
  440         GC TC 450
  441   445 RUY(N,K,I)=0.C
```

```
  442   450 CONTINUE
  444         DC 470 K=1,6
  445         IF(ABSIFSDZ(N,K,I)).LT.S(1))GC TO 460
  450         RDZ(N,K,I)=1.0/VN(1)
  451         GC TC 470
  452   460 IF(ABSIFSDZ(N,K,I)).LT.S(3))GO TO 461
  455         RDZ(N,K,I)=((FSDZ(N,K,I)/S(2))**BSN(1))/VN(2)
  456         GO TC 470
  457   461 IF(ABSIFSDZ(N,K,I)).LT.S(4))GC TC 462
  462         RDZ(N,K,I)=((FSDZ(N,K,I)/S(3))**BSN(3))/VN(3)
  463         GO TO 470
  464   462 IF(ABSIFSDZ(N,K,I)).LT.S(5))GO TO 465
  467         RDZ(N,K,I)=((FSDZ(N,K,I)/S(4))**BSN(4))/VN(4)
  47C         GU TO 470
  471   465 ROZ(N,K,I)=0.D
  472   47C CUNTINUE
  474   600 CCNTINUE
        C
        C      DELODX(N,I)TCTAL PART DAMAGE FCR X-AXIS LOADING,AT N PERCENT OF
        C      MCDE I.
        C
  477         DU 650 I=1,6
  500         JO 650 N=1,17
  501         DELDDX(N,I)=C.0
  502         DELDDY(N,I)=0.D
  503         DELDDZ(N,I)=D.D
  504         DO 650 K=1,6
  505         DELODX(N,I)=DELDDX(N,I)+RDX(N,K,I)*SUMNX(K,N,I)
  506         DELDDY(N,I)=DELDDY(N,I)+RDY(N,K,I)*SUMNY(K,N,I)
  507         DELODZ(N,I)=DELDDZ(N,I)+RDZ(N,K,I)*SUMNZ(K,N,I)
  510   650 CUNTINUE
        C
        C      SUMDX(I)=TOTAL PART DAMAGE IN MDOE I FOR X-AXIS LOADING.
        C
  514         DO 675 I=1,6
  515         SUMDX(I)=0.0
  516         SUMDY(I)=0.0
  517         SUMDZ(I)=0.0
```

```
        52C          UC 675 N=1,17
        521          SDMDX!(I)=SDMDX1I)+CELDDX(N,I)
        522          SDMDY(1)=SDMCY(I)+CELDDY(N,I)
        523          SUMDZ(I)=SUMCZ(I)+CEL    Z(N,I)
        524      675 CONTINUE
        C
        C            DDX= TCTAL PART CAMAGE DUE TC X-AXIS LCADING, SUMMING THE MODAL
        C            DAMAGE.
        C
        527          GDX=0.0
        530          DDY=0.0
        531          CDZ=0.0
        532          DO 700 I=1,6
        533          CCX=CDX+SDMDXI(I)
        534          CCY=DDY+SDMDY(I)
        535          DDZ=CDZ+SDMDZ(I)
        536      700 CLNTINUE
        C
        C            CDM(I)= TOTAL PART CAMAGE PER MODE, SUMMING THE LCAD AXIS DAMAGE.
        C
        54C          UC 710 I=1,6
        541          DDM(I)=C.D
        542      710 CCNTINUE
        544          DC 720 I=1,6
        545          DCM(I)=DOM(I)+SDMCX(I)+SCMCY(I)+SDMDZ(I)
        546      720 CONTINUE
        C
        C            DD= TOTAL CF ALL PART CAMAGE DUE TC SPECTRUM.
        C
        550          DD=DDX+DDY+DCZ
        551          WRITE(6,800)TITLE1,TITLE2
        552      80C FORMAT(1H1,47X,4A6/51X,16HFATIGUE ANALYSIS/47X,4A6/52X,14HFATIGUE
                     20AMAGE /)
        553          WRITE(6,8C5)ZR,ANS
        554      805 FURMAT(3X,11HSWEEP RATE=,F5.2,10X,31HNUMBER CF SWEEPS (UP AND DOWN
                     21=,F5.2 /)
        555          WRITE(6,810)TITLE3,(MCDE,MCDE=1,6)
        562      810 FURMAT(/47X,4A6///57X,4HMCDE/3X,7HLCADING/4X,4HAXIS,6I12,11X,3HSUM
```

```
                     2)
        5E3          WRITE(6,820)((SDMDXI(I),I=1,6),DDX)
        574      820 FURMAT(6X,1HX,7X,7E12.3 /)
        575          WRITE(6,830)((SDMDY(I),I=1,6),DDY)
        6C6      830 FORMAT(6X,1HY,7X,7E12.3 /)
        6C7          WRITE(6,840)((SDMDZ(I),I=1,6),DDZ)
        62C      843 FORMAT(6X,1HZ,7X,7E12.3 /)
        621          WRITE(6,850)((DDM(I),I=1,6),DD)
        632      850 FORMAT(/5X,3HSUM,6X,7E12.3/1H-)
        633     1000 CONTINUE
        635     2CCC CONTINUE
        637          GU TO 50
        64C          END
```

```
        0  $IBFTC SCRT
        1            SUBROUTINE SCRT(A,B,N)
        2            DIMENSION A(1),B(1)
        3            DC 1000 I=2,N
        4            DC 1000 J=2,I
        5            JJ=I+2-J
        E            IF(A(JJ-1).GE.A(JJ)) GC TC 1000
        11           ADUM=A(JJ)
        12           BDUM=B(JJ)
        13           A(JJ)=A(JJ-1)
        14           B(JJ)=B(JJ-1)
        15           A(JJ-1)=ADUM
        16           B(JJ-1)=BDUM
        17     1C00 CONTINUE
        22           RETURN
        23           END
```

30

```
(SN       SCURCE STATEPENT

0  $ICFTC SLM
1          SLBRUUTINE SLM(A,B,C,R,JC,X,Y,Z)
2          DIMENSICN A(1(,B1I(,C(1(,X(1(,Y(1(,Z(1)
3          X(1(=A(1(
4          Y(1)=B(1(
5          Z(1(=C(1)
6          JC=(
7          DO 2000 (=2,R
1C         IF(A11-1).EC.A11(( CC TC 1000
13         JC=JC+1
14         X(JC)=A(1(
15         Y(JC(=Y(JC-1)+B1I(
1C         Z1JC)=Z(JC-1)+C(1(
17         GC TC 2000
2C    1CC0 Y(JC(=Y(JC(+B(1(
21         Z1JC(=Z1JC(+C11(
22    2000 CCNTINUE
24         RETURN
25         ENO
```

IBM 7040 INPUT FORM · 80 COLUMN

IBM 7040 INPUT FORM - 80 COLUMN

XXR (I,1)					XXR (6,1)	
NC CARDS		INPUT LOADING				
XXR (I,NC)					XXR (6,NC)	

Appendix B

EXAMPLE PROBLEM

This analysis was conducted on the LEM PS/TCA, Reaction Control System aft engine support structure. In this structure, static stress analysis indicated that the most highly stressed points were on adjacent pieces of structure loaded simultaneously by a single bolt. While the stress of one of the parts was only 94 percent of the stress in the other part, they were of different materials and, therefore, both were analyzed. A schematic of this assembly, with the critical loading, is shown in Fig. B-1.

MAGNIFICATION FACTORS

Since the input is applied sequentially along each of the three reference axes, three matrices of magnification factors result, one for each axis of loading:

X-Axis Loading

$$[H_{rii}] = \begin{bmatrix} +2.59 & -0.52 & +0.46 & -0.33 & -0.13 & -0.09 \\ 1.10 & -1.17 & 0.76 & 0.73 & -1.12 & -0.74 \\ +1.65 & +2.40 & -2.77 & -0.63 & +0.36 & +0.31 \\ 2.70 & -0.81 & 1.71 & 0.25 & 0.99 & 0.63 \\ +0.31 & -0.15 & -0.14 & - & +0.04 & -0.03 \\ 0.21 & 0.12 & 0.07 & - & 0.03 & -0.05 \end{bmatrix}$$

32
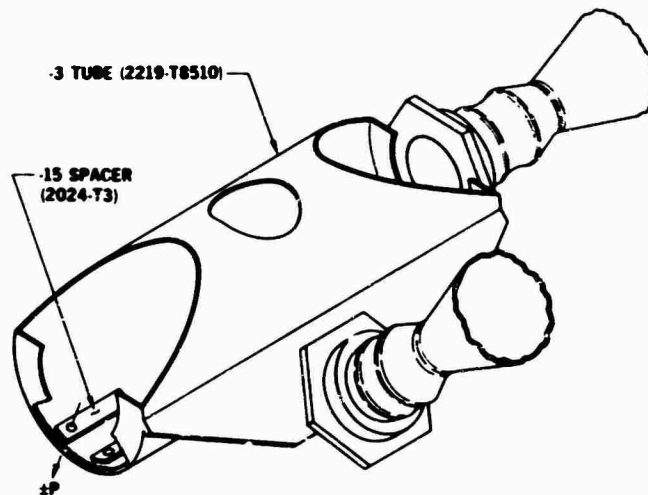
Fig. B-1. Schematic of LEM
PS/TCA cluster mount

Y-Axis Loading

$$[H_{ri2}] = \begin{bmatrix} -0.52 & 2.43 & -1.86 & 1.42 & 0.07 & 0.08 \\ -1.17 & +1.02 & -0.20 & -0.38 & +0.12 & +0.08 \\ +2.40 & +4.32 & -4.84 & -1.10 & +0.20 & +0.33 \\ -0.80 & +0.50 & -1.79 & -0.18 & -0.30 & -0.20 \\ -0.13 & 6.37 & 6.03 & -0.11 & -0.66 & 0.68 \\ 0.10 & 2.87 & 1.88 & -0.10 & 0.60 & -0.99 \end{bmatrix}$$

Z-Axis Loading

$$[H_{ri3}] = \begin{bmatrix} +0.46 & -1.86 & +2.24 & -1.32 & -0.06 & -0.07 \\ 0.76 & -0.20 & 1.18 & 0.37 & -0.08 & -0.05 \\ -2.77 & -4.85 & 5.84 & 1.29 & -0.24 & -0.38 \\ 1.72 & -1.79 & 1.46 & 0.29 & 0.66 & 0.43 \\ -0.13 & 6.03 & 5.70 & -0.11 & -0.63 & 0.65 \\ 0.06 & 1.88 & 1.60 & -0.06 & 0.35 & -0.58 \end{bmatrix}$$

NATURAL FREQUENCIES

The six calculated modal frequencies are listed below.

Mode	F_n (cps)	Mode	F_n (cps)
1	57.1	4	113.3
2	69.6	5	173.6
3	96.7	6	200.8

MASS MATRIX

In this problem, the input spectra are in units of g. The mass matrix is, therefore, written in terms of the cluster weight and weight moments of inertia:

$$W = 25 \text{ lb,}$$
$$I_X = 318 \text{ psi,}$$
$$I_Y = 592 \text{ psi, and}$$
$$I_Z = 591 \text{ psi,}$$

and

$$\begin{bmatrix} M_i \end{bmatrix} = \begin{bmatrix} 25 & & & & & \\ & 25 & & & & \\ & & 25 & & & \\ & & & 318 & & \\ & & & & 592 & \\ & & & & & 591 \end{bmatrix}$$

33

STRESS COEFFICIENT MATRIX

A static stress analysis yielded the following stress coefficient matrices for the two parts (see Eq. (26)):

-15 Spacer

$$\left\lfloor A_i \right\rfloor_{15} =$$

$$\begin{bmatrix} 0.1339 & & & & & \\ & -14.6 & & & & \\ & & 0.3842 & & & \\ & & & 18.86 & & \\ & & & & 1.653 & \\ & & & & & 2.423 \end{bmatrix} \cdot$$

-3 Tube

$$\left\lfloor A_i \right\rfloor_{3} =$$

$$\begin{bmatrix} 0.1258 & & & & & \\ & -13.71 & & & & \\ & & 0.3608 & & & \\ & & & 17.71 & & \\ & & & & 1.55 & \\ & & & & & 2.275 \end{bmatrix} \cdot$$

INPUT SPECTRA

Three sinusoidal spectra, shown in Fig. B-2, are applied sequentially in x-, y-, and z-axis directions. These spectra are logarithmically swept at the rates, and for the number of times, shown in Table B-1.
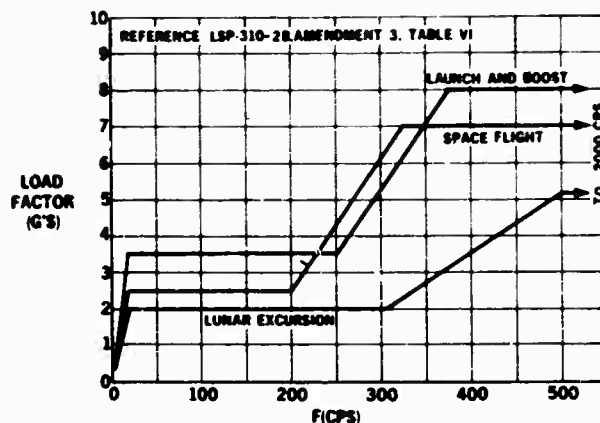
Fig. B-2. Sinusoidally applied load factors qualification test

TABLE B-1

Spec-trum	Condition	Sweep Rate (octaves/min)	No. of Sweeps Up and Down
1	Launch and boost	3	2
2	Space flight	1.5	2
3	Lunar excursion	0.5	2

DATA SHEETS

Completed data input sheets are shown in Fig. B-3.

RESULTS

The damage resulting from the three loading conditions for the -15 spacer and the -3 tube are shown in the following printout. The total damage for the -3 tube is

$$D = 0.01925 + 0.00104 + 0.00002 = 0.02031,$$

and for the -15 spacer,

$$D = 0.04758 + 0.00197 + 0.00004 = 0.04959.$$

IBM 7040 INPUT FORM - 80 COLUMN

FORM TWC 1940 REV. 7-00

JOB NO.	JOB NAME	NAME	EXTENSION	DEPT.	PAGE
3402	FATIGUE ANALYSIS	S. FOGELSON	1198	153	1 OF

LEM PS/TCA AFT CLUSTER	2	3	2		1
2.59	-0.52	0.96	-0.33	-0.13	-0.09	2
1.0	-1.17	0.76	0.73	-1.12	-0.74	3
1.65	2.4	-2.77	-0.63	0.36	0.31	4
2.7	-0.81	1.71	0.25	0.99	0.63	5
0.31	-0.15	-0.14		0.04	-0.03	6
0.21	0.12	0.07		0.03	-0.05	7
-0.52	2.43	-1.86	1.42	0.07	0.08	8
-1.17	1.02	-0.2	-0.38	0.12	0.08	9
2.40	1.32	-4.84	-1.1	0.2	0.33	10
-0.8	0.5	-1.79	-0.18	-0.3	-0.2	11
-0.13	6.37	6.03	-0.11	-0.66	0.68	12
0.10	2.87	1.88	-0.1	0.6	-0.99	13
0.46	-1.86	2.24	-1.32	-0.06	-0.07	14
0.76	-0.20	1.18	0.37	-0.08	-0.05	15
-2.77	-4.85	5.84	1.29	-0.24	-0.38	16
1.72	-1.79	1.46	0.29	0.66	0.43	17
-0.13	6.03	5.70	-0.11	-0.63	0.65	18
0.06	1.88	1.60	-0.06	0.37	-0.58	19
57.1		69.6	96.7	113.3	173.6	200.8	20
25.0	318.0	592.0	541.0		21
6.0	+04	3.4	+04	2.6	+04	2.1	+04	1.8	+04	22
6.0	+04	3.625	+04	2.7	+04	2.16	+04	1.75	+04	23
7.64	+02	1.0	+05	1.0	+06	1.0	+07	1.0	+08	24
1.948	+03	1.0	+05	1.0	+06	1.0	+07	1.0	+08	25

Fig. B-3(a). Completed data input sheets

35

IBM 7040 INPUT FORM · 80 COLUMN

FORM TWC 1540 REV. 7-05

JOB NO.	JOB NAME	NAME		EXTENSION	DEPT.	PAGE

PAGE 2 of

```
8.583        8.583       19.937      10.782      0.0
7.816        7.816       10.319      10.935      0.0
          -15 SPACER          1
           -3 TUBE            2
  .2339       -19.6         .3892      18.859     1.6527      2.4226
  .1258       -13.71        .3608      17.712     1.552       2.275
      LAUNCH AND BOOST       3.0     2.0
        SPACE FLIGHT         1.5     2.0
       LUNAR EXCURSION       0.5     3.0
3.5          3.5          3.5         3.5        3.5         3.5
2.5          2.5          2.5         2.5        2.5         2.5
2.0          2.0          2.0         2.0        2.0         2.0
```

Fig. B-3(b). Completed data input sheets

LEM PS/TCA AFT CLUSTER
FATIGUE ANALYSIS
-3 TUBE
FATIGUE DAMAGE

SWEEP RATE= 3.00   NUMBER OF SWEEPS (UP AND DOWN)= 2.00

LAUNCH AND BOOST

LOADING AXIS	MODE 1	MODE 2	MODE 3	MODE 4	MODE 5	MODE 6	SUM
X	0.	0.221E-04	0.	0.	0.	0.	0.221E-04
Y	0.833E-02	0.	0.148E-02	0.	0.	0.	0.981E-02
Z	0.376E-02	0.	0.566E-02	0.	0.	0.	0.942E-02
SUM	0.121E-01	0.221E-04	0.714E-02	0.	0.	0.	0.193E-01

LEM PS/TCA AFT CLUSTER
FATIGUE ANALYSIS
-3 TUBE
FATIGUE DAMAGE

SWEEP RATE= 1.50   NUMBER OF SWEEPS (UP AND DOWN)= 2.00

SPACE FLIGHT

LOADING AXIS	MODE 1	MODE 2	MODE 3	MODE 4	MODE 5	MODE 6	SUM
X	0.	0.221E-04	0.	0.	0.	0.	0.221E-04
Y	0.540E-03	0.	0.591E-04	0.	0.	0.	0.599E-03
Z	0.138E-03	0.	0.284E-03	0.	0.	0.	0.422E-03
SUM	0.678E-03	0.221E-04	0.343E-03	0.	0.	0.	0.104E-02

LEM PS/TCA AFT CLUSTER
FATIGUE ANALYSIS
-3 TUBE
FATIGUE DAMAGE

SWEEP RATE= 0.50   NUMBER OF SWEEPS (UP AND DOWN)= 2.00

LUNAR EXCURSION

LOADING AXIS	MODE 1	MODE 2	MODE 3	MODE 4	MODE 5	MODE 6	SUM
X	0.	0.221E-04	0.	0.	0.	0.	0.221E-04
Y	0.	0.	0.	0.	0.	0.	0.
Z	0.	0.	0.162E-05	0.	0.	0.	0.162E-05
SUM	0.	0.221E-04	0.162E-05	0.	0.	0.	0.237E-04

LEM PS/TCA AFT CLUSTER
FATIGUE ANALYSIS
-15 SPACER
FATIGUE DAMAGE

SWEEP RATE= 3.00   NUMBER OF SWEEPS (UP AND DOWN)= 2.00

LAUNCH AND BOOST

MODE

LOADING AXIS	1	2	3	4	5	6	SUM
X	0.	0.271E-04	0.	0.	0.	0.	0.271E-04
Y	0.206E-01	0.	0.393E-02	0.	0.	0.	0.246E-01
Z	0.547E-02	0.	0.135E-01	0.	0.	0.	0.230E-01
SUM	0.301E-01	0.271E-04	0.174E-01	0.	0.	0.	0.476E-01

LEM PS/TCA AFT CLUSTER
FATIGUE ANALYSIS
-15 SPACER
FATIGUE DAMAGE

SWEEP RATE= 1.50   NUMBER OF SWEEPS (UP AND DOWN)= 2.00

SPACE FLIGHT

MODE

LOADING AXIS	1	2	3	4	5	6	SUM
X	0.	0.271E-04	0.	0.	0.	0.	0.271E-04
Y	0.612E-03	0.	0.166E-03	0.	0.	0.	0.578E-03
Z	0.547E-03	0.	0.413E-03	0.	0.	0.	0.961E-03
SUM	0.136E-02	0.271E-04	0.580E-03	0.	0.	0.	0.157E-02

LEM PS/TCA AFT CLUSTER
FATIGUE ANALYSIS
-15 SPACER
FATIGUE DAMAGE

SWEEP RATE= 0.50   NUMBER OF SWEEPS (UP AND DOWN)= 2.00

LUNAR EXCURSION

MODE

LOADING AXIS	1	2	3	4	5	6	SUM
X	0.	0.271E-04	0.	0.	0.	0.	0.271E-04
Y	0.	0.	0.	0.	0.	0.	0.
Z	0.	0.	0.169E-04	0.	0.	0.	0.169E-04
SUM	0.	0.271E-04	0.169E-04	0.	0.	0.	0.440E-04

DISCUSSION

Mr. Holland (Allied Research Associates): Fatigue damage is sensitive to the response amplitude, and you have determined damping analytically. Have you tried to find the effect different values derived from the damping matrix have on the cumulative fatigue damage?

Mr. Fogelson: The greater the damping, of course, the lower would be the applied stress and, therefore, the damage would be less.

Mr. Holland: How sensitive is it to this matrix? Since it is analytically determined, would small errors create a large difference in response?

Mr. Fogelson: We haven't found that. We applied various damping ratios differing by as much as 10 percent, and the difference was less than 10 percent, less than a 1:1 relationship.

Mr. Holland: What is your damping ratio?

Mr. Fogelson: We use 10 percent.

Mr. Holland: What is the critical damping; is it modal damping?

Mr. Fogelson: Yes.

Mr. Bratkowski (Westinghouse Research Laboratories): How were you measuring modal damping? This has been a problem for most dynamicists in the past, but it seems that you have solved it.

Mr. Fogelson: I haven't solved the problem. The program has been used only in the design and analysis stage in which we have assumed a certain amount of modal damping. We have run a test on the system, but the data are not yet reduced.

Mr. Bratkowski: How have you correlated the results of your theory and experimental results as far as damage is concerned?

Mr. Fogelson: That, too, is waiting for completion of the test now under way.

Mr. DiTaranto (PMC Colleges): Why were you using each of the three stresses at a point individually, instead of the combined stresses?

Mr. Fogelson: I did not make myself clear. I do combine the stresses. There are six stress components, one for each response direction. But I combine them based on the number of times each of these stress levels is applied. The stress level with the greatest number of cycles is used only for the number of cycles that it is applied minus the number of cycles that the next greatest stress is applied. Then the next two stresses are added together to get a new total stress which is applied only for the difference in the number of times these stresses are applied. All stresses are finally added together, but only for the minimum number of cycles.

Mr. DiTaranto: These are not added linearly?

Mr. Fogelson: Yes, they are.

Mr. DiTaranto: Rather than using a more circular approach?

Mr. Fogelson: No, because this stress was uniaxial and, therefore, the individual stress components, since they were all acting in the same direction, were added linearly.

Mr. Ip (Aerospace Corp.): Miner's hypothesis is based on a simple fatigue test. Is there any question of how well it applies to three-dimensional fatigue?

Mr. Fogelson: I cannot answer that.

Mr. Stallard (AVCO Corp.): A test was run about ten years ago using random vibration as the load on pieces of metal. This again approaches the idealized test. By performing that test using Miner's hypothesis of $\Sigma (n/N)$ equal to 1, we found that $\Sigma (n/N)$ varied between 3/10 and 5 and 6, which makes me wonder about this test. Of course, you are using sinusoidal rather than random vibration. In the last two or three years, most of the papers in the Shock and Vibration Bulletins indicated that Miner's $\Sigma (n/N)$ ratio holds for a sinusoidal flexing load produced by a small round beam with a wheel in the center and a weight hanging on the end of it. However, $\Sigma (n/N)$ is not equal to 1 for random loading; it varies over a wide range. I am sure that anyone else in this audience who has seen this type of test has found the same answer.

Mr. Rubin (Aerospace Corp.): This is very true. I think a paper was presented a few weeks ago at a Society of Automotive Engineers'

meeting which pointed out that the choice of the criterion of failure will affect the result. For example, if you define a 1 percent change in the natural frequency as failure for a small beam specimen, you will get one result. If you then want to call failure a 2 percent change in the natural frequency, you will get an entirely different result. So your failure criterion is also very important in establishing the exact fatigue hypothesis.

*   *   *

ANALYSIS OF VIBRATION DISTRIBUTIONS
IN COMPLEX STRUCTURES

Eric E. Ungar
Bolt Beranek and Newman Inc.
Cambridge, Massachusetts

and

Terry D. Scharton
Bolt Beranek and Newman Inc.
Van Nuys, California

This paper is intended to serve as an introduction to the "statistical energy analysis" approach, which provides one with a relatively simple means for understanding and estimating the most significant properties of multi-modal random vibrations of complex structures. The theoretical basis for this approach is summarized, some insights resulting from its use are presented, and some applications of it to spacecraft vibration analysis and testing are discussed.

E. E. Ungar

INTRODUCTION

Recent technological trends have brought with them more powerful sources of high-frequency random vibrations, and simultaneously have led to lighter, smaller, and more delicate structures and equipments which are susceptible to damage from such vibrations. As these trends have developed, vibration analysts have found that the various techniques that served them so well in the low-frequency domain (near the fundamental resonances) could not deal realistically with high-frequency problems.

To be sure, the time-honored classical analysis techniques are also theoretically valid for high frequencies; however, one encounters difficulties in their application to practical problems. The classical techniques generally involve determination of the lowest few mode shapes, calculation of the response of each mode to a prescribed excitation, and superposition of these responses to obtain the total response. Since only the lowest few modes respond significantly to low-frequency excitation, computations based only on these modes uffice for low-frequency analyses. This is not the case for broadband high-frequency excitations.

In analyzing the responses to high-frequency excitations, particularly where the excitations have broad frequency band spectra, one finds that one must take into account a large number of modes. Determination of all of these mode shapes, of the associated natural frequencies, and of the modal responses generally requires an excessive amount of computation.

Further, and perhaps more significantly, one finds that one cannot calculate the high-frequency mode shapes of practical structures meaningfully. To perform such calculations one would need to have available complete and precise mathematical descriptions of the geometries, boundary conditions, and elastic properties of all structural components. Since such descriptions are usually not available, one is tempted to perform the required calculations for a fictitious structure which is similar to the actual one. Unfortunately, however, at a given location on the structure the responses associated with the higher modes tend to be much more affected by small changes in

41

geometry and boundary conditions than those associated with the lower modes. Analysis of a fictitious structure thus gives results which are devoid of meaning for the higher modes, although a similar analysis may be useful where only the lower modes are involved.

If one could somehow perform adequately the multi-mode calculations required for high-frequency response predictions, one would still be faced with interpreting the large volume of data generated by such calculations. Generally, one would desire to perform further computations, e.g., to determine various response averages, to reduce these data to more easily interpretable form.

An approach, which has come to be known as statistical energy analysis, has been developed in the past few years to circumvent the aforementioned problems. This approach permits one to calculate average responses and their distribution over complex structures with relative ease, being concerned with the details of the various modes.

This paper is intended to serve as an introduction to "statistical energy analysis." The theoretical basis for this analysis approach is summarized in the first of the following sections. Some applications of this approach to two coupled systems are indicated in the second section, whereas the third section discusses some practical applications to more complex systems.

THEORETICAL BACKGROUND [1,2]

Modes

Modes describe a special class of free vibrations of undamped elastic systems where all points move in unison sinusoidally in time. Accordingly, one may describe a modal vibration of an extended (one-dimensional*) system by

$$w(x,t) = \psi_n(x) \sin \omega_n t . \qquad (1)$$

Here w denotes a deformation of the system from equilibrium and is a function of the spatial coordinate x and of time t. The function $\psi_n(x)$ is called the "mode shape" and is independent of time. The time dependence of $w(x,t)$

---

*The discussion is here presented only for a one-dimensional system, such as a beam or shaft. Results for two- or three-dimensional systems may readily be obtained by analogy.

is embodied in the $\sin \omega_n t$ term, where ω_n denotes the (radian) frequency associated with the mode.

Continuous systems have an infinite number of modes, each with an associated modal (natural) frequency. The modes are usually numbered, beginning with the lowest (i.e., the fundamental) mode. The subscript "n" in Eq. (1) indicates the mode number. The mode shapes ψ_n and modal frequencies satisfy the system equations of motion (in the absence of damping and excitation) and the boundary conditions.

The mode shapes also satisfy

$$\int_0^L \psi_n(x) \, \psi_k(x) \, m(x) \, dx = \begin{cases} 0 & \text{for } n \neq k \\ M & \text{for } n = k \end{cases}, \qquad (2)$$

where $m(x)$ denotes the distribution of mass per unit length, L the total length, and M the total mass of the system. (M is, of course, equal to the integral of $m(x)$ over the entire length.) The property that the product of two different mode shapes integrates to zero is called "orthogonality," and only holds for systems whose boundaries are clamped, simply supported, and/or elastically restrained. Integration of $\psi_n^2(x) m(x)$ to M is a "normalization" condition (one of many possible ones) which is imposed on the mode shapes to define them uniquely (since the differential equations of motion define them only within an arbitrary multiplicative constant).

The mode shapes are useful functions for studying the responses of systems, since they permit one to expand any physically realizable system deflection $w(x,t)$ or velocity $v(x,t)$ and most excitation distributions $p(x,t)$ in series:

$$w(x,t) = \sum_{n=1}^{\infty} W_n(t) \, \psi_n(x) ,$$

$$v(x,t) = \sum_{n=1}^{\infty} V_n(t) \, \psi_n(x) , \qquad (3)$$

and

$$p(x,t) = \sum_{n=1}^{\infty} F_n(t) \, \psi_n(x) .$$

For constant or small damping, each displacement coefficient W_n and velocity coefficient V_n depends only on the corresponding force coefficient F_n, according to

42

$$M \ddot{W}_n + C_n \dot{W}_n + K_n W_n = F_n .$$

$$V_n = \dot{W}_n . \tag{4}$$

Here C_n is a modal viscous damping coefficient, and $K_n = M \omega_n^2$ is a modal stiffness; F_n is called the modal force.

Equation (4) may be recognized to be completely analogous to the relation which governs the displacement W_n of a mass M to a force F_n, where the mass is mounted on a parallel combination of a spring (of stiffness K_n) and a dashpot (with viscous damping coefficient C_n). Thus, one may study the responses of modes simply by studying the responses of analogous single-degree-of-freedom mass-spring-dashpot systems.

One may also show that the kinetic energy of a vibrating elastic system and its (spatially averaged) mean square velocity is simply related to the modal coefficients. By use of Eqs. (2) and (3), one finds that the total kinetic energy T_T of the system obeys

$$T_T = \frac{1}{2} \int_0^L m(x) \, v^2(x,t) \, dx$$

$$= \frac{1}{2} \sum_{n=1}^{\infty} \sum_{n=1}^{\infty} V_n V_k \int_0^L m(x) \, \psi_n(x) \, \psi_k(x) \, dx \tag{5}$$

$$= \frac{M}{2} \sum_{n=1}^{\infty} V_n^2(t)$$

and that the (mass-weighted) mean square velocity $\overline{v^2(t)}$ is given by

$$\overline{v^2(t)} = \frac{1}{M} \int_0^L m(x) \, v^2(x,t) \, dx = \sum_{n=1}^{\infty} V_n^2(t) . \tag{6}$$

Equation (5) shows that the system kinetic energy is equal to the sum of all modal kinetic energies $M V_n^2/2$, and Eq. (6) indicates that the system mean square velocity is equal to the sum of the squares of all modal velocities V_n. These important results will be put to use later.

Energy Analysis of Two
  Coupled Modes

Before studying the interaction between two coupled elastic systems, one may do well to develop an understanding of the interaction between two modes, where one mode belongs to

the first and one to the second system. In accordance with the previous discussion, one may visualize each mode as a mass-spring-dashpot system, so that one may study the interaction of two modes in terms of a system like that diagrammed in Fig. 1.
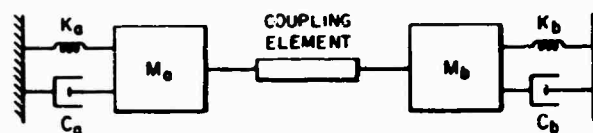
Fig. 1. Schematic representation
of two coupled modes

Keeping in mind that the present objective is to develop an "energy balance" approach to replace the more complex detailed dynamic analyses which are commonly used, one may at once note that the time-average power D_a dissipated by mode a is given by

$$D_a = C_a \langle V_a^2 \rangle = \frac{2 C_a}{M_a} \langle T_a \rangle . \tag{7}$$

where the brackets $\langle \cdots \rangle$ indicate time averages; $\langle V_a^2 \rangle$ thus denotes the mean square velocity and $\langle T_a \rangle$ the average kinetic energy of mode a.

If one knows the time-average power inputs A_a and A_b to the two modes of Fig. 1, then one still cannot perform an energy balance analysis unless one can describe the time-average net power flow P_{ab} from mode a to mode b. It turns out, fortunately, that under some conditions that are often encountered in practice the net mode-to-mode power flow is proportional to the difference between the time-average modal kinetic energies; that is,

$$P_{ab} = \phi_{ab} (\langle T_a \rangle - \langle T_b \rangle) . \tag{8}$$

Equation (8) has been shown to hold, at least approximately, if (a) the coupling between the two modes is linear (giving rise to a linear differential equation), conservative (neither supplying nor dissipating mechanical energy), and light and/or purely springlike and/or gyroscopic, and (b) the forces acting on the two modes are uncorrelated and have spectra that are flat (compared to the systems admittance spectra) within the frequency band encompassed by the resonances of the coupled system.

The proportionality coefficient $\dot{\phi}_{ab}$ may be calculated if the coupling element is defined. For example, for coupling that may be represented in Fig. 1 by a spring of stiffness K_c, one finds

$$\phi_{ab} = \frac{2K_c^2 \, a_k / M_a M_b}{a_k \, a_c - (\omega_a^2 - \omega_b^2)^2} . \qquad (9a)$$

where

$$a_k = \frac{C_a}{M_a} + \frac{C_b}{M_b} .$$

$$a_c = \frac{C_a K_b + C_b K_a}{M_a M_b} . \qquad (9b)$$

$$\omega_a^2 = \frac{K_a + K_c}{M_a} .$$

and

$$\omega_b^2 = \frac{K_b + K_c}{M_b} .$$

One may show for any type of "loose" coupling (i.e., coupling that has relatively little effect on the average response of a mode to a force acting directly on it) which satisfies the aforementioned conditions, that

$$\dot{\phi}_{ab} \approx \frac{2C_a C_b}{\pi} \int_{-\infty}^{\infty} |Y_{ab}(\omega)|^2 \, d\omega , \qquad (10)$$

where Y_{ab} is the transfer admittance, that is, the ratio of the velocity (phasor) $V_a(\omega)$ of mode a to the force (phasor) $F_b(\omega)$ which acts on b to produce $V_a(\omega)$.

It is of interest to note that Eq. (8), Eq. (7), and an analogous relation pertaining to mode permit one to analyze the two coupled modes problem in terms of energies, and to visualize it in terms of a diagram like Fig. 2. One may also recognize that Fig. 2 is analogous to a diagram one may draw to represent the heat transfer between two systems; then $\langle T_a \rangle$ and $\langle T_b \rangle$ are analogous to the system temperatures, P_{ab} is analogous to the heat flow between the systems, A_a and A_b are analogous to heat supplied from sources, and D_a and D_b are analogous to heat rejected to sinks.

If one, for example, considers the mode a in absence of any coupling, then one may determine that $A_a = D_a$; that is, that the average power received by a mode is in the steady state equal to the average power dissipated by the
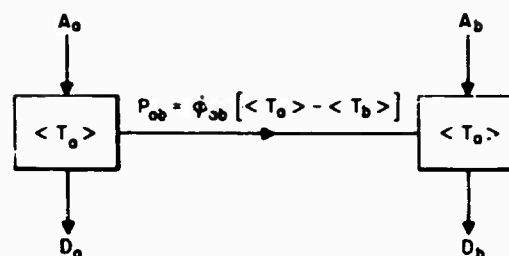
Fig. 2. Power flow diagram for two coupled modes

mode. In the absence of coupling (or for loose coupling) one may express the power received by mode a as

$$A_a \approx \pi S_a / M_a \qquad (11)$$

in terms of S_a, the value of the mean square spectral density (also called power spectral density) of the force F_a at and near the resonance of mode a. (S_a is again assumed to be a relatively flat function of frequency.)

By use of Eqs. (7) and (11) one may then directly arrive at the following expression for the steady state mean square velocity of an uncoupled mode:

$$\langle V_a^2 \rangle = \pi S_a M_a C_a . \qquad (12)$$

As one may visualize with the aid of Fig. 2, if mode b has no force acting on it directly ($A_b = 0$), then this mode receives power only through the coupling element. In the steady state this power must be equal to the power dissipated by mode b, so that if Eq. (8) holds, then

$$\dot{\phi}_{ab}(\langle T_a \rangle - \langle T_b \rangle) = \phi_{ab}\left[\frac{M_a}{2} \langle V_a^2 \rangle - \frac{M_b}{2} \langle V_b^2 \rangle \right]$$

$$= C_b \langle V_b^2 \rangle . \qquad (13)$$

From the foregoing relation one may readily determine that the velocity ratio between the two modes may be written as

$$\frac{\langle V_a^2 \rangle}{\langle V_b^2 \rangle} = \frac{2C_b + \phi_{ab} M_b}{\phi_{ab} M_a} \qquad (14)$$

Energy Analysis of Two Mode Sets

The previously discussed expression pertaining to power flow between two individual

44
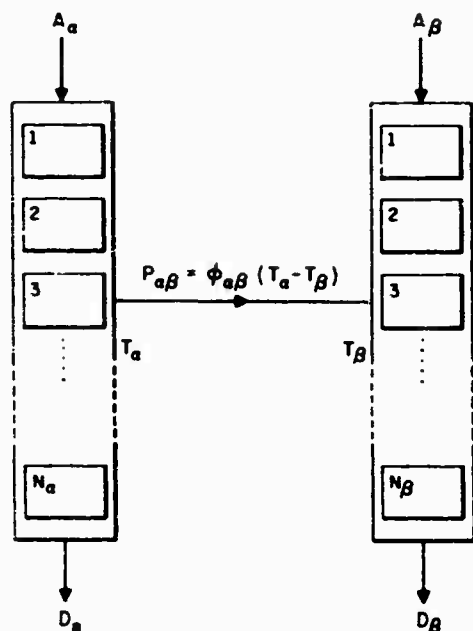
Fig. 3. Power flow diagram for two coupled sets of modes

modes may be extended to apply to the power flow between two sets of modes (Fig. 3), where, for example, the two sets of modes may be groups of modes of two different structures. One finds that the time average power flow $P_{\alpha\beta}$ from a mode set α to a mode set β may be written as

$$P_{\alpha\beta} = \phi_{\alpha\beta}(T_\alpha - T_\beta),\qquad (15)$$

analogously to Eq. (8). Here T_α represents the average kinetic energy per mode of the α set; thus, if T_{T_α} represents the total kinetic energy of all modes of the set, and if there are N_α modes in the set, then

$$T_\alpha = \frac{T_{T_\alpha}}{N_\alpha} = \frac{1}{N_\alpha} \sum_{j=1}^{N_\alpha} \langle T_j \rangle. \qquad (16)$$

A corresponding expression applies also for T_β, of course.

Equation (15) may be shown to hold if (a) the mode-to-mode power flow from all modes of the α set to all modes of the β set satisfies Eq. (8), and (b) either the mode-to-mode coupling is the same for all mode pairs composed of one of the α and one of the β modes, or all modes in a set have equal time-average kinetic energies. Equation (15) also applies for the ensemble average power flow from one mode set to another mode set of an ensemble, if (a) the first of the foregoing conditions is satisfied,

(b) the mode-to-mode coupling coefficients and modal kinetic energies are statistically independent, and (c) the modal kinetic energies in the ensemble average are uniformly distributed within a set. However, here T_α, T_β, and $\phi_{\alpha\beta}$ must be taken as the corresponding ensemble average parameters.

Under the aforementioned conditions the set-to-set coupling factor $\phi_{\alpha\beta}$ turns out to be the sum of all possible mode-to-mode coupling factors between the sets, or

$$\phi_{\alpha\beta} = \sum_{j=1}^{N_\alpha} \sum_{k=1}^{N_\beta} \phi_{\alpha j,\beta k} = N_\alpha N_\beta \phi_{\alpha a,\beta b}, \qquad (17)$$

where $\phi_{\alpha a,\beta b}$ denotes the average (over all mode pairs) of the mode-to-mode coupling factors and $\phi_{\alpha j,\beta k}$ denotes the factor pertaining to power from the jth mode of the α set to the kth mode of the β set.

The total power D_α dissipated by mode set α is equal to the sum of all the dissipation contributions of the individual modes. Therefore,

$$D_\alpha = \sum_{j=1}^{N_\alpha} C_j \langle V_j^2 \rangle = C_\alpha \langle V_\alpha^2 \rangle, \qquad (18)$$

where $\langle V_\alpha^2 \rangle$ represents the total mean square velocity of system α due to the N_α modes; according to Eq. (6), $\langle V_\alpha^2 \rangle$ is equal to the sum of all the individual modal velocities, since all of the α modes belong to the same elastic system. C_α is an "effective" viscous damping coefficient for the whole set α and may be seen to obey

$$C_\alpha = \frac{\Sigma C_j \langle V_j^2 \rangle}{\Sigma \langle V_j^2 \rangle} = \frac{\Sigma C_j \langle T_j \rangle}{T_{T_\alpha}}, \qquad (19)$$

where all summations are implied to extend from $j=1$ to $j=N_\alpha$. The second form of Eq. (19) follows from Eq. (5) and from the equality of all modal masses in a set of modes of the same system, as evident from Eq. (2).

Loss Factors

It is useful to restate some of the previously given results by introducing loss factors as measures of energy dissipation and conduction. Loss factors may be defined in terms of energy quantities and thus have greater generality than viscous damping coefficients. In addition, use of loss factors for both dissipation and conduction of energy serves to draw attention

45

to the fact that both of these mechanisms may have the same effect on a system.

The loss factor is related to the viscous damping coefficient C and the critical damping coefficient c_c as

$$\eta = C/M\omega_a = C/\sqrt{KM} = 2C/c_c .$$

The loss factor η of a mode a oscillating in steady state may be expressed as

$$\eta_a = D_a/2\omega_a \langle T_a \rangle . \qquad (20)$$

where D_a denotes the time-average power dissipated by the system, $\langle T_a \rangle$ the time-average kinetic energy of the mode, and ω_a the modal frequency [3]. An expression like Eq. (20) may also be applied to a set of modes. The loss factor η_a of a set a may be written as

$$\eta_a \approx D_a/2\omega_o T_{Ta} \approx \Sigma\eta_j \langle T_j \rangle/\Sigma\langle T_j \rangle . \qquad (21)$$

where ω_o here represents the center frequency of a band which encompasses all modal frequencies of the set, and where the summations on j extend from 1 to N_a. The right-hand expression of Eq. (21), which is similar to Eq. (19) and shows that η_a is a weighted average of the modal loss factors, follows from Eqs. (16), (18), and (20).

"Coupling loss factors" η_{ab} and $\eta_{\alpha\beta}$, which are indicative of power flow in the same way that the loss factors of Eqs. (20) and (21) are indicative of power dissipation, may be defined by expressions which are the same as Eqs. (20) and (21), except that D_a and D_a are replaced by

$$P_{ab}\Big|_{\langle T_b \rangle=0} = \phi_{\alpha\beta}\langle T_a \rangle \quad \text{and} \quad P_{\alpha\beta}\Big|_{T_{\beta=0}} = \phi_{\alpha\beta}T_a .$$

From the appropriately modified Eq. (21) and from an analogous expression pertaining to the mode set β, one finds that the coupling loss factor $\eta_{\alpha\beta}$ (which refers to power flow from set α to set β) and the loss factor $\eta_{\beta\alpha}$ (which refers to power flow from the β to the α set) obey

$$\eta_{\alpha\beta} N_\alpha = \eta_{\beta\alpha} N_\beta = \phi_{\alpha\beta}/2\omega_o . \qquad (22)$$

The usefulness of this notation will become apparent in the illustrations which follow.

Modal Densities

One usually studies the interactions of elastic systems on a band-by-band basis by

determining the power flow from modes of one system which have their resonances in a given frequency band to a set of modes of another system which have their resonances in the same band. One may in general choose any convenient bandwidth, and one may often wish to use different bandwidths for different calculations. The number of modes which fall within the various sets depends on the bandwidths one chooses, so that it is useful to introduce the concept of modal density, in terms of which the dependence of some of the previous results on bandwidth can be stated more explicitly.

The modal density of an elastic system is defined as the average number of modes per unit frequency interval. If a system exhibits N_a modes whose resonances fall within a frequency interval $\Delta\omega$, then the modal density of the system at the center frequency ω of the interval is defined as

$$n_a(\omega) = N_a/\Delta\omega ,$$
$$n_a(f) = N_a/2\pi\Delta f . \qquad (23)$$

The modal densities of systems may be determined from their "frequency equations," i.e., from the equations which give the system resonance frequencies as a function of the system parameters. For simple systems these calculations may be carried out without great difficulty [4].

Table 1 lists the modal densities of some uniform elastic systems, obtained largely from Smith and Lyon [4] and from related calculations. The expressions listed in the table apply strictly only for frequencies considerably above the system fundamental (by perhaps at least two octaves), where boundary conditions have no important effects on the natural frequencies; however, these expressions generally also provide reasonable estimates for the modal densities at frequencies only slightly above the fundamental.

The modal density of a composite system is approximately equal to the sum of the modal densities of the component systems. Thus, for example, the modal density of a plate with attached beams is roughly equal to the modal density of the plate by itself, plus the modal densities of all of the beams by themselves.

APPLICATIONS TO SIMPLE SYSTEMS

Two Coupled Plates

Consider two coupled systems, as represented by two irregularly shaped plates, joined

46

TABLE 1
Modal Densities of Some Uniform Systems

System	Motion	Modal Density, $n(\omega)$	Auxiliary Expressions
String	Lateral	$L/\pi c_s$	$c_s = \sqrt{T/\rho A}$
Shaft, beam	Torsion	$L/\pi c_T$	$c_T = \sqrt{Gk/\rho J}$
Shaft, beam	Longitudinal	$L/\pi c_\ell$	$c_\ell = \sqrt{E/\rho}$
Beam	Flexure	$L/2\pi \, (\omega \kappa_b c_\ell)^{-1/2}$	$\kappa_b c_\ell = \sqrt{EI/\rho A}$
Membrane	Lateral	$A_s \, \omega/2\pi c_m^2$	$c_m = \sqrt{S/\rho h}$
Plate	Flexure	$A_s/4\pi \, \kappa_p c_\ell$	$\kappa_p c_\ell = \sqrt{D/\rho h} = \sqrt{Eh^2/12\rho(1-\nu^2)}$
Room (acoustic volume)	Sound (compression)	$V\omega^2/2\pi^2 \, c_a^3$	
Cylindrical shells [5]	Flexure	$\begin{cases} \approx n_p & \text{for } \omega/\omega_r > 1 \\ \approx n_p(\omega/\omega_r)^{2/3} & \text{for } \omega/\omega_r < 1 \end{cases}$	$\omega_r = c_\ell/a$ $n_p = A_s/4\pi \, \kappa_p c_\ell$
Doubly curved shells	Flexure	Expressions are complex, see Ref. 6	

Symbol Definitions

A = cross-sectional area

A_s = surface area

a = mean radius of cylindrical shell

c_a = acoustic wave velocity

c_ℓ = longitudinal wave velocity

c_m = membrane wave velocity

c_s = string wave velocity

c_T = torsional wave velocity

D = plate rigidity

E = Young's modulus

G = shear modulus

h = thickness

I = centroidal moment of inertia of A

J = polar moment of inertia of A

K = torsional constant of A

L = length

S = membrane tension force/unit edge length

T = string tension force

V = volume

κ_b = radius of gyration of A

κ_p = radius of gyration of plate cross section

ν = Poisson's ratio

ω = frequency (rad/time)

ρ = material density

by a reinforcing beam (Fig. 4). If plate α is exposed to a broadband excitation of bandwidth $\Delta\omega$ (considerably above the plate fundamental) so that it vibrates a given amount, how much will plate β vibrate? This is clearly a difficult (or at least a tedious) problem to solve by classical means. However, one may obtain an estimate very easily and rapidly by the statistical energy approach.

The beam of Fig. 4 is likely to result in loose coupling between the modes of plate α (which have their resonances in the band of interest) and the corresponding modes of plate β. If one assumes all modes of a set to be uniformly excited, so that the previously outlined concepts apply, one may write an energy balance for set β as
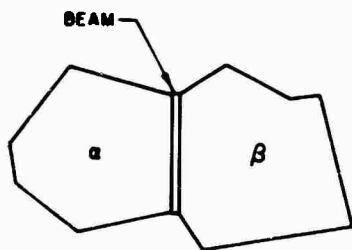
Fig. 4. Two coupled plates

$$\phi_{\alpha\beta}(T_\alpha - T_\beta) = D_\beta = \eta_\beta 2\omega_o N_\beta T_\beta . \qquad (24)$$

and from it determine

$$\frac{T_\beta}{T_\alpha} = \frac{\phi_{\alpha\beta}}{\phi_{\alpha\beta} + 2\omega_o \eta_\beta N_\beta} = \frac{\eta_{\beta\alpha}}{\eta_{\beta\alpha} + \eta_\beta} . \qquad (25)$$

From Eqs. (16), (23), and the expression of Table 1 for the modal density of plates one finds that if the plates are made of the same material, then

$$\frac{T_\beta}{T_\alpha} = \frac{n_\alpha M_\beta \langle V_\beta^2 \rangle}{n_\beta M_\alpha \langle V_\alpha^2 \rangle} \frac{A_{s\alpha} h_\beta^2 \langle V_\beta^2 \rangle}{A_{s\beta} h_\alpha^2 \langle V_\alpha^2 \rangle} , \qquad (26)$$

where h and A_s denote the thickness and area, respectively, of the plate indicated by the subscript.

By combining Eqs. (25) and (26), one may obtain an expression for the ratio of the mean square velocities in terms of only the gross geometric parameters of the two plates, the dissipation loss factor η_β, and the coupling loss factor $\eta_{\alpha\beta}$. The loss factor η_β generally can be estimated from available data, or it can be determined from some simple measurements, e.g., of the rate of decay of free vibrations of plate β by itself. As yet there is available no adequate means for estimating the coupling loss factor $\eta_{\beta\alpha}$. However, $\eta_{\beta\alpha} + \eta_\alpha$ may also be deduced from some simple measurements, e.g., of the rate of decay of free vibrations of plate β when it is attached to plate α as in Fig. 4. (Note that the coupling loss factor $\eta_{\beta\alpha}$ which appears in Eq. (25) refers to power flow from plate β to plate α, but power flows from α to β when α is excited.)

It is of interest to note that the aforementioned result reduces to a particularly simple one if the plate β is lightly damped ($\eta_\beta \ll \eta_{\beta\alpha}$), so that the right-hand side of Eq. (5) reduces to unity.

The grouping of the loss factor terms appearing in Eq. (25) permits one also to make some observations concerning the effectiveness of adding damping to the indirectly excited plate β. If the damping of the β plate is small initially, that is, if $\eta_\beta \ll \eta_{\beta\alpha}$, then added damping will reduce the system vibrations only if this added damping is large enough so that the resulting η_β is no longer insignificant compared to $\eta_{\beta\alpha}$. On the other hand, if $\eta_\beta \gg \eta_{\beta\alpha}$, then $\langle V_\beta^2 \rangle$ varies inversely as η_β and any increase in η_β will result in a corresponding decrease in $\langle V_\beta^2 \rangle$.

From an energy balance on the directly excited plate α one may determine that

$$\frac{A_\alpha}{2\omega_o T_\alpha N_\alpha} \equiv \eta_{\alpha_{app}} = \eta_\alpha + \frac{\eta_{\alpha\beta} \eta_\beta}{\eta_{\beta\alpha} + \eta_\beta} . \qquad (27)$$

The "apparent loss factor" $\eta_{\alpha_{app}}$ introduced in the foregoing equation corresponds to the value of the dissipation loss factor which one would ascribe to set α (on the basis of measurements performed on set α) if one were not aware that this set is coupled to set β. It is evident from Eq. (27) that the apparent loss factor $\eta_{\alpha_{app}}$ is never smaller than the actual dissipation loss factor η_α. Thus, if one is unaware that a system whose loss factor one is measuring is coupled to another system, then one always obtains a loss factor value which is too large, an "obvious" result. The error is insignificant, however, if the coupling is poor ($\eta_{\alpha\beta}, \eta_{\beta\alpha} \approx 0$) and/or if the coupled set is relatively lossless ($\eta_\beta \ll \eta_\alpha$).

From Eq. (27) one may also deduce that the response $\langle V_\alpha^2 \rangle$ of plate α to a given excitation A_α is not controlled by the actual dissipation loss factor η_α of that plate, but rather by the apparent loss factor $\eta_{\alpha_{app}}$.

Interaction of Sound and Structures

The statistical energy approach may also be applied to cases where one of the elastic systems considered is an acoustic volume. Thus, the approach may be used for estimating the sound field produced by structural vibrations or for predicting the structural vibrations induced by sound.

Consider the case where a structure S is directly excited by random forces acting on it, and where these structural vibrations produce noise in a room R in which the structure is located. Here the structural modes in a

frequency band of interest correspond to a directly excited mode set s, the modes of the acoustic space R correspond to the indirectly excited set R.

The total energy E_R in a diffuse acoustic field within a fluid volume V in a frequency band $\Delta\omega$ is related to the mean square acoustic pressure $\langle \bar{p}^2 \rangle$ measured in the same frequency band as

$$E_R = \langle \bar{p}^2 \rangle V / \rho_a c_a^2 . \qquad (28)$$

where ρ_a denotes the density and c_a the sound velocity of the fluid. This total energy is, on the average, half potential and half kinetic, hence the average total kinetic energy T_{TR} is one half of the total. The average modal kinetic energy T_R may be obtained by dividing T_{TR} by $n_R \times \Delta\omega$, the number of modes in the interval. With the modal density expression given in Table 1 for acoustic volumes, one finds the average kinetic energy of an acoustic mode of a room to be given by

$$T_R = \frac{E_R}{2 n_R \Delta\omega} = \frac{\pi^2 c_a}{\rho_a \omega^2} \frac{\langle \bar{p}^2 \rangle}{\Delta\omega} . \qquad (29)$$

If one applies Eq. (16) to the structure under consideration and replaces the number of modes N_S by $n_s \times \Delta\omega$, then one finds that the average kinetic energy of a structural mode may be written

$$T_S = \frac{M_s \langle V_s^2 \rangle}{2 n_s \times \Delta\omega} = \frac{M_s \langle a_s^2 \rangle}{2 \omega^2 n_s \Delta\omega} , \qquad (30)$$

where $\langle V_s^2 \rangle$ represents the mean square velocity and $\langle a_s^2 \rangle = \omega^2 \langle V_s^2 \rangle$ the mean square acceleration of the structure, as measured in the frequency band $\Delta\omega$ with center frequency ω. From an energy balance on the indirectly excited system, i.e., the room, one may then obtain

$$\frac{\langle \bar{p}^2 \rangle}{\langle a_s^2 \rangle} = \frac{\rho_a M_s}{2\pi^2 c_a n_s} \frac{\eta_{RS}}{\eta_{RS} + \eta_R} . \qquad (31)$$

In most practical cases the room-to-structure coupling loss factor will be much smaller than the dissipation loss factor of the room. Then, if one uses Eq. (22) to replace η_{RS} by $\eta_{SR} n_s / n_R$ and replaces the loss factor η_{SR} by an equivalent viscous coefficient C_{RS}, one obtains

$$\frac{\langle \bar{p}^2 \rangle}{\langle a_s^2 \rangle} = \frac{\rho_a C_{SR}}{2\pi^2 c_a \omega_0 n_R \eta_R} = \frac{\rho_a c_a^2 C_{SR}}{V \omega^3 \eta_R} . \qquad (32)$$

where the last form is obtained by substituting for n_R the appropriate expression from Table 1. The structure-to-room coupling coefficient C_{SR} may be shown to be the same as the rather well-known acoustic "radiation resistance" of the structure, which may be estimated reasonably readily [4].

One may also readily develop an expression which describes the response of a structure to sound. For the case where sound in an acoustic enclosure excites a structure, one may write an energy balance for the (here indirectly excited) structure, and from it determine that

$$\frac{\langle a_s^2 \rangle}{\langle \bar{p}^2 \rangle} = 2\pi^2 \frac{c_a n_s}{\rho_a M_s} \frac{\eta_{SR}}{\eta_{SR} + \eta_S} . \qquad (33)$$

PRACTICAL APPLICATIONS

Rationale

In applying "statistical energy analysis" one takes advantage of properties which largely are peculiar to high-frequency random vibrations. Calculations involving structural and excitation details are avoided by averaging over possible excitation and measurement positions, since at high frequencies the vibration of uniform structural regions is usually insensitive to details of the excitation or measurement positions. By considering a complex structure as composed of a number of simple, lightly coupled substructures, one may often study the vibrations of each substructure in terms of the vibration characteristics of that substructure considered as completely isolated from adjacent substructures; the power flow between the substructures then can be calculated from simple power balance relations similar to Eq. (24).

Coupled structures may be shown to exhibit a certain tendency toward assuming equal average modal energies, and one often finds it advantageous to use this "equipartition" tendency in estimating vibration distributions in composite structures. Since the coupling and dissipation loss factors are always positive, one may deduce from Eq. (25), for example, that the average modal energy T_β of the indirectly excited system is always less than that of the directly excited system T_α. The two modal energies are essentially equal in those cases where the loss factor η_β of the indirectly excited system is much smaller than the coupling loss factor $\eta_{\beta\alpha}$. One may use the fact that $T_\beta \leq T_\alpha$ to determine a simple upper bound to the vibration levels that result in various

components of a complex structure due to localized random excitation.

Vibration Responses of Space Vehicles

The statistical energy approach has been applied to a number of problems involving vibration response and transmission in space vehicles. The approach has proven particularly useful for evaluating the relative importances of various excitation sources and transmission paths. For example, statistical energy calculations have shown, in agreement with recent experimental work, that over a significant frequency range turbulent boundary layer excitation is more efficient in exciting mechanical vibrations than is acoustic excitation [7]. The use of the statistical energy approach to calculate the response of a launch vehicle to acoustic and aerodynamic excitation sources is discussed by Chandiramani and Lyon [8].

Figure 5 shows a schematic diagram of the OGO spacecraft and the energy paths that have been considered in calculating the vibration distributions that result from the action of the exterior acoustic field [9]. The "acoustic path" involves the exterior acoustic space, shroud, interior acoustic space, and spacecraft panels; the "mechanical path" involves the exterior acoustic space, shroud, ring frame, mounting trusses, and spacecraft panels. Calculations [9] predict 10 to 20 db greater vibration levels due to transmission via the acoustic path than via the mechanical path. An experimental investigation of vibration transmission in the OGO spacecraft is in progress.

The relative importance of various vibration transmission paths in the Surveyor spacecraft are currently under study. As indicated in Fig. 6, this study considers a direct acoustic path from the interior acoustic space to compartment A, in addition to a mechanical path which involves transmission from the adapter to the spacecraft trusses and then to compartment A. The adapter is excited by three sources: the interior acoustic space, the vented acoustic space, and the tank dome.

The statistical energy calculations indicate that high-frequency vibration transmission in a wide class of complex structures depends largely on a few characteristic properties of the structure, such as length of transmission path, mass of typical elements, average modal density, and internal damping. Some preliminary

COMPONENTS

1 Exterior Acoustic Space
2 Shroud
3 Interior Acoustic Space
4 Spacecraft Panels
5 Ring Frame
6 Mounting Trusses

TRANSMISSION PATHS:

Fig. 5. Vibration transmission in the OGO spacecraft

COMPONENTS

1 Interior Acoustic Space
2 Compartment A
3 Adapter
4 Spacecraft Trusses
5 Vented Acoustic Space
6 Tank Dome
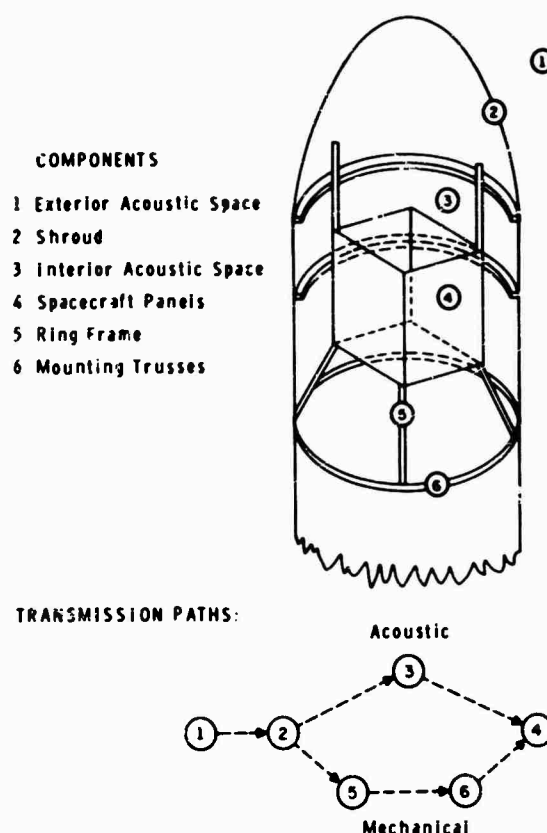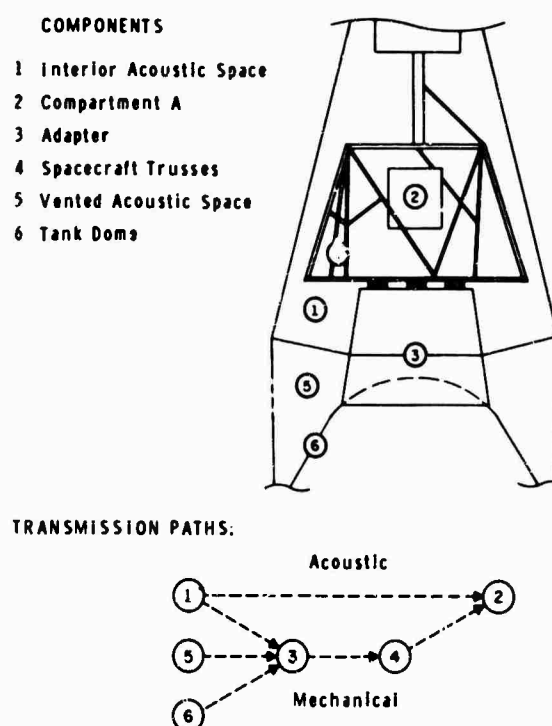
TRANSMISSION PATHS:

Fig. 6. Vibration transmission in the Surveyor spacecraft

58

work has been done, which indicates that vibration transfer functions experimentally determined on Ranger, Mariner and Surveyor spacecraft can be reduced to a common form by scaling the frequency axis with respect to a transmission length [10].

Implications Relative to High-Frequency Vibration Testing

In present practice one generally attempts to obtain very stiff test fixtures to set the first fixture resonance at a relatively high frequency. However, the first bending resonance of conventional fixtures often occurs within the frequency range of interest in random vibration tests. Fixture resonances result in amplification of the vibration level, for which one usually must compensate by using expensive equalization equipment) and in spatial variations in the fixture vibration, which complicate the problem of excitation control.

As a possible means of avoiding the problems associated with stiff test fixtures, the statistical energy view suggests the use of light, flexible, multi-modal test fixtures. Such a fixture would have many resonances in any measurement bandwidth, and would result in a vibration field quite uniformly distributed over the fixture. (It has been demonstrated [11] that the spatial variation in mean square response of a structure excited with noise is inversely proportional to the number of structural modes which contribute to the response. Therefore, whereas the spatial variation in the response of a very rigid fixture vibrating in a low mode may be quite large, the vibration field of a thin panel-like fixture responding in many modes generally is quite uniform.)

Multi-modal test fixtures also have the added advantage that they usually can simulate the impedance of typical aerospace mounting configurations much better than conventional fixtures. Conventional rigid test fixtures provide a coherent excitation source and, therefore, severely overtest equipment which in practice is attached to lightweight structure and subjected to an incoherent excitation source. Some preliminary tests with multi-modal test fixtures have been rather encouraging.

By use of the multi-modal test fixture approach one also may avoid the conceptual,

instrumentation, and computation problems associated with interface vibration measurements and specifications. One merely needs to use in-flight measurements of the reverberant vibration on multi-modal structures to set the reverberant test levels on the multi-modal fixtures. This method of specifying the vibration test levels is analogous to specifying the sound pressure level for acoustic tests in a reverberant chamber.

CONCLUDING REMARKS

The ideas which underlie the statistical energy analysis approach have been summarized to give the reader some insight into the range of validity and applicability of this potentially very useful approach. Extended discussions of these ideas and a more complete list of references appears in Ref. 1.

A number of cases have been indicated where the statistical energy analysis approach has led to a better qualitative understanding of this behavior of coupled systems. Practical applications of the approach to the prediction of vibration levels and to the comparison of the relative importances of parallel vibration transmission paths have also been discussed.

Statistical energy analysis provides one with a simple and powerful means for obtaining a qualitative understanding and quantitative estimates of the most important aspects of multi-modal random vibrations of complex structural systems. At present the lack of information on power-flow coupling coefficients often limits the validity of the quantitative response estimates one desires to make for practical systems, but related further work is in progress.

ACKNOWLEDGMENTS

REFERENCES

1. E. E. Ungar, "Fundamentals of Statistical Energy Analysis of Vibrating Systems," AFFDL TR 66-52, Apr. 1966

2. E. E. Ungar, "Statistical Energy Analysis of Vibrating Systems," submitted for publication in Trans. Am. Soc. Mech. Eng.

3. E. E. Ungar and E. M. Kerwin, Jr., "Loss Factors of Viscoelastic Systems in Terms of Energy Concepts," J. Acoust. Soc. Am., Vol. 34, pp. 454-457, July 1962

4. P. W. Smith, Jr., and R. H. Lyon, "Sound and Structural Vibration," NASA CR-160, Mar. 1965

5. M. Heckl, "Vibrations of Point-Driven Cylindrical Shells," J. Acoust. Soc. Am., Vol. 34, pp. 1553-1557, Oct. 1962

6. V. V. Bolotin, "On the Density of Distributions of Natural Frequencies of Thin Elastic Shells," J. Appl. Math. and Mech., Vol. 27, No. 2, pp. 538-543; transl. from Soviet PMM 27, No. 2, pp. 362-364, 1963

7. P. A. Franken and R. H. Lyon, "Energy-Method Estimates of Response to Inflight Dynamic Loads," 1966 Ann. Tech. Meeting, IES

8. K. L. Chandiramani and R. H. Lyon, "Response of Structural Components of a Launch Vehicle to Inflight Acoustic and Aerodynamic Environments," Shock and Vibration Bull. No. 36, Part 5, 1967

9. J. E. Manning, R. H. Lyon, and T. D. Scharton, "An Analytical Procedure for Determining the Random Load Acting on a Spacecraft Due to a Primary Random Load Acting on an Exterior Structure," Bolt Beranek and Newman Rept. 1431, Contract No. NAS5-9601, July 1966

10. T. D. Scharton and P. A. Franken, "Cascade Models of Vibration Transmission in Flight Vehicles," to be presented at the November 1966 meeting of the Acoust. Soc. Am.

11. R. H. Lyon et al., "Studies of Random Vibration of Coupled Structures," Bolt Beranek and Newman Rept. 967, Appendix I, p. 28, Eq. 3.12, 1965

BIBLIOGRAPHY

Franken, P. A., T. H. Mack, and T. D. Scharton, "Comparison of Mariner Assembly-Level and Spacecraft-Level Vibration Tests," Shock and Vibration Bull. No. 36, Part 3, 1967

Karnopp, D. C., "Basic Theory of Random Vibration," Chap. 1 of Random Vibration,

Vol. 2, ed. by S. H. Crandall, MIT Press, Cambridge, 1963

Scharton, T. D., "Random Vibration of Coupled Oscillators and Coupled Structures," Doctoral Thesis, MIT, Oct. 1965

DISCUSSION

Mr. Bookstein (Jet Propulsion Laboratory): Have you made any comparison between your method and the so-called stone-age method for computing responses?

Mr. Ungar: No. The problems we have attempted by this method are completely impossible by any other method. So ours is the best.

Mr. Kaplan (General Electric Co.): It appears that you still have to go through the cumbersome stone-age procedures, namely, getting the modes of vibration of the subsystems or the portions of the structure.

Mr. Ungar: I was not careful enough to point out the savings which we make. We do not have to determine the mode shapes. All we need to know is the average number of modes per frequency interval and this is a very dirty number which depends only on gross system properties.

Mr. Kaplan: But here again, for an example such as you postulated, a complicated spacecraft structure, there would be resonances within the various higher frequency bands that might be attributed to local breathing, secondary resonances on the equipment support structure, and the like. Therefore, wouldn't you

still have to know the content within each of the frequency bands to associate the various phenomena in terms of what is happening physically, and wouldn't you still need the mode shapes?

Mr. Ungar: We do not need to know the mode shapes. We need to know only the type and number of modes.

Mr. Lyon (Bolt Beranek and Newman): A few of the more difficult modes to calculate, for example, in-plane motions or extensional modes of the structure, may be missed by the simpler ways of counting the number of modes in a band. Fortunately, there is a tendency for an equal amount of energy to exist in all modes. Therefore, if you miss 5 percent of them, you have only missed 5 percent of the energy or 2 percent of the motion.

Mr. Smith (Bell Aerosystems Co.): Classical or statistical, you are still faced with the last step, aren't you? If you are handling a fatigue problem, you want stresses in the structure, not modal displacement. Neither the classical attack, with the shortcomings you outlined, nor the statistical will indicate whether you have a well or a badly designed structure.

Mr. Ungar: That is certainly true to some extent. We are, incidentally, working on an application or extension of this method in which we calculate, from the mean square response obtained, the maximum stresses near the edges. Incidentally, we are doing this by applying the dynamic edge condition principle discovered by Bolotin. I realize this is only a partial answer to your question, but it is the best I can give.

Mr. Crocker (LTV Research Center): Can you tell me how good your method is at low frequencies? I suspect that the classical method might be more accurate for the lower modes.

Mr. Ungar: If you can use the lowest modes, you should. The method is well established. However, to do a reasonable analysis involving the lowest 20 modes, you need to deal with the lowest 14 modes and a 40×40 matrix,

and so on up. You very quickly run out of computer space. If you have a program and you want to worry only about the lowest three modes, by all means use classical methods.

Mr. Crocker: I did a problem by computer where we took into account 400 modes. It would have taken me 20 years by hand; the computer did it in about 20 minutes. The method seems fairly accurate at low and high frequencies, and is quite quick once the program is set up.

Mr. Ungar: I am glad you went through this stone-piling procedure. I recently saw some similar calculations where people calculate transmissibilities of structures when they were really only interested in the transmissibility peaks at reasonably high frequencies. So they did something very similar, based on an assumed value of damping. I think if you had assumed the value of damping, using the simple method, you would have had the answer, without the use of a computer, in 1/10th the time, perhaps at half the cost.

Mr. Himelblau (North American Aviation): I would like to come to your defense because I believe it is very difficult to get any kind of a computer solution for the higher modes that will adequately describe the modes and the modal responses. If you are averaging over several modes, the statistical energy method is very effective for problems not particularly susceptible to a narrow-band type of failure. For example, whether fatigue occurs in the 40th or the 43rd mode generally does not determine that a different lifetime exists. However, in certain problems involving subsequent narrow-band oscillators which provide an input to a particularly narrow-band resonant structure, you would not want to know what would happen in the 43rd mode. Taking the average response over a range involving, say, the 40th to the 50th mode, would not give assurance that your design was adequate. Any comment on that?

Mr. Ungar: You covered a lot of ground, and I think I agree with you in just about everything, particularly in coming to our defense.

* * *

DYNAMIC ANALYSIS OF CONTINUUM BODIES
BY DIRECT STIFFNESS METHOD

W. E. Baker
Rocketdyne
Division of North American Aviation
McGregor, Texas

and

J. M. Daly
Arde Engineering Company
Asheville, North Carolina

Problems frequently encountered in the field of structural dynamics require an analysis of structures having complex geometry and non-homogeneous materials. A method is presented for dynamic analysis of complex continuum bodies by extension of the finite element method, to circumvent the severe oversimplification often required in treating these problems by classical methods. Axisymmetric and plane stress-strain formulations, with the associated computer programs, have been developed. The analysis was developed using viscous damping and the assumption that classical modes exist. The undamped frequencies and mode shapes are first calculated, then used to uncouple the damped equations of motion by diagonalization of the mass, damping and stiffness matrices. Thus, single-degree-of-freedom modal response equations are formed and solved for the response contribution of each mode. Through superposition of each modal contribution coupled with a transformation back to the original coordinate system, the response to an arbitrary forcing function is determined. Theoretical development, correlation studies, applications and some of the limitations of the analysis are discussed.

W. E. Baker

INTRODUCTION AND SUMMARY

In the field of structural dynamics, problems frequently encountered require an analysis of structures having complex geometry and non-homogeneous material properties. This is particularly true in the solid rocket motor field, where the propellant grains often have irregular internal surfaces. Classical methods of analysis are somewhat limited, particularly where irregular geometries and nonhomogeneous materials are involved; often severe over-simplifications are required to obtain classical solutions.

Recent achievements in finite element methods, accompanying the continuing advances in speed and capacity of digital computers, have enhanced the scope and detail practical in structural analysis. The finite element method, which has been found to be a powerful and versatile tool in the static analysis of complex structures, is being extended into the field of dynamics to allow a whole new realm of dynamic problems to be solved at minimal cost. Some of the problems that may be solved are:

1. Dynamic elastic analysis of thick-walled vessels, including spheres, cylinders and general axisymmetric shapes. Both longitudinal and radial modes may be analyzed.

2. Plane stress and plane strain analyses of arbitrary configuration and material property

55

distribution, subjected to transverse dynamic loading.

3. Analysis of elastic half spaces in which pressure waves emanate radially from a point source acting on the surface.

4. Longitudinal waves in rods of varying nonuniform cross section.

5. Analysis of circular plates of arying nonuniform general thickness subjected to axisymmetric loading.

A major portion of the dynamic analysis, the stiffness matrix, had already been formulated in the development of the static analysis [1-4]. A recent study has extended the two-dimensional plane stress finite element method to include dynamic effects [5]; and at Rocketdyne the method has been extended to axisymmetric bodies. The extension of the finite element method to dynamic analysis required the development of a mass matrix. Initially, a lumped mass method was used, but later a displacement consistent mass matrix suggested by Archer [6] was developed to improve the accuracy of the program. Comparisons of the two mass expressions showed that the consistent mass method generally provided greater accuracy, especially in the higher modes.

With the computer programs developed, a large number of sample problems have been solved, the majority of which involve bodies of regular shapes such as spheres, cylinders, and thick plates. The accuracy of the method is shown by comparison of the calculated natural frequencies and mode shapes with results available from experiments and classical theoretical solutions. Agreement was very good, especially in the lower modes.

THEORETICAL PROCEDURE

Direct Stiffness Method

Details of the development of the stiffness matrix for a solid body are not presented here, except to the extent necessary for a general introduction to the concept; the missing details may be found in Refs. 1 through 4. Due to the similarity between the plane stress and axisymmetric formulation, only the axisymmetric case will be discussed.

The finite element concept is the idealization of an actual continuum body as an assemblage of discrete elements (Fig. 1) connected at their nodal points. The basic element is

triangular in cross section, as shown in Fig. 2. For compatibility to be maintained at the edge of the elements, linear displacement functions were assumed:

$$u(r, z) = a + br + cz,$$

and   (1)

$$v(r, z) = d + er + fz.$$

By assuming the displacement functions and knowing the strain-displacement and the stress-strain relations, the energy function may be calculated for the element. The element stiffness coefficients are then obtained by minimization of the energy function. The coefficients relate nodal displacements to nodal forces; for a triangle having six degrees of freedom, a 6×6 element stiffness matrix is formed.
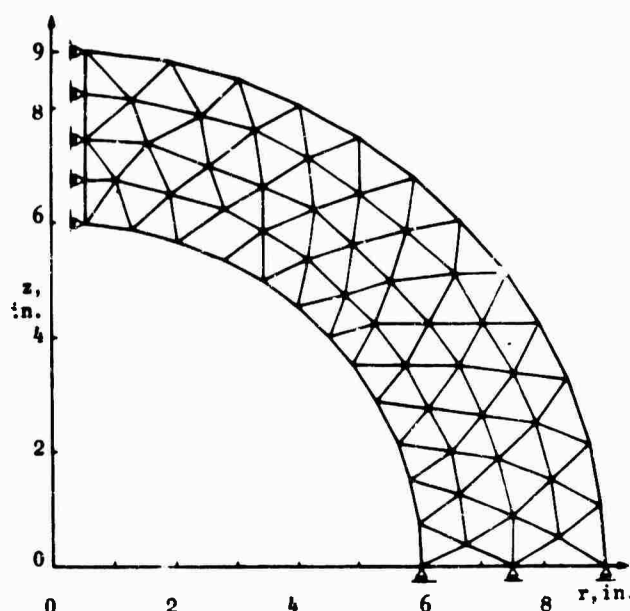
Fig. 1. Typical axisymmetric model

The complete assembly stiffness matrix is then formed by superposition of the appropriate stiffness coefficients of the elements connecting each nodal point, and the matrix will be equal in size to twice the number of nodal points. Boundary conditions that impose displacement constraints are accounted for by removal of appropriate rows and columns in the matrix. The assembly stiffness matrix relates the nodal forces to nodal displacements and the relationship expressed in matrix form is

$$\{F\} = [K]\{u\}.$$ (2)

56

(a) Element for the plane stress
or plane strain case

(b) Element for the axi-
symmetric case

Fig. 2. Finite elements used in dynamic
stiffness method

Dynamic Analysis

The equations of motion in a damped finite element system may be expressed in matrix form as

$$[M]\{\ddot{u}\} + [C]\{\dot{u}\} + [K]\{u\} = \{F(t)\} . \quad (3)$$

where

  K is the nodal stiffness matrix as described in the previous section,

  $[M]$ is the mass matrix,

  $[C]$ is the equivalent viscous damping matrix, and

  $\{F(t)\}$ is the dynamic force vector.

The mass matrix used in these programs is defined by one of the following methods: (a) one-third of the mass of each element is lumped at each of its nodal points, or (b) mass distribution is based on the assumed displacement shape of the element. The displacement-consistent mass matrix (method b) will be discussed later.
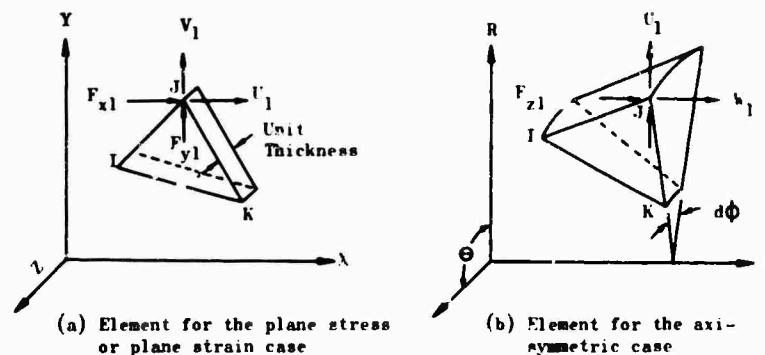
The general procedure followed in the method presented in this paper is (a) to solve the characteristic equation of an undamped system for the natural frequencies and mode shapes, and (b) to evaluate the forced dynamic response by mode superposition. The eigenvectors of the characteristic equation are used to form a transformation matrix that will uncouple the equations of motion, forming single-degree-of-freedom modal response equations. These equations are then solved for the response

contribution of each mode; and, through superposition of the mode contributions combined with a transformation back to the original coordinate system, the structural response is calculated.

The method used to decouple the equations of motion required the assumption of the existence of classical modes. This assumption requires the damping matrix to be diagonalized by the same transformation that diagonalizes the mass and stiffness matrix. In general, this is not entirely true for many practical problems, and the error introduced remains to be proven. Another approximation which may introduce error is the use of only the first 20 modes to evaluate the transient response plus the loss in accuracy in calculating some of the higher mode shapes.

The effective forcing function is determined using the assumption that all displacement constrained nodal points are rigidly attached to the body supplying the external force to the system. Thus, the effective force becomes the difference of the applied external force and the resulting internal force. No provision has been made to provide for absolute fixity of a nodal point.

Displacement Consistent Mass Matrix

It has been shown by Archer [6] that improved accuracy in dynamic analysis may be attained by a mass distribution consistent with the assumed element displacement function. Because of computer storage limitation, it was of interest to develop a method whereby accuracy could be improved in a manner other than

57

by increasing the number of elements used to define a structure. Therefore, a mass matrix consistent with the displacement field within the element was developed. The resulting element mass matrix is similar to the element stiffness matrix. Use of the consistent mass method required some additional matrix manipulation and was somewhat of a disappointment in that it required a prohibitive amount of computer storage space, thus limiting the grid size. Improvements in frequency and mode shapes were not sufficient to warrant use of the consistent mass method; no studies have been made to determine the effects on the forced response.

CORRELATION STUDIES

Discussion of Correlation Studies

During development of this new application of the finite element method, various structural dynamics problems were analyzed to serve as checkout runs to evaluate the numerical accuracy and scope of the method.

For every example analyzed, excellent correlation was achieved with data available from other sources. Most of the examples studied were chosen for availability of both theoretical and experimental correlated data. These examples include structures of simple geometrical shapes, such as flat circular plates, spheres, rods, and rectangular beams.

The agreement has been excellent, as indicated in the examples presented in this section. The high degree of accuracy is especially impressive, since in most instances relatively coarse element models were used to expedite the gathering and reduction of data and to limit the total computer time required throughout development and checkout of the computer program.

In addition to simple examples used for evaluation of the accuracy of the method, rocket motors of complex shapes were analyzed. The utility and power of the dynamic stiffness method becomes apparent in the analysis of structures of complex shape. The same finite elements that form a thick-walled sphere, flat circular plate or uniform cantilever beam can readily be reassembled to represent a pressure vessel, rocket motor, or irregular piece of hardware. For such cases, there exists no other known practical approach to calculating the dynamic structural response, without the introduction of grossly simplifying assumptions.

Examples

In the examples presented, natural frequencies and mode shapes calculated by the dynamic finite element method have been compared with results from other methods. In all instances, excellent agreement as to both frequencies and mode shapes has been achieved. Following determination of frequencies and mode shapes, overall structural response to a forcing function is calculated using the mode superposition method.

Examples presented to illustrate accuracy of the method are:

1. Flexural and extensional (radial) vibrations of thick circular plates;

2. Radial vibrations for spherical bodies; and

3. Longitudinal and radial vibrations of hollow tubes and rings.

To illustrate typical rocket motor grain structural response calculations, examples of stresses, displacement, velocities and accelerations throughout the body, varying with time, are presented in Example 4.

Even for the first three seemingly simple examples, solutions by classical theoretical methods are extremely difficult. For several of these three classes of problems, satisfactory theoretical solutions have been developed only in recent years.

The first three examples are problems in three-dimensional elasticity that may be formulated in two parameters. Further complicating the classical theoretical approaches is the fact that separate solutions may be involved for flexural vs extensional modes of vibration, for a given body. In contrast, the dynamic analysis of these and many other classes of structures may be performed by a single dynamic finite element method program.

Example No. 1, Circular Disk — A particularly useful series of cases were analyzed for vibrations of thick circular disks. Vibrations of bodies of this class have been intensively studied, providing good data for comparison; both experimental and theoretical results are available.

Theoretical solutions for flexural modes of vibration have been published by Deresiewicz

58

and Mindlin [7], and corresponding experimental results have been published by Sharma [8].

Theoretical solutions for extensional (or radial) modes of vibration have been developed by Gazis and Mindlin [9], and experimental results obtained by Shaw [10] have been compared with the theoretical.

Table 1 summarizes a comparison of frequencies of extensional (or radial) modes of vibration. Figure 3 shows the model used in this analysis. As noted, the finite element method agrees very well with the theoretical results. In the range of disk diameter-to-thickness ratio of 10:1 used in this example, the theoretical results of Gazis and Mindlin [9] and experimental results of Shaw [10] were in close agreement. For smaller diameter-to-thickness ratios, about 5:1, results from these two sources differed by about 12 percent for several modes. In this region, the finite element results were about 4 percent below experimental results, and about 8 percent above theoretical results, which seems very good correlation, considering the discrepancies in the data available.

Good agreement is also shown in Table 2 for flexural vibrations of the same circular disk.

Deflected mode shapes as calculated by the finite element method show clearly extensional and flexural modes of vibration. Extensional mode shape data are presented in Fig. 4. Some flexural mode shapes are shown in Fig. 5. Little has been published as to predicted mode shapes

TABLE 1

Comparison of Natural Frequencies Obtained by Finite Element Program and Theoretical Results

Fundamental Mode No.	Normalized Frequency, Ω		α Diff. (%)
	Finite Element Program	Theoretical Results [9]	
1	0.221	0.220	0.4
2	0.568	0.570	-0.4
3	0.872	0.880	-1.0
4	1.115	1.143	-2.5
5	1.271	1.290	-1.6
6A[b]	1.369[b]	--	--
6B[b]	1.385[c]	1.47[d]	-5.8
		1.31[e]	+5.7
7	1.472	1.5	-2.0
8	1.58	1.61	-1.9

[a]Of radial vibration for thick circular disk, diameter:thickness ratio of 10:1.
[b]Apparent shear-extensional mode.
[c]Edge mode.
[d]Experimental edge mode.
[e]Theoretical edge mode.

No. of Elements = 98
No. of Nodal Points = 65
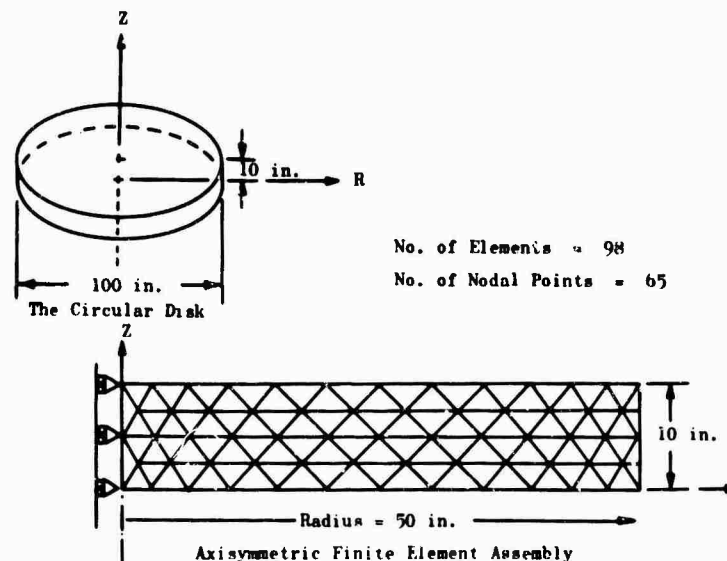
Fig. 3. Circular disk and axisymmetric finite element model

59

TABLE 2
Natural Frequencies in Flexural Modes of Vibration
of Thick Circular Disk by Finite Element Program

Fundamental Mode Number[a]	Normalized Frequency			Max. Diff. (%)
	Finite Element Program	Theoretical [7]	Experimental [8]	
1	0.0533	0.0515[b]	0.0515[b]	3.5
2	0.205	0.197	0.194	5.7
3	0.400	0.371	0.371[b]	7.8

[a]Applicable results for first three modes only are given in the references.
[b]Approximate — curve extended beyond range given in Refs. 7 and 8.

Fig. 4. Radial and axial deflections for
extensional modes of vibration

60

Fig. 5. Deflected shapes for disk vibrating in flexural modes

for circular plates, but efforts will continue to determine the accuracy of the calculated shapes. The accuracy of these shapes directly influences the accuracy of calculated stresses and strains in forced vibration, when using the mode superposition method. Based on the present study it seems reasonable to assume tentatively that accuracy of the mode shapes will be of the same order as that attained in calculating the natural frequencies.
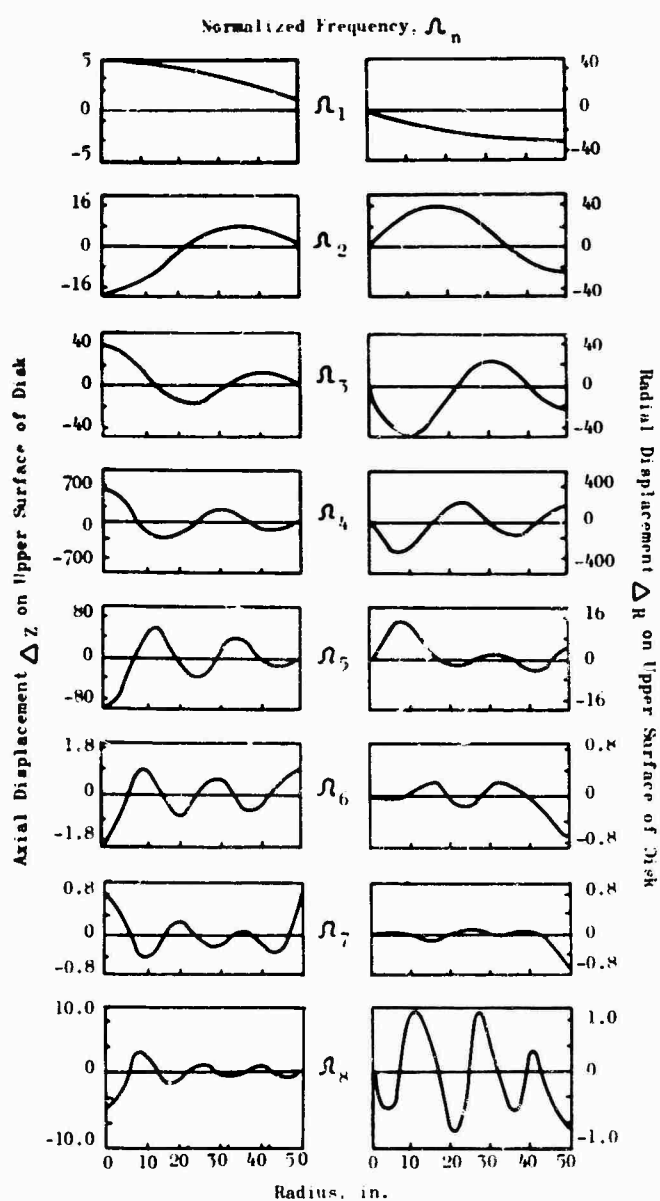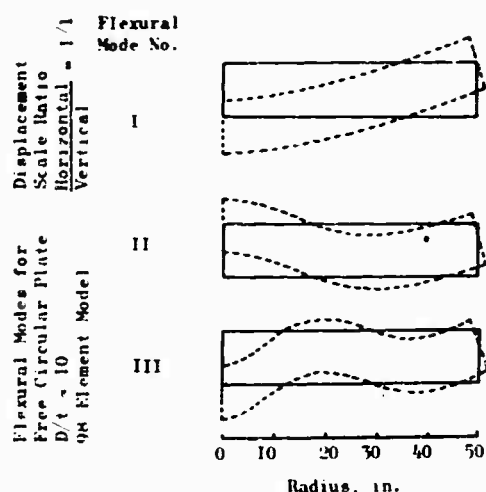
A review of data in Tables 1 and 2 reveals the maximum error in natural frequency to be about 7.8 percent. Also, it can be seen that much higher accuracy is obtained in the extensional than in the flexural modes, as might be expected from consideration of the basic assumptions of the finite element method. The relevant assumption is that each element undergoes extension or compression and shear, but not pure flexural distortion [1, 2, 3].

A better grid system than the one chosen would perhaps give better flexural results, although this particular finite element method would not be recommended for dynamic analysis of, for example, thin shell structures where flexural modes predominate. However, the method is ideally suited for analysis of relatively thick bodies, such as solid rocket motor grains encased in relatively stiff cases where case bending is neglected.

Example No. 2, Spherical Bodies — Additional correlation of the finite element program was made with the theory for vibration of spherical bodies. Three bodies were analyzed: a solid sphere, a hollow body with a wall thickness

50 percent of its outer radius, and a hollow sphere with a wall thickness equal to 33.3 percent of the outer radius.

Theoretical solutions for the fundamental radial frequency are given by Love [11]. With this approach a computer program was written to find the theoretical natural frequency, using an iterative procedure on an IBM 1401 computer. Table 3 summarizes and compares the results obtained by the finite element method and by Love's theory [11]. The models are shown in Fig. 6.

TABLE 3
Natural Radial Frequency of Spheres

Sphere	Natural Radial Frequencies (rad/sec)		Diff. (%)
	Finite Element	Theoretical [11]	
Solid (90 element model)	729	726	0.41
Hollow, wall thickness 50% (51 element model)	605	605	0
Hollow, wall thickness 33.3% (98 element model)	535	533	0.37
Hollow, wall thickness 33.3% (48 element model)	539	533	1.13

Example No. 3, Tubes, Rings, and Cylinders — A variety of tubes, rings, and cylinders were also analyzed by the finite element method. Several hollow cylinder models were analyzed and checked against applicable theories. Simple classical theories for vibrations of finite length, hollow cylinders do not include this important physical parameter. Therefore, to provide a basis for correlating the finite element analyses with theory, Poisson's ratio was permitted to approach zero in correlation data for this example. Results of including Poisson's ratio are also given to demonstrate the effect of varying the ratio in the analysis.

Table 4 presents the natural frequencies for a long hollow cylinder, with an element model as shown in Fig. 7. Mode shapes are calculated by the dynamic finite element program and plotted as shown in Fig. 8.

61

A. Solid Sphere

90 Elements
58 Nodal Points

B. Hollow Sphere

$\dfrac{\text{Wall Thickness}}{\text{Outside Radius}} = 50\%$
51 Elements
36 Nodal Points

C. Hollow Sphere

$\dfrac{\text{Wall Thickness}}{\text{Outside Radius}} = 33.3\%$
98 Elements
65 Nodal Points

D. Hollow Sphere

$\dfrac{\text{Wall Thickness}}{\text{Outside Radius}} = 33.3\%$
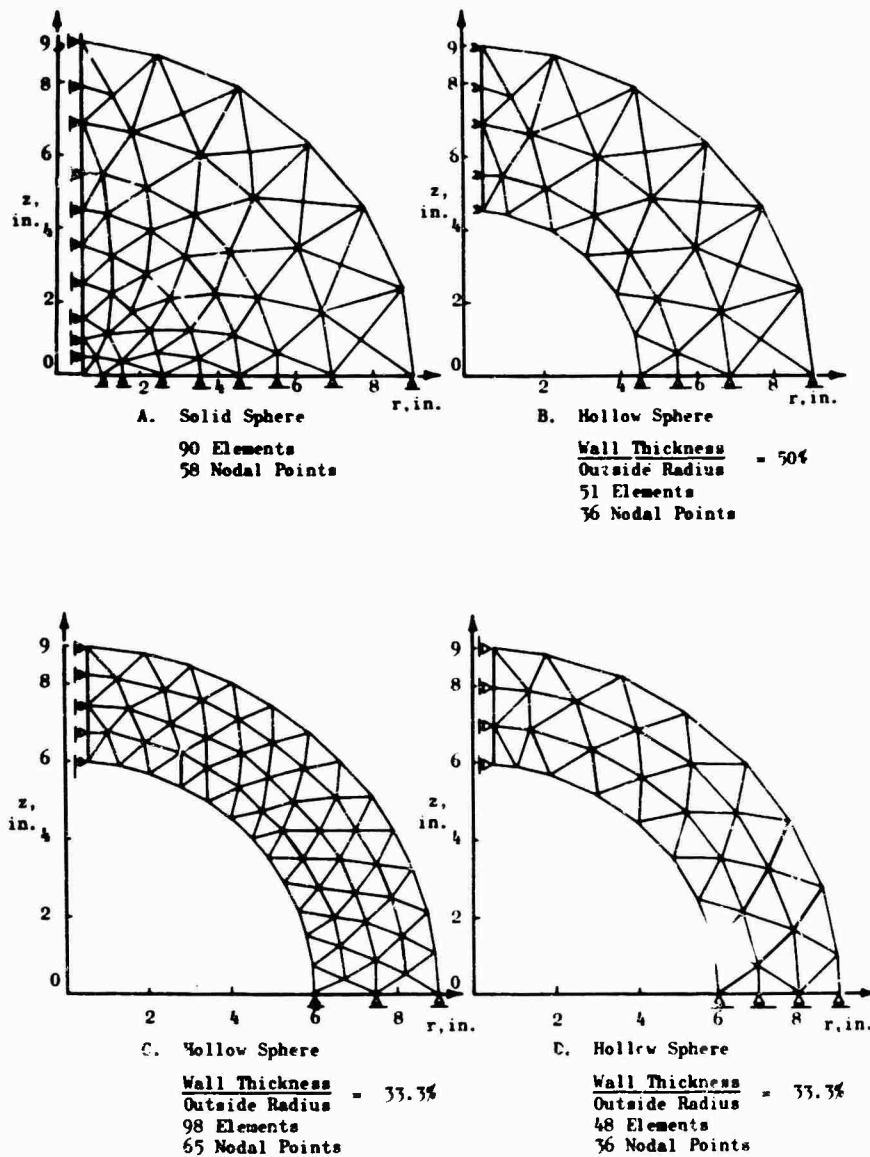48 Elements
36 Nodal Points

Fig. 6. Axisymmetric finite element models for solid and
hollow spheres

TABLE 4
Natural Frequencies of Longitudinal Vibration for a Hollow Cylinder

Mode No.	Natural Frequencies (rad/sec)			
	Theoretical	Finite Element Program, Poisson's Ratio ≈ 0.0	Diff.[a] (%)	Finite Element Program, Poisson's Ratio = 0.45
1	48.25	48.23	-0.04	48.15
2	144.75	144.30	-0.31	142.19
3	241.25	239.16	-0.87	228.97
4	337.50	331.64	-1.74	302.72

[a]Percent difference = (program frequency - theoretical frequency)/theoretical frequency × 100 percent; theoretical frequency calculated by

$$\omega_n = (n - 0.5)\frac{\pi}{L}\sqrt{\frac{gE}{\rho}}$$

where n = mode number, 1, 2, 3, 4;
  ρ = unit weight, 0.065 pci;
  E = elastic modulus, 1000 psi; and
  L = length, 80 in.

The Hollow Cylinder

No. of Elements = 80
No. of Nodal Points = 63
Boundary Conditions are base
 nodal points restrained only
 in axial direction, free in
 radial direction.

Finite Element Assembly
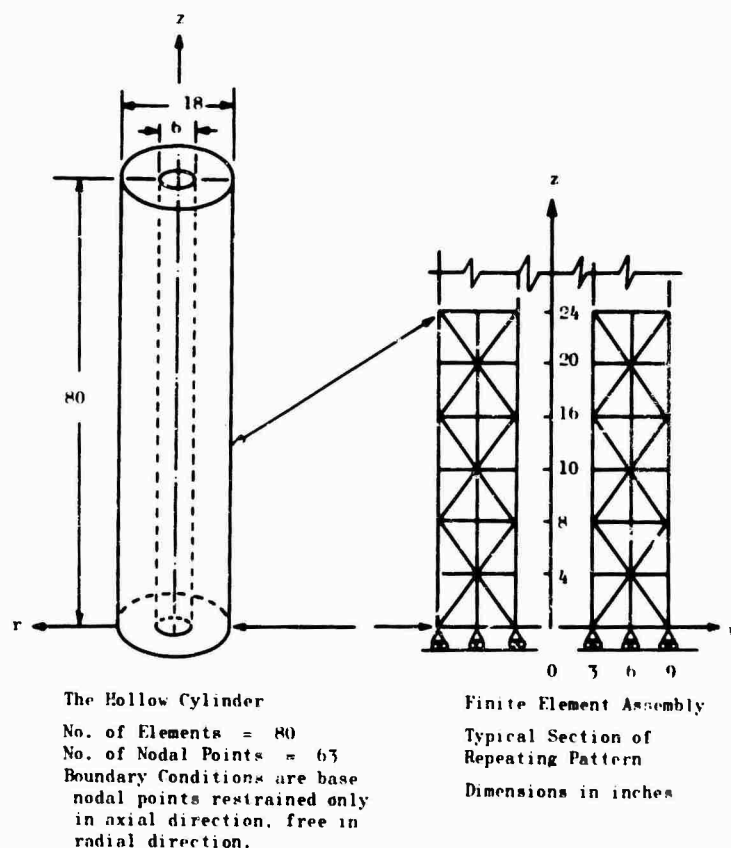
Typical Section of
Repeating Pattern

Dimensions in inches

Fig. 7. 80-in. long hollow cylinder and finite
element assembly
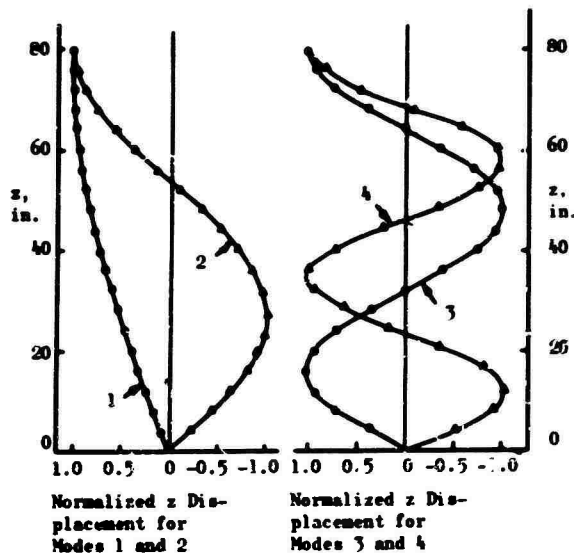
Fig. 8. Mode shapes of longitudinal vibrations for 80-in. cylinder

TABLE 5
Natural Frequencies of Longitudinal and Ring Extensional Vibrations for Short Hollow Cylinder[a]

| Mode Type | Natural Frequency (rad/sec) | | Diff. (%) |
	Theoretical	Finite Element Program, Poisson's Ratio = 0.0	
Extensional ω_R'	65.6	66.7	1.5
Longitudinal			
1	182.7	180.5	1.2
2	548.0	573.9	4.7

[a]See Fig. 9.

Theoretical mode shapes are calculated by the equation

$$\delta_z = C_1 \sin\left(\frac{Z}{\ell} \times \frac{\pi n}{2}\right) . \qquad (4)$$

where

$n = 1, 3, 5, 7 \ldots$, the number of quarter waves per length of cylinder;

δ_z = axial displacement;

Z = axial location;

ℓ = length, 80 in.; and

C_1 = amplitude of maximum displacement, a constant not defined for free vibrations.

Table 5 summarizes the results for a thick ring, illustrated in Fig. 9. The ring chosen has a very coarse model of eight elements, yet results appear satisfactory for the ring extensional (radial) modes and for the lower order longitudinal modes. Theoretical frequencies of longitudinal vibrations are calculated as for a long cylinder.

Ring extensional (or radial) frequency is calculated by

$$\omega_R = \frac{1}{\bar{R}} \sqrt{\frac{Eg}{e}} \quad \text{and} \quad \bar{R} = \sqrt{\frac{I}{a}} = 35.355 \text{ in.},$$

where

E = elastic modulus, 910 psi;

g = acceleration of gravity, 32.2 x 12 in./sec^2;

e = unit weight, 0.065 pci;

I = moment of inertia of ring; and

a = cross-sectional area of ring.

Example No. 4 — Figure 10 summarizes the information available from the dynamic finite element analysis. The problem is defined as follows:

Grain outside diameter = 3.960 in.;

Case thickness = 0.064 in.;

Grain modulus = 1000 psi;

Poisson's ratio = +0.48;

Boundary condition: outer boundary rigidly fixed to forcing body;

Load resonant acceleration:

$$P_X = 1 \, (g) \sin (\omega_{(1)} t) .$$

where

$1 \, (g)$ = the assumed maximum amplitude of load,

$\omega_{(1)}$ = the first resonant frequency (rad/sec), and
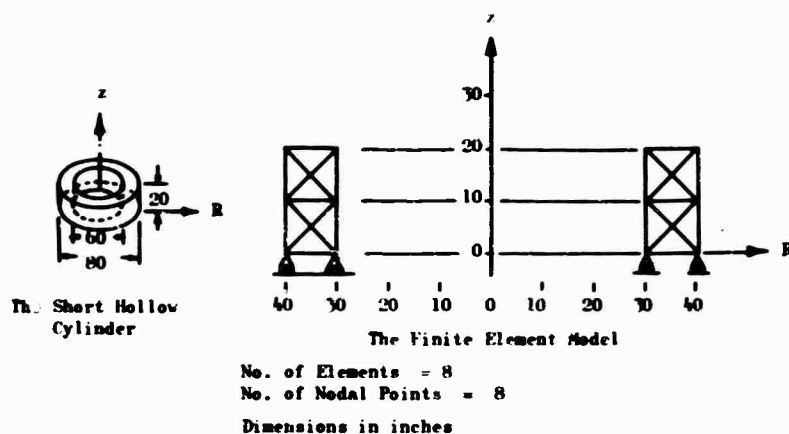
t = time (sec).

64

Fig. 9. Short hollow cylinder and finite element model

The element model and curves shown are re-produced from cathode ray tube plots, automatically drawn by the computer to aid in rapid interpretation of the data from the computer run, as well as to provide documentation of the analysis as shown in Fig. 10:

Part (a) pictures the element model of a section of a typical grain, to be analyzed for transverse accelerations.

Part (b) is a trace of acceleration loads input to the grain through the case, mounted on a vibrating fixture.

Part (c) shows traces of acceleration and displacement of the tip of the grain during load-ing. Maximum displacements and accelerations asymptotically approach a maximum value during resonant load of constant maximum ampli-tude. Accelerations and displacements quickly die out due to energy absorption of the propel-lant following removal of the applied load.

Part (d) is a plot of stresses in a critical element of the grain, at the side of the filleted star point. Stresses also approach a maximum, to die out quickly after removal of load.

Comparison of Program Versions
    Using Lumped Mass and Consistent
    Mass Matrix Representations

A comparison is made of natural frequen-cies and mode shapes calculated by the lumped mass program (AXDY) and by the consistent mass program (AXMQ) for identical finite ele-ment models. All solid bodies analyzed to compare the two approaches were treated in the preceding paragraphs; only those additional data required for comparison are now introduced.

The results presented in Table 6 show that, in general, for a given element assembly the two programs agree about equally well with correlated data. An exception was shown in the case of Example 1, a very coarse model of a short hollow cylinder.

In evaluating accuracy of the results, con-sideration of the effect of the stiffness matrix is also pertinent. From the fundamental as-sumption of constant strains through an element, a limitation is placed on the displaced shape the body can take. As a result, the finite element model is invariably stiffer than the real struc-ture, tending to produce calculated frequencies that are higher than the correct value. Fur-thermore, use of the displacement-consistent mass matrix approach yields frequencies that represent an upper bound to the true frequen-cies [6].

In general, lumped mass representation may yield frequencies either higher or lower than the correct value. However, in most of the cases analyzed by the lumped mass program, the calculated frequencies were below the cor-rect values. In these cases, errors introduced by the mass representation were apparently larger and of opposite sign from those intro-duced by the stiffness representation. Thus, the errors tended to be canceling, improving the agreement with theoretically correct re-sults for the lumped mass program.

Results of previous work have indicated the consistent mass matrix can be expected to yield results superior to those obtained using a lumped mass approach. However, results of this study show that, for those element models finely enough divided to represent the stiffness characteristics of the structure, the lumped mass approach gives results with about equal accuracy.
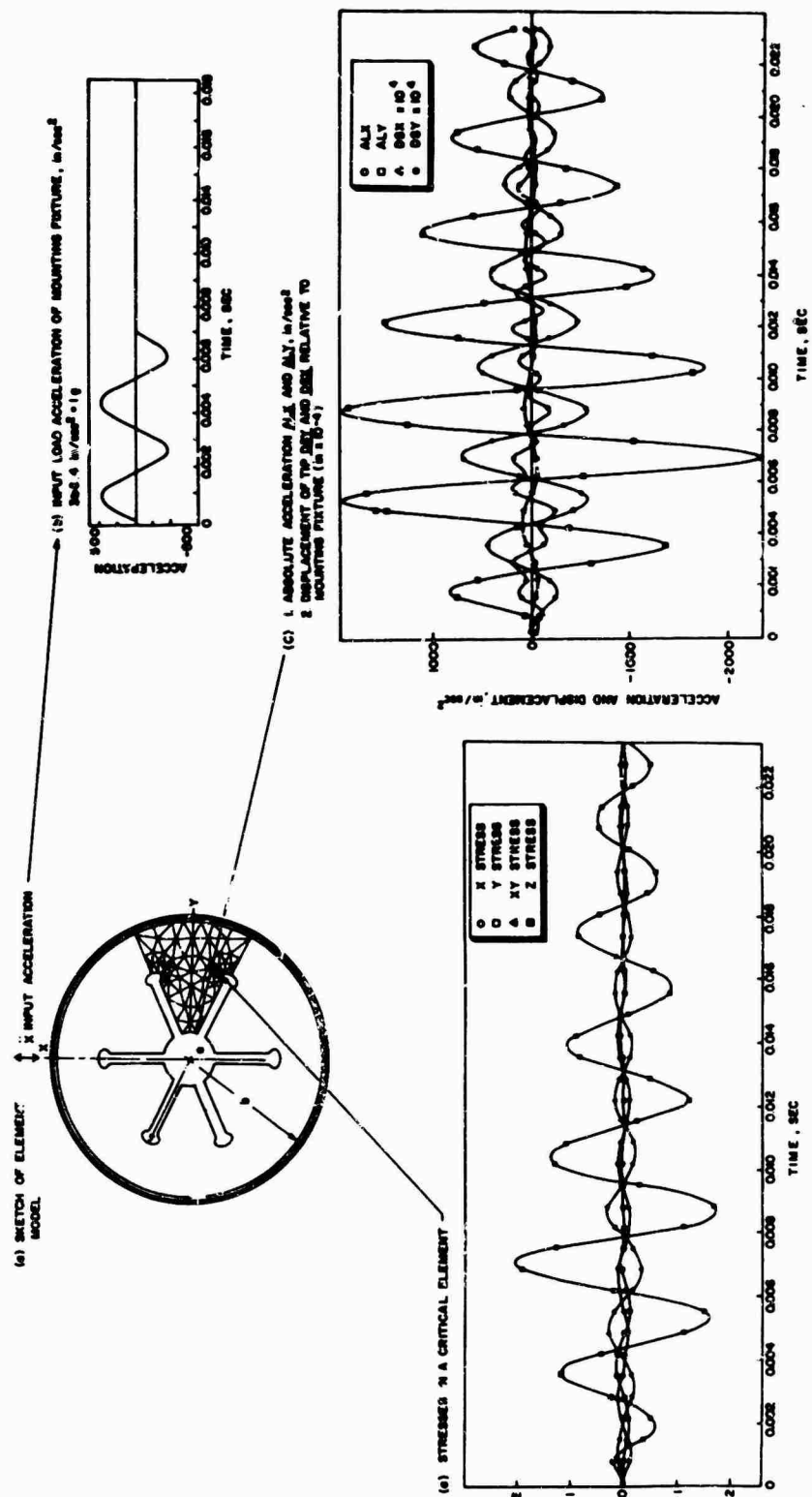
65

Fig. 10. Results from typical grain analysis

TABLE 6
**Natural Frequencies Calculated by Programs AXDY and AXMQ
Compared with Theoretical Values**

Example	Theoretical	Program AXDY		Program AXMQ	
		Natural Frequency (cps)	Diff. (%)	Natural Frequency (cps)	Diff. (%)
1. Short hollow cylinder:					
Ring extensional mode, ω_r	66.3	62.5	-5.7	66.6	+0.3
Longitudinal mode -1	182.7	160.0	-12.6	185.0	+1.2
-2	548.0	701.0	+27.9	601.0	+8.8
2. 44-in. long cylinder:					
Longitudinal mode -1	83.03	83.0	-0.035	83.01	-0.02
-2	249.1	248.2	-0.36	249.9	+0.32
-3	415.15	411.1	-0.967	419.6	+1.06
-4	581.2	570.0	-1.93	593.4	+2.1
-5	747.3	723.0	-3.25	764.7	+2.34
-6	914.0	867.6	-5.07	961.4	+5.19
3. Hollow spheres:					
$t/r_0 = 0.50$, radial mode	576.5	581.6	+0.71	584.1	+1.32
$t/r_0 = 0.333$, radial mode	532.0	539.0	+1.12	545.0	+240

DISCUSSION AND CONCLUSIONS

Dynamic analyses using the finite element method have been applied to a variety of test cases on elastic bodies of regular shape. Correlation with available natural frequency and mode shape results of theoretical and experimental solutions has been excellent. It appears that with some refinement, this method of analysis will provide an excellent tool for analyzing bodies of complex geometry and nonhomogeneous materials.

The forced response portion of the analysis has several shortcomings, which may make the results questionable for many classes of problems. Attempts to allow for arbitrary forcing function and transient response calculations led to the use of the mode superposition method. For many problems, the assumption of the existence of classical modes, used in the mode superposition method, does not hold and the deviation from the actual response, in many cases, is now known. Making the forcing function less general (steady-state sinusoidal) would allow the use of better solution techniques and improve the results in steady-state vibration problems.

With modification the method could be extended to include analysis of bodies with orthotropic material properties, analysis of bodies encased in thin shells, structural damping, and three-dimensional analyses. Structural damping in steady-state sinusoidal vibration may be

included by multiplying the stiffness by a factor of $(1 + ig)$, where i is $\sqrt{-1}$ and g is the damping proportionality factor. Isothermal viscoelastic analyses may be performed with a program of this type for calculation of the stiffness matrix using the storage modules and letting g become the loss tangent.

In many problems a three-dimensional analysis would be most appropriate. The formulation of such a program is fundamentally easy but because of computer storage limitations it does not appear feasible at this time. However, the two-dimensional program may be used to obtain good approximations.

REFERENCES

1. M. J. Turner, R. W. Clough, H. C. Martin, and L. J. Topp, "Stiffness and Deflection Analysis of Complex Structures," J. Aerospace Sci., Vol. 23, pp. 805-824, 1956

2. E. L. Wilson, "Finite Element Analysis of Two-Dimensional Structures," U. of Calif. Structures and Materials Res. Lab., Dept. of Civil Eng., Rept. 63-2, June 1963

3. R. W. Clough and Y. Rashid, "Finite Element Analysis of Axisymmetric Solids," J. Eng. Mech. Div., ASCE, Vol. 91, No. EM1, Proc. Paper 4229, Feb. 1965

4. R. J. Melosh, "Basis for Derivation of Matrices for the Direct Stiffness Method," AIAA J., Vol. 1, No. 7, July 1963

5. R. W. Clough and A. K. Chopra, "Earthquake Stress Analysis in Dams," Proc. ASCE, Vol. 92, No. EM-2, April 1966

6. J. S. Archer, "Consistent Mass Matrix for Distributed Mass Systems," J. Structural Div., 3rd Conf. on Electronic Computation, Vol. 89, No. ST4, Pt. 1, Proc. ASCE, p. 161, Aug. 1963

7. H. Deresiewicz and R. D. Mindlin, "Axially Symmetric Flexural Vibrations of a Circular Disk," J. Appl. Mech., pp. 86-88, March 1955

8. R. L. Sharma, "Dependence of Frequency Spectrum of a Circular Disk on Poisson's Ratio." J. Appl. Mech., pp. 641-642, Dec. 1957

9. D. C. Gazis and R. D. Mindlin, "Extensional Vibrations and Waves in a Circular Disk and a Semi-Infinite Plate," J. Appl. Mech., pp. 541-547, Sept. 1960

10. E. A. G. Shaw, "On the Resonant Vibrations of Thick Barium Titanate Disks," J. Acoust. Soc. Am., Vol. 28, pp. 38-50, 1956

11. A. E. H. Love, The Mathematical Theory of Elasticity, 4th Ed. Dover Publications, New York, 1944

DISCUSSION

Mr. Howard (Aerospace Corp.): Do you use a solid or a two-dimensional element in your model?

Mr. Baker: This is a two-dimensional element and the plane-stress plane-strain formulation is a triangle of unit thickness. In the axisymmetric formulation it is a segment of a ring. Actually we eliminate the whole ring and use a one-radian segment, triangular in cross section. This can be done in three dimensions by using a tetrahedral solid element, although this may cause trouble with computer storage capacity.

Mr. Langland (Naval Ordnance Test Station, China Lake): You mentioned earlier that you assume a linear displacement function for these elements. Would you care to elaborate?

Mr. Baker: It has generally been found that the linear displacement function is satisfactory for this type of analysis. It is the easiest one to use. The displacements are set along the two coordinate directions and are written in terms of either the rz or the xy coordinates, e.g., $A + Br$ Cz. By using this displacement, the forces are determined in terms of nodal point displacement. We minimize energy by using these linear displacement functions, writing an energy function and then using a Rayleigh-Ritz procedure to minimize it for the lower values.

Mr. Langland: Is the tetrahedral element you mentioned the one Gallagher developed and described in some papers?

Mr. Baker: There are several papers about it. I think some one at General Dynamics published a paper using the tetrahedron.

* * *

MIN-MAX RESPONSE PROBLEMS OF DYNAMIC SYSTEMS
AND COMPUTATIONAL SOLUTION TECHNIQUES

Eugene Sevin and Walter Pilkey
IIT Research Institute
Chicago, Illinois

Analysis and design problems of dynamic systems are considered in which the system and/or disturbances are not completely prescribed and the extremal peak responses are of interest. Discussions are presented of mathematical techniques of linear and nonlinear programming and dynamic programming which can be used to solve these so-called min-max problems. These techniques serve to determine not only the extremal responses but also the unknown properties of the system (the optimum design problem) and/or the disturbance (the extremal response analysis problem) which generate these responses. Detailed consideration is limited to single-degree-of-freedom dynamic systems.

E. Sevin

INTRODUCTION

Various analysis and design-oriented problems in dynamics are concerned with achieving some minimum-maximum deviation of the response, though they may not always be stated in this form. For example, it may be desired to design a shock isolator for which either the maximum transmitted acceleration or the maximum relative displacement is to be minimized. Or perhaps the response of a system to the "worst" loading of a prescribed class is sought. This might correspond to finding the particular loading among the class for which the system's maximum displacement is itself a maximum. The problem may be of a compound type in which, for example, an isolator is desired having a minimum-maximum response under the "worst" loading. Still another possibility is a design for minimum response sensitivity where the system is sought for which the spread between the maximum responses, corresponding

to the "worst" and the "best" loadings, is minimized.

This paper deals with min-max problems for which the properties of the system and/or disturbances are not completely prescribed. Computational techniques are discussed which, under these circumstances, serve to determine both the maximum (or minimum) system response as well as the unknown system and/or disturbance characteristics. Consideration is limited to single-degree-of-freedom dynamic systems. While the methods are easily generalized to higher dimensions, in some instances the associated computational burden appears to be a formidable one.

CLASS OF PROBLEMS

By way of introduction, consider the single-degree-of-freedom shock absorber and shock isolator shown in Figs. 1 and 2, respectively. For unit mass the equation of motion for a shock absorber is

$$\ddot{x} + u(x,\dot{x}) = g(t), \qquad (1a)$$

and for a shock isolator is

$$\ddot{x} + u(x,\dot{x}) = -\ddot{g}(t), \qquad (1b)$$

where $u(x,\dot{x})$ denotes the system function and $g(t)$ the disturbance (input) function. The system function generally is expressed in terms of
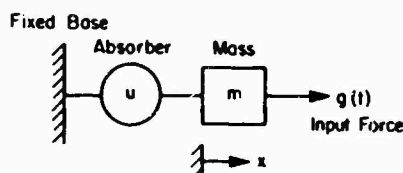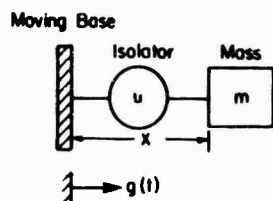
Fig. 1. Single-degree-of-freedom shock absorber

Fig. 2. Single-degree-of-freedom shock isolator

the state variables, i.e., for a linear spring-dashpot system

$$u(x, \dot{x}) = kx + c\dot{x} ,$$

and is only an implicit function of time. In some instances, however, it is more appropriate to treat u as an explicit function of time.

It is convenient to introduce a state variable notation where the symbol x denotes the vector $\{^x_{\dot{x}}\}$, whose elements are displacement x and velocity $\dot{x}$. Then the types of systems we will consider are those covered by a set of first-order ordinary differential equations of the vector form

$$\dot{x} = f(x, u, g) , \qquad (2)$$

$x(0)$ = prescribed. Equations (1) are merely special forms of Eq. (2).

We will define the response function h as being that aspect of the system response whose maximum deviation is to be either minimized or maximized. Thus, for the isolator whose relative displacement is to be minimized, $h = x_j$, however, for the absorber we may wish to minimize the maximum transmitted force, so that $h = u$. In general, then

$$h = h(x, u)$$

and we will seek to determine the maximum deviation of h from some preassigned quantity in a time interval of interest, $0 \leq t \leq T$. This is designated

$$\max_t h(x, u) .$$

We may now consider three types of min-max problems, the first two being a simple type and the third a compound type.

Problem 1

Given a system $u(x)$ and a class of disturbances $g(t)$, find

$$\min_g \max_t h(x) \qquad (3a)$$

or

$$\max_g \max_t h(x) \qquad (3b)$$

and the associated $g(t)$. This is the analysis problem of determining the upper and lower bounds to the system response for incompletely prescribed disturbances or, equivalently, the problem of finding the response to the "best" and "worst" disturbances among a specified class. A way of prescribing the class of $g(t)$ might be to specify total impulse and duration and/or to specify a band within which $g(t)$ must lie. This problem can be generalized immediately to multidegree-of-freedom systems, for example, for the study of stress and displacement bounds on continuous structural members for incompletely prescribed loadings.

Problem 2

Given constraints $L(x, u) \leq 0$ on the system response and a disturbance $g(t)$, find

$$\min_u \max_t h(x, u) \qquad (4)$$

and the associated $u(t)$. (In this problem u cannot be found directly as $u(x)$, unless a class of $u(x)$ is first prescribed [1]. The latter approach would represent a less general minimization of h. Therefore, in the present formulation the determination of $u(x)$ is considered a separate problem which ultimately requires that some class of $u(x)$ be specified.) This is the design problem of determining a system whose response is optimum in a prescribed sense. At the same time,

$$\max_t h(x, u)$$

represents optimal performance specifications against which the "efficiency" of any suboptimal system can be measured and the margin for improvement determined. The ability to establish

70

the optimal $u(t)$ also suggests improved techniques for determining the best $u(x)$ from among a prescribed class, since what has heretofore been treated as a constrained minimization problem now can be viewed as the much more simple problem of approximating $u[x(t)]$ to $u(t)$, e.g., by the method of least squares.

Problem 3

Given constraints $L(x,u) \leq 0$ on the system response and a class of disturbances $g(t)$, find

$$\min_{g} \min_{u} \max_{t} h(x,u) \qquad (5a)$$

or

$$\max_{g} \min_{u} \max_{t} h(x,u) \qquad (5b)$$

and the associated $u(t)$ and $g(t)$. This type of compound problem corresponds to designing a system which is optimum for either the "best" or "worst" possible disturbances among a prescribed class. A problem of this sort related to the design of space vehicles is discussed by Blair, Lovingood and Geissler [2]. Examples in terms of shock absorbers and isolators are obvious.

It might be noted that these problems have their counterparts in the theory of differential games. Roughly speaking, Eq. (5b) corresponds to a player g whose goal is to maximize $\max h$ while an opposing player u is seeking to minimize it.

DISCRETE FORMULATION

Since we intend to seek computational procedures utilizing high-speed digital computers, it is essential that a discrete formulation of the min-max problems be developed. Various approaches are possible, depending on the discretization of $u(t)$ and $g(t)$.

Let the total time interval T be divided into n subintervals Δt_i, $i = 1, 2, \ldots, n$. Denote the value of x at the beginning of the ith interval by x_i. If the subintervals are of equal length Δt, then

$$x_i = x[(i - 1)\Delta t].$$

A piecewise constant representation of the system function $u(t)$ is

$$u(t) = \sum_{i=1} (u_i - u_{i-1}) H(t - t_i), \qquad (6)$$

where $H(t - t_i)$ is the unit step function, u_i is a constant in the interval $t_i \leq t \leq t_i + \Delta t$, $t_i = (i - 1)\Delta t$, and $u_o = 0$. A continuous representation of $u(t)$ is

$$u(t) = \sum_{i=1} (u_i' - u_{i-1}') H(t - t_i)(t - t_i). \qquad (7)$$

where

$$u'(t) = \sum_{i=1} (u_i' - u_{i-1}') H(t - t_i)$$

with u_i' constant in $t_i \leq t \leq t_i + \Delta t$.

Possible representations for the disturbance function include a series of a discrete impulse applied at the beginning of each interval, i.e.,

$$g(t) = \sum_{i=1} g_i \delta(t - t_i), \qquad (8)$$

where $\delta(t - t_i)$ is the Dirac delta function, and the piecewise constant form

$$g(t) = \sum_{i=1} (g_i - g_{i-1}) H(t - t_i). \qquad (9)$$

The solution to Eq. (2) provides, in effect, a transformation of state variables from the ith to the $(i + 1)$st state. That is, we may write

$$x_{i+1} = F(x_i, u_i, g_i), \qquad (10)$$

where the function F may be either an exact expression if a closed form solution to Eq. (2) is available or an approximating difference equation.

Finally, we represent the response function h in discrete form, so that the maximization over time t is equivalent to maximization over all stages i, i.e.,

$$\max_{t} h(x,u) = \max h(x_i, u_i), \quad i = 1, 2, \ldots, n+1. \qquad (11)$$

COMPUTATIONAL TECHNIQUES

Linear and Nonlinear Programming

The general problem of linear and nonlinear programming is the selection of the set of parameters y_i which minimizes (or maximizes) some objective function (performance index) $q(y_i)$ subject to certain conditions of constraint on the parameters, $p(y_i) < 0$. When both the objective function and each of the constraining

functions are linear in the y_i, the problem is one of linear programming; otherwise, it is one of nonlinear programming. The solution techniques and relative ease of computation are far more advanced for linear programming problems. Thus, while we will consider the problem "solved" when reduced to either a linear or nonlinear programming formulation, a numerical solution in the latter case may not be easily obtained.

For the min-max problems, the maximization over time of $h(x,u)$ is placed in a form leading to mathematical programming formulations by setting

$$\max_i h(x_i, u_i) = \phi. \tag{12}$$

The problem is now to extremize ϕ, subject to the prescribed constraints, with the addition of the requirement

$$h(x_i, u_i) \leq \phi, \quad i = 1, 2, \ldots, n+1. \tag{13}$$

As a first example, consider a problem 1 situation in which the bounds to the maximum displacement of a damped linear absorber are sought for a class of disturbances characterized by total impulse and duration.

Here, the specific form of Eq. (2) is

$$\dot{x} = \begin{Bmatrix} \dot{x} \\ \ddot{x} \end{Bmatrix} = \begin{Bmatrix} \dot{x} \\ -kx - c\dot{x} + g(t) \end{Bmatrix}, \tag{14}$$

where the disturbance will be represented by a series of impulses as given by Eq. (8). The response function is merely the displacement, so that

$$h(x_i, u_i) = x_i. \tag{15}$$

An exact solution of Eq. (14) is possible and the state transformation, Eq. (10), can be extended for zero initial conditions to the form

$$x_i = \sum_{j=1}^{i-1} \frac{g_j \, e^{-\beta\omega(t_i - t_j)}}{\lambda\omega} \sin\left[\lambda\omega(t_i - t_j)\right], \tag{16}$$

where

$\lambda \quad (1 - \beta^2)^{1/2}$,

$\beta \quad c/c_c < 1$, and

$c_c = 2\omega = 2\sqrt{k}$.

The class of disturbance functions is characterized by

$g_j \geq 0, \quad j = 1, 2, \ldots, n+1$ (non-negative loading),

$g_j = 0, \quad j \geq n + 2$ (pulse of duration $T = n\Delta t$),

and

$$\int_0^T g(t) \, dt = \sum_{j=1}^{n+1} g_j \tag{17}$$

$$= R \text{ (prescribed total impulse, } R). $$

From Eqs. (12) and (15),

$$\phi = \max_i |x_i|. \tag{18}$$

Then the mathematical programming problem is one of finding the set of g_j satisfying the conditions set by Eqs. (17) such that ϕ is a minimum (or maximum), where the x_i are given by Eq. (16). In the form stated, the problem is one of linear programming since ϕ and the constraints of Eqs. (17) are all linear functions of the unknown g_j. However, we have yet to state an explicit condition for insuring that the $\max |x_i|$, found in $0 \leq t \leq T$, is not exceeded at some $t > T$. One approach is to recognize that there exists a functional relationship between x and $\dot{x}$ (i.e., a region of the phase plane) which insures that $\max |x_i|$ is not exceeded at some later time. In general, this will be a nonlinear relationship among the g_j, destroying the linearity of the problem. In the present example, this relationship is easily shown to be quadratic for Eq. (16). To retain the linearity it is necessary to either approximate the nonlinear function by a polygonal path in the phase space or, more simply, to extend sufficiently the time interval of interest. Clearly, the latter approach would be followed here.

A second example is the problem 2 type, in which we seek to design an isolator whose relative displacement does not exceed a prescribed value and whose maximum transmitted acceleration is minimized. The disturbance function is specified.

The system function, $u(t)$, will be taken to be piecewise constant as in Eq. (6), and the state transformation obtained from the solution of

$$\ddot{x} + u(t) = -\ddot{g}(t)$$
$$x(0) = 0 \tag{19}$$

is

$$x_i = -\frac{1}{2} \sum_{j=1}^{i-1} (u_j - u_{j-1})(t_i - t_j)^2 - g(t_i). \tag{20}$$

The response function is $h(x_i, u_i) = -u_i$ and, hence, $\phi = \max_i |u_i|$. The linear programming problem is the determination of the set of u_i for which

$$x_i \leq X_i \tag{21}$$

(prescribed displacement bound) and ϕ is a minimum, the x_i and u_i being related through Eq. (20). The solution to this problem is reported by Liber and Sevin [1]; typical results are shown in Fig. 3.

Problem 3 is considered as a final example of the linear programming formulation. The example is interesting in its own right and also serves to indicate that not all such problems admit to a linear, or even nonlinear, approach. We want to design an isolator whose response, for the "best" of a given class of disturbances, is such that the maximum acceleration does not exceed a prescribed value and the maximum relative displacement is minimized. That is, we seek to determine

$$\min_{u_i} \min_{g_i} \max_i h \tag{22}$$

where the response function is $h(x_i, u_i) = x_i$. We specify the class of disturbance functions to be of prescribed duration, total impulse and bounded intensity. Both the system and disturbance functions will be represented as piecewise constant, as in Eqs. (6) and (9), respectively. The state transformation now is

$$x_i = -\sum_{j=1}^{i+1} \left[\frac{1}{2} (u_j - u_{j-1})(t_i - t_j)^2 + (g_j - g_{j-1}) \right]. \tag{23}$$

Again, with

$$\phi = \max_i |x_i|.$$

the linear programming problem is to find the set of u_i and the set of g_i satisfying Eq. (23) for which

$$|u_i| \leq U_i$$

(prescribed acceleration bound),

$$|g_i| \leq G_i$$

(prescribed force bound),

$$\sum_{j=1}^{n} (g_j - g_{j-1})(t_{n+1} - t_j) = R$$

(prescribed total impulse), and such that ϕ is a minimum.

Examination of Eq. (23) will indicate that the problem yields to a linear programming formulation simply because we are minimizing ϕ with respect to both the u_i and g_i. Were we instead to attempt to construct

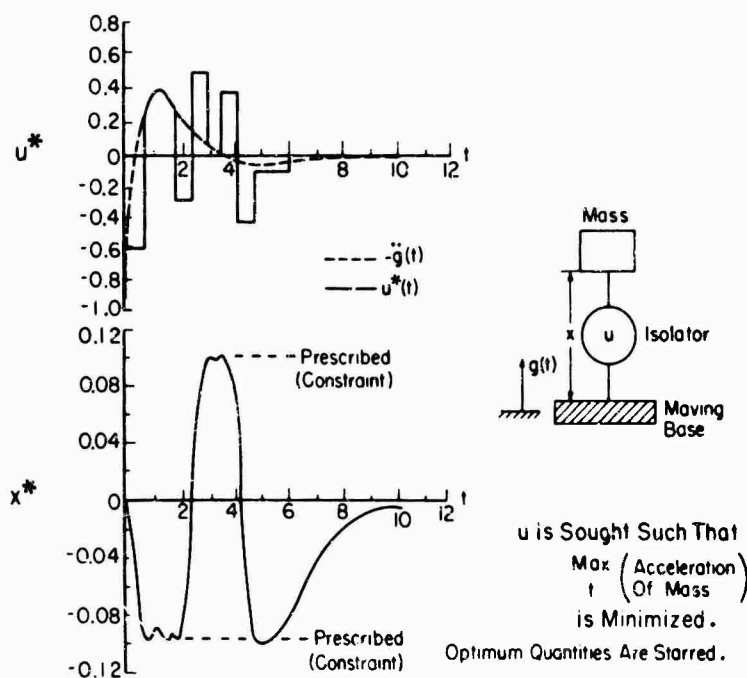$$\min_{u_i} \max_{g_i} \phi,$$

Fig. 3. Optimum shock isolator

73

where an order of minimization and maximization has to be preserved, an alternate approach would be necessary. In this instance, the matter of linearity is of no consequence, so nonlinear programming offers nothing new. We are forced to turn then to dynamic programming.

DYNAMIC PROGRAMMING

The computational technique of dynamic programming can be used to solve all three classes of min-max problems, and hence is a more general formulation than either linear or nonlinear programming. The method is computationally quite straightforward; there is more of a problem in getting lost in a sea of notation. We will first illustrate the technique with respect to a problem 2 example considered earlier and then generalize to cover all three classes.

We want to establish the system function $u(t)$, characterized by the set of u_i, for which $|x_i| < X_i$ (X_i specified) and $z = \max u_i$ is a minimum. The state transformation is given by Eqs. (10); note that the system starts from rest, i.e., $x_1 = 0$. Assume for the moment that at time $t_j (\leq t_{n+1})$, the system is in state x_j and that the min-max solution for the subsequent motion is known. Moreover, assume that this solution is known for M different values of the state x_j. That is, we know

$$z(x_j^m) = \min_{u_i} \max_i |u_i| ; \quad i = j, j+1, \ldots, n+1 .$$

$$m = 1, 2, \ldots, M . \quad (24)$$

In this notation $m = 1$, $j = 1$ corresponds to the value of the initial state originally prescribed. Thus, the desired min-max value is represented by $z(x_1^1) = z_1(0)$.

We seek now a means for computing $z(x_{j-1}^m)$. Consider the system to be in the state x_{j-1} at time t_{j-1} and investigate its response under the choice of some value of u_{j-1} consistent with the constraint of Eq. (21). At time t later, i.e., at t_j, the system will be in state x_j, as determined from Eq. (10), corresponding to which can be found the value of $z(x_j)$. The maximum of the two quantities u_{j-1} and $z(x_j)$ is recorded. This process is repeated for a range of admissible u_{j-1}, so that

$$\min_{u_{j-1}} \max \left[u_{j-1} , z(x_j) \right]$$

can be determined. Clearly, this value then corresponds to $z(x_{j-1}^m)$ for the particular choice

of m. The entire process must be repeated for a sufficient range of m so that subsequently, at any stage $j-1$, the resulting state x_j will be close enough to some x_j^m in the matrix of known $z(x_j^m)$ values to permit accurate interpolation. The process is easily started at $j = n+1$ since at t_{n+1}, $z_{n+1} = 0$ for all x_{n+1}^m. We recognize that with dynamic programming the $n+1$ dimensional minimization required in the linear (or nonlinear) programming formulation has been replaced by a sequence of $n+1$ unidimensional minimizations. Since dynamic programming does not consider linearity, it represents a most powerful approach.

The notation is improved somewhat if we distinguish better between the subscript denoting the stage of the computational process and the state of the system response. Thus, the computational algorithm becomes

$$z_{n+2-j}(x_j) = \min_{u_j} \max \left[u_j , z_{n+1-j}(x_{j+1}) \right] .$$

$$j = n, n-1, \ldots, 1 . \quad (25)$$

with

$$z_1(x_{n+1}) = 0 .$$

where subscript j represents the state of the system and the subscript on z denotes the stage of the computational process. The minimization, of course, is only with respect to admissible values of u_j as determined from the system constraints of Eq. (21). The optimal choice of the u_j is retained in the computer memory at each stage. Once the desired $z_{n+1}(0)$ is determined, knowledge of u_1 permits the process to be repeated forward in time to select the appropriate set of u_i.

Equation (25) follows directly from Bellman's principle of optimality, which in essence says that regardless of the decisions made in reaching a particular state, subsequent decisions must constitute an optimal policy with respect to this state. This permits us to generalize the formulation immediately. Let

$$extrem$$

represent any of the minimizations, maximizations or min-max combinations appropriate to the three types of problems considered earlier. That is,

$$extrem = \min_{s_i} \text{ or } \min_{u_i} \text{ or } \max_{g_i} \text{ or } \min_{g_i} \text{ max or } \min_{u_i} \min_{g_i} .$$

Then, if at the $(n-1-j)$th stage of the process, corresponding to the system being in its $(j+1)$st state, we denote the min-max value by

$$\phi_{n+1-j}(x_{j+1}) = \text{extrem max } h(x_i, u_i) . \quad (26)$$
$$s_i \quad i$$

the next stage in the process is given by

$$\phi_{n+2-j}(x_j) = \text{extrem max} \left[h(x_j, u_j), \phi_{n+1-j}(x_{j+1}) \right] . \quad (27)$$

The process starts with

$$\phi_1(x_{n+1}) = \max_t h(x, u), \quad t \geq t_{n+1} . \quad (28)$$

and is conducted for $j = n, n-1, \ldots, 1$. The extremes are taken only with respect to admissible values of s_j as determined by the stagewise constraints

$$S_j^- \leq s_j \leq S_j^+ .$$

In the dynamic programming formulation it is necessary to distinguish between stagewise and process (overall or terminal) constraints. In the linear programming formulation, these appeared either as inequalities (stagewise constraint) or equalities (process constraint), and both could be handled automatically. It is usually said that the greater the number of constraints, the easier is the dynamic programming solution since the space to be searched is reduced accordingly. This is true enough with respect to stagewise constraints, but the computational burden is increased in the presence of process constraints. Specifically, the process constraint enters the problem as an additional state variable. Consider, for example, the case in which the disturbance function is to have a prescribed total impulse,

$$r(g, T) = \int_0^T g(t) dt = R . \quad (29)$$

We define a new state variable z_j as

$$z_j \left\{ \begin{array}{c} x_j \\ \dot{x}_j \\ r(g, t_j) \end{array} \right\} = \left\{ \begin{array}{c} x_j \\ \dot{x}_j \\ r(g, t_j) \end{array} \right\} , \quad (30)$$

where $r(g, t_j)$ is the value of the constraint at time t_j. The additional state transformation needed to supplement Eq. (10) is

$$r(g, t_{j+1}) = r(g, t_j) + \Delta r_j .$$

where Δr_j is the change caused in the constraint variable r by application of g_j.

Unfortunately, the addition of another state variable increases the already bothersome burden of dimensionality. An alternate approach possessing the original dimensionality is available for some systems. It has been shown [3] for a certain class of absorbers, including linear systems, that the response function and process constraint can be interchanged without increasing the dimension of the dynamic programming formulation. In the case of min-max displacement for an absorber with prescribed total impulse and time duration, the equivalent problem becomes that of finding the $g(t)$ of duration T, such that $|x| \leq X$ (X prescribed) and the total impulse $r(g, T)$ is maximized. Here

$$\phi_{n+1-j}(x_{j+1}) = \max_{g_i} \sum_{i=j+1}^{n+1} g_i . \quad (31)$$

and in accord with the principle of optimality

$$\phi_{n+2-j}(x_j) = \max \left\{ g_j + \phi_{n-j+1}(x_{j+1}) \right\} \quad (32)$$

is computed for $j = n, n-1, \ldots, 1$. Typical results for this problem are shown in Fig. 4.

SUMMARY

A number of practical problems of a minimum-maximum deviation, or min-max, sort have been described and classified as three types. These have been represented by discrete formulations amenable to solution by such general mathematical programming techniques as linear and nonlinear programming and dynamic programming. Where applicable, linear programming constitutes the most efficient computational approach. Dynamic programming is the most general technique but presents the greatest computational burden for higher order systems. The method is eminently practical, however, for single-degree-of-freedom dynamic systems. Certain of the more interesting problems formulated have not as yet been solved numerically. These will be the subject of future publications.
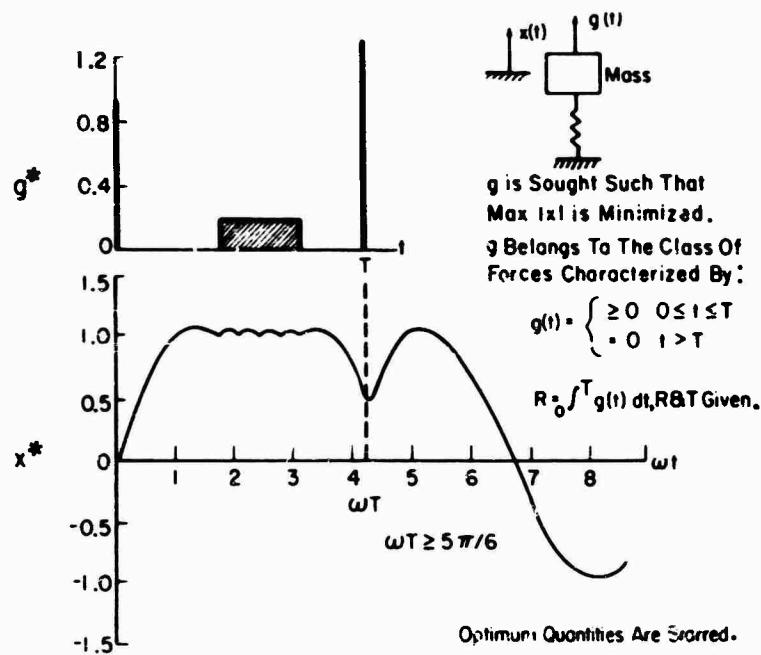
ACKNOWLEDGMENT

Fig. 4. Min-max solution for systems with prescribed
total impulse and time duration of forcing function

REFERENCES

1. T. Liber and E. Sevin, "Optimum Shock Isolation Synthesis," Shock and Vibration Bull., Vol. 35, Part 5, pp. 203-215, Feb. 1966

2. J. C. Blair, J. A. Lovingood, and E. D. Geissler, "Advanced Control Systems for Launch Vehicles," Astronautics and Aeronautics, Vol. 4, No. 8, pp. 30-39, Aug. 1966

3. E. Sevin and W. Pilkey, "Computational Approaches to the Min-Max Response of Dynamic Systems with Incompletely Prescribed Input Functions," to be published in J. Appl. Mech.

*   *   *

STRAIN RESPONSE OF SIMPLY SUPPORTED BEAMS
TO POINT AND ACOUSTIC LOADING

Tony L. Parrott and Joseph A. Drischler
NASA Langley Research Center
Langley Station, Hampton, Va.

Although dynamic strain response is the basic ingredient in fatigue life estimation schemes, there is a lack of documented comparisons of measured and predicted strains for responses of either complex or simple structures. Many investigators have been concerned with measurements of strain responses on structural components under operational conditions for which calculations are impractical to perform. On the other hand, theoretical investigations have been carried out for relatively simple structures for which few experimental strain response tests have been conducted, perhaps primarily because of the difficulty of obtaining a sufficiently close approximation to a set of classical boundary conditions.

It is the purpose of this paper to present a comparison of measured and predicted strain responses for carefully controlled experiments on beams whose boundary conditions approximate, to a high degree of accuracy, those of a simple support. The simply supported boundary condition was found to be readily amenable to mathematical analysis and characterized by low damping. Considerable development work was required in perfecting beam boundary attachments having satisfactory simple support behavior. Dimensions of the beams were chosen so that significant vibration amplitudes (in excess of the beam thickness) could be obtained in the fundamental mode. The beams were excited by sinusoidal and random loadings applied both acoustically (uniformly distributed along beam) and mechanically (at a point location). In addition to strain measurements, both the total equivalent viscous damping and the magnitude of the exciting force were obtained.

In general, good agreement between measured and predicted dynamic bending strain was obtained; however, for sinusoidal point loading the theory overpredicted, and for sinusoidal acoustic loading it underpredicted the dynamic strains. For random loading the theory and experiment were in close agreement. The total equivalent viscous damping, measured by the log decrement technique, was found to have amplitude and modal dependence.

T. L. Parrott

INTRODUCTION

Present-day strain response prediction schemes are intended to provide engineering estimates of the strain levels at critical locations in complex structures loaded by spatially distributed forces characterized by continuous spectra with or without discrete frequencies superimposed. The prediction of strain response is useful for the purpose of estimating fatigue life and for determining noise transmission characteristics. The dynamic strain response of an aircraft or space vehicle structural component to various types of complex dynamic loading depends, in addition to the detailed characteristics of the loading, on the geometry of the structure, the distribution of the structural mass and elasticity, the ability of the structure to dissipate vibrational energy,

and the boundary conditions imposed on the particular structural component of interest by the remaining structure.

Many investigators have been concerned with measurements of strain responses on structural components under operational conditions for which calculations are impractical to perform. On the other hand, theoretical investigations have been carried out for relatively simple structures for which few experimental strain response tests have been conducted, perhaps primarily because of the difficulty of obtaining a sufficiently close approximation to a set of classical boundary conditions.

It is the purpose of this paper to present a comparison of measured and predicted strain responses for carefully controlled experiments on beams whose boundary conditions approximate those of a simple support. It was found that the simply supported boundary condition was readily amenable to mathematical analysis and was characterized by low damping. Considerable development work was required, however, in perfecting beam boundary flexure attachments having satisfactory simple support behavior.

TEST MODEL

Illustrated in Fig. 1 are the boundary conditions associated with the various idealized models used in the classical description of beam behavior. The free-free beam was eliminated from consideration in the present investigation because of the practical difficulty of supporting it in such a manner as to permit the excitation of the higher modes, as well as the infrequent encounter with anything approaching this type of support in existing hardware. The clamped-clamped support was also eliminated from consideration because of the unwieldy mathematics needed to describe the response to random loading and also because of the inherently high joint damping. Finally, the simple support (hinged-hinged) was chosen because of the ease with which the mathematics could be handled, the low damping that could be achieved, and because this type of boundary condition is not too far removed from some practical situations. The last entry illustrates an idealized model of the beam boundary conditions which actually existed. The development work centered around attempting to make the spring stiffness, which governed the vertical displacement, very stiff without introducing an appreciable resistive bending moment [1]. This resistive bending moment is represented by the torsional springs. By using a combination of

Fig. 1. Boundary conditions of end supported beams

analytical and empirical methods, a very close approach to true simple support conditions was achieved.

A schematic diagram of the beam geometry, including flexure support details and strain measuring locations, is shown in Fig. 2. The analytical work indicated that the resisting bending moment would be negligible if the beam thickness to flexure thickness ratio were on the order of 25. The flexures were spot welded to the beam as close as possible to the right-angle bend. Observations indicated that the best performance could be obtained if the flexures were clamped approximately 0.032 in. from the beam. Apparently, this clearance minimized the torsional spring compliance.

As criteria for evaluating the success to which simply supported conditions were
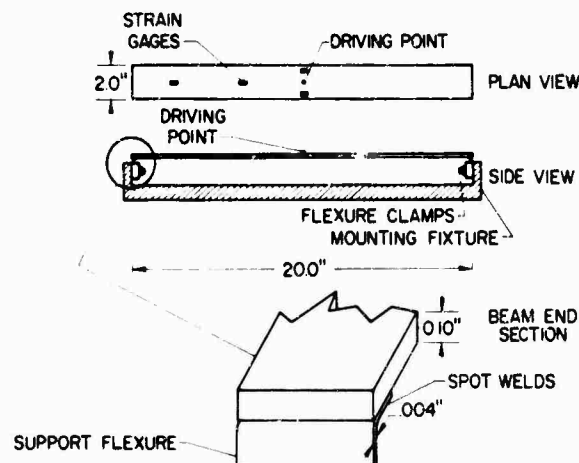

Fig. 2. Schematic diagrams of test beam and support system

78

approached, both natural frequencies and mode shapes were measured. Figure 3 shows a comparison of the measured and calculated frequencies for the first five symmetric modes for a typical beam installation. In this plot the ratio of calculated to measured frequencies is plotted as a function of mode number. It will be seen that the measured frequencies are within 5 percent of the calculated frequencies for all measured modes. However, the agreement is not quite as good at the higher frequencies. This is probably due to the spring action of the flexures, which calculation indicates should become predominant at the higher frequencies.

Fig. 4. Comparison of calculated and measured beam flexural mode shapes
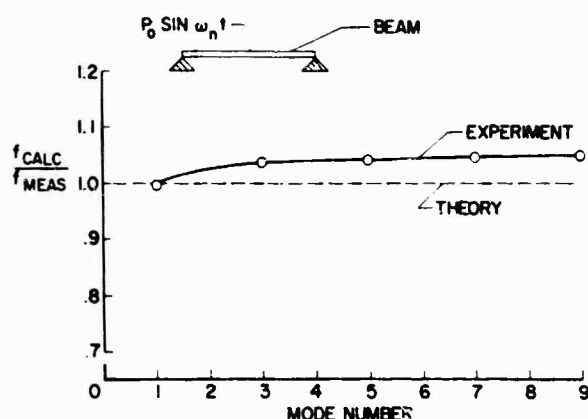

Fig. 3. Comparison of calculated and measured resonant frequencies of test beam

As a further test for the closeness of approach to the simple support condition, the measured mode shapes for the first three symmetrical modes are compared to the theoretical mode shapes in Fig. 4. In these plots the measured strain at two off-center locations on the beam is ratioed to the strain measured at the midspan location and plotted as a function of the beam length. The theoretical mode shape for the simply supported beam is a sinusoid of the appropriate wavelength as shown for the first three symmetric modes. Note that the measured strain ratios are very close to their proper relative magnitudes. Thus, it appears that a close approximation to simple support conditions has been attained based on measured frequencies and mode shapes.

A number of beams, constructed to be as nearly identical as possible, were tested in this experiment to evaluate individual differences of behavior. It was found that as far as frequencies were concerned, the deviation from
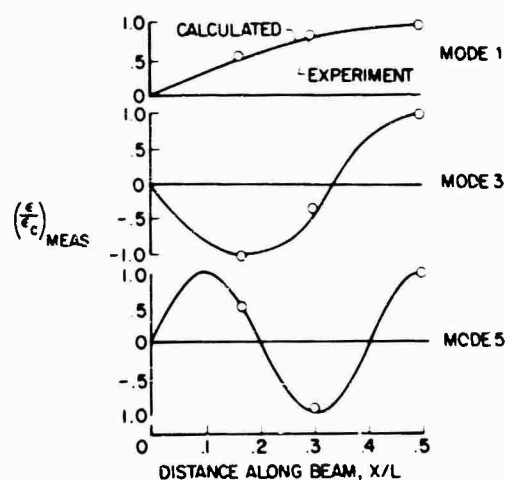
calculations did not exceed 10 percent. Also, nodal patterns were in excellent agreement with calculations. By far the greater part of the differences in behavior between beams was in the dynamic strain response which, in turn, was due to relatively large differences in the damping between the beams.

ANALYSIS

The test program and the data acquired were directed toward the comparison of the measured and the predicted strain response taking into account the detailed nature of the modal damping and the driving force. The equation of motion for a beam undergoing a general time varying distributed loading is given by:

$$EIW_{xxxx} + \rho \ddot{W} + \beta \dot{W} = P(x,t) \qquad (1)$$

where

E = modulus of elasticity ($lb_f/in.^2$),

I = moment of inertia ($in.^4$),

W = deflection (in.),

ρ = mass per unit length ($lb_m/in.$),

β = damping coefficient (lb_f-sec/in.^{2}),

$P(x,t)$ = load distribution along beam ($lb_f/in.$),

W_x = $\partial W/\partial x$, and

$\dot{W}$ = $\partial W/\partial t$.

79

This equation was solved for the four cases corresponding to the type of driving force used in the tests:

    1. Sinusoidal point load,

    2. Random point load,

    3. Sinusoidal acoustic load with normal incidence, and

    4. Random acoustic load with normal incidence.

The normal mode technique used to solve Eq. (1) made use of the characteristic functions for a simply supported beam to express the beam displacement response as a series [2]. The strain response was then obtained by taking the second space derivative of the displacement response. For the point load cases, use was made of the Dirac delta function to express the loading as an idealized point load.

The solutions of Eq. (1) for the rms strain at the midspan location for the above four cases are as follows:

    1. Point sinusoidal load

$$\epsilon(f_n)_{rms} = \left(\frac{6L}{Eb\,h^2\pi^2}\right)\left(\frac{1}{n^2}\right)\frac{P(f_n)_{rms}}{\delta}\,, \qquad (2)$$

    2. Random point load

$$\epsilon_{rms} = \left(\frac{6L}{Eb\,h^2\pi^2}\right)\frac{\sqrt{\pi\omega_n}}{n^2}\frac{P_{rms}}{\delta}\,, \qquad (3)$$

    3. Sinusoidal acoustic loading for normal incidence

$$\epsilon(f_n)_{rms} = \left(\frac{6L}{Eb\,h^2\pi^3}\right)\left(\frac{1}{n^3}\right)\frac{P(f_n)_{rms}}{\delta}\,, \qquad (4)$$

    4. Random acoustic loading for normal incidence

$$\epsilon_{rms} = \left(\frac{12\sqrt{2}\,L}{Eb\,h^2\pi^2}\right)\left(\frac{\sqrt{f_n}}{n^3}\right)\frac{P_{rms}}{\delta}\,, \qquad (5)$$

where

    $\epsilon(f_n)_{rms}$ = root mean square strain response for pure mode excitation (μin/in.),

    L = length of beam (in.),

    b = width of beam (in.),

    h = thickness of beam (in.),

    n = mode number,

    ζ = ratio of damping to critical damping,

    ω = angular frequency (rad/sec),

    f_n = normal mode frequency, and

    $P(f_n)_{rms}$ = sinusoidal loading at a normal mode frequency (lb).

MEASURED DAMPING

The ability to predict the absolute strain magnitude at a given location on a beam undergoing dynamic excitation depends in part on an exact knowledge of the total equivalent viscous damping for each mode of interest as well as how it changes as a function of the response amplitude. Damping was measured by the free decay technique since this was believed to be the most expedient technique available. In Fig. 5, a sample of the measured damping is shown for the first three symmetric modes of a beam as a function of the rms value of the driving force. In this plot, the damping is given on the vertical scale in percentage of critical damping and the driving force is plotted on the abscissa in millipounds of force. Note that the damping in the first mode is essentially independent of response amplitude, having a value of approximately 0.35 percent. However, the higher modes are seen to be dependent on response amplitude; the second mode damping varies from 0.10 percent to about 0.24 percent for the driving force range applied, and the third mode damping varies from about 0.09 to 0.20 percent.

COMPARISONS OF EXPERIMENTAL RESULTS AND THEORY

As indicated previously, a knowledge of the damping and driving force enables prediction of the strain response at any location on a given simply supported beam. Measured strain responses have been obtained at the midspan location of the beam for the four types of dynamic loadings for which analytical expressions have been derived. Comparisons of these measured responses with the analytical estimates are given below.
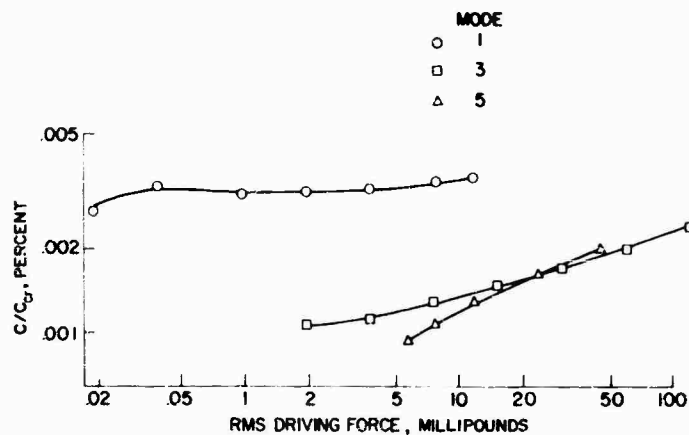
80

Fig. 5. Measured damping for three modes
of test beam as function of driving force

Sinusoidal Point Loading

In Fig. 6, the strain response in micro-
inches per inch is plotted as a function of the
driving force in millipounds. The measured
and predicted strain by use of Eq. (2) is shown
for the first three symmetric modes at the
midspan of the beam. Predicted strain is shown
by the dashed curves and the experimental
strain values are indicated by the symbols.
The driving force in this case was sinusoidal
point loading with a frequency corresponding to
that of the particular mode of the beam being
driven. Note that the agreement between theory
and experiment is quite good.

Random Point Loading

The frequency spectrum of the point load-
ing applied to the beam midspan is shown in
Fig. 7. Note that the spectrum is flat from
20 Hz to approximately 800 Hz. Strain re-
sponses of the beam have been measured for
the first three symmetrical modes to such a
spectrum of force for various levels of force
input. These measured strain responses are
shown in Fig. 8 along with the predicted strain
response of Eq. (3) (modal theory) as a function
of the mode number. Also included for compar-
ison is the strain predicted for the first mode
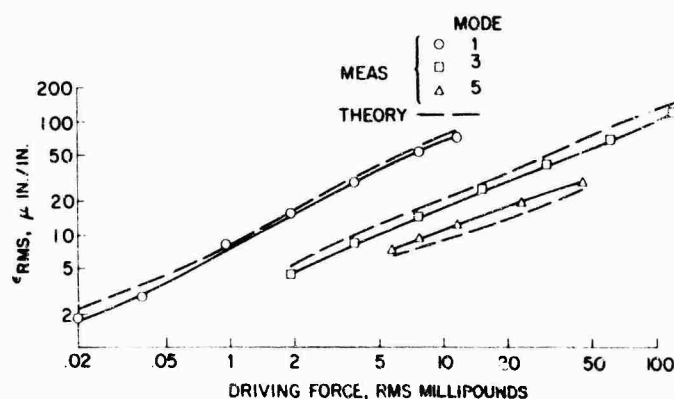response by the well-known Miles theory [3].

Fig. 6. Comparison of calculated and
measured modal strain responses of
test beam as function of sinusoidal point
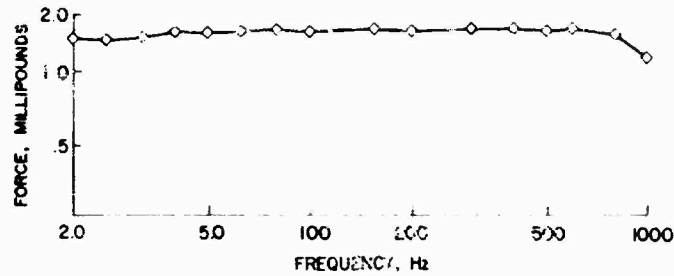driving force

81

Fig. 7. Frequency spectrum of
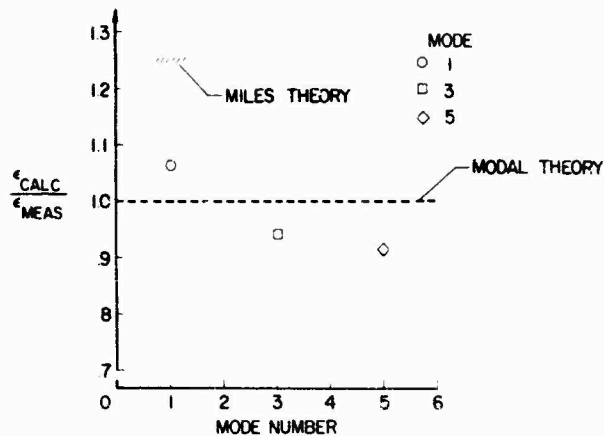random point loading

Fig. 8. Comparison of calculated and
measured strain responses for random
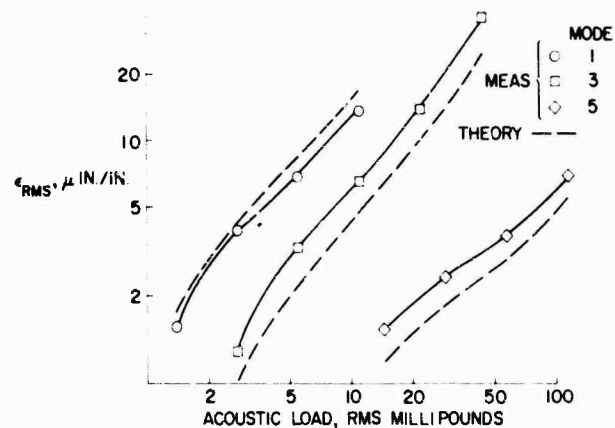point loading

Fig. 9. Comparison of calculated and
measured modal strain responses for
sinusoidal acoustic loading

Note that the Miles theory is overpredicting as expected, being approximately 25 percent high. The modal theory is also overpredicting and varies from 7 to 15 percent above the experimentally observed strain response.

Uniform Sinusoidal Acoustic Loading

In Fig. 9 is shown the measured strain response and strain response predicted from Eq. (4) for acoustic loading of the sinusoidal type where the acoustic loading is expressed in millipounds of force. The acoustic loading was measured by microphones flush mounted into a surface in which the beam was also mounted to provide baffling. In the first mode, theory and experiment are again in good agreement, with theory overpredicting. In the two higher modes, however, this trend is reversed. Here the theory seems to be underpredicting, although the general trend of the strain response is still predicted very well. Greater discrepancies will probably be encountered between theory and experiment when acoustic measurements are

involved because of the inherent lack of precision associated with extrapolating an acoustic pressure measurement from a rigid surface to a nearby vibrating surface.

Uniform Random Acoustic Loading

The frequency spectrum of the random acoustic loading is shown in Fig. 10. A flat spectrum cannot be obtained with the means available for producing acoustic loading. The beam resonance frequencies of 20, 200, and 500 Hz are indicated on the plot by the vertical lines. Note that the beam frequencies are located at points on the spectrum where there is a local minimum or where the spectrum is changing rapidly. Hence, it was surmised that this type of spectrum would provide a severe test for the theory since the assumption was made that the excitation for each mode consisted of white noise with a level corresponding to that of the actual spectrum level at the resonant frequency of the particular mode of interest.
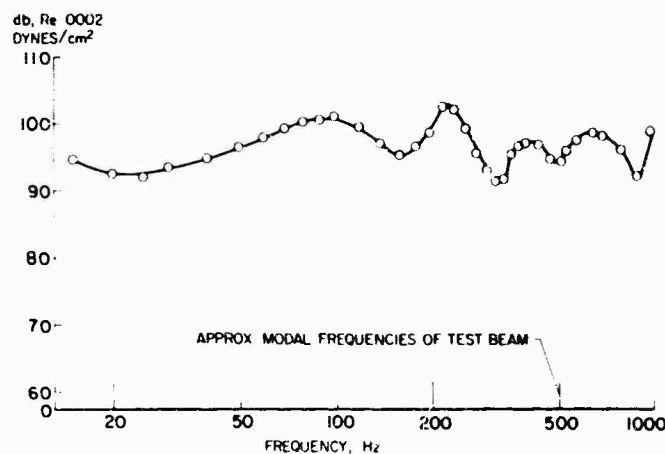
82

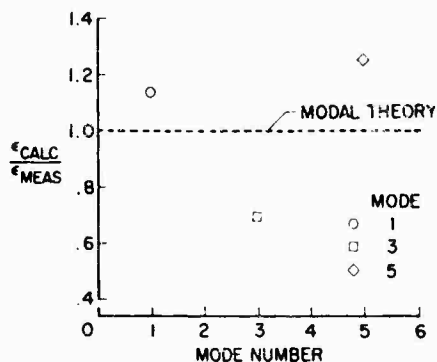Fig. 10. Frequency spectrum of random acoustic loading applied to test beam

Fig. 11. Comparison of calculated and measured strain responses for random acoustic loading

The results in Fig. 11 indicate the deviation of experiment from theory for the input spectrum shown in Fig. 10. The data are plotted as the ratio of calculated to measured strain response as a function of the mode number. Note that the theory predicts the strain response to within about 40 percent. The greater deviation of experiment from theory for the third mode may somehow be related to the fact that the spectrum was changing rapidly with respect to frequency for this mode; however, for the most part the discrepancies are believed to be due to experimental error. These results indicate that the present assumptions and approximations used in the modal analysis schemes for predicting strain levels are adequate for strain response estimates for the simple structures used in this experiment.

CONCLUDING REMARKS

A technique has been employed for the design of simple structures to approximate simply supported boundary conditions characterized by low damping. The use of this technique on a simple beam has established confidence in modal analysis methods for providing good engineering estimates of strain levels for loadings ranging in complexity from simple sinusoidal point loading to random acoustic loading.

REFERENCES

1. Dennis U. Noiseux, Norman Doelling, Preston W. Smith, and James J. Coles, "The Response of Electronics to Intense Sound Fields," WADD TR 60-754, Jan. 1961

2. R. L. Barnoski, "Response of Elastic Structures to Deterministic and Random Excitation," AFFDL-TR-64-199, May 1965

3. John W. Miles, "On Structural Fatigue Under Random Loading," J. Aero. Sci., Vol. 21, No. 11, pp. 573-762, Nov. 1954

DISCUSSION

Mr. Smith (Bell Aerosystems Co.): Did you investigate how the damping of the specimen was distributed between the joints at the two ends, the material itself, the internal material damping, and the basic acoustic damping? I assume the test was not conducted in a vacuum. Second, when you compared the responses for the random point loading, the analysis of this spectrum appeared to be coarse. This might account for the differences between the experimental and theoretical results. Third, how was the random acoustic loading correlated along the length of the beam? It obviously plays a vital part, again, in the comparison between theory and experiment.

Mr. Parrott: I did not try to distinguish between the various components of damping; I only measured the total equivalent viscous damping, using the logarithmic decrement, exciting the specimen sinusoidally, letting it decay, and taking the first 3 db of the record.

Mr. Smith: In the spectral analysis of the point random loading, the points on your graph appear to be quite wide apart in frequency. You are playing with three lightly damped modes, and your spectrum might not be as flat as you think it is.

Mr. Parrott: We assumed in the calculations that the spectrum was actually white noise at the point where the beam was resonating. We thought we could do this because with the low damping, less than 1 percent of critical for this beam, there was no intermodal coupling. We simply assumed all the strain response to be due to that particular mode; we filtered out

all modes of the strain response except one and looked at it.

Mr. Smith: I assume that spectrum was your input spectrum of the point loading.

Mr. Parrott: Yes. This is a 1/3-octave band analysis of the force loading.

Mr. Smith: Your modes are very much less damped than a 1/3-octave analysis of your input spectrum could handle. Your spectrum might not be flat, and this could account for the scatter between theoretical and measured responses.

Mr. Parrott: Right, but in the experimental analysis we centered the filter of the 1/3-octave band analyzer on the beam resonant frequency and looked with several other widths of filters. It seemed that we were getting all the strain response in that particular mode. Damping may have played a part in some of our analysis scatter here because we measured damping using a sinusoidal excitation and had to extrapolate back to the approximate amplitudes at which we felt the specimen was responding under random loading. Perhaps the damping values are off in the region in which we are interested for random loading.

Mr. Smith: The third question was the spatial correlation of the acoustical loading on the beam.

Mr. Parrott: The loading was normal impingement, and we have no reason to believe that it was anything but unity throughout the total length of the beam.

*　　*　　*

PREDICTION OF FLIGHT VIBRATION LEVELS
FOR THE SCOUT LAUNCH VEHICLE

Robert B. Bost
LTV Aerospace Corporation
LTV Astronautics Division
Dallas, Texas

A widely used technique for establishing random vibration criteria is based on scaling of measured vibration data by such factors as acoustic sound pressure level, mass loading, and surface weight density. This paper presents a prediction procedure developed in the process of establishing random vibration criteria for the Scout launch vehicle. The prediction procedure was designed to define the acoustically induced random vibration environment throughout the Scout vehicle by using the limited data sample from six vehicles.

A transfer function relating the internal vibration level to the external noise level was established by use of the measured vibration data and the calculated external noise levels at the point of measurement. This transfer function was then used to calculate the expected vibration levels in each area of the vehicle from the noise level at each location. Statistical methods were used to establish confidence levels for these calculations.

The success of the prediction procedure is demonstrated by comparison of the predicted vibration levels with measured data obtained on subsequent Scout flights. In addition, the applicability of the procedure to other vehicles is demonstrated by comparison of predicted and measured vibration levels for the Atlas-launched fire velocity package.

R. B. Bost

INTRODUCTION

The prediction of environmental vibration levels for a new vehicle is a problem continually facing the vibration engineer. The difficulty of this problem is only slightly mitigated when the engineer is subsequently required to modify the predicted environment on the basis of limited measured data obtained in the vehicle flight test program.

Several methods of predicting environmental vibration levels have been formulated by various investigators in the dynamics field. These methods are, in general, based on empirical information. Some of the methods have been employed with considerable success, particularly where the vibrations are induced solely by acoustic excitation. In this case, a strong correlation usually exists between the external noise level and the induced vibration level, so a transfer function may be defined which reflects the observed correlation.

It is the purpose of this paper to present a transfer function method for the prediction of acoustically induced random vibrations. This method was developed for the Scout launch vehicle to aid in revising the vibration test requirements to simulate better the actual flight environment. The method was developed from analysis of measured vibration data obtained during the boosted flight phase of six different Scout vehicles. These vehicles were equipped with 19 vibrometers located in three of the four vehicle interstage structures and with sensitive axes in both the longitudinal and transverse directions.

The success of the prediction procedure is demonstrated by comparison of the predicted vibration levels with measured data obtained at different locations on subsequent Scout flights. In addition, the applicability of the procedure to other launch vehicles is demonstrated by comparison of measured and predicted vibration levels for the fire velocity package launched by the liquid-propellant Atlas booster.

REVIEW OF SCOUT FLIGHT DATA

An examination of the flight vibration data from the six Scout vehicles indicated that the maximum random vibration levels occur at a flight time corresponding to maximum dynamic pressure and are induced by the turbulent boundary layer surrounding the vehicle at this time. These vibrations are broadband random in character and approximate a stationary Gaussian random process for several seconds of flight time. These characteristics were verified by amplitude probability density analyses and by autocorrelation analyses.

Since the Scout vibration environment at maximum dynamic pressure arises solely from acoustic excitation, it was elected to devise an analysis procedure whereby all vibration data arising from this source could be considered as a single statistical sample. This was accomplished by the transfer function approach [1] which consists of relating the external sound pressure level to the internal vibration level through a transfer function. Since the vibration data currently available for the Scout are quite limited for some portions of the vehicle, this was considered to afford the best estimate of the overall vehicle vibration environment consistent with the current data sample.

PREDICTION OF EXTERNAL NOISE LEVELS

The application of the transfer function method required a knowledge of the external noise levels existing at maximum dynamic pressure. Since measured data were not available, a prediction procedure was used to estimate these levels.

External sound pressure fluctuations induced by turbulent boundary layers have been shown by several authors [2,3] to be strongly correlated with the free-stream dynamic pressure. The correlation is represented by a relation of the form

$$P_R = K q_\infty \qquad (1)$$

where P_R is root mean square (rms) boundary layer pressure, q_∞ is the free-stream dynamic

pressure, and K is a factor which may vary over a wide range depending on the aerodynamic "cleanliness" of the vehicle. Measurements on the Scout vehicle [4] indicate a value of K on the order of 0.005. Equation (1), written in terms of the overall sound pressure level (OASPL), for a K value of 0.005 is

$$OASPL = 20 \log P_R = 20 \log q_\infty + 82 \text{ db}. \qquad (2)$$

relative to 0.0002 dynes/sq cm. This equation is shown graphically in Fig. 1 by the curve labeled "conventional."

Experimental data indicate that the correlation represented by the above equation tends to overestimate the magnitude of the external pressure levels in the supersonic region of flight. The deviation from the conventional curve suggested by Van Houten [3] for higher dynamic pressures is shown in Fig. 1 superimposed on the conventional curve. This curve was used to estimate the Scout boundary layer noise levels at maximum dynamic pressure.

The spectrum of sound pressures have been correlated with the Reynolds, Strouhal, and Mach numbers as a combined parameter [2] (Fig. 2). The parameters defining the coordinates of the graph in Fig. 2 are as follows: C_o is the speed of sound at sea level; V is the free-stream velocity; ν_o and ν_o are the kinematic viscosities at sea level and at the altitude of operation, respectively; and $\cdot$ is the thickness of the boundary layer.

The boundary layer thickness was determined by the flat-plate approximation [5],

$$\cdot = 0.37 L (\nu_\infty VL)^{1/5}. \qquad (3)$$

where L is the distance from the leading edge of the structure initiating the disturbance, and the quantity within the parentheses is the inverse of the Reynolds number. For these calculations, the nose of the vehicle was assumed to initiate the disturbance.

The one-third octave band sound pressure level (1/3 OBSPL) was calculated from the sound pressure spectrum level (SPL) by the relation

$$1/3 \, OBSPL = SPL + 10 \log \Delta f. \qquad (4)$$

where the SPL was established at the geometric mean frequency, $f_M = (f_L f_H)^{1/2}$, and $\Delta f = f_H - f_L$ is the one-third octave bandwidth.

The application of this procedure to a typical Scout vehicle operating at a free-stream dynamic pressure of 2600 psf at an altitude of 35,000 ft is shown in Fig. 3.
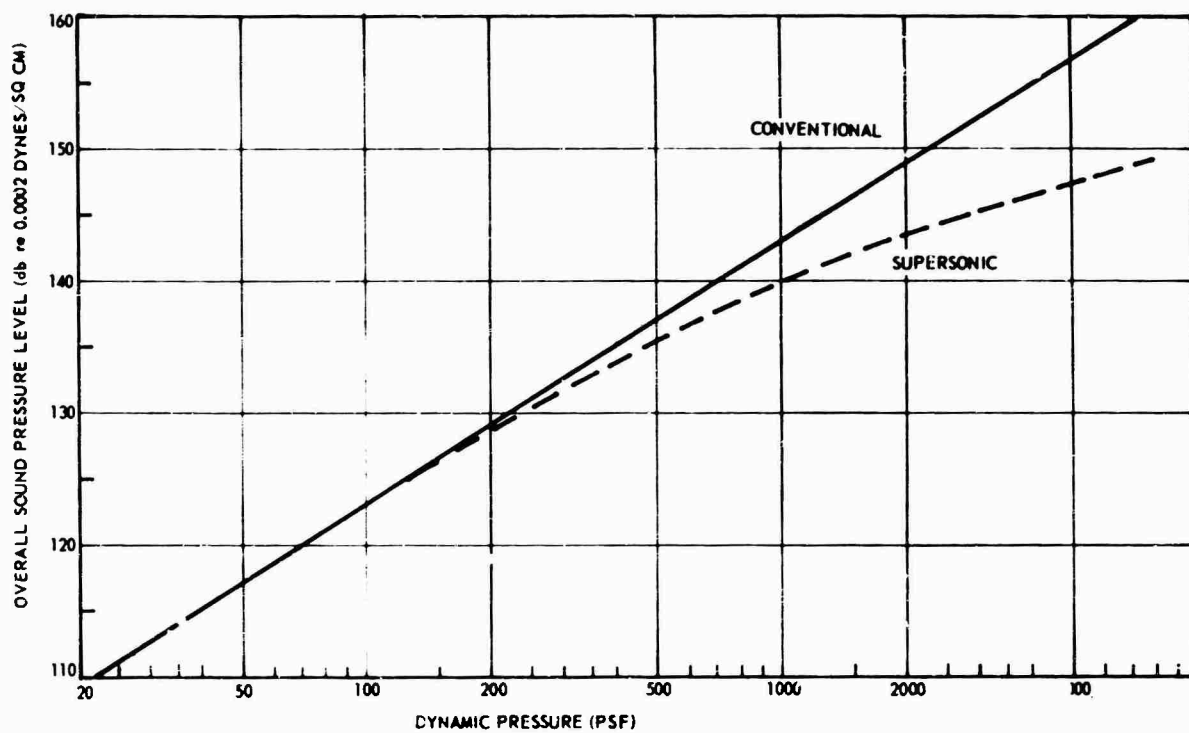
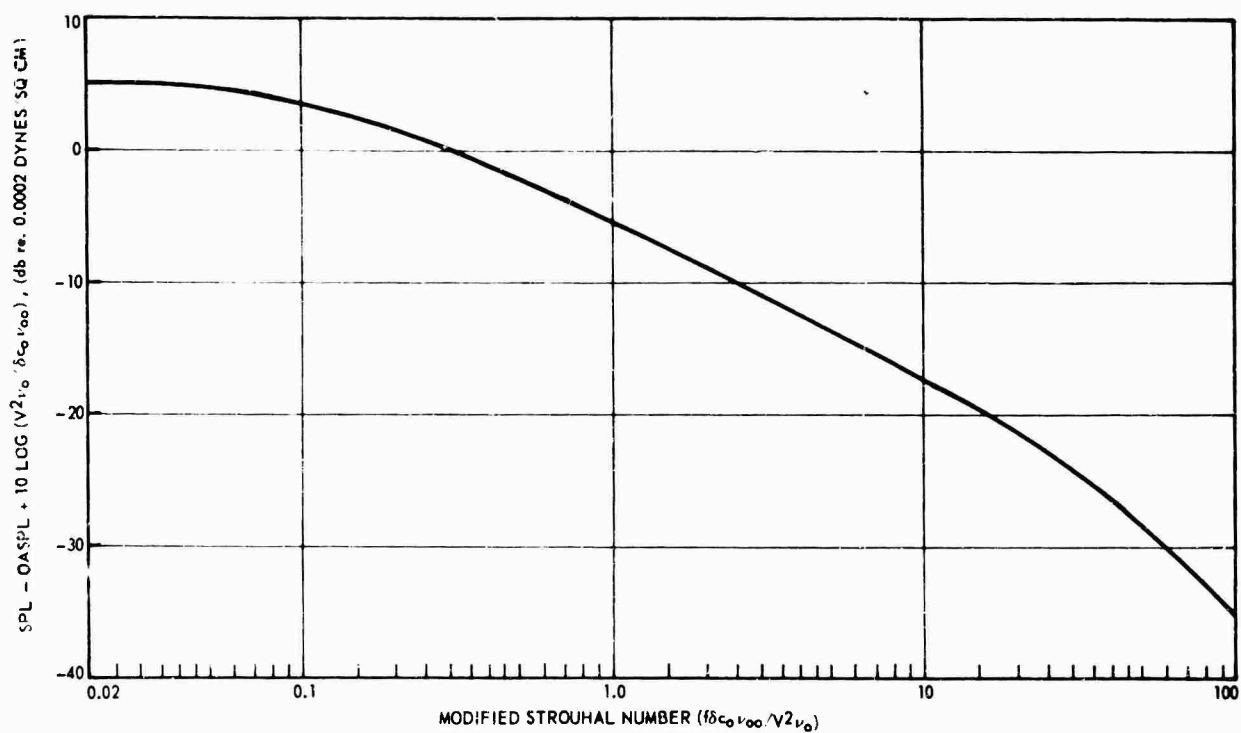Fig. 1. Boundary layer noise external overall sound pressure level

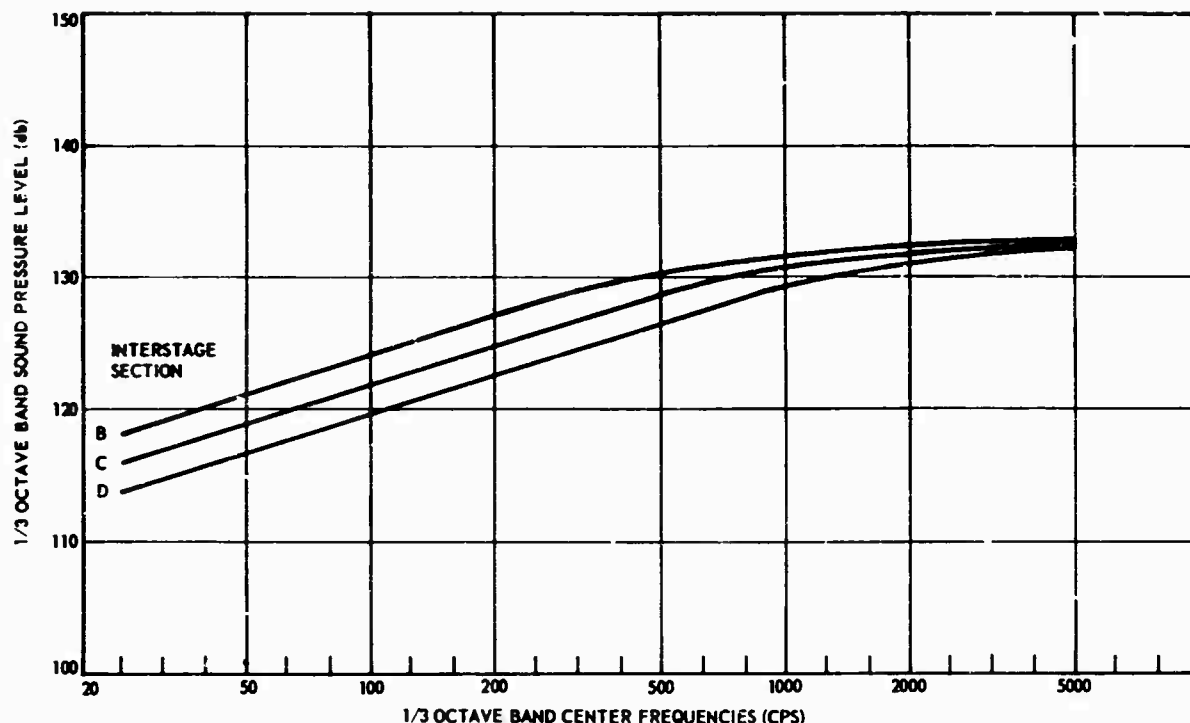Fig. 2. Normalized boundary layer pressure spectrum

87

Fig. 3. One-third octave band sound pressure levels at
maximum dynamic pressure for typical Scout vehicle

DEVELOPMENT OF TRANSFER
FUNCTION

The transfer function approach to the pre-
diction of random vibration environments in-
duced by acoustic excitation is limited prima-
rily to the prediction of the broadband
characteristics of the vibration. Some authors
[6] have used a transfer function to define the
octave band vibration levels, while others [1]
have attempted a finer definition by considering
one-third octave band levels. Both approaches
apply an arbitrary "correction factor" to ac-
count for possible narrow-band peaks in the
vibration spectrum.

The transfer function considered here is in
terms of one-third octave band levels, but the
appropriate correction factors are obtained by
correlation with measured narrow-band data
rather than by specifying some arbitrary factor.

Details of Transfer Function
Definition

The one-third octave band external sound
pressure levels in decibels relative to 0.0002
dynes/sq cm were calculated by the procedure
outlined in the preceding paragraphs for each
measurement location on each of the instru-
mented Scout vehicles. The corresponding

measured one-third octave band rms vibration
levels were extracted from the acceleration
time histories and converted to decibels rela-
tive to 1g rms. The difference of these two
quantities, 1/3 OBSPL - 1/3 OBGRMS, was defined
as the transfer function relating external sound
pressure level at maximum dynamic pressure
to the internal vibration levels. These data are
shown as a function of the one-third octave
band center frequencies by the scattered points
in Fig. 4.

A regression analysis was performed on
these data to provide a "best fit" in the least
squares sense. This analysis was conducted to
smooth the data and to provide a statistical
basis for establishing confidence in predictions
made from it. Quartic regression was found to
provide the minimum standard deviation of er-
ror about the regression line, and this fit is
shown superimposed on the data points of Fig. 4
along with the corresponding 80 and 95 percent
confidence limits.

The external sound pressure levels shown
in Fig. 3 were used in conjunction with the
transfer function shown in Fig. 4 to predict the
one-third octave band g rms vibration levels
for a typical Scout vehicle. The resulting levels
were then converted to an acceleration power
density spectrum by assuming the spectrum
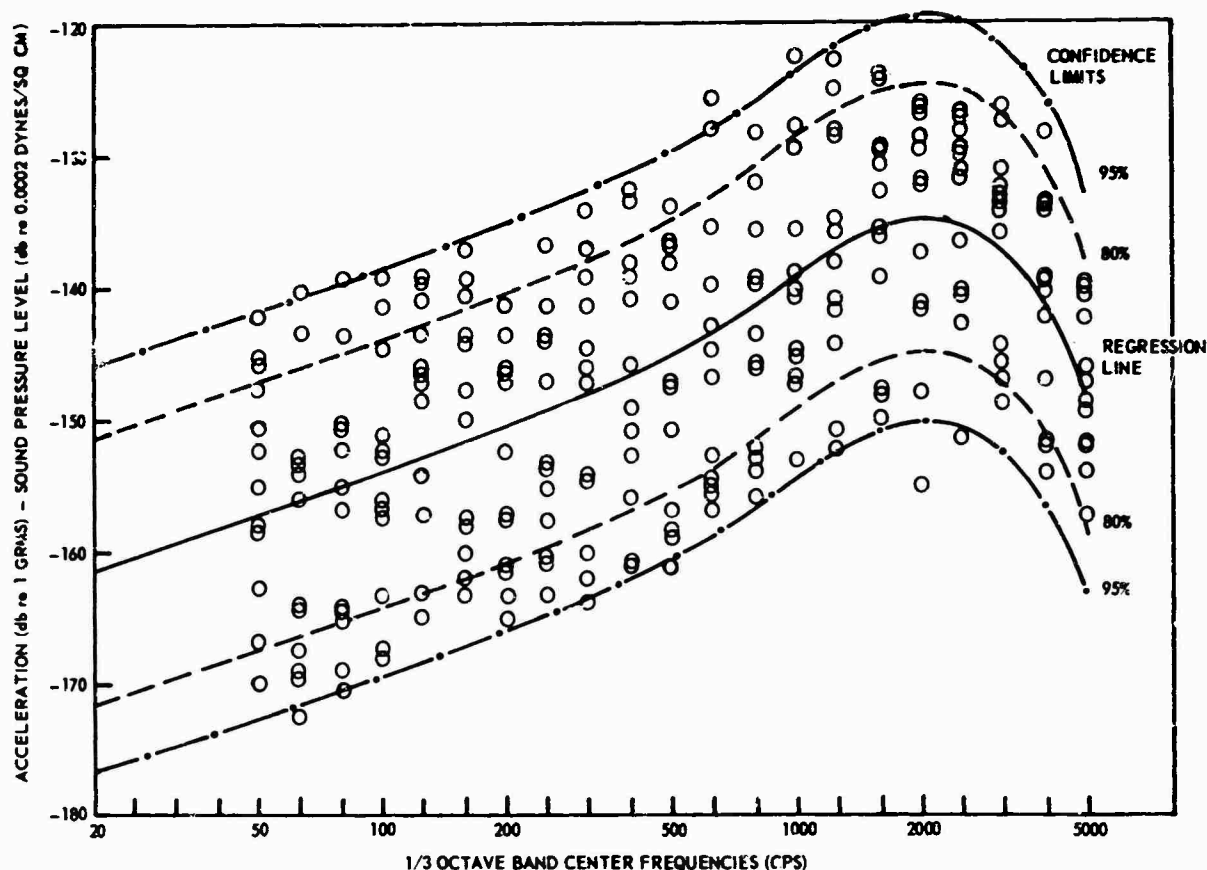was flat within each one-third octave band.

88

Fig. 4. Structural response to acoustic loading in one-third octave band levels

The calculated acceleration power density spectra for the three Scout interstage sections designated "B", "C" and "D" are shown in Figs. 5 through 7. These spectra are based on the transfer function defined by the regression line and by the upper 80 and 95 percent confidence lines of Fig. 4. The spectra presented represent a smooth envelope of the spectra calculated by assuming a flat spectrum in each of the one-third octave bands.

CORRELATION WITH MEASURED DATA

The calculated acceleration power density spectra of Figs. 5 through 7 were compared with measured narrow-band data to establish the appropriate correction factors to be placed on the vibration levels predicted on the basis of the regression line of Fig. 4. This comparison is shown in Figs. 5 through 7 in terms of an envelope of all of the measured data from each of the three interstage sections. As can be seen, the upper 95 percent confidence line provides a satisfactory envelope of all of the peaks in

the measured narrow-band data. On this basis, the upper 95 percent confidence line of Fig. 4 was chosen as the appropriate "transfer function" relating the external noise levels and the induced vibration levels for each of the Scout interstage sections.

APPLICATION TO OTHER VEHICLES

While the data presented here were collected from the Scout launch vehicle, these empirical curves have been used to predict vibration levels for other launch vehicles where vibration data are available. The predicted levels fit the measured data with about the same degree of accuracy as they do the Scout data. This is illustrated in Figs. 8 and 9 by comparison of measured and predicted vibration spectra at two locations on the fire velocity package launched by a liquid-propellant Atlas booster. As for the Scout data, the upper 95 percent confidence level provides a satisfactory envelope of all of the peaks in the measured spectra.

89
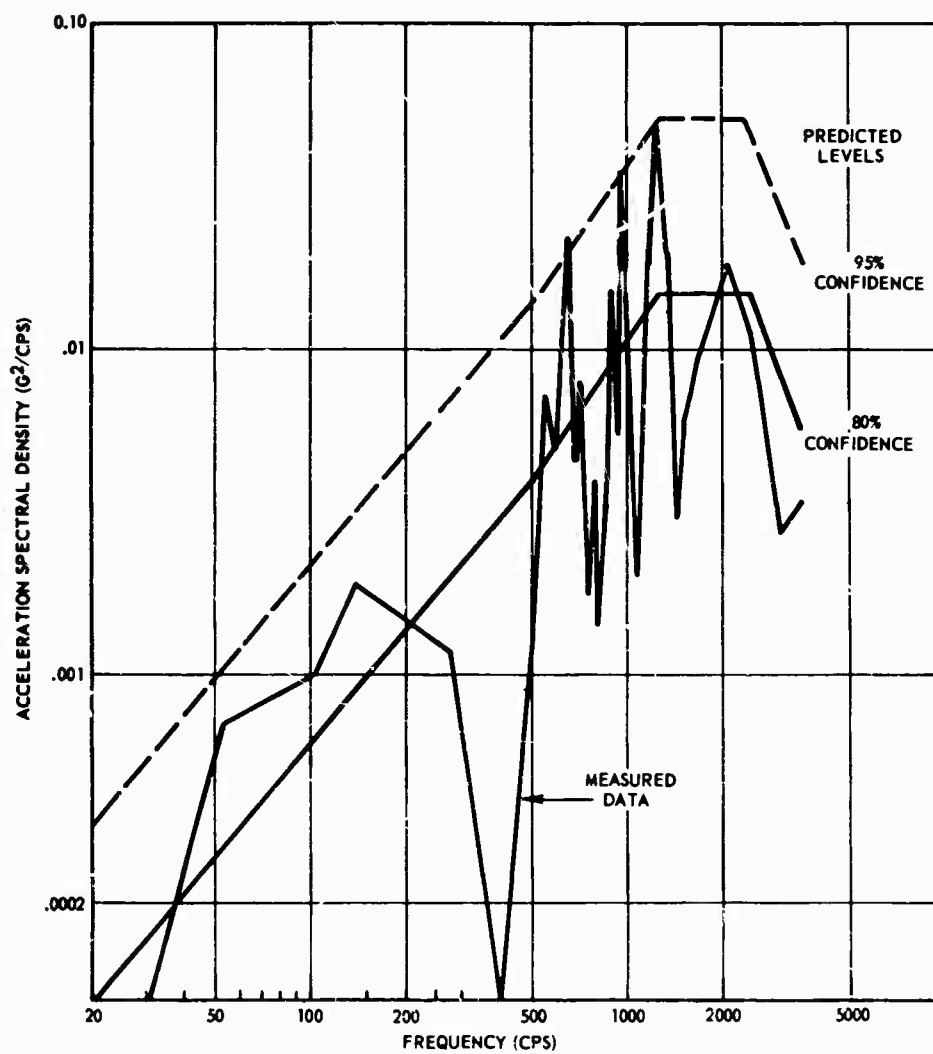
Fig. 5. Measured and predicted acceleration power
density spectra for Scout vehicle "B" section
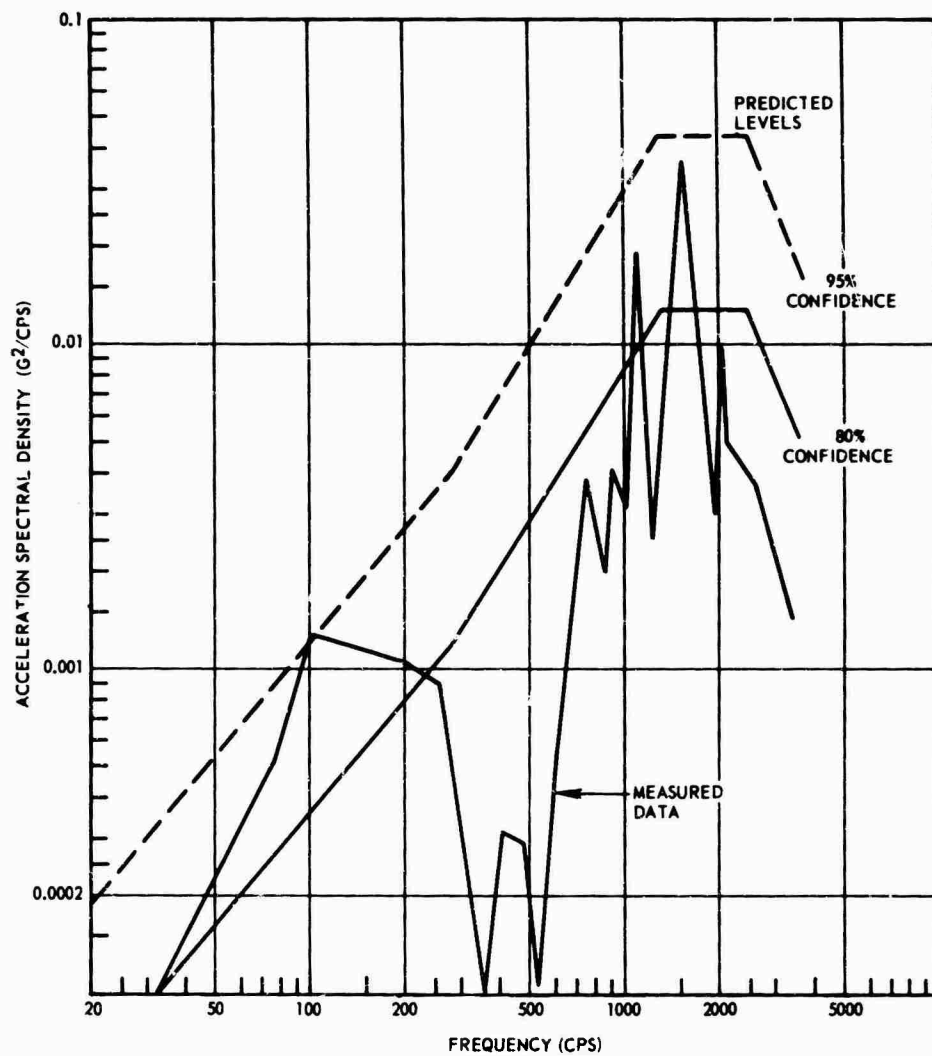
Fig. 6. Measured and predicted acceleration power
density spectra for Scout vehicle "C" section
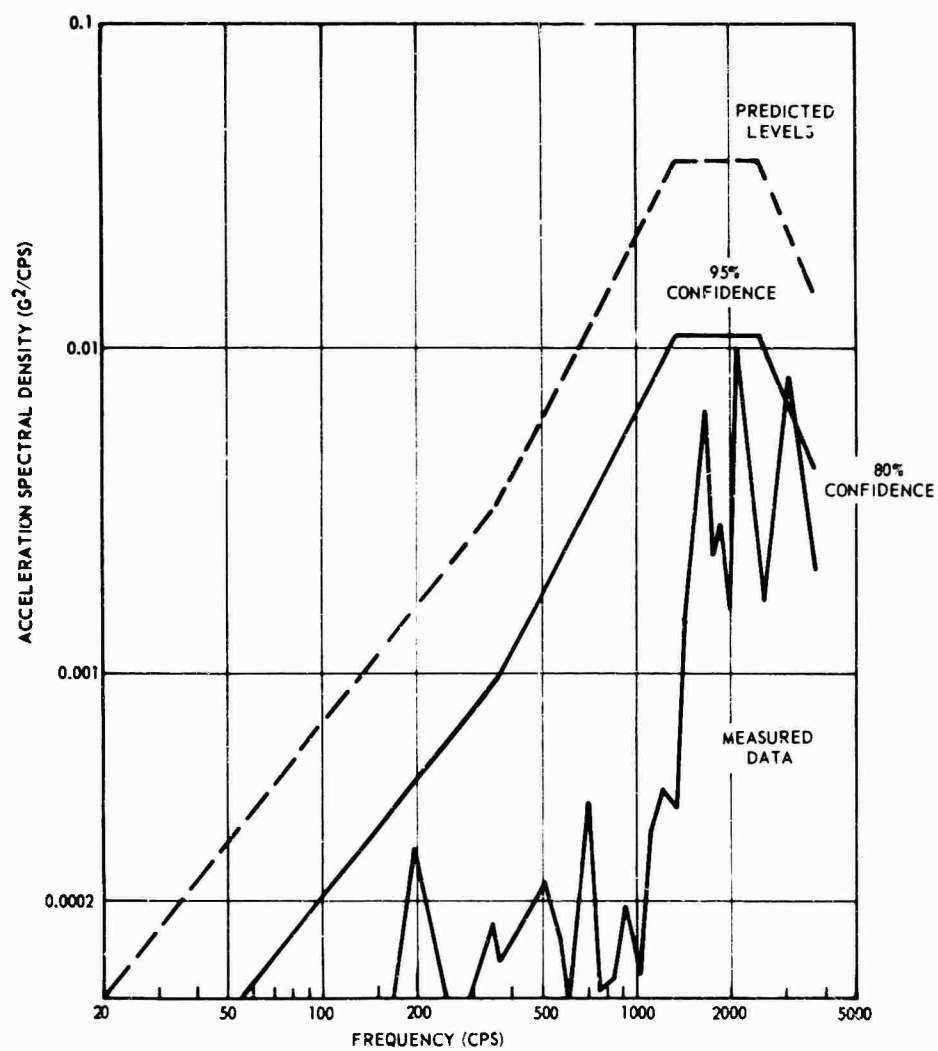
Fig. 7. Measured and predicted acceleration power
density spectra for Scout vehicle "D" section
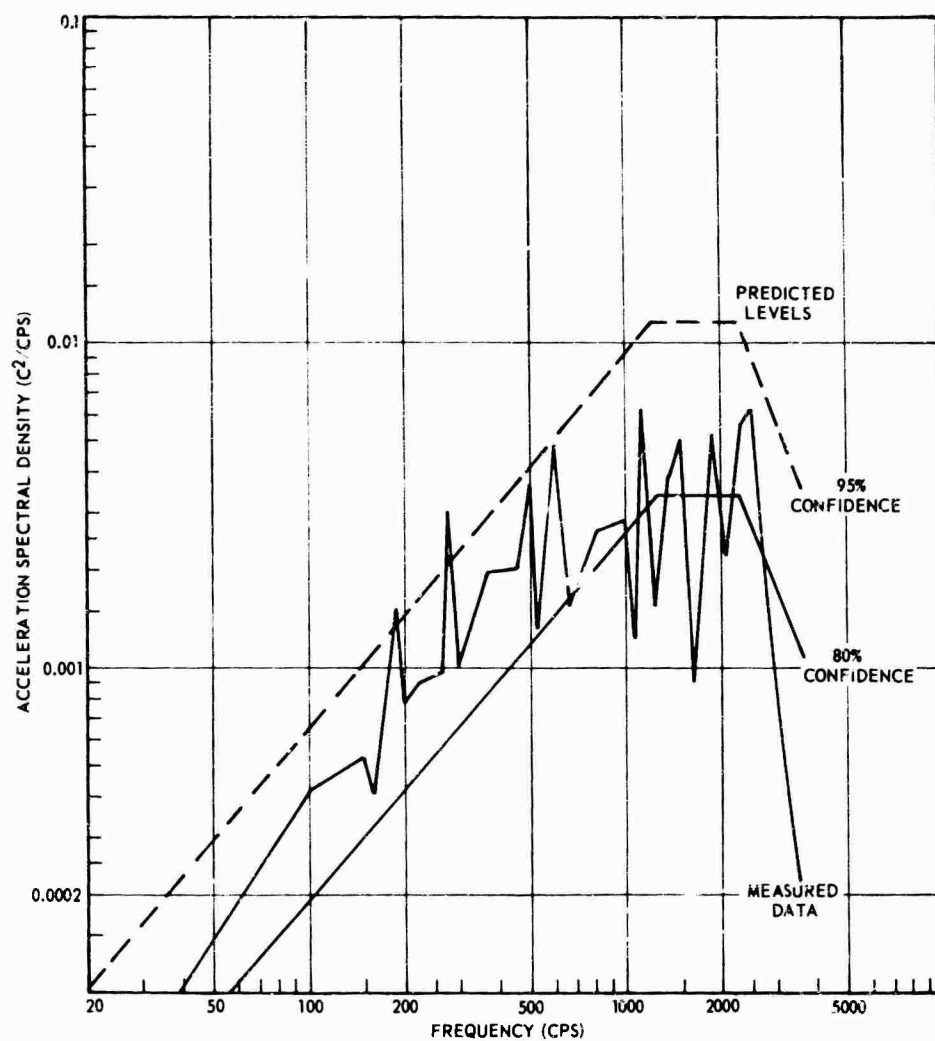
Fig. 8. Measured and predicted acceleration power density
spectra for fire velocity package -- equipment shelf
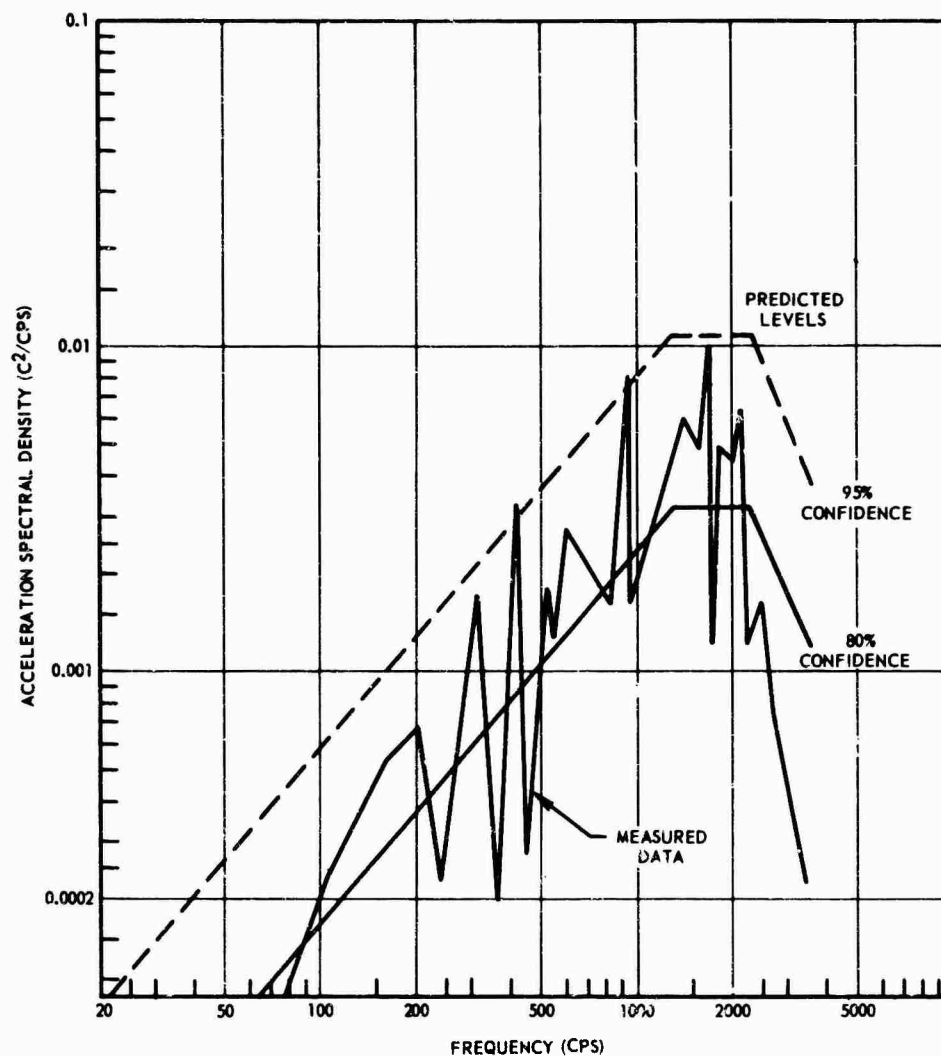
Fig. 9. Measured and predicted acceleration power density
spectra for fire velocity package -- aft separation ring

CONCLUDING REMARKS

By choosing the desired risk level (confidence line), the transfer functions presented in Fig. 4 may be used with reasonable success on other launch vehicles. In particular, the 95 percent level should satisfactorily envelop most narrow-band peaks and, hence, provide a good first estimate of the vibration environment of a new vehicle.

REFERENCES

1. R. W. Mustain, "Prediction of Random Environments," SAE National Aeronautic and Space Engineering and Manufacturing Meeting, Los Angeles, Sept. 23-27, 1963

2. K. M. Eldred, W. J. Roberts, and R. White, "Structural Vibrations in Space Vehicles," WADD TR 61-62, Dec. 1961

3. J. J. Van Houten, "Analysis Procedures for Predicting Boundary-Layer-Induced Noise," LTV Appl. Res. Div. Rept. 718-01, Jan. 1962

4. D. A. Hilton, "Scout-Vehicle Aerodynamic Noise Measurements," Noise Control, Vol. 2, pp. 28-31, Oct. 1963

5. H. Schlichting, "Boundary Layer Theory," p. 35. Pergamon Press, New York, 1955

6. P. T. Mahaffey and K. W. Smith, "Method for Predicting Environmental Vibration Levels in Jet Powered Vehicles," Noise Control, Vol. 6, pp. 20-26, July 1960

DISCUSSION

Mr. Whiteley (Ampex Corp.): Did you develop a transfer function from acoustical noise to mechanical vibration?

Mr. Bost: Yes, that is correct.

Mr. Whiteley: Is this felt applicable to various space vehicles?

Mr. Bost: I think it is definitely applicable to aerodynamically generated noise. We have tried it in a few cases for engine-generated noise, and it seems to give a fairly good correlation there also. We have tried it on other vehicles where measured data are available, and generally it gives a pretty good prediction of the maximum level.

Mr. Whiteley: This acoustic coupling, then, is felt to come through the skin. Is it structurally or acoustically coupled on the inside?

Mr. Bost: It is structurally coupled. It is transmitted through the skin to the basic structure. All these measurements were made on primary structure which was fairly heavy and stiff.

Mr. Franken (Bolt Beranek and Newman): What is the typical diameter of the Scout vehicle on which the empirical procedure was based?

Mr. Bost: It varies from about 40 to 30 in.

Mr. Franken: With this diameter of about 2-1/2 to 3 ft, the ring resonance would be somewhere around 1500 cycles. Perhaps the peak in your transfer function is due to some cylindrical behavior which ought to be scaled by the diameter of the vehicle you are dealing with.

*   *   *

RESPONSE OF STRUCTURAL COMPONENTS OF A LAUNCH VEHICLE TO IN-FLIGHT ACOUSTIC AND AERODYNAMIC ENVIRONMENTS

Khushi L. Chandiramani and Richard H. Lyon
Bolt Beranek and Newman Inc.
Cambridge, Massachusetts

A unified system of procedures is developed for estimating some important classes of in-flight noise environments and the resulting surface vibration on a typical launch vehicle. Noise environments are classified according to the nature of the spatial and temporal correlations of the associated fluctuating pressure fields. The structural elements considered are a cylinder and a flat plate. The presentation is general enough to apply to orthotropic and liquid-loaded structures. Some numerical examples are presented for estimates of frequency spectra of acceleration on the vibrating structures.

R. H. Lyon

INTRODUCTION

This paper summarizes a recent study [1] undertaken to establish a system of procedures for estimating some important classes of in-flight noise environments and resulting surface vibration levels experienced by skin segments of a typical launch vehicle. The in-flight noise environments are estimated empirically, based largely on available laboratory and field data and well-accepted similarity arguments. The procedures for response estimation draw heavily on the available pool of completed analyses, which have been modified to apply to vehicle skin segments that are orthotropic because of stringers and stiffening rings or filled with liquids.

The study results in a basic system of simple procedures and solutions that are comprehensive enough to establish some preliminary design specifications and intelligible enough that an intuitive understanding of the results can be gained.

The study was undertaken with the following objectives in mind:

1. The final estimates should be in more or less closed form, so that the effect of various input parameters can be easily appraised, and so that detailed calculations (such as numerical integration or numerical solution of a differential equation) are not necessary for final predictions.

2. The input parameters themselves should be as few as possible and should relate easily to trajectory and geometric parameters.

The above objectives dictated certain compromises — for example, ignoring of variations in convection velocity and eddy decay in the mathematical model for pressure fluctuations under a turbulent boundary layer, use of thin-shell theory, and ignoring of flutter-type interaction between the vibrating structure and the exciting pressure field.

IN-FLIGHT ACOUSTIC AND AERODYNAMIC ENVIRONMENTS

Classification of Noise Sources

Figure 1 presents a summary of environmental noise sources in terms of vehicle configuration and Mach number. The letters in the figure refer to different types of noise sources.

The noise sources can be broadly classified into two categories: the acoustic noise associated with rocket jet exhaust stream which dominates during or shortly after vehicle lift-off, and the aerodynamic noise which dominates during the rest of the trajectory. Table 1 shows the classification and coding of these noise sources. Table 1 and Fig. 1 broadly define the range of trajectory and geometric parameters over which a particular type of environment is
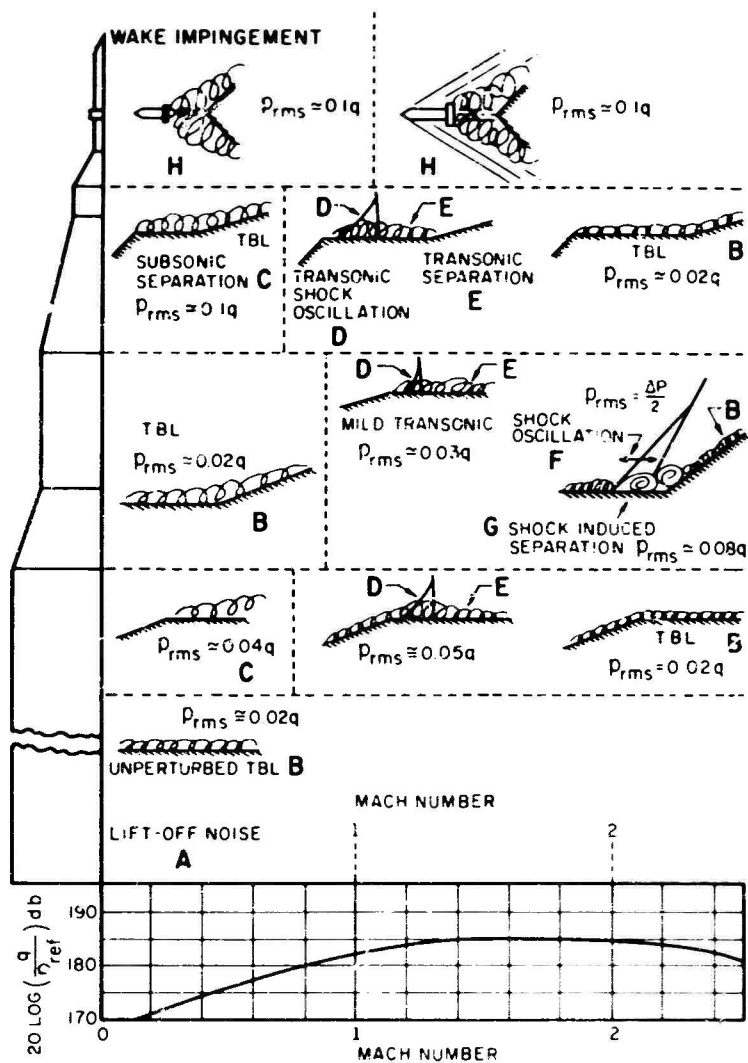
Fig. 1. Summary of environmental noise sources as a function of vehicle configuration and Mach number

TABLE 1
Classification and Coding of In-Flight Acoustic and Aerodynamic Environments

Environment	Flight Mach No.	Code
Acoustic noise during lift-off	—	A
Unperturbed and attached turbulent boundary layer	—	B
Separation aft of flares at subsonic speeds	1	C
Shock oscillation aft of flares at transonic speeds	1	D
Separation aft of transonic shock oscillation (D)	1	E
Shock oscillation forward of flares at supersonic speeds	1	F
Separation aft of supersonic shock oscillation (E)	1	G
Wake impingement	—	H

manifested, and the associated overall root mean square level p_{rms} of fluctuating pressure in terms of free-stream dynamic head q. Here the detailed procedures for estimating the environmental parameters are omitted; they may be found in Ref. 1. Extensive use of available laboratory and flight data was made for this purpose.

Grouping of Noise Sources for
Response Estimation

For vibration analysis, it is convenient to group the environments in accordance with the nature of the spatial and temporal correlations of the associated fluctuating pressure fields. The environments are, therefore, grouped and modeled mathematically.

Environment A. Acoustic Noise During Lift-Off — The sound pressure field surrounding a segment of the vehicle is modeled approximately by a diffuse sound field; that is, at any frequency, uncorrelated plane sound waves are assumed to impinge with equal intensity from all possible directions exterior to the structure surface. The pressure field acting on the structure surface is statistically homogeneous and stationary in space and time, and its spatial correlation is isotropic.

The sound pressure levels of the noise field exciting the structure are estimated by dimensional scaling of field data; the scaling parameters are the total lift-off thrust, jet exhaust velocity, effective nozzle diameter, and overall dimensions of the vehicle.

Environments B, C, E, G and H. Turbulent Boundary Layer and Similar Noise Sources — We can assume the fluctuating pressure fields associated with these environments to be statistically homogeneous and stationary in space and time. However, unlike a diffuse sound field, these pressure fields show dominant propagation only in the direction of the mainstream flow. An adequate representation of these environments is given by a simple mathematical model of a convecting and decaying fluctuating pressure field completely defined by the following: a constant convection velocity U_c; normalized wave number spectra $\Phi_1(k_1)$ and $\Phi_3(k_3)$, in the directions parallel and transverse to the main flow; and the normalized "temporal" or "moving-axis" spectrum $\Phi_m(\cdot)$. The combined wave number and frequency spectrum $\Phi_p(k,\omega)$ is given by

$$\Phi_p(k,\omega) = p^2_{rms} \, \Phi_1(k_1) \, \Phi_3(k_3) \, \Phi_m(\omega - k_1 U_c) . \quad (1)$$

where k is the wave number vector (k_1, k_3), and p^2_{rms} is the overall mean square value of

the pressure fluctuations. The familiar frequency spectrum measured by means of a fixed microphone is then $p^2_{rms} \, \Phi_f(\omega)$, given by

$$p^2_{rms} \, \Phi_f(\omega) = \int_{-\infty}^{\pi} \int_{-\pi}^{\pi} \Phi_p(k,\omega) \, dk . \quad (2)$$

The flow parameters that must be estimated for calculation of structural response are the boundary-layer displacement thickness δ^*, the convection velocity U_c, p_{rms}, and the spectra $\Phi_f(\cdot)$ and $\Phi_3(k_3)$. The displacement thickness δ^* can be related to the distance from the leading edge, U_c can be related to the free stream velocity, and p_{rms} can be related to the free stream dynamic head. The shapes of $\Phi_f(\omega)$ and $\Phi_3(k_3)$ can be obtained in terms of δ^* and U_c. A dominant component of the structural response of airborne vehicles, as a result of the excitation by the environments under discussion, occurs at "coincidence" which is the match between the spatial patterns of vibration on the structure surface and those of fluctuations in the exciting pressure field. In such a case, details of eddy decay become unimportant and one can bypass the necessity for specifying the spectra $\Phi_1(k_1)$ and $\Phi_m(\omega)$ separately [1].

Environments D and F. Shock Oscillation — The oscillation of shock fronts is a result of shock/boundary layer interaction. It is a relatively low-frequency phenomenon. At transonic speeds the shock oscillation occurs downstream of the flares; at supersonic speeds it occurs upstream of the flares. The empirical evidence for shock oscillation is obtained by noting that the static pressure measured near the mean shock-front location consists of a random rectangular wave with a dominant frequency [2,3].

For the purpose of estimation of structural response from environments D and F, we idealize the environment in the following way. The pressure in front of and behind the shock front has constant values. There is a discrete jump Δ_p in the pressure across the shock front. The shock front oscillates in the direction x_1 of the main flow and always remains straight in the transverse direction x_3. The displacement $y(t)$ of the shock front from its mean position is represented by a narrow-band random Gaussian process with zero mean, centerband frequency ω_{osc}, and rms value σ. The statistical properties of $y(t)$ are identical to those of the displacement of an oscillator of resonance frequency ω_{osc}, when excited by white Gaussian noise. Note that the random pressure field, assumed to be associated with an oscillating shock front, is statistically homogeneous in time but not in space.

For estimation of response, the parameters Δ_p, ω_{osc} and c of the exciting environment are determined empirically by relating them to the flow and geometric parameters such as Mach number, dynamic head, ambient static pressure, and flare geometry.

STRUCTURAL COMPONENTS

We have studied various dynamic properties of two simple structural elements, a flat plate and a cylinder. To handle most situations of interest, these structures have been studied in both their finite and infinite form, and in their isotropic as well as orthotropic form. We have considered also the case where a liquid (inside the cylinder or on one side of the plate) forms an integral part of the structure. Here we present some of the major results.

Infinitely Extended Structures

When the exciting pressure field is statistically homogeneous over the surface of the responding structure and when the structure boundaries or the discontinuities on the structure surface do not play a significant role, it is worthwhile to exploit these simplifications by considering an infinitely extended model of the structure.

Infinitely Extended Isotropic Cylinder or Plate — Consider vibration (in the radial direction) of an infinitely long, isotropic, thin cylindrical shell of radius a, thickness h, and surface mass density ρ_s. Let x_1, x_3 be the axial and circumferential coordinates. The resonance frequency ω for a vibration pattern with wave number $k = (k_1, k_3)$ on the cylinder surface is found to be given by the resonance condition,

$$\nu^2 = r^4 + \cos^4 \theta . \tag{3}$$

where ν and (r, θ) are the dimensionless frequency and wave number defined as

$$\nu = \omega a / c_\ell . \tag{4}$$

$$r = k(\kappa a)^{1/2} . \tag{5}$$

$$k = |k| = (k_1^2 + k_3^2)^{1/2} . \tag{6}$$

and

$$\tan \theta = k_3 / k_1 = r_3 / r_1 . \tag{7}$$

Here, $\kappa = h \sqrt{12}$ is the radius of gyration and c_ℓ is the velocity of longitudinal waves in the cylinder material. In deriving Eq. (3), the influence of bending and membrane stresses is

accounted for in the simplest possible way; the influence of shear deformation and of axial and tangential inertias is neglected. In spite of these approximations, the final result has been found to be quite accurate, especially for thin cylinders with thickness-to-diameter ratio of 10^{-2} or less [4].

If we think of the resonance condition of Eq. (3) in terms of energy functions, the kinetic energy of the vibrating structure is proportional to ν^2, the contribution to the potential energy from the bending stresses is proportional to r^4, and the contribution to the potential energy from the membrane stresses is proportional to $\cos^4 \theta$. The resonance condition for an infinite flat plate can be obtained by simply omitting the term $\cos^4 \theta$ in Eq. (3), since the effect of curvature and resulting membrane stresses is absent in a flat plate.

The loci of constant resonance frequency ν in the wave number plane (r, θ) are shown in Fig. 2. In the membrane region of the (r, θ) plane, $\cos \theta$ is larger than r; hence membrane stresses dominate and the resonance condition becomes approximately

$$\nu = \cos^2 \theta . \tag{8}$$

The resonance loci in the membrane region are thus radial straight lines. In the bending region of the (r, θ) plane, r is larger than $\cos \theta$; therefore, bending stresses dominate, the cylinder responds like a flat plate, and the resonance condition becomes approximately

$$\nu = r^2 . \tag{9}$$

The resonance loci in the bending region are, therefore, circles. The boundary between the membrane and bending regions is given by

$$r = \cos \theta . \tag{10}$$

Infinitely Extended Orthotropic Cylinder or Plate — For analyzing an orthotropic structure, the inertial, extensional, and bending properties of the structure are averaged over the sources of its orthotropy, such as axial stringers and circumferential stiffeners in the structure. The average properties thus defined are valid for vibration with wavelengths larger than the spatial extent over which the structural properties are averaged.

The averaged surface mass density enters into the kinetic energy of vibration. The averaged extensional and bending rigidities of the structure (these can be different in the axial and circumferential directions) enter, respectively,
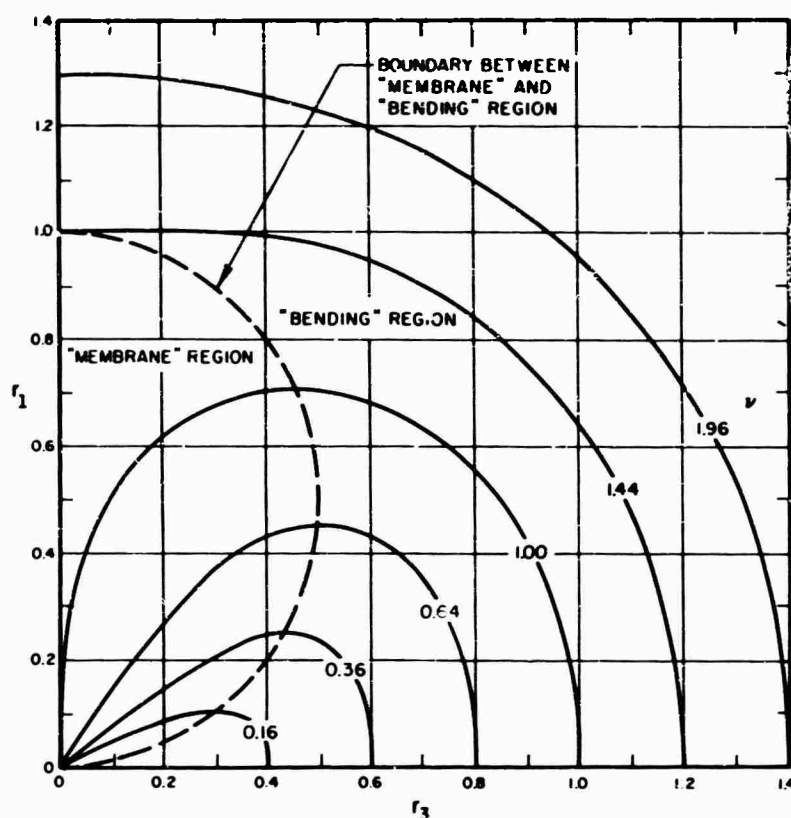
Fig. 2. Loci of constant resonance frequency in the dimensionless wave number plane (r,θ), isotropic cylinder

into the components of potential energy controlled by the membrane and bending stresses. The description of the resonance loci in the wave number plane is qualitatively the same as that for the corresponding isotropic structure [1].

Infinitely Extended, Liquid-Loaded Cylinder or Plate — We consider only the liquids whose sound velocity exceeds the phase velocity of vibration on the structure surface. For such cases, no net energy is radiated from the vibrating structure into the liquid, and the impedance offered by the liquid pressure to the structural vibration is inertial. The mass loading m_f per unit surface area owing to the liquid is approximately given by

$$m_f = \rho_o/k , \qquad (11)$$

where ρ_o is the liquid density and k is the magnitude of the wave number of vibration on the structure surface.

This additional mass loading effect can easily be incorporated into the dynamic properties described above for the "empty" structures. This liquid mass loading, in general,

tends to reduce the resonance frequencies and suppress the membrane effects induced by the curvature. For example, if the isotropic cylinder shown in Fig. 2 were filled with a heavy liquid, the resonance loci in the membrane region of the (r,θ) plane would no longer be radial straight lines; the loci would tend, rather, to be extensions of the circular resonance loci in the bending region, thus reflecting the suppression of the curvature-induced membrane effects.

Structures of Finite Extent

When the excitation field is not statistically homogeneous over the surface of the responding structure, or when the discontinuities such as the structure boundaries are expected to play a significant role, it becomes necessary to consider the modal representation of the finite structure. Often, the analyses performed on highly idealized structures with simple boundary conditions yield concepts (and answers) powerful enough to find application in more general situations.

Modal Representation for Finite Cylinder or Plate — Consider a rectangular plate of

101

dimensions ℓ_1, ℓ_3, simply supported along its edges. The flexural vibration of the plate can be resolved into a double infinity of its orthogonal modes. The spatial pattern $\psi_{mn}(x)$ of the mode (m,n) of this series is given by

$$\psi_{mn}(x) = \sin(m\pi x_1/\ell_1)\,\sin(n\pi x_3/\ell_3) . \quad (12)$$

where x_1, x_3 are the coordinates parallel to ℓ_1 and ℓ_3, and m,n are positive integers. The modal wave number k associated with the mode (m,n) is given by

$$k = (k_1, k_3) = (m\pi/\ell_1,\ n\pi/\ell_3) . \quad (13)$$

This is the dominant wave number corresponding to the spatial pattern of Eq. (12). In other words, the spatial Fourier transform of Eq. (12) would peak at the wave number k given by Eq. (13). The larger the dimensions ℓ_1 and ℓ_3 of the plate, the sharper this peak in the Fourier transform will be, until in the limit the peak approaches a Dirac delta function for an infinite plate.

For a cylinder, odd numbers of half-wavelengths of vibration along the circumference are not possible. However, for every even number $2n$ of half-wavelengths along the circumference, two independent modal shapes must be specified. Thus, for a cylinder of length ℓ_1 and circumference ℓ_3, simply supported along its edges, the modal shapes $\psi_{mn}(x)$ are

$$\psi_{mn}(x) = \sin(m\pi x_1/\ell_1)\,\sin(2n\pi x_3/\ell_3) .$$

and $\qquad\qquad\qquad\qquad\qquad (14)$

$$\psi_{mn}(x) = \sin(m\pi x_1/\ell_1)\,\cos(2n\pi x_3/\ell_3)$$

The structures we have considered are simply supported along their boundaries. The resonance frequencies of their modes are, therefore, related to the associated modal wave numbers by the resonance conditions (such as Eqs. (3), (8), (9)) for the corresponding infinite structures.

Modal Densities for Finite Structures —
Modal density $n(\omega)$ is defined as the number of modes whose natural frequencies lie in a unit radian frequency bandwidth around frequency ω. The simplest way of calculating modal densities is to represent the structural modes as a lattice of points in the wave number plane k, where the location of each mode is determined by its associated modal wave number. By considering the geometry of the resonance loci in the k plane, we can easily calculate the modal densities [1,5].

Calculations show that for an isotropic cylinder, below the ring frequency $\omega_r = c_\ell/a$, the

modal density increases with frequency. It attains its peak value at the ring frequency and maintains a constant value, roughly two-thirds of the peak value, above the ring frequency. This constant value of modal density above the ring frequency applies also to a flat plate of the same area as the surface area of the cylinder. As noted before in connection with Eqs. (3), (8), (9) and Fig. 2, above the ring frequency ω_r (i.e., $\nu > 1$), a cylinder is dynamically equivalent to a flat plate.

Detailed calculations of the modal density for orthotropic and liquid-loaded structures are reported in Ref. 1.

STRUCTURAL VIBRATION INDUCED BY ACOUSTIC AND AERODYNAMIC ENVIRONMENTS

Response of Cylinder or Flat Plate to Turbulent Boundary Layer Pressure Field (Environments B, C, E, G, or H)

Consider a turbulent boundary layer (TBL) pressure field over an isotropic cylinder, the pressure field being convected along the generators of the cylinder. Figure 3 shows the geometry of the situation in the wave number plane k for three different frequency ranges. At each frequency ω, most of the excitation from the TBL pressure field is shown to be concentrated in a narrow strip centered around $k_1 = \omega/U_c$, where k_1 is the wave number in the flow direction and U_c is the convection velocity. The width of this strip in the k_1 direction depends on the eddy decay time or the temporal spectrum $\Phi_m(\omega)$ (see Eq. (1)). As shown in Fig. 3, this "excitation strip" divides the wave number plane into regions of hydrodynamically slow (HS), hydrodynamically coincident (HC), and hydrodynamically fast (HF) modes. These modes are defined by the trace in the axial direction of the phase velocity of vibration at frequency ω. The trace velocity for a HS mode is less than U_c. The HF and HC modes are defined similarly.

The three frequency ranges represented in Fig. 3 are defined by the two critical frequencies, the ring frequency ω_r, and the hydrodynamic critical frequency ω_h, defined as

$$\omega_h = U_c^2/\kappa c_\ell \quad (15)$$

Almost invariably, the hydrodynamic critical frequency is higher than the ring frequency for structures of current interest. For $\omega < \omega_h$, the strip of excitation in the wave number plane intersects the resonance locus (Figs. 3b and 3c);

VARIATION OF $\Phi_p(k,\omega)$
IN THE k_1 DIRECTION

HF RESONANT MODES

(a)

HC RESONANT MODES

(b)

HS RESONANT MODES

MEMBRANE
CONTRIBUTION
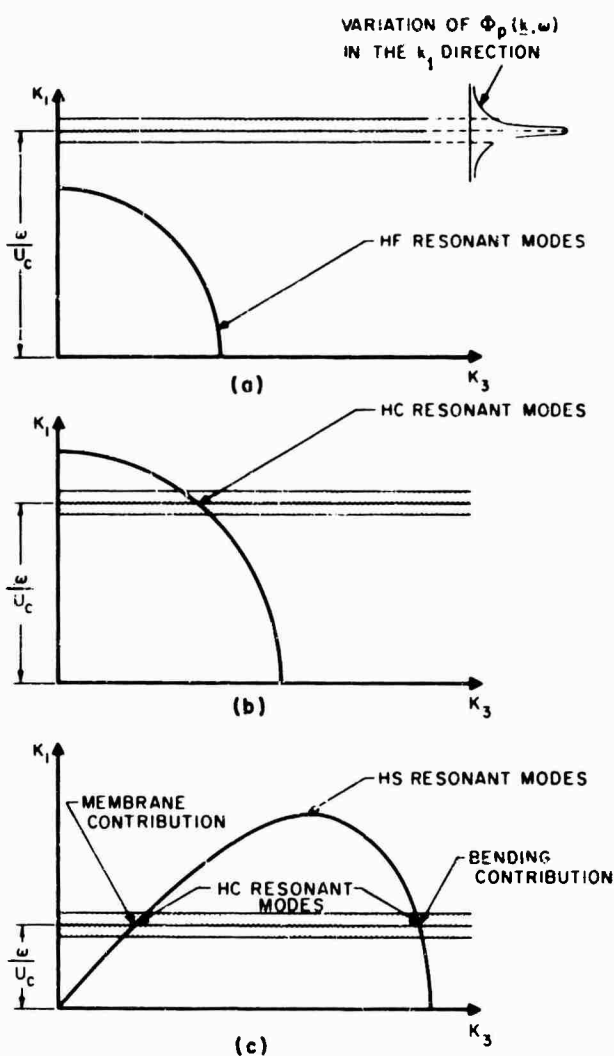
BENDING
CONTRIBUTION

HC RESONANT
MODES

(c)

Fig. 3. Resonance loci and domain of excitation in the wave number plane, isotropic cylinder, TBL pressure field: (a) $\omega > \omega_h$, (b) $\omega_r < \omega < \omega_h$, and (c) $\omega < \omega_r$

for $\omega > \omega_h$, it does not (Fig. 3a). For $\omega_h < \omega < \omega_r$, only the bending stresses are dominant and the cylinder behaves like a flat plate (Fig. 3b); for $\omega < \omega_r$, both the bending stresses and the membrane stresses become important (Fig. 3c).

In the wave number plane, the domain of excitation at any frequency is quite narrow and sharply defined; therefore, the HC modes find the best spatial match or coincidence with the excitation field. The excitation of the HS and HF modes arises from relatively secondary effects. The first of these effects is the result of the extension, or "tail," of the excitation field beyond the narrow strip defining the coincident region in the wave number plane. These tails of the excitation field (see the variation of $\Phi_p(k,\omega)$ in Fig. 3a) are governed by the temporal fluctuations, that is, the spectrum $\Phi_m(\omega)$, of the pressure field in the TBL. The second

effect is due to the finite extent of any real structure. If the structure has many edges and discontinuities (i.e., a small mean free path), the edge effects will contribute to some coupling with the excitation field.

For the situation considered in Fig. 3a, the frequency ω is higher than the hydrodynamic critical frequency. Any resonant response of the structure at this frequency must arise from the secondary effects described above. In this frequency range, most of the resonant response is controlled by the temporal spectrum $\Phi_m(\omega)$, the contribution from the edge effects being relatively negligible [6]. Below the hydrodynamic critical frequency ω_h, the dominant structural response is not only resonant but also coincident, and is caused by the interaction between the exciting pressure field and the structural modes that lie in the wave number plane near the intersection of the resonance locus and the excitation strip (Figs. 3b and 3c).

For the noncoincident and resonant response above ω_h where response is controlled by $\Phi_m(\omega)$, as well as for the coincident and resonant response below ω_h, the interaction between the pressure environment and the appropriate structural modes is characterized by the matching of the wave numbers in the pressure field and the modal wave numbers. This interaction takes place over the entire surface of the structure and is more or less independent of the edges. Therefore, we can simplify the calculations for power transfer and vibration response by considering a corresponding structure that is infinitely extended or "edgeless."

The following general procedure is used to calculate the vibration response of structures excited by a TBL or by similar convecting-and-decaying pressure fields. Consider the corresponding edgeless structure. In different frequency bands, find the mechanical power that the fluctuating pressure field transfers to the structure via the matching wave numbers of vibration at resonance. Equate this power input to the power dissipated as a result of the structural vibration. (The power can be dissipated inside the vibrating structure as well as into the surroundings.) Solve for the velocity spectrum of structural response. The resulting estimate pertains to resonant vibration averaged over the surface of the structure. This technique has been successfully applied to isotropic, orthotropic, and liquid-loaded cylinders and plates [1].

We omit the mathematical details and present only the results of a typical calculation. Figure 4 shows the spectrum for resonant acceleration of an isotropic cylinder excited by
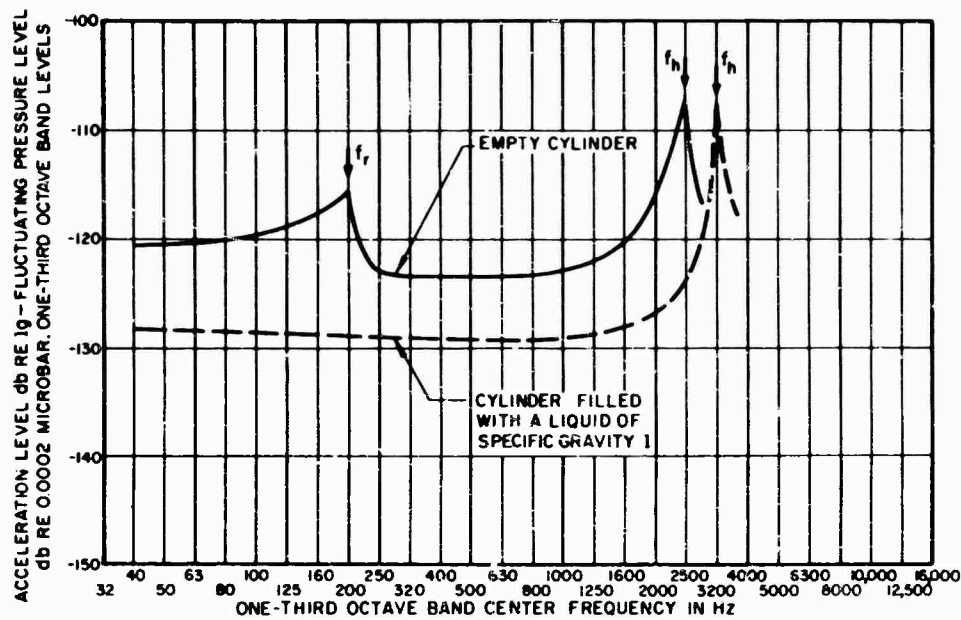
103

Fig. 4. Response of cylinder to TBL pressure field

a TBL pressure field. The cylinder is 25 ft in diameter, 200 mils thick, and has a dissipation loss factor of 0.01. The boundary layer pressure fluctuations have a mean convection velocity of 1250 fps with a free-stream velocity of 1800 fps. The boundary layer displacement thickness is 0.25 ft. The response spectrum is calculated up to the hydrodynamic critical frequency f_h. For the empty cylinder, the response is seen to peak at f_h and at the ring frequency f_r. When the same cylinder is filled with a liquid of specific gravity ρ, the liquid mass loading brings down the response levels and suppresses the membrane effects as well as the peak at the ring frequency.

Response of Cylinder or Flat Plate to
Diffuse Sound Field (Environment A)

Consider a diffuse sound field impinging on the exterior of an isotropic cylinder. Figure 5 shows the geometry of the situation in the wave number plane k for three different frequency ranges. At each frequency ω, the excitation from the diffuse sound field is shown to be restricted to wave number magnitudes ranging from 0 to $k_a = \omega/c$, where c is the sound speed. This region is shown as a shaded quarter-circle in the wave number plane. The structural modes situated in the wave number plane inside this shaded circular region are acoustically fast (AF) modes, those situated outside are acoustically slow (AS) modes. The magnitude of the phase velocity of vibration at frequency ω of an AF (AS) mode is higher (lower) than the sound velocity c.

The three frequency ranges represented in Fig. 5 are defined by the two critical frequencies, the ring frequency ω_r, and the acoustic critical frequency ω_c, defined as

$$\omega_c = c^2/\kappa c_\ell . \tag{16}$$

For most structures of interest, $\omega_c > \omega_r$. At a frequency $\omega > \omega_c$ (Fig. 5a), all the resonant modes of the structure find a good spatial match or coincidence with some wave number components of the impinging sound field. The resonant vibration here is controlled by the bending stresses or the flat-plate behavior of the structure. At a frequency $\omega < \omega_r$ (Fig. 5c), only some of the resonant modes that are controlled essentially by membrane stresses are coincident. Thus, for the situations depicted in Figs. 5a and 5c (namely, $\omega > \omega_c$, and $\omega < \omega_r$), the dominant structural response arises from the surface interactions between the environment and the resonant and coincident modes. The vibration analysis in these frequency regimes can, therefore, be performed equally well on an infinitely extended or edgeless structure. In the intermediate frequency range, $\omega_c < \omega < \omega_r$ (Fig. 5b), a fairly important frequency range, no coincidence or surface interaction is possible between the resonant modes and the sound field. Any interaction causing resonant response in this frequency range must arise from the effects due to the boundaries and discontinuities on the structure surface. The analysis on the corresponding infinite or edgeless structure would give zero resonant response in this frequency range.
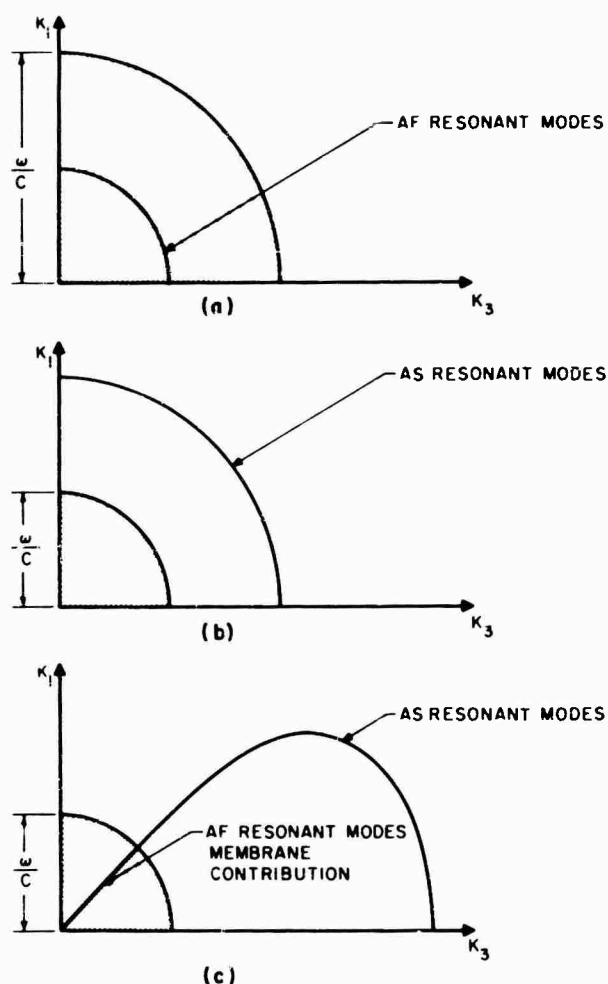
104

Fig. 5. Resonance loci and domain of excitation in the wave number plane, isotropic cylinder, diffuse sound field: (a) ··· ·ᶜ, (b) ·ᵣ · ·· ·ᶜ, and (c) ᶜ· · ·ᵣ

Response calculations for excitation from a diffuse sound field are based on a modal approach, so the size, boundaries, and discontinuities of the structure can be taken into consideration. The interaction between the sound field and different classes of modes over the surface, perimeter, edges, and corners of the structure can be expressed in terms of coupling parameters, which, in turn, can be related to the radiation efficiencies of modes. These calculations have been successfully completed for isotropic, orthotropic, and liquid-loaded cylinders and plates [1,7,8]. The vibrational energy of a structure is dissipated partly by radiation into the surrounding acoustic medium; therefore, the radiation efficiency, in addition to determining the extent of coupling between the structural modes and the sound field, modifies the total dissipation loss factors of modes. Our approach is to calculate the response of a single mode to a diffuse sound field, and then extend the concepts to include groups of structural modes resonating in different frequency bands.

Again, we omit the mathematical details and present only the results of a typical calculation. Figure 6 shows the spectrum for resonant acceleration of an isotropic cylinder excited by a diffuse sound field. The cylinder is 30 ft long, 25 ft in diameter, 200 mils thick, and has a structural dissipation loss factor of 0.01. In the response calculations, this loss factor of 0.01 is increased slightly by the addition of the effective radiation loss factor. The acceleration spectrum for a cylinder with discontinuities, shown in Fig. 6, is calculated for the case where line sources of discontinuities are spaced 5 ft
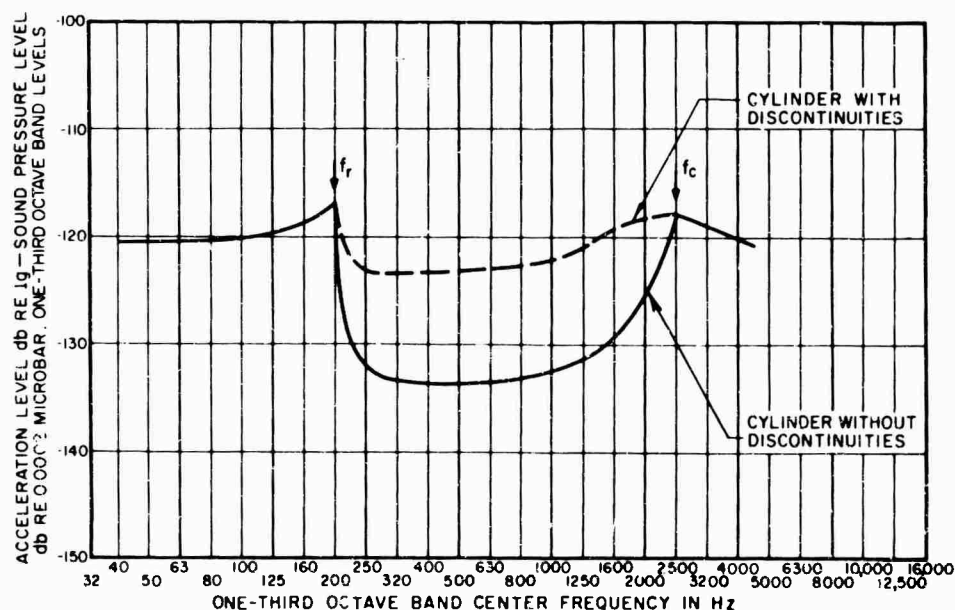

Fig. 6. Response of cylinder to diffuse sound field

105

apart, along the axial and circumferential directions of the cylinder. As we noted before, the response at frequencies above the acoustic critical frequency f_c and below the ring frequency f_r is dominated by the surface interactions and is, therefore, hardly influenced by the presence or absence of structural discontinuities, edges, or boundaries. However, between the ring frequency and the acoustic critical frequency, the edge coupling is important and the response level depends on the mean free path of vibration or on the ratio of structural surface area to total length of the edges. The discontinuities reduce the mean free path and increase the resonant response.

Response of Cylinder or Flat Plate to Oscillating Shock Front (Environment D or F)

As explained before, the pressure field associated with an oscillating shock front is not spatially homogeneous. When a shock front over a structure surface undergoes a random oscillatory motion, the portion of the structure near the mean shock position experiences a fluctuating pressure field. Consequently, energy flows from the environment into the structure in this localized region, and the resulting vibration is transmitted to the other parts of the structure. Since the structural vibration is derived from a localized source of excitation, t ibration level averaged over the structure su. e clearly depends on the extent of the structure. Also, shock oscillation frequency is generally found to be quite low (20 to 100 cps). As a result, only a few lowest order modes of the structure determine the vibration response. These facts dictate consideration of a finite structure with well-defined boundary conditions and estimation of individual modal response for the first 5 or 10 modes. Thus, in this case, statistical concepts (like modal density) cease to apply to the very few modes involved. The statistical concepts can, however, be applied to the random oscillatory motion of the shock front. Details of the response estimation for oscillating shock are given in Ref. 1.

REFERENCES

1. K. L. Chandiramani, S. E. Widnall, R. H. Lyon, and P. A. Franken, "Structural Response to Inflight Acoustic and Aerodynamic Environments," Bolt Beranek and Newman Inc., Contract NAS8-20026, BBN Rept. 1417, 31 July 1966

2. A. L. Kistler, "Surface Pressure Fluctuations Produced by Attached and Separated Supersonic Boundary Layers," NATO, AGARD Rept. 458, 1963

3. D. R. Wiley and M. G. Seidl, "Aerodynamic Noise Tests on X-20 Scale Models," Boeing Co., Tech. Rept. AFFDL-TR-65-192, Vols. I and II, 1965

4. M. Heckl, "Vibrations of Point-Driven Cylindrical Shells," J. Acoust. Soc. Am., Vol. 32, pp. 1553-1557, 1962

5. P. W. Smith, Jr., and R. H. Lyon, "Sound and Structural Vibration," NASA CR-160, 1965

6. J. E. Ffowcs Williams and R. H. Lyon, "The Sound Radiated From Turbulent Flows Near Flexible Boundaries," Bolt Beranek and Newman Inc., Rept. 1054, Contract Nonr 2321(00), 15 Aug. 1963

7. G. Maidanik, "Response of Ribbed Panels to Reverberant Acoustic Fields," J. Acoust. Soc. Am., Vol. 34, pp. 809-862, 1962

8. P. W. Smith, Jr., "Response and Radiation of Structural Modes Excited by Sound," J. Acoust. Soc. Am., Vol. 34, pp. 640-647, 1962

BIBLIOGRAPHY

Bies, D A., and P. A. Franken, "Notes on Scaling Jet and Rocket Noise," J. Acoust. Soc. Am., Vol. 33, pp. 1171-1173, 1961

*   *   *

DYNAMIC VIBRATIONS OF THICK-WALLED
ELASTIC ANISOTROPIC CYLINDERS AND
SPHERES WITH INTERNAL DAMPING*

Gabriel Cinelli
Argonne National Laboratory
Argonne, Illinois

A new finite Hankel transform is used to find the transient displacement
and stresses in thick elastic cylinders and spheres composed of mate-
rial with transverse curvilinear isotropy and internal viscous damping
for the following problems: (a) plane strain motion of an infinitely long
circular cylindrical shell, (b) torsional motion of a finite circular cy-
lindrical shell, and (c) radially symmetric motion of a spherical shell.
The dynamic loads on the surfaces are taken as arbitrary functions of
space (torsional case only) and time.

It is shown that the problems of the solid body, the thin shell, and cavity
in an infinite medium can be obtained from the thick shell solution as
limiting cases. Specializing the surface tractions to standard forms
such as an impulse or a sinusoid, the free, harmonic, and static mo-
tions are recovered. Physical quantities such as resonance and me-
chanical impedance are derived and studied. Using the displacement
equations, it is shown that the radially symmetric motion is analogous
to the plane-strain motion of the cylinder. The results for isotropic
bodies are found by specifying certain values for the elastic constants.

An extended Weber transform is also introduced, permitting solution of
infinite media problems in a manner which is more direct than existing
techniques.

G. Cinelli

INTRODUCTION

In recent years considerable effort has
been expended on study of dynamic wave propa-
gation and vibration in elastic isotropic bodies
of finite and infinite dimensions. In contrast to
this has been the small amount of work done
regarding elastic anisotropic bodies, although
many materials of practical interest are of this
nature. What work has been accomplished is
mostly harmonic wave propagation and vibra-
tions. Very few transient problems have been
solved, especially for finite regions. A good
review and evaluation of the field is given by
Harmon [1] and Scott and Miklowitz [2].

For some classes of anisotropy and axes
orientation, the equations of motion of an elas-
tic solid admit plane strain and torsional solu-
tions. These are the class of problems studied
in this paper. The purpose of this study was to
determine the transient displacement and
stresses in elastic bodies of material with
transverse curvilinear isotropy and viscous
internal damping for the following problems:
(a) plane strain motion of a thick infinitely long

circular cylindrical shell, (b) torsional motion of a finite thick circular cylindrical shell, and (c) radially symmetric motion of a thick spherical shell. The surface loads in these problems are taken as arbitrary functions of space (torsional case only) and time. The only previous work on such problems has been that by Eason on harmonic loads [3].

The paper is divided into five parts. The first section lists the pertinent finite and infinite transforms used in solving the various problems. The second portion treats in considerable detail the plane strain motion of the cylindrical shell. The general solution is obtained by means of a finite Hankel transform [4]. By specifying certain values for the elastic constants, the solution for the isotropic body is given. Next the cases of the solid body and the thin shell are shown to be limiting cases of the thick shell solution. An extended Weber transform is then introduced which solves the problem of a cylindrical cavity in an infinite medium. The surface tractions are specialized to standard forms, such as step function and sinusoid, which enable the free, harmonic, and static motions to be recovered as special cases. Physical quantities such as resonance and mechanical impedance are then derived. In the next section, it is shown that the radially symmetric motion of a sphere is analogous to the plane strain problem which enables the solutions for the sphere to be obtained directly from those in the plane strain problem. The general solution for the torsional motion of the finite cylindrical shell is given in the fourth part. Finally, the results and conclusions of the study are presented.

TABULATION OF TRANSFORMS

The various transforms and their properties are listed in this section to make the paper self-contained. In these formulas, a bar over a lower case letter indicates the transform variable, whereas a prime on a letter indicates differentiation.

Extended Finite Hankel Transform [4]

$$H[f(r)] \quad \overline{f} \quad \overline{f}(\xi_i) = \int_a^b rf(r)\, C_i(r, \xi_i)\, dr\,.$$

$$a \le r \le b, \quad \nu > -1/2. \quad (1)$$

$$C_i(r, \xi_i) \quad J_\nu(\xi_i r)[\xi_i Y'_\nu(\xi_i a) + hY_\nu(\xi_i a)]$$
$$- Y_\nu(\xi_i r)[\xi_i J'_\nu(\xi_i a) + hJ_\nu(\xi_i a)]. \quad (2)$$

$$f(r) \quad \frac{\pi^2}{2} \sum_i \xi_i^2 \xi_i J'_\nu(\xi_i b)$$

$$\cdot kJ_\nu(\xi_i b)]^2\, \overline{f}(\xi_i)\, \frac{C_i(r, \xi_i)}{F_i(\xi_i)}\,. \quad (3)$$

$$F_i(\xi_i) \quad \left\{ k^2 + \xi_i^2\left[1 - \left(\frac{\nu}{\xi_i b}\right)^2\right] \right\}[\xi_i J'_\nu(\xi_i a) + hJ_\nu(\xi_i a)]^2$$

$$- \left\{ h^2 + \xi_i^2\left[1 - \left(\frac{\nu}{\xi_i a}\right)^2\right] \right\}[\xi_i J'_\nu(\xi_i b) + kJ_\nu(\xi_i b)]^2. \quad (4)$$

where ξ_i is a positive root of

$$[\xi_i Y'_\nu(\xi_i a) + hY_\nu(\xi_i a)][\xi_i J'_\nu(\xi_i b) + kJ_\nu(\xi_i b)] \quad \xi_i Y'_\nu(\xi_i b)$$

$$+ kY_\nu(\xi_i b)][\xi_i J'_\nu(\xi_i a) + hJ_\nu(\xi_i a)]. \quad (5)$$

$$H\left(\frac{d^2 f}{dr^2} + \frac{1}{r}\frac{df}{dr} - \frac{\nu^2}{r^2} f\right) \quad \frac{2}{\pi}\left\{ \frac{\xi_i J'_\nu(\xi_i a) + hJ_\nu(\xi_i a)}{\xi_i J'_\nu(\xi_i b) + kJ_\nu(\xi_i b)}\right\}$$

$$\cdot [f'(b) + kf(b)] - [f'(a) + hf(a)]\} - \xi_i^2 \overline{f}(\xi_i). \quad (6)$$

Extended Weber Transform

$$H[f(r)] \quad \overline{f} = \overline{f}(\lambda) = \int_a^\infty rf(r)\, C_\nu(r, \lambda)\, dr\,.$$

$$a \le r < \infty, \quad \nu > -1/2. \quad (7)$$

$$C_\nu(r, \lambda) \quad J_\nu(\lambda r)[\lambda Y'_\nu(\lambda a) + hY_\nu(\lambda a)]$$
$$- Y_\nu(\lambda r)[\lambda J'_\nu(\lambda a) + hJ_\nu(\lambda a)]. \quad (8)$$

$$f(r) \int_0^\infty \frac{\lambda \overline{f}(\lambda)\, C_\nu(r, \lambda)\, d\lambda}{[\lambda J'_\nu(\lambda a) + hJ_\nu(\lambda a)]^2 + [\lambda Y'_\nu(\lambda a) + hY_\nu(\lambda a)]^2}\,. \quad (9)$$

$$H\left(\frac{d^2 f}{dr^2} + \frac{1}{r}\frac{df}{dr} - \frac{\nu^2}{r^2} f\right) \quad -\frac{2}{\pi}[f'(a) + hf(a)] - \lambda^2 \overline{f}(\lambda). \quad (10)$$

Finite Hankel Transform [5]

$$H[f(r)] \quad \overline{f} \quad \overline{f}(\xi_i) \quad \int_0^b rf(r)\, J_\nu(\xi_i r)\, dr\,.$$

$$0 \le r \le b, \quad \nu > -1/2. \quad (11)$$

$$f(r) = \frac{2}{b^2} \sum_{i} \frac{\gamma_i^2 \bar{f}(\gamma_i)}{k^2 + \left(\gamma_i^2 - \frac{\nu^2}{b^2}\right)} \frac{J_\nu(\gamma_i r)}{[J_\nu(\gamma_i b)]^2} \cdot \quad (12)$$

where γ_i is a positive root of

$$\gamma_i J'_\nu(\gamma_i b) + k J_\nu(\gamma_i b) = 0 . \quad (13)$$

$$H\left(\frac{d^2 f}{dr^2} + \frac{1}{r}\frac{df}{dr} - \frac{\nu^2}{r^2} f\right) = bJ_\nu(\gamma_i b)[f'(b) + kf(b)]$$

$$- \gamma_i^2 \bar{f}(\gamma_i) . \quad (14)$$

Finite Cosine Transform

$$C[f(x)] = \bar{f} = \bar{f}(n) = \int_0^a f(x) \cos\frac{n\pi x}{a} dx, \quad n = 0, 1, 2. \quad (15)$$

$$f(x) = \frac{1}{a}\bar{f}(0) + \frac{2}{a}\sum_{n=1}^{\infty} \bar{f}(n) \cos\frac{n\pi x}{a} , \quad (16)$$

$$C\left(\frac{d^2 f}{dx^2}\right) = (-1)^n f'(a) - f(0) - \frac{n^2\pi^2}{a^2}\bar{f}(n) . \quad (17)$$

In these formulas the following notation holds:

J_ν, Y_ν = Bessel functions of the first and second kind, respectively, and of order ν;

H, C = linear integral operators;

a, b = inner and outer radii of shell, respectively;

h, k = constant coefficients whose value can be positive, negative, or zero; and

f = arbitrary function.

PLANE STRAIN MOTION OF AN INFINITELY LONG CIRCULAR CYLINDRICAL SHELL

The basic equations of motion for the radial vibrations of an infinitely long cylindrical shell with transverse curvilinear isotropy and internal viscous damping are:

$$\frac{\partial\sigma_r}{\partial r} + \frac{\sigma_r - \sigma_\theta}{r} = \rho^*\frac{\partial^2 u}{\partial t^2} + D\frac{\partial u}{\partial t} , \quad a \leq r \leq b, \ t > 0. \quad (18)$$

$$\sigma_r = c_{11}\frac{\partial u}{\partial r} + c_{12}\frac{u}{r} , \quad (19)$$

$$\sigma_\theta = c_{12}\frac{\partial u}{\partial r} + c_{22}\frac{u}{r} , \quad (20)$$

where

σ_r, σ_θ = radial and circumferential stress components, respectively;

u = radial displacement of cylinder;

ρ^* = density of elastic medium;

c_{11}, c_{12}, c_{22} = elastic constants; and

D = viscous damping coefficient.

Putting Eqs. (19) and (20) into Eq. (21) gives

$$\frac{\partial^2 u}{\partial r^2} + \frac{1}{r}\frac{\partial u}{\partial r} - \frac{\nu^2}{r^2} u = \frac{\rho^*}{c_{11}}\frac{\partial^2 u}{\partial t^2} + \frac{D}{c_{11}}\frac{\partial u}{\partial t} , \quad (21)$$

where

$$\nu^2 = \frac{c_{22}}{c_{11}} . \quad (22)$$

Equations (2), (3), and (21) can be transformed into the following nondimensionalized coordinate system as

$$\frac{\partial^2 u}{\partial\rho^2} + \frac{1}{\rho}\frac{\partial u}{\partial\rho} - \frac{\nu^2}{\rho^2} u = \frac{\partial^2 u}{\partial\tau^2} + C\frac{\partial u}{\partial\tau} , \quad 1 \leq \rho \leq p, \ \tau > 0. \quad (23)$$

$$\rho = \frac{r}{a} , $$

$$p = \frac{b}{a} , \quad (24)$$

$$C = \frac{avD}{c_{11}} ; $$

$$v = \left(\frac{c_{11}}{\rho^*}\right)^{1/2} , \quad (25)$$

$$\tau = \frac{v}{a} t ; $$

$$\frac{a}{c_{11}}\,\sigma_\rho(\rho,\tau) \;=\; \frac{\partial u}{\partial \rho} + \frac{c_{12}}{c_{11}}\,\frac{u}{\rho}\;; \qquad (26)$$

$$\frac{a}{c_{12}}\,\sigma_\theta(\rho,\tau) \;=\; \frac{\partial u}{\partial \rho} + \frac{c_{22}}{c_{12}}\,\frac{u}{\rho}\;. \qquad (27)$$

The appropriate initial conditions are

$$u(\rho,0) \;=\; f(\rho)\,,$$
$$\left.\frac{\partial u}{\partial \tau}\right|_{\tau=0} \;=\; \dot{u}(\rho,0) \;=\; g(\rho)\;; \qquad (28)$$

the boundary conditions are

$$\sigma_\rho(P,\tau) \;=\; B(\tau)\,,$$
$$\sigma_\rho(1,\tau) \;=\; A(\tau)\,. \qquad (29)$$

The appropriate transform for the solution of this problem is, from Eq. (1),

$$\bar{u} \;=\; \bar{u}(\xi_i,\tau) \;=\; \int_1^P \rho\,u(\rho,\tau)\,C_\nu(\rho,\xi_i)\,d\rho\,. \qquad (30)$$

Define

$$h \;=\; \frac{c_{12}}{c_{11}}\,, \qquad (31)$$
$$k \;=\; \frac{c_{12}}{c_{11}P} \;=\; \frac{h}{P}\,.$$

Applying Eq. (30) to Eq. (23) and using Eqs. (6), (26), (29), and (31) gives

$$\frac{d^2\bar{u}}{d\tau^2} + C\,\frac{d\bar{u}}{d\tau} + \xi_i^2\,\bar{u} \;=\; \frac{2a}{\pi c_{11}}\left\{\frac{[\xi_i J_\nu'(\xi_i) + hJ_\nu(\xi_i)]}{[\xi_i J_\nu'(\xi_iP) + kJ_\nu(\xi_iP)]}\right.$$
$$\left. \cdot \sigma_\rho(P,\tau) - \sigma_\rho(1,\tau)\right\}\,. \qquad (32)$$

By following standard techniques, Eq. (32) can be rewritten as

$$\frac{d^2\bar{u}}{d\tau^2} + 2\zeta\omega_n\frac{d\bar{u}}{d\tau} + \omega_n^2\bar{u} \;=\; \frac{2a}{\pi c_{11}}\left\{\frac{[\xi_i J_\nu'(\xi_i) + hJ_\nu(\xi_i)]}{[\xi_i J_\nu'(\xi_iP) + kJ_\nu(\xi_iP)]}\right.$$
$$\left. \cdot \sigma_\rho(P,\tau) - \sigma_\rho(1,\tau)\right\}\;; \qquad (33)$$

$$C = C_{CR}\,,$$
$$C_{CR} = 2\omega_n\,, \qquad (34)$$
$$\omega_n = \xi_i\,.$$

The solution to Eq. (33) via the Laplace transform and Eq. (28) is

$$\bar{u}(\xi_i,\tau) = \frac{2a}{\pi c_{11}}\int_0^\tau e^{-\zeta\omega_n(\tau-v)}$$

$$\cdot\left\{\frac{[\xi_i J_\nu'(\xi_i) + hJ_\nu(\xi_i)]}{[\xi_i J_\nu'(\xi_iP) + kJ_\nu(\xi_iP)]}\,\sigma_\rho(P,v) - \sigma_\rho(1,v)\right\}$$

$$\cdot \sin\omega(\tau-v)\,dv + \bar{f}(\xi_i)\,e^{-\zeta\omega_n\tau}\cos\omega\tau$$

$$+ \frac{[\bar{g}(\xi_i) + \zeta\omega_n\bar{f}(\xi_i)]}{\omega}\,e^{-\zeta\omega_n\tau}\sin\omega t\,, \qquad (35)$$

$$\begin{array}{c}\bar{f}(\xi_i)\\ \bar{g}(\xi_i)\end{array} = \int_1^P\rho\,\begin{array}{c}f(\rho)\\ g(\rho)\end{array}\,C_\nu(\rho,\xi_i)\,d\rho\,. \qquad (36)$$

$$\omega = \omega_n\sqrt{1-\zeta^2} = \xi_i\sqrt{1-\zeta^2}\,. \qquad (37)$$

The solution for the displacement is, from Eq. (3),

$$u(\rho,\tau) = \frac{\pi^2}{2}\sum_{\xi_i}\xi_i^2\,[\xi_i J_\nu'(\xi_iP)$$
$$+ kJ_\nu(\xi_iP)]^2\,\bar{u}(\xi_i,\tau)\,\frac{C_\nu(\rho,\xi_i)}{F_\nu(\xi_i)}\,. \qquad (38)$$

When the relationships given by Sneddon [5] are used,

$$\frac{dZ_\nu}{d\rho} = \frac{\nu}{\rho}Z_\nu - Z_{\nu+1}\,, \qquad (39)$$

$$Z_\nu = AJ_\nu + BY_\nu\,. \qquad (40)$$

The stresses found from Eqs. (26), (27), and (38) are

$$\sigma_\rho(\rho,\tau) = \frac{\pi^2}{2a}\sum_{\xi_i}\frac{\xi_i^2[\xi_i J_\nu'(\xi_iP) + kJ_\nu(\xi_iP)]^2\,\bar{u}(\xi_i,\tau)}{F_\nu(\xi_i)}$$

$$\times \xi_i\left[\left(\nu c_{11} + \frac{c_{12}}{\zeta_i}\right)C_\nu(\rho,\xi_i) - c_{11}C_{\nu+1}(\rho,\xi_i)\right]\,. \qquad (41)$$

$$\sigma_\theta(\rho,\tau) = \frac{\pi^2}{2a}\sum_{\xi_i}\frac{\xi_i^2[\xi_i J_\nu'(\xi_iP) + kJ_\nu(\xi_iP)]^2\,\bar{u}(\xi_i,\tau)}{F_\nu(\xi_i)}$$

$$\times \xi_i\left[\left(\nu c_{12} + \frac{c_{22}}{\xi_i}\right)C_\nu(\rho,\xi_i) - c_{12}C_{\nu+1}(\rho,\xi_i)\right]. \qquad (42)$$

110

Equations (35), (38), (41), and (42) represent the general solutions to the basic equations.

The case of the isotropic solid is obtained by defining the elastic constants as:

$$: \quad 1 ,$$

$$c_{11} \quad c_{22} \quad \lambda + 2\mu .\qquad(43)$$

$$c_{12} \quad \cdot \cdot$$

The general solutions then reduce to those in Ref. 6.

The thin shell solution is contained in Eqs. (35) and (38). Using Eq. (38) and taking the difference between the displacements at the surfaces gives

$$u(p, \cdot) - u(1, \cdot) \quad \frac{-2}{2} \sum_{\xi_i} \xi_i^2 [\xi_i J_i'(\xi_i p) + k J_\nu(\xi_i p)]^2$$

$$\cdot \frac{\bar{u}(\xi_i, \tau)}{F_\nu(\xi_i)} [C_\nu(p, \xi_i) - C_\nu(1, \xi_i)] .$$

$$\qquad(44)$$

As p approaches one, the difference in the bracket in Eq. (44) goes to zero. Hence, the usual assumptions of shell theory apply here, thereby showing that the general solutions hold over the range of shell thicknesses from very thin to very thick.

The solid cylinder is obtained by letting the inner radius approach zero. The initial conditions are those of Eq. (28), but the boundary conditions become

$$\frac{b}{c_{11}} \sigma_\rho(p, \tau) = \left(\frac{\partial u}{\partial \iota} + \frac{c_{12}}{c_{11}} u \right)_{\rho=1} .\qquad(45)$$

For this case the nondimensionalized form of Eq. (21) is

$$\frac{\partial^2 u}{\partial \iota^2} + \frac{1}{\iota} \frac{\partial u}{\partial \iota} - \frac{\nu^2}{\iota^2} u = \frac{\partial^2 u}{\partial \tau^2} + C \frac{\partial u}{\partial \tau} , \quad 0 \le \iota \le 1, \quad \tau > 0;$$

$$\qquad(46)$$

$$\iota = \frac{r}{b} ,$$

$$\tau = \frac{v}{b} t ,\qquad(47)$$

$$C = \frac{bvD}{c_{11}} .$$

The transform for this case is from Eq. (11)

$$\bar{u} = \bar{u}(\xi_i, \tau) = \int_0^1 \rho u(\rho, \xi_i) C_\nu(\rho, \xi_i) d\rho .\qquad(48)$$

Applying Eq. (48) to Eq. (46) and using Eqs. (14), (31), and (45) gives

$$\frac{d^2 \bar{u}}{d\tau^2} + 2\zeta \omega_n \frac{d\bar{u}}{d\tau} + \omega_n^2 \bar{u} \quad \frac{J_\nu(\xi_i)}{c_{11}} \sigma_\rho(1, \tau) .\qquad(49)$$

where ζ, ω_n are as defined by Eq. (34). The solution to Eq. (49) is

$$\bar{u}(\xi_i, \tau) \quad \frac{J_\nu(\xi_i)}{c_{11} \omega} \int_0^\tau e^{-\zeta \omega(\tau - v)} \sigma_\rho(1, v) \sin \omega(\tau - v) dv$$

$$+ \bar{f}(\xi_i) e^{-\zeta \omega_n \tau} \cos \omega \tau + \frac{[\bar{g}(\xi_i) + \zeta \omega_n \bar{f}(\xi_i)]}{\omega} e^{-\zeta \omega_n \tau} \sin \omega \tau .$$

$$\qquad(50)$$

$$\begin{matrix} \bar{f}(\xi_i) \\ \bar{g}(\xi_i) \end{matrix} = \int_0^1 \rho \begin{matrix} f(\rho) \\ g(\rho) \end{matrix} J_\nu(\xi_i \rho) d\rho ,\qquad(51)$$

where ω is as defined in Eq. (37). The solution for the displacement is obtained from Eq. (12) as

$$u(\iota, \tau) = 2 \sum_{\xi_i} \frac{\xi_i^2 \bar{u}(\xi_i, \tau)}{k^2 + (\xi_i^2 - \nu^2)} \frac{J_\nu(\xi_i \rho)}{[J_\nu(\xi_i)]^2} .\qquad(52)$$

The corresponding stress is found from Eq. (45).

The case of the cavity in an infinite medium is solved by using the extended Weber transform. The basic equations, Eqs. (23) through (28), remain the same. The boundary conditions now become

$$\sigma_\rho(1, \tau) = A(\tau) ,$$

$$\qquad(53)$$

$$\lim_{\rho \to \infty} \sigma_\rho(\rho, \tau) \to 0 .$$

The transform for this case is

$$\bar{u} = \bar{u}(\alpha, \tau) = \int_1^\infty \rho u(\rho, \tau) C_\nu(\rho, \alpha) d\rho .\qquad(54)$$

Applying Eq. (54) to Eq. (23) and using Eqs. (10), (26), (31), and (53) gives

$$\frac{d^2 \bar{u}}{d\tau^2} + C \frac{d\bar{u}}{d\tau} + \alpha^2 \bar{u} = -\frac{2a}{\pi c_{11}} \sigma_\rho(1, \tau) .\qquad(55)$$

111

The solution to Eq. (55) is

$$\bar{u}(a,\tau) = -\frac{2a}{\pi c_{11}\omega}\int_0^\tau e^{-C/2(\tau-v)}\,\sigma_\rho(1,v)\,\sin\omega(\tau-v)\,dv$$

$$+ e^{-C/2}\left[\bar{f}(a)\cos\omega\tau + \frac{2\bar{g}(a)+C\bar{f}(a)}{2\omega}\sin\omega\tau\right]. \tag{56}$$

$$\begin{aligned}\bar{f}(a)\\\bar{g}(a)\end{aligned} = \int_1^\infty \rho \begin{aligned}f(\rho)\\g(\rho)\end{aligned} C_\nu(\rho,a)\,d\rho. \tag{57}$$

$$\omega = \left(a^2 - \frac{C^2}{4}\right)^{1/2}. \tag{58}$$

From Eq. (9) the displacement is

$$u(\rho,\tau) = \int_0^\infty \frac{a\bar{u}(a,\tau)\,C_\nu(\rho,a)\,da}{[aJ_\nu'(a)+hJ_\nu(a)]^2 + [aY_\nu'(a)+hY_\nu(a)]^2}. \tag{59}$$

The corresponding stresses are found from Eqs. (26) and (27). This problem has also been solved [7] using the Laplace transform. The advantage of the solution given here is that the complex integration used by Eason is avoided. However, it remains true that for most cases the integral in Eq. (59) must be evaluated numerically.

Returning to the thick shell, the surface tractions are now specialized so that particular cases of interest can be studied. Setting the surface tractions in Eq. (28) equal to zero, that is,

$$\sigma_\rho(p,\tau) = \sigma_\rho(1,\tau) = 0, \tag{60}$$

gives the solution for free vibrations. Harmonic vibrations are studied by specifying the surface loads as follows:

$$\sigma_\rho(1,\tau) = -A e^{i\omega\tau},$$
$$\sigma_\rho(p,\tau) = f(\rho) = g(\rho) = 0. \tag{61}$$

Putting Eq. (61) into Eq. (33) and solving for $\bar{u}$ gives

$$\bar{u} = \frac{2aA}{\pi c_{11}\omega_n^2}\frac{e^{i(\omega\tau-\phi_n)}}{\left[\left(1-\frac{\omega^2}{\omega_n^2}\right)^2 + \left(2\zeta\frac{\omega}{\omega_n}\right)^2\right]^2}, \tag{62}$$

$$\phi_n = \tan^{-1}\frac{2\zeta\frac{\omega}{\omega_n}}{1-\frac{\omega^2}{\omega_n^2}}. \tag{63}$$

Resonance is obtained by letting $\omega\to\omega_n$ in Eq. (62), which gives

$$\bar{u}|_{RES} = \frac{2aA}{\pi c_{11}\omega_n^2}Q_n e^{i(\omega_n\tau-\tau/2)}. \tag{64}$$

$$Q_n = \frac{1}{2\zeta}, \tag{65}$$

where Q_n is the "magnification factor" for each mode. Static motion is then found by letting ω approach zero in Eq. (62) which gives

$$\bar{u}_{ST} = \frac{2aA}{\pi c_{11}\omega_n^2}. \tag{66}$$

By using Eq. (66), Eq. (62) is rewritten as

$$\frac{\bar{u}}{\bar{u}_{ST}} = \frac{e^{i(\omega\tau-\phi_n)}}{\left[\left(1-\frac{\omega^2}{\omega_n^2}\right)^2 + \left(2\zeta\frac{\omega}{\omega_n}\right)^2\right]^{1/2}}. \tag{67}$$

Equations (61) through (67) show that under harmonic excitation each normal mode of the shell responds very much like a single degree of freedom with viscous damping. Another form of the harmonic solution which has practical use is the transfer function or the ratio of the displacement to the surface load $\sigma_\rho(1,\tau)$. By using Eqs. (38), (62), and (67), it is easily shown that the transfer function is

$$\frac{u(\rho,\omega)}{\sigma_\rho(1,\omega)} = -\frac{\pi^2}{2A}\sum_{\xi_i}\xi_i^2\,[\xi_i J_\nu'(\xi_i p) + kJ_\nu(\xi_i p)]^2$$

$$\times \frac{C_\nu(\rho,\xi_i)}{F_\nu(\xi_i)}\frac{e^{-i\phi_n}}{\left[\left(1-\frac{\omega^2}{\omega_n^2}\right)^2 + \left(2\zeta\frac{\omega}{\omega_n}\right)^2\right]^{1/2}}\bar{u}_{ST}. \tag{68}$$

Equation (68) clearly shows the interrelationship of the static displacement, driving force, and shell response. Mechanical impedance is another concept which has widespread practical use. For a continuous elastic system of finite dimensions, this is defined as

$$Z(e_1, e_2, e_3, \omega) = \frac{P(e_1, e_2, e_3) e^{i \cdot \tau}}{\dot{u}(e_1, e_2, e_3, \omega)} \quad . \quad (69)$$

where

Z = mechanical impedance,

e_1, e_2, e_3 = orthogonal coordinates,

P = spatial distribution of applied force, and

$\dot{u}$ = velocity of elastic system.

To apply this concept to elastic systems of finite dimensions, two restrictions must be made: (a) all initial conditions must be zero, and (b) for loads on more than one surface, the mechanical impedance must be determined separately for each surface. For the loads specified in Eq. (61), the mechanical impedance found from Eqs. (61), (62), and (68) is

$$\frac{1}{Z(\rho, \omega)} = -\frac{\pi^2}{2} \sum_{\xi_i} \xi_i^2 [\xi_i J_\nu'(\xi_i \rho) + k J_\nu(\xi_i \rho)]^2$$

$$\times \frac{C_\nu(\rho, \xi_i)}{F_\nu(\xi_i)} \frac{\omega e^{-i(\phi_n - \pi/2)} \bar{u}_{ST}}{\left[\left(1 - \frac{\omega^2}{\omega_n^2} \right)^2 + \left(2\zeta \frac{\omega}{\omega_n} \right)^2 \right]^{1/2}} \quad . \quad (70)$$

The reciprocal of the impedance has been used in Eq. (70) because of the length and complexity of the expression and the fact that such an expression can be implemented in an analyzer. The use of the complete expression in Eq. (70) is, of course, cumbersome. Fortunately, for most structural materials the damping is so low ($\zeta < 0.01$) that contributions to the total motion from modes other than the first constitute only a few percent. Hence, a good approximation to Eq. (70) is

$$Z(\rho, \omega) \equiv$$

$$\frac{2\bar{u}_{ST} F_\nu(\xi_1) \left[\left(1 - \frac{\omega^2}{\omega_1^2} \right)^2 + \left(2\zeta \frac{\omega}{\omega_1} \right)^2 \right]^{1/2} e^{i(\phi_n - \pi/2)}}{\pi^2 \omega \xi_1^2 [\xi_1 J_\nu'(\xi_1 \rho) + k J_\nu(\xi_1 \rho)]^2 C_\nu(\rho, \xi_1)} \quad (71)$$

The "point" impedance is found in Eqs. (70) and (71) by choosing $\rho = 1$. The "transfer" impedance is found by taking $\rho \neq 1$. All of the results in Eqs. (61) through (71) were obtained for a load on the inner surface. The same procedure

can be repeated for a load on the outer surface with similar results.

The specification of the surface loads enables the transient solution to be put into a form that is more convenient for physical interpretation than Eqs. (35) and (38). To illustrate the basic method, the following conditions are chosen:

$$\sigma_\rho(1, \tau) = -1(\tau) \ .$$
$$\sigma_\rho(p, \tau) = f(\rho) = g(\rho) = 0 \ . \quad (72)$$

Taking the Laplace transform of Eq. (33) and using Eq. (72) gives

$$\bar{u}(\xi_i, s) = \frac{2a}{\pi c_{11}} \frac{1}{s[(s + \zeta \omega_n)^2 + \omega^2]} \ . \quad (73)$$

The final value theorem of Laplace transform theory is

$$\lim_{t \to \infty} F(x, y, z, t) = \lim_{s \to 0} \bar{F}(x, y, z, s) \ . \quad (74)$$

When Eq. (74) is applied to Eq. (73), the static solution to Eq. (23) is

$$\bar{u}(\xi_i)_{ST} = \bar{u}_{ST} = \frac{2a}{\pi c_{11} \omega_n^2} \ . \quad (75)$$

Equation (73) can be rewritten as

$$\bar{u}(\xi_i, s) = \frac{\omega_n^2 \bar{u}_{ST}}{s[(s + \zeta \omega_n)^2 + \omega^2]} \ . \quad (76)$$

By inverting Eq. (76) and using Eq. (38), the solution for the displacement is

$$u(\rho, \tau) = \frac{\pi^2}{2} \sum_{\xi_i} \xi_i^2 [\xi_i J_\nu'(\xi_i \rho) + k J_\nu(\xi_i \rho)]^2 \frac{C_\nu(\rho, \xi_i)}{F_\nu(\xi_i)}$$

$$\times \bar{u}_{ST} \left[1 + \frac{\omega}{\omega_n} e^{-\zeta \omega_n \tau} \sin(\omega \tau - \psi) \right] \ , \quad (77)$$

$$\psi = \tan^{-1} \frac{\omega}{\zeta \omega_n} \ . \quad (78)$$

Equation (77) shows that the dynamic response can be related directly to the static deformation. This is similar to the case of harmonic vibration in Eq. (67). As the damping ζ goes to zero, the standard result is that a dynamic displacement of twice the static deformation is recovered. The basic procedure shown here can be repeated for other types of loading with

113

similar results and for loads on the outer surface.

All of the results in this section shown for specific loads can be easily extended to the limiting cases of the solid cylinder and cavity in an infinite medium. The standard case of no damping for all of the results in this section can be obtained by letting the damping ratio ζ go to zero. Although the approximation of the internal damping as a viscous effect is undoubtedly oversimplified in many materials, the incorporation of more complex viscoelastic behavior can be solved by the same methods. Hence, extension to linear damping models of wider applicability can be accomplished by the interested reader.

RADIAL MOTION OF A SPHERICAL SHELL

The basic equations for the radially symmetric motion of a spherical shell with internal viscous damping and transverse curvilinear isotropy are

$$\frac{\partial \sigma_r}{\partial r} + \frac{2\sigma_r - \sigma_\theta - \sigma_\phi}{r} = \rho^* \frac{\partial^2 u}{\partial t^2} + D \frac{\partial u}{\partial t}, \quad a \le r \le b, \quad t > 0, \tag{79}$$

$$\sigma_r = c_{11} \frac{\partial u}{\partial r} + 2c_{12} \frac{u}{r} . \tag{80}$$

$$\sigma_\theta = \sigma_\phi = c_{12} \frac{\partial u}{\partial r} + (c_{22} + c_{23}) \frac{u}{r} . \tag{81}$$

where

u = radial displacement of the sphere;

$\sigma_r, \sigma_\theta, \sigma_\phi$ = radial and circumferential stresses, respectively;

$c_{11}, c_{12}, c_{22}, c_{23}$ = elastic constants; and

ρ^*, D = material density and viscous damping coefficient, respectively.

Substitution of Eqs. (80) and (81) into Eq. (79) gives

$$\frac{\partial^2 u}{\partial r^2} + \frac{1}{r} \frac{\partial u}{\partial r} - \frac{(\mu^2 - 1/4)}{r^2} u = \frac{\rho^*}{c_{11}} \frac{\partial^2 u}{\partial t^2} + \frac{D}{c_{11}} \frac{\partial u}{\partial t} . \tag{82}$$

$$\mu = \frac{1}{2} \left[\frac{8(c_{22} + c_{23} - c_{12})}{c_{11}} + 1 \right]^{1/2} . \tag{83}$$

When the same variables defined in Eqs. (24) and (25) are used, the dimensionless form of the basic equations for the sphere are:

$$\frac{\partial^2 u}{\partial \rho^2} + \frac{2}{\rho} \frac{\partial u}{\partial \rho} - \frac{(\mu^2 - 1/4)}{\rho^2} u = \frac{\partial^2 u}{\partial \tau^2} + C \frac{\partial u}{\partial \tau}, \quad 1 \le \rho \le p, \quad \tau > 0, \tag{84}$$

$$\frac{a}{c_{11}} \sigma_\rho(\rho, \tau) = \frac{\partial u}{\partial \rho} + \frac{2c_{12}}{c_{11}\rho} u , \tag{85}$$

$$\frac{a}{c_{12}} \sigma_\theta(\rho, \tau) = \frac{a}{c_{12}} \sigma_\phi(\rho, \tau) = \frac{\partial u}{\partial \rho} + \frac{c_{22} + c_{23}}{c_{12}\rho} u . \tag{86}$$

The appropriate initial and boundary conditions are, respectively,

$$u(\rho, 0) = m(\rho) , \tag{87}$$

$$\left. \frac{\partial u}{\partial \tau} \right|_{\tau = 0} = n(\rho) :$$

$$\sigma_\rho(1, \tau) = A(\tau) , \tag{88}$$

$$\sigma_\rho(p, \tau) = B(\tau) .$$

If

$$u(\rho, \tau) = \rho^{-1/2} f(\rho, \tau) , \tag{89}$$

then Eqs. (84) through (88) become

$$\frac{\partial^2 f}{\partial \rho^2} + \frac{1}{\rho} \frac{\partial f}{\partial \rho} - \frac{\mu^2}{\rho^2} f = \frac{\partial^2 f}{\partial \tau^2} + C \frac{\partial f}{\partial \tau} , \quad 1 \le \rho \le p, \quad \tau > 0, \tag{90}$$

$$\frac{a\rho^{1/2}}{c_{11}} \sigma_\rho(\rho, \tau) = \frac{\partial f}{\partial \rho} + \frac{4c_{12} - 1}{2c_{11}\rho} f . \tag{91}$$

$$\frac{a\rho^{1/2}}{c_{12}} \sigma_\theta(\rho, \tau) = \frac{a\rho^{1/2}}{c_{12}} \sigma_\phi(\rho, \tau)$$

$$= \frac{\partial f}{\partial \rho} + \frac{2(c_{22} + c_{23}) - 1}{2c_{12}\rho} f . \tag{92}$$

Initial Conditions:

$$f(\rho, 0) = \rho^{1/2} m(\rho) ,$$

$$\left. \frac{\partial f}{\partial \tau} \right|_{\tau = 0} = \dot{f}(\rho, 0) = \rho^{1/2} n(\rho) . \tag{93}$$

Boundary Conditions:

$$\sigma_\rho(1, \tau) = A(\tau) ,$$

$$\sigma_\rho(p, \tau) = B(\tau) . \tag{94}$$

114

A comparison of Eqs. (90) through (94) with Eqs. (23) through (29) indicates that there is a direct analogy between the plane strain and radially symmetric problems if the following analogous quantities are defined:

Cylinder	Sphere
$u(\xi_i, \tau)$, ξ_i	$f(\xi_i, \tau)$, μ, ξ_i
$\sigma_\rho(\cdot, \tau)$, $\sigma_\beta(\cdot, \cdot)$	$\rho^{-1/2}\sigma_\rho(\cdot, \tau)$, $\rho^{-1/2}\sigma_\mu(\cdot, \tau)$
$u(\rho, 0)$, $\dot{u}(\rho, 0)$	$f(\rho, 0)$, $\dot{f}(\cdot, 0)$
$h = \dfrac{c_{12}}{c_{11}}$	$h = \dfrac{2c_{12} - 1/2}{c_{11}}$
$k = \dfrac{c_{22}}{c_{12}}$	$k = \dfrac{c_{22} + c_{23} - 1/2}{c_{12}}$

Thus, the solution for $f(\rho, \tau)$ in the general case and all the various subcases can be written directly from the solution for $u(\rho, \tau)$ in the cylindrical case merely by replacing the cylindrical quantities in the expression by their spherical counterpart. The radial displacement is then found from Eq. (89). The spherical stresses are obtained from the expressions in Eqs. (41) and (42) for the cylindrical stresses in exactly the same manner as $f(\rho, \tau)$. Eason [7] has shown that the plane stress solution also has a plane stress analog. As a result of the present study, any plane strain, plane stress, or radial symmetric problem has a corresponding solution in the other two analogs.

TORSIONAL MOTION OF A FINITE CYLINDRICAL SHELL

Transient torsional wave propagation problems in elastic media have been studied extensively in the recent past with most papers concentrating on isotropic bodies [6,8-19]. Achenbach [11] and Berry [20] have extended the studies to viscoelastic materials. Anisotropic materials have been treated in only a few cases, as in Refs. 2, 18 and 19 which concern an infinite plate and semi-infinite media. All of the papers in which the radial direction is finite assume that the lateral surface is free from tractions. The problem treated here is the vibration of a finite hollow cylinder with internal viscous damping and transverse curvilinear isotropy with all of its surfaces subject to loads.

The basic equations of motion for this problem are [2]:

$$\frac{\partial^2 u}{\partial z^2} + a^* \left(\frac{\partial^2 u}{\partial r^2} + \frac{1}{r} \frac{\partial u}{\partial r} - \frac{1}{r^2} u \right) = \frac{\rho^*}{c_{44}} \frac{\partial^2 u}{\partial t^2} + D \frac{\partial u}{\partial t} ,$$

$$\left\{ \begin{matrix} a \leq r \leq b \\ 0 \leq z \leq \ell \\ t > 0 \end{matrix} \right\} , \quad (95)$$

$$\sigma_{r\theta}(r, z, t) = c_{44} a^* \left(\frac{\partial u}{\partial r} - \frac{u}{r} \right) , \quad (96)$$

and

$$\sigma_{\theta z}(r, z, t) = c_{44} \frac{\partial u}{\partial z} , \quad (97)$$

where

  u = torsional displacement of the cylinder,

  c_{44} = elastic constant, and

  a^* = dimensionless constant whose value depends on the type of material crystal being used [2].

The new variables are defined as

$$\rho = \frac{r}{a \sqrt{a^*}} ,$$

$$x = \frac{z}{a} ,$$

$$v^2 = \frac{c_{44}}{\rho^*} , \quad (98)$$

$$\mu' = \frac{c_{44}}{a} ;$$

$$\tau = \frac{vt}{a} ,$$

$$p = \frac{b}{a} ,$$

$$q = \frac{\ell}{a} , \quad (99)$$

$$C = \frac{avD}{c_{44}} .$$

The basic equations in nondimensionalized coordinates are

$$\frac{\partial^2 u}{\partial x^2} + \left(\frac{\partial^2 u}{\partial \rho^2} + \frac{1}{\rho} \frac{\partial u}{\partial \rho} - \frac{1}{\rho^2} u \right) = \frac{\partial^2 u}{\partial \tau^2} + C \frac{\partial u}{\partial \tau} , \quad \left\{ \begin{matrix} 1 \leq \rho \leq p \\ 0 \leq x \leq q \\ \tau > 0 \end{matrix} \right\} .$$

$$(100)$$

115

$$\sigma_{\rho\theta}(\cdot, x, \tau) = \mu' \sqrt{a^*} \left(\frac{\partial u}{\partial \rho} - \frac{u}{\rho} \right). \quad (101)$$

and

$$\sigma_{\theta x}(\cdot, x, \tau) = \mu' \frac{\partial u}{\partial x}. \quad (102)$$

The appropriate initial conditions are

$$u(\cdot, x, 0) = F(\cdot, x),$$

$$\left. \frac{\partial u}{\partial \tau} \right|_{\tau=0} = G(\cdot, x); \quad (103)$$

boundary conditions are

$$\sigma_{\rho\theta}(1, x, \tau) = A(x, \tau),$$

$$\sigma_{\rho\theta}(p, x, \tau) = B(x, \tau); \quad (104)$$

$$\sigma_{\theta x}(\cdot, 0, \tau) = D(\cdot, \tau),$$

$$\sigma_{\theta x}(\cdot, q, \tau) = E(\cdot, \tau); \quad (105)$$

The appropriate transform for the axial variable (x) is, from Eq. (15),

$$\bar{u} = \bar{u}(\rho, n, \tau) = \int_0^q u(\cdot, x, \tau) \cos \frac{n\pi x}{q} \, dx. \quad (106)$$

By applying Eq. (106) to Eq. (100) and using Eqs. (17), (102), and (105),

$$\frac{1}{\mu'} \left[(-1)^n E(\cdot, \tau) - D(\cdot, \tau) \right] + \left(\frac{\partial^2 \bar{u}}{\partial \rho^2} + \frac{1}{\rho} \frac{\partial \bar{u}}{\partial \rho} - \frac{1}{\rho^2} \bar{u} \right)$$

$$= \frac{\partial^2 \bar{u}}{\partial \tau^2} + C \frac{\partial \bar{u}}{\partial \tau} + \frac{n^2 \pi^2}{q^2} \bar{u}. \quad (107)$$

The transform for the radial variable (·) is, from Eq. (1),

$$\bar{\bar{u}} = \bar{\bar{u}}(\xi_i, n, \tau) = \int_1^p \rho u(\cdot, n, \tau) C_1(\cdot, \xi_i) \, d\rho. \quad (108)$$

If by definition

$$h = -1,$$

$$k = -\frac{1}{p} = \frac{h}{p}, \quad (109)$$

then using Eq. (108) along with Eqs. (6), (101), and (104) on Eq. (107) gives

$$\frac{d^2 \bar{\bar{u}}}{d\tau^2} + C \frac{d\bar{\bar{u}}}{d\tau} + \left(\xi_i^2 + \frac{n^2 \pi^2}{q^2} \right) \bar{\bar{u}} = \frac{1}{\mu'} \left[(-1)^n \bar{E}(\xi_i, \tau) - \bar{D}(\xi_i, \tau) \right]$$

$$+ \frac{2}{\pi \mu' \sqrt{a^*}} \left\{ \frac{[\xi_i J_1'(\xi_i) + h J_1(\xi_i)]}{[\xi_i J_1'(\xi_i p) + k J_1(\xi_i p)]} \quad \bar{B}(n, \tau) - \bar{A}(n, \tau) \right\}, \quad (110)$$

$$\begin{array}{l} \bar{A}(n, \tau) \\ \bar{B}(n, \tau) \end{array} = \int_0^q \begin{array}{l} A(x, \tau) \\ B(x, \tau) \end{array} \cos \frac{n\pi x}{q} \, dx. \quad (111)$$

$$\begin{array}{l} \bar{D}(\xi_i, \tau) \\ \bar{E}(\xi_i, \tau) \end{array} = \int_1^p \rho \begin{array}{l} D(\cdot, \tau) \\ E(\cdot, \tau) \end{array} C_1(\cdot, \xi_i) \, d\rho. \quad (112)$$

If

$$\lambda_n^2 = \xi_i^2 + \frac{n^2 \pi^2}{q^2}. \quad (113)$$

then by using the same definitions of Eq. (34) in Eq. (110), the solution for $\bar{\bar{u}}$ is

$$\bar{\bar{u}}(\xi_i, n, \tau) = \frac{2}{\pi \mu' \sqrt{a^*} \, \omega} \int_0^\tau \left\{ \frac{\pi \sqrt{a^*}}{2} \left[(-1)^n \bar{E}(\xi_i, v) - \bar{D}(\xi_i, v) \right] \right.$$

$$+ \left[\frac{\xi_i J_1'(\xi_i) + h J_1(\xi_i)}{\xi_i J_1'(\xi_i p) + k J_1(\xi_i p)} \quad \bar{B}(n, v) - \bar{A}(n, v) \right] \right\}$$

$$\times e^{-\zeta \omega_n \tau} \sin \omega(\tau - v) \, dv + e^{-\zeta \omega_n \tau}$$

$$\times \left[\bar{\bar{F}}(\xi_i, n) \cos \omega\tau + \frac{\bar{\bar{G}}(\xi_i, n) + \zeta \omega_n \bar{\bar{F}}(\xi_i, n)}{\omega} \sin \omega\tau \right], \quad (114)$$

$$\begin{array}{l} \bar{\bar{F}}(\xi_i, n) \\ \bar{\bar{G}}(\xi_i, n) \end{array} = \int_1^p \int_0^q \rho \begin{array}{l} F(\rho, x) \\ G(\rho, x) \end{array} C_1(\rho, \xi_i) \cos \frac{n\pi x}{q} \, d\rho \, dx. \quad (115)$$

The solution for the displacement is obtained from the inversion series in Eqs. (3) and (16) as

$$u(\cdot, x, \tau) = \frac{\pi^2}{2q} \sum_{\xi_i} \xi_i^2 \left[\xi_i J_1'(\xi_i p) \right.$$

$$+ k J_1(\xi_i p)]^2 \, \bar{\bar{u}}(\xi_i, 0, \tau) \frac{C_1(\cdot, \xi_i)}{F_1(\xi_i)}$$

$$+ \frac{\pi^2}{q} \sum_{\xi_i} \sum_{n=1}^\infty \xi_i^2 \left[\xi_i J_1'(\xi_i p) \right.$$

$$+ k J_1(\xi_i p)]^2 \, \bar{\bar{u}}(\xi_i, n, \tau) \frac{C_1(\cdot, \xi_i)}{F_1(\xi_i)} \cos \frac{n\pi x}{q}. \quad (116)$$

116

The solution is obtained by placing Eq. (114) into Eq. (116). It can easily be shown [11] that the lowest torsional mode ($\epsilon_i = 0$) is nondispersive, thereby making anisotropic finite hollow cylinders useful as delay lines in ultrasonic studies.

The special cases of free, harmonic, and static motion plus the limiting cases of the solid cylinder and thin shell can be solved using the techniques and methods outlined for the circular cylindrical shell. Using the extended Weber transform, the case of the infinite plate with a circular hole in it can be solved. The solution for the semi-infinite medium with a circular hole is obtained by using the extended Weber transform and semi-infinite cosine transform. The infinite medium with a circular hole in it is solved by the combined use of the extended Weber transform and complex Fourier transform. Because of the ease with which these subproblems can be solved and to conserve paper length, they are left as an exercise for the reader.

This section treated the case where all four surface tractions were specified. Other cases which have displacements and tractions specified on the surfaces can be solved by choosing appropriate transforms that are available in the literature. Mixed boundary conditions which lead to dual integral equations are treated by Shail [15] and Sneddon et al. [16].

RESULTS AND CONCLUSIONS

The dynamic response of thick elastic anisotropic cylinders and spheres has been found in certain problems, where the boundary conditions are Cauchy in nature, by new integral transforms. The solutions were obtained in a manner which is more direct and concise than existing techniques. It was shown that there exists a direct analog between plane strain motion of a cylinder and radially symmetric motion of a sphere. These results have application to such diverse fields as pressure vessels, solid rocket propellants, geophysics, and ultrasonics.

REFERENCES

1. R. F. S. Harmon, Applied Anisotropic Elasticity. Oxford Univ. Press, London, Eng., 1961

2. R. A. Scott and J. Miklowitz, "Transient Elastic Waves in Anisotropic Plates," Div. of Eng. and Appl. Sci., California Inst. of Technology, ONR Contract Nonr-220(57) NR-064-487 TR-1, AD 623917, Sept. 1965

3. G. Eason, "On the Vibration of Anisotropic Cylinders and Spheres," Appl. Sci. Res., Sect. A, Vol. 12, p. 81, June 1962

4. G. Cinelli, "An Extension of the Finite Hankel Transform and Application," Intern. J. Eng. Sci., Vol. 3, No. 5, p. 539, Oct. 1965

5. I. N. Sneddon, Four Transforms. McGraw-Hill, New York, 1951

6. G. Cinelli, "Dynamic Vibrations and Stresses in Elastic Cylinders and Spheres," 5th U. S. National Cong. of Appl. Mech., Univ. of Minnesota, June 1966; to appear in J. Appl. Mech.

7. G. Eason, "Propagation of Waves from Spherical and Cylindrical Cavities," ZAMP, Vol. 14, p. 12, 1963

8. J. J. McCoy, "Propagation of Torsional Waves in a Circular Elastic Rod," ZAMP, Vol. 15, p. 456, 1964

9. W. L. Wainwright, "On Torsional Oscillations in a Finite Circular Cylinder," JASA, Vol. 36, No. 3, p. 511, Mar. 1964

10. G. Cinelli, "Torsional Wave Propagation and Its Application to Ultrasonic Delay Lines," 1965 IEEE Ultrasonics Symp., Boston, Mass., Dec. 1965

11. J. D. Achenbach, "Torsional Oscillations of an Encased Hollow Cylinder of Finite Length," AIAA/ASME 7th Structures and Materials Conf. Proc., Coca Beach, Fla., Apr. 1966

12. S. K. Clark, "Torsional Wave Propagation in Hollow Cylindrical Bars," JASA, Vol. 28, No. 6, p. 1163, 1956

13. M. S. Macrakis, "Study of Torsional Waves in a Laminated Elastic Rod," MIT Lincoln Lab. Rept. 250-0015

14. A. E. Armenakas, "Torsional Waves in Composite Rods," JASA, Vol. 38, p. 439, Mar. 1965

15. R. Shail, "On the Forced Torsional Oscil-
    lations of an Elastic Cylinder," Proc.
    Cambridge Phil. Soc., Vol. 61, p. 955, 1965

16. I. N. Sneddon et al., "The Reissner-Sagoci
    Problem for a Long Cylinder of Finite
    Length," Quart. J. Mech. and Appl. Math.,
    Vol. 19, No. 2, p. 123, May 1966

17. M. L. Ghosh, "Disturbance in an Elastic
    Half Space Due to an Impulsive Twisting
    Moment Applied to an Attached Rigid Disc,"
    Appl. Sci. Res., Sec. A, Vol. 14, No. 1-2,
    p. 31, 1964-65

18. M. Mitra, "Disturbance Produced in an
    Elastic Half Space by an Impulsive Twist-
    ing Moment Applied to an Attached Rigid
    Disc," ZAMM, Vol. 38, No. 1-2, p. 40,
    Jan.-Feb. 1958

19. G. Eason, "On the Torsional Impulsive
    Loading of an Elastic Half Space," Quart.
    J. Math. and Appl. Mech., Vol. 17, No. 3,
    p. 279, 1964

20. D. S. Berry, J. Mech. Phys. Solids, Vol. 6,
    p. 177, 1958

*   *   *

EFFECT OF ASYMMETRICAL TRAPEZOIDAL PULSE
ON SINGLE-DEGREE-OF-FREEDOM SYSTEMS*

H. Saunders
General Electric Company
Philadelphia, Pennsylvania

The behavior of components when subjected to a shock may be approx-
imated by a single-degree-of-freedom mass-spring system subjected
to a prescribed pulse. A number of specifications require a rectangu-
lar input pulse. Due to the limitations of the physical laboratory equip-
ment, the theoretical rectangular pulse is unattainable and an asym-
metrical trapezoidal pulse must be used. Equations are derived for
predicting the maximum acceleration response of a physically obtain-
able asymmetrical trapezoidal pulse. The equations employ the actual
rise, decay and dwell portions of the pulse. Since most physical sys-
tems contain little or no damping, an undamped one degree of freedom
is employed. The solution is obtained by utilizing the Laplace trans-
form method in terms of the Dirac delta function. Comparisons are
made between the theoretical rectangular pulse and a few trapezoidal
pulses having different rise, decay and dwell times. The rectangular
pulse is the most severe. The rise and decay times have a secondary
effect on the response; the dwell time has the most important effect.
By using the derived equations, the designer can evaluate the degree of
departure between the idealized and actual test condition and can thus
define an equivalent trapezoidal pulse capable of furnishing a similar
response in the component.

INTRODUCTION

Great costs and prodigious engineering ef-
forts are involved in attempting to achieve high
reliability in the launch of space payloads.
High reliability is based on a strong foundation
of rigid quality control and preflight tests, par-
ticularly shock and vibration tests. Space pay-
loads are subjected to shock loads before and
during flight and at touchdown. In the preflight
phase, shock loads occur during transportation
and handling of the payload. From launch to
reentry, the primary sources of shock are en-
gine ignition, shutdown and staging. From re-
entry to the successful end of the mission, the
main sources of shock excitation are parachute
deployment, earth or water impact and, in the
case of the LEM vehicle, touchdown on the
moon. Since space payloads are exotic struc-
tures consisting of fabricated mechanical and
electronic parts, the response analysis of such
a system may be of questionable value in as-
sessing the system reliability. It thus becomes
apparent that, where possible, these payloads

must be subjected to the anticipated shock
loads. Under simulated operating conditions,
all components should be energized and prop-
erly functioning to prove their ability in with-
standing the induced shock. The components
must either perform flawlessly or passively
survive during the shock environment. The
shock loadings may tend to compromise their
ability to complete the intended flight mission.

DISCUSSION

At present, most aerospace manufacturers
subject components to shock load tests to verify
their capability before going into system test.
Each type of shock testing machine creates a
particular pulse defined by an acceleration-
time curve. The area under the acceleration
curve is the velocity change and is considered
to be a primary parameter in the damage effect.
There are certain applicable principles concern-
ing component damage which are directly re-
lated to the results of a shock.

---

*This paper was not presented at the Symposium.

MATHEMATICAL ANALYSIS

A one-degree-of-freedom vibrating system subjected to various shock impulses applied to the base has been analyzed by a number of authors in terms of acceleration response and its resulting amplification factor. A majority of the present specifications stipulate that the shock pulse inputs must be either peak terminal sawtooth, half-sinusoidal, simulated blast pulse (right triangular), or rectangular [1]. Consider a one-degree-of-freedom system with an elastic restraint, as shown in Fig. 1. The illustration shows the absolute displacement x_1 of the mass m, the absolute displacement of the chassis x_0, and the idealized spring stiffness k. The differential equation governing the behavior of the system during the shock phase of motion is

$$m\ddot{x}_1 + k(x_1 - x_0) = 0 , \quad 0 \le t \le \tau \quad (1a)$$

or

$$\ddot{x}_1 + \omega_1^2(x_1 - x_0) = 0 , \quad (1b)$$

where

$$\omega_1^2 = \frac{k}{m}$$
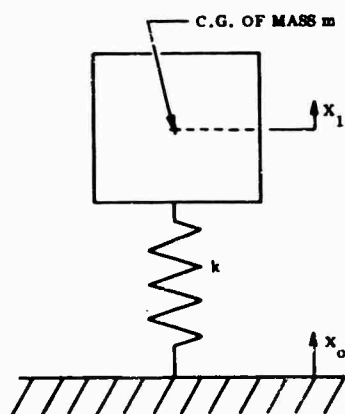
and τ is the pulse period.

Fig. 1. Schematic representation of single-degree-of-freedom system

In present specifications, the shock pulse inputs are prescribed in terms of accelerations. For convenience, the following transformations are used:

$$x_1 - x_0 = y , \quad (2a)$$

$$\dot{x}_1 - \dot{x}_0 = \dot{y} , \quad (2b)$$

and

$$\ddot{x}_1 - \ddot{x}_0 = \ddot{y} . \quad (2c)$$

Likewise, the original differential equation is transformed to the following form:

$$\ddot{y} + \omega_1^2 y = -\ddot{x}_0 , \quad 0 \le t \le \tau . \quad (3)$$

This indicates that $\ddot{x}_0$ represents the base excitation and y represents the relative displacement of the mass m with respect to the base. Equation (3) can be readily solved for y, together with the conditions that the initial velocity $\dot{x}(0)$ and displacement $x(0)$ are zero. For most components, damping is considered to be small and is neglected.

In practical design, the maximum absolute acceleration response is of primary concern. The relationship between $\ddot{x}_1$ and y is determined from Eqs. (1) and (2a):

$$\ddot{x}_1 = -\omega^2 y . \quad (4)$$

A characteristic value of the displacement x_1 is the maximum static displacement under the maximum absolute value of the force, i.e.,

$$\delta = \max \left| \frac{F(t)}{k} \right| = \frac{\max F(t)}{m \omega_1^2} . \quad (5)$$

Based on this equation, it is most natural to express the displacement spectrum in a dimensionless form in terms of the static deflection δ. The ratio of the displacement spectrum to δ is defined as the dynamic amplification factor or acceleration spectrum:

$$\text{amplification spectrum} = \frac{|x_1| \max (\omega_1 t)}{\delta}$$

$$= \frac{\text{displacement spectrum}}{\text{max. static displacement}} .$$

$$(6)$$

For most practical problems, the amplification spectrum for acceleration is desired and is represented by

$$\frac{a_1}{a_2} = \frac{\text{max. absolute acceleration of mass}}{\text{max. acceleration of pulse}}$$

If the shock pulse is defined, one approach to shock analysis is the use of Laplace transforms. This was first applied by Muller [2].

Many specifications prescribe the rectangular pulse as a shock input. A number of
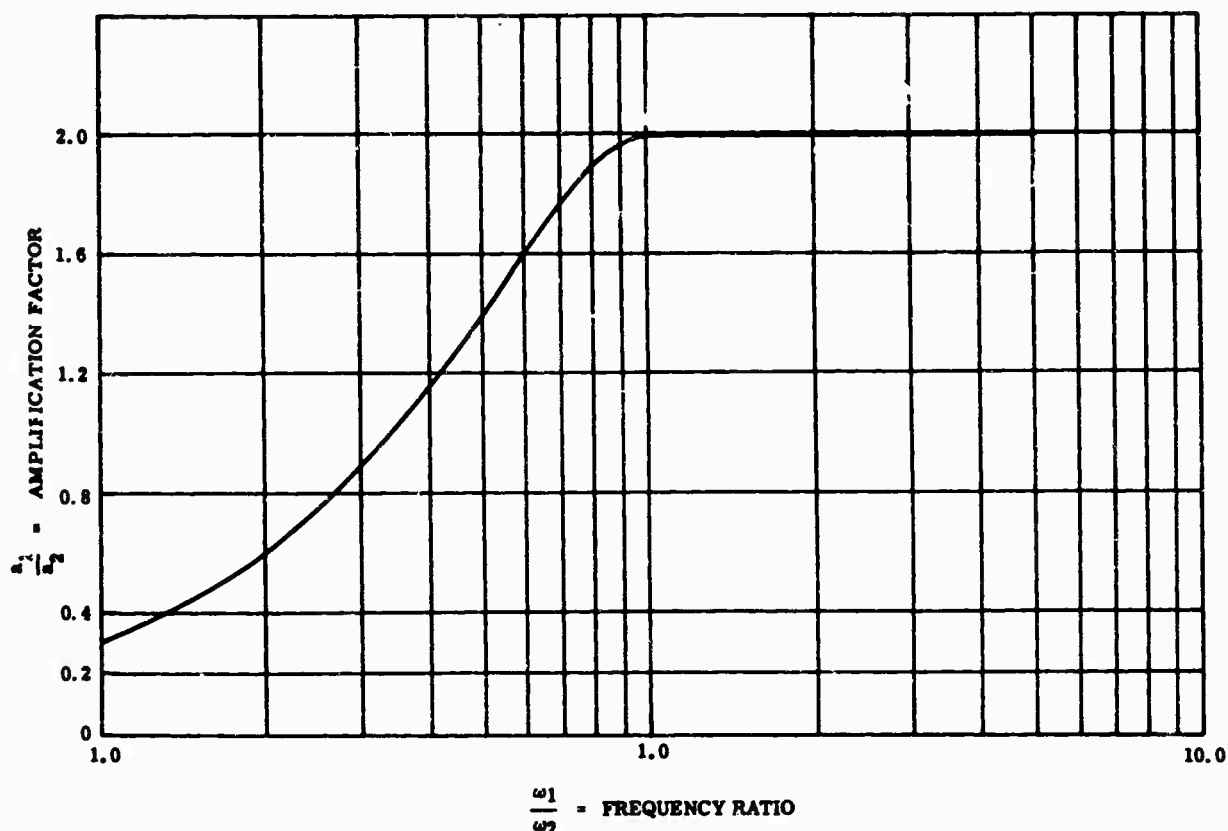
120

Fig. 2. Maximum acceleration response for rectangular pulse

authors have derived its shock spectrum by various methods. During the pulse, the maximum acceleration ratio is

$$\left|\frac{a_1}{a_2}\right|_{max} = 1 - \cos \omega_1 t , \quad t < \tau, \qquad (7)$$

where ω_2 is the forcing frequency and $\tau = \pi/\omega_2$. This reaches a maximum of 2 when $\omega_1/\omega_2 = 1$. After the pulse, the maximum acceleration ratio is

$$\left|\frac{a_1}{a_2}\right|_{max} = \sqrt{2}\left(1 - \cos \frac{\omega_1}{\omega_2} \pi\right)^{1/2}$$

$$= 2 \sin\left(\frac{\omega_1}{\omega_2} \frac{\pi}{2}\right), \quad t > \tau . \qquad (8)$$

When $\omega_1 = \omega_2$, the maximum acceleration ratio again attains the value of 2. This is illustrated in Fig. 2. In the laboratory, the specified rectangular pulse is difficult to obtain. Due to the inherent characteristics of present-day machines, the rectangular pulse acquires definite rise, dwell and decay times. The desired rectangular pulse thus becomes an asymmetrical

trapezoidal pulse (Fig. 3). Jacobsen and Ayre [3] derived a symmetrical trapezoidal pulse, i.e., equal rise and decay time.

The derivation of the asymmetrical pulse consists of describing the three phases, i.e., rise, dwell and decay positions, by an impulse function in Laplace transform notation. For the asymmetrical trapezoidal pulse, the base acceleration applied to the single-degree-of-freedom system, as defined in Fig. 3, is
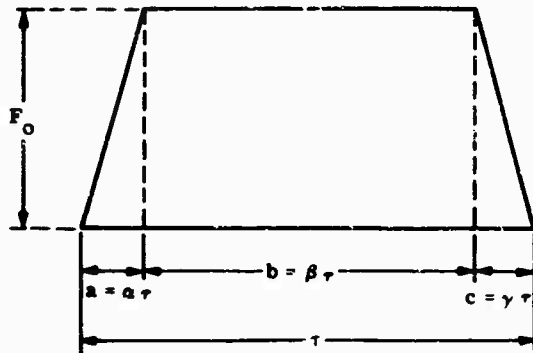
$$\ddot{x}_0 = a_2 (A + B + C) , \qquad (9)$$

where

$$\text{rise period} = A = \frac{t}{\alpha\tau} [\mu(t) - \mu(t - \alpha)\tau] , \quad (10)$$

$$\text{dwell period} = B = [\mu(t - \alpha) - \mu(t - (\alpha + \beta)\tau)] , \qquad (11)$$

$$\text{decay period} = C = \frac{t - \tau}{\gamma\tau} [\mu(t - (\alpha + \beta)\tau) - \mu(t - \tau)] , \qquad (12)$$

and $\mu(t)$ is the Dirac impulse function where $a = \alpha\tau$, $b = \beta\tau$, $c = \gamma\tau$, and $\alpha + \beta + \gamma = 1$. The

121

NOTES

F_o = APPLIED PULSE FORCE

τ = PULSE PERIOD

$\alpha + \beta + \gamma = 1$

Fig. 3. Asymmetrical
trapezoidal pulse

expressions of Eqs. (10) through (12) are sub-
stituted into Eq. (9) and the resulting equation
is described in transform notation:

$$s^2 X_o(s) = \frac{a_2}{\alpha \tau s^2}\left[1 - e^{-\alpha \tau s} - \frac{\alpha}{\gamma}e^{-(\alpha+\beta)\tau s} + \frac{\alpha}{\gamma}e^{-\tau s}\right].$$
(13)

Equation (3) can be represented in transform
notation by

$$(s^2 + \omega_1^2)\, y(s) = -s^2 X_o(s) .$$
(14)

Substituting Eq. (13) into Eq. (14) and simplify-
ing yields

$$y(s) = -\frac{a_2}{\alpha \tau}\left[\frac{1 - e^{-\alpha \tau s} - \frac{\alpha}{\gamma}e^{-(\alpha+\beta)\tau s} + \frac{\alpha}{\gamma}e^{-\tau s}}{s^2(s^2 - \omega_1^2)}\right].$$
(15)

The inverse transformation results in the
acceleration ratio equation after utilizing
Eq. (4):

$$\left|\frac{a_1}{a_2}\right| = \frac{t}{\alpha \tau} - \frac{\sin \omega_1 t}{\alpha \omega_1 \tau} - \left\langle\frac{t}{\alpha \tau} - 1 - \frac{\sin \omega_1(t - \alpha \tau)}{\alpha \omega_1 \tau}\right\rangle \mu(t - \alpha \tau)$$

$$- \left\langle\frac{t}{\gamma \tau} - \frac{\alpha+\beta}{\gamma} - \frac{\sin \omega_1[t - (\alpha+\beta)\tau]}{\gamma \omega_1 \tau}\right\rangle \mu[t - (\alpha+\beta)\tau]$$

$$+ \left\langle\frac{t}{\gamma \tau} - \frac{1}{\gamma} - \frac{\sin \omega_1(t - \tau)}{\gamma \omega_1 \tau}\right\rangle \mu(t - \tau) .$$
(16)

The acceleration ratio during the pulse, i.e.,
$t < \tau$, then becomes

$$\left|\frac{a_1}{a_2}\right| = 1 - \frac{t}{\gamma \tau} + \frac{\alpha+\beta}{\gamma} + \frac{M \sin \omega_1 t}{\omega_1 \tau} - \frac{N \cos \omega_1 t}{\omega_1 \tau} .$$
(17)

where

$$M = \frac{\cos \alpha \omega_1 \tau}{\alpha} + \frac{\cos \omega_1(\alpha+\beta)}{\gamma} - \frac{1}{\alpha} \quad (18a)$$

and

$$N = \frac{\sin \omega_1(\alpha+\beta)\tau}{\gamma} + \frac{\sin \alpha \omega_1 \tau}{\alpha} . \quad (18b)$$

To maximize the expression in Eq. (17),
the first derivative is set equal to zero, solved
for $\sin \omega_1 t$ and $\cos \omega_1 t$, and substituted back
into Eq. (17). This results in an expression for
the maximum absolute acceleration response in
terms of ω_1 and ω_2.

After some mathematical manipulation, the
maximum acceleration ratio reduces to:

$$\left|\frac{a_1}{a_2}\right|_{max} = \frac{1}{\gamma} - \frac{t}{\gamma \tau} + \frac{M \sin \omega_1 t}{\omega_1 \tau} - \frac{N \cos \omega_1 t}{\omega_1 \tau} . \quad (19)$$

where

$$\sin \omega_1 t = \frac{M - N\sqrt{\gamma^2(M^2+N^2) - 1}}{\gamma(M^2+N^2)} \quad (20a)$$

and

$$\cos \omega_1 t = \frac{M - N\sqrt{\gamma^2(M^2+N^2) - 1}}{\gamma(M^2+N^2)} . \quad (20b)$$

This can be further simplified to

$$\left|\frac{a_1}{a_2}\right|_{max} = \frac{1}{\gamma} - \frac{t}{\gamma \tau} + \frac{1}{\gamma \omega_1 \tau}\left[\gamma^2(M^2+N^2) - 1\right]^{1/2} .$$
(21)

After the shock phase, the forcing function
is no longer operative. The resulting acceler-
ation ratio becomes

$$\left|\frac{a_1}{a_2}\right| = \frac{G \sin \omega_1 t}{\omega_1 \tau} + \frac{H \cos \omega_1 t}{\omega_1 \tau} , \quad (22)$$

where

122

$$G = \frac{\cos \omega_1\tau}{2} + \frac{\cos \omega_1(a+\beta)\tau}{\gamma} - \frac{1}{2} - \frac{\cos \omega_1\tau}{\gamma} \tag{23a}$$

and

$$H = -\frac{\sin \omega_1(a+\beta)\tau}{\gamma} - \frac{\sin \omega_1 t}{a} + \frac{\cos \omega_1\tau}{\gamma} . \tag{23b}$$

To obtain the maximum acceleration ratio, the procedure as outlined above for Eq. (19) is followed. After much algebraic manipulation, the maximum acceleration ratio reduces to

$$\left|\frac{a_1}{a_2}\right|_{max} = \frac{\omega_2}{\omega_1\pi}$$

$$\times \left[\left(-\frac{1}{a} + \frac{\cos a\frac{\omega_1}{\omega_2}\pi}{a} + \frac{\cos \frac{\omega_1}{\omega_2}(1-\gamma)\pi}{\gamma} - \cos \frac{\omega_1}{\omega_2}\pi\right)^2 \right.$$

$$\left. + \left(-\frac{\sin a\frac{\omega_1}{\omega_2}\pi}{a} - \frac{\sin \frac{\omega_1}{\omega_2}(1-a)\pi}{\gamma} + \sin \frac{\omega_1}{\omega_2}\pi\right)^2\right]^{1/2} . \tag{24}$$

When $a = \gamma$, Eq. (24) becomes a symmetrical trapezoidal pulse, and the equation reduces to that given by Jacobson and Ayre [3] when expressed in their terminology.

Equation (24) can be further simplified by expanding the quantities in the parenthesis and collecting terms. After much manipulation, Eq. (24) reduces to the following:

$$\left|\frac{a_1}{a_2}\right|_{max} = \frac{\sqrt{2}}{\left(\frac{\omega_1}{\omega_2}\right)\pi a} \left\langle 1 + n^2\left\{1 - \frac{\cos\left(\frac{\omega_1}{\omega_2}\right)n a}{n}\right\}\right.$$

$$-4n\left\{\cos\left(\frac{\omega_1}{\omega_2}\right)\pi\left[1 - \left(\frac{1+1}{2n}\right)a\right]\sin\left(\frac{\omega_1}{\omega_2}\right)\pi a \sin\left(\frac{\omega_1}{\omega_2}\right)\frac{\pi a}{2n}\right\}$$

$$\left. - \cos\left(\frac{\omega_1}{\omega_2}\right)\pi a\right\rangle^{1/2} . \tag{25}$$

where $n = a/\gamma$.

Example

As an example of the use of the developed equation, consider a theoretical rectangular pulse having an 11-msec dwell. There are three other pulses, one symmetrical (LRP) and two asymmetrical trapezoidal pulses (ASTP No. 1 and No. 2) which may be obtained by use of the laboratory equipment. The question arises, "Which of the pulse shapes will simulate the theoretical rectangular pulse?"

Table 1 gives the quantities necessary for the problem solution. After substituting the values for the rectangular pulse into Eq. (8) and LRP, ASTP No. 1, ASTP No. 2 into Eq. (25), one finds that the rectangular pulse is the most severe (as to be expected) and the ASTP pulses are approximately the same (Fig. 4).

TABLE 1

Pulse	a	b	c	α	β	γ	n
Rectangular (theoretical)	—	0.011	—	—	—	—	—
LRP	0.002	0.011	0.002	0.1333	0.7334	0.1333	1.0
ASTP No. 1	0.002	0.011	0.004	0.118	0.647	0.235	0.5
ASTP No. 2	0.004	0.011	0.002	0.235	0.647	0.118	2.0

TABLE 2

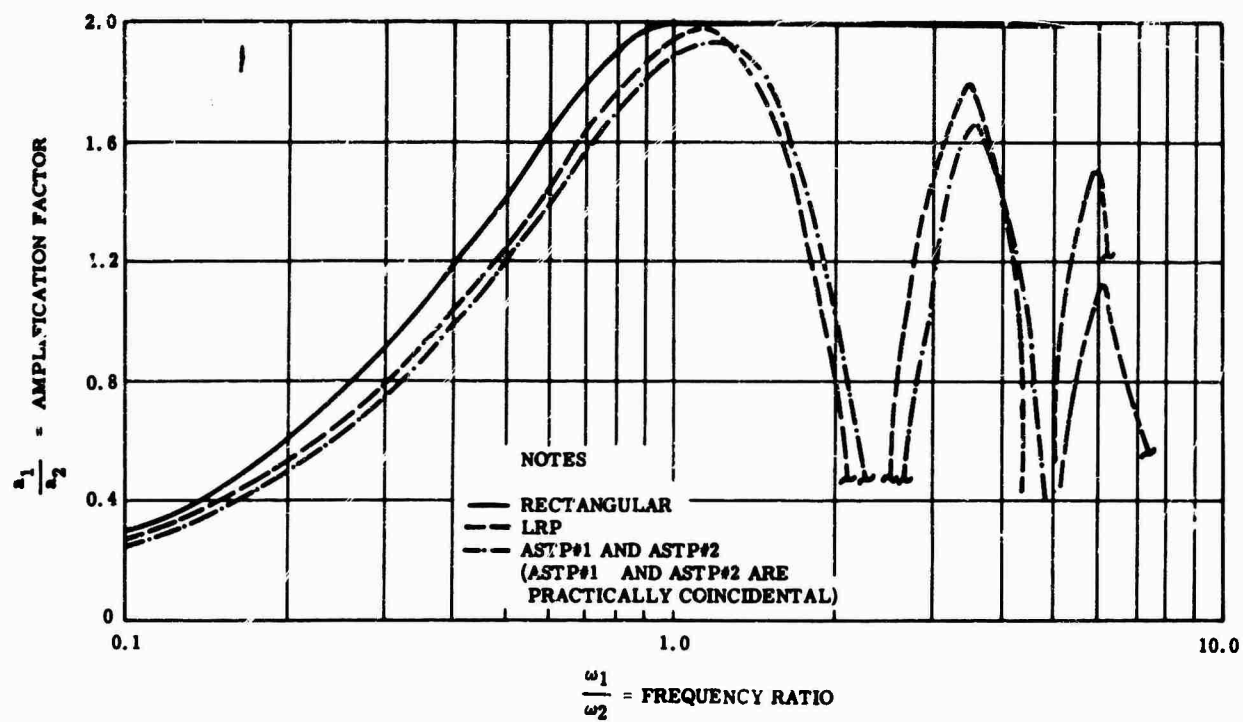| Pulse	a	b	c	α	β	γ	n
ASTP No. 3	0.002	0.001	0.001	0.6452	0.3226	0.0322	20.037
ASTP No. 4	0.002	0.004	0.0025	0.320	0.640	0.040	8.0
ASTP No. 5	0.002	0.006	0.00035	0.2395	0.7186	0.0419	5.716

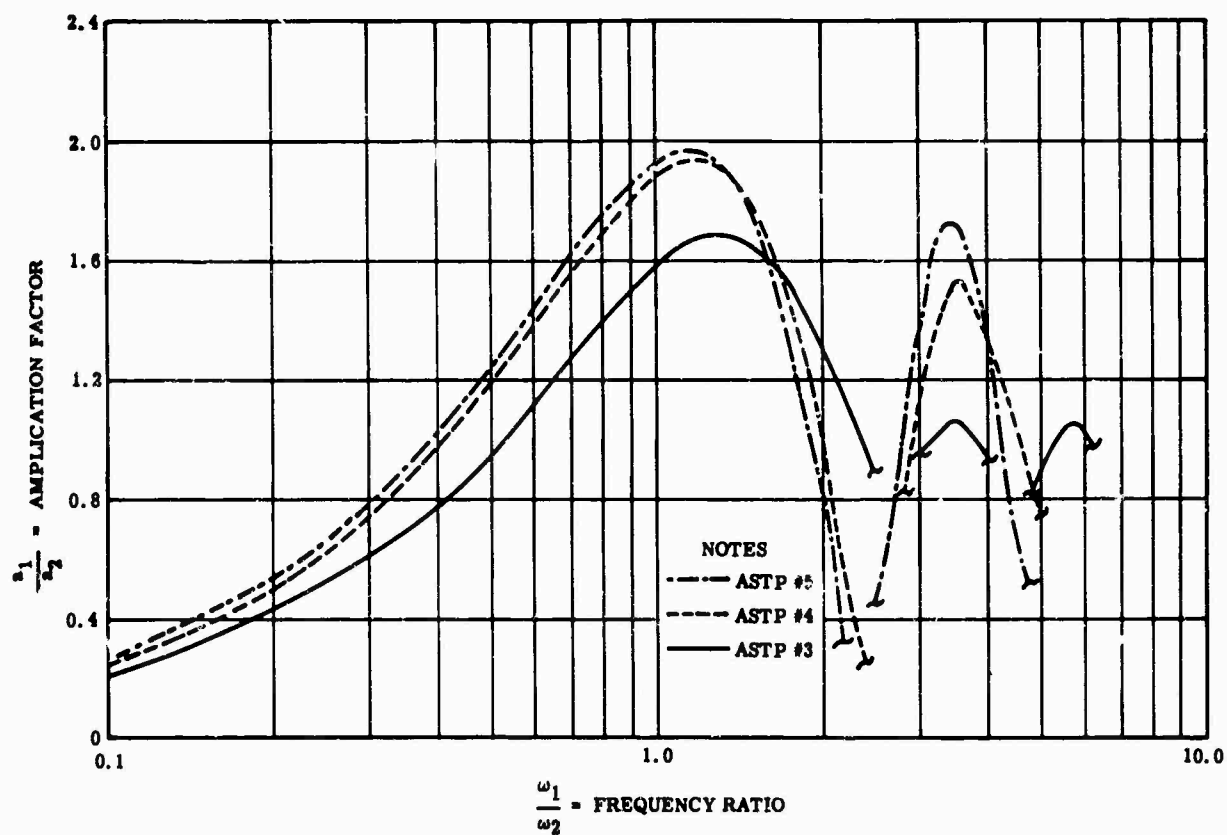Fig. 4. Shock spectra for rectangular, LRP, ASTP No. 1 and ASTP No. 2

Fig. 5. Shock spectra for ASTP No. 3, ASTP No. 4, and ASTP No. 5

As a further indication of the relative effects of the rise, decay and dwell times, three other asymmetrical trapezoidal pulses having the same rise time but increasing dwell and decay times were computed. The inputs for the pulses are given in Table 2. Based on calculated results of these three pulses, ASTP No. 5 was the most severe, with ASTP No. 3 the mildest (Fig. 5).

CONCLUSIONS

A simple equation has been presented for determining the maximum acceleration ratio of an asymmetrical trapezoidal pulse. This pulse results from the inability of laboratory equipment to simulate physically a specified rectangular pulse. It has been shown that the asymmetrical trapezoidal pulse is less severe than the theoretical rectangular pulse. The dwell time is the determining factor, with the rise and decay portions performing secondary roles. The results of this study will enable the designer to assess the degree of deviation between the idealized and the actual test conditions; in

this way he can specify an equivalent trapezoidal pulse capable of providing similar response in the test item. The relationship between rise and decay portions of a pulse has been extensively discussed by Lowe and Cavanaugh [4] and Schell [5].

ADDITIONAL EFFORTS IN PROGRESS

The General Electric Re-Entry Systems Department is continuing studies of the asymmetrical trapezoidal pulse by extending the method to include damping and by developing spectra for determining the maximum acceleration response composed of all variables.

ACKNOWLEDGMENT

The author would like to thank V. Warkulwiz who aided in the programming and L. E. Chaump who stimulated discussions concerning the use of the method.

REFERENCES

1. C. Harris and C. Crede, "Shock and Vibration Handbook," Vol. 1, Chap. 8. McGraw-Hill, New York, 1961

2. J. T. Muller, "Transients in Mechanical Systems," Bell Telephone Tech. Jour., Vol. 27, No. 4, pp. 657-683, Oct. 1948

3. L. S. Jacobsen and R. S. Ayre, "A Comparative Study of Pulse and Step-Type Loads in Single Vibratory System," Stanford

University Tech. Rept. 16, A.T.I. 139914, Jan. 25, 1952

4. R. Lowe and R. D. Cavanaugh, "Correlation of Shock Spectra and Pulse Shape with Shock Environment," presented at Eastern Regional Meeting, IES, Nov. 1958

5. E. H. Schell, "Spectral Characteristics of Some Practical Variations in the Half-Sine and Sawtooth Pulses," AFFDL-TR-64-175, Jan. 1965

* * *